T H È S E

pour obtenir le grade de

Docteur

de

Université Paris Ouest Nanterre La Défense

Spécialité "Mécanique et Génie Mécanique"
présentée et soutenue publiquement le 12 Décembre 2014
par

Jefri Semuel BALE

THE DAMAGE OBSERVATION OF COMPOSITE USING NON DESTRUCTIVE TESTING (NDT) METHOD

M. Dedi PRIADI	University of Indonesia	Président
M. Jacques RENARD	Ecole des Mines de Paris	Raporteur
Mme Anne Zulfia SYAHRIAL	University of Indonesia	Raporteur
M. Claude BATHIAS	Université Paris Ouest Nanterre La Défense	Co-directeur
Mme Martine MONIN	PSA Peugeot Citroen	Examinateur
M. Olivier POLIT	Université Paris Ouest Nanterre La Défense	Directeur
M. Tresna SOEMARDI	University of Indonesia	Co-directeur
M. Emmanuel VALOT	Université Paris Ouest Nanterre La Défense	Examinateur

CONTENTS

ABSTRACT

The aim of this study is to investigate the damage behavior of composite material in static and fatigue condition with non destructive testing (NDT) thermography method and supported by acoustic emission and also computed tomography (CT) scan. Thermography and acoustic emission are used in real-time monitoring techniques during the test. On the other hand, NDT observation of tomography is used for a post-failure analysis. In order to achive this, continuous glass fiber composite (GFRP) and discontinuous carbon fiber composite (DCFC) have been used as the test specimens which supplied by PSA Company, France.

A series of mechanical testing was carried out to determine the damage behavior under static and fatigue loading. During all the mechanical testing, thermography was used in real-time observation to follow the temperature change on specimen surface and supported by acoustic emission in certain condition.

This study used rectangular shape and consist of specimen with and without circular notches (hole) at the center. The constant displacement rate is applied to observe the effect on damage behavior under tensile static loading. Under fatigue testing, the constant parameter of frequency and amplitude of stress was explored for each load level to have the fatigue properties and damage evolution of specimen. The tomography was used to confirm the appearance of damage and material condition after fatigue testing.

The analysis from the experiment results and NDT observation shown the good agreement between mechnical results and NDT thermography with supported by acoustic emission observation in detect the appearance and propagation of damage for GFRP and DCFC under static loading. Fatigue testing shows that thermal dissipation is related to the damage evolution and also thermography and can be successfully used to determine high cycle fatigue strength (HCFS) and S-N curve of fiber composite material. From post failure analysis, CT scan analysis successfully measured and evaluated damage and material condition after fatigue test for fiber composite material.

RÉSUMÉ

L'objectif de ce travail de thèse est d'étudier le comportement de l'endommagement des matériaux composites sous chargement statique et fatigue par contrôle non destructif (C.N.D) thermographie et soutenu par émission acoustique et la tomographie (CT scan). Pour cela, ce unidirectionnels composite à fibres de verre (GFRP) et discontinue composite à fibres de carbone (DCFC) ont été utilisés comme les éprouvettes qui ont fourni par PSA peugeot citröen, France.

Une série d'essais mécaniques a été réalisée pour déterminer le comportement de l'endommagement sous chargement statique et fatigue. Pendant tout des essais mécanique, la thermographie a été utilisé pour l'observation en temps réel pour suivre l'évolution des températures sur la surface de l'éprouvette et supporté par émission acoustique dans certaines conditions. Cette étude a utilisé une forme rectangulaire et se compose d'éprouvettes trouées et non trouées au centre de l'éprouvette. La vitesse de déplacement constante est appliquée pour observer l'effet sur le comportement de l'endommagement sous chargement de traction statique. Sous les essais de fatigue, le paramètre constant de la fréquence et de l'amplitude de stress a été étudiée pour chaque niveau de charge pour avoir les propriétés de fatigue et l'évolution de l'endommagement de l'éprouvette. La tomographie a été utilisée pour confirmer l'apparition de l'endommagement et l'etat du matériau après l'essai de fatigue.

L'analyse des résultats de l'expérimentation et de l'observation NDT montré le bon accord entre les résultats mechnical et NDT thermographie avec prise en charge par l'observation de l'émission acoustique en détecter l'apparition et la propagation de l'endommagement de GFRP PRV et DCFC sous chargement de statique en traction. Les essais en fatigue montrent que la dissipation thermique est liée à l'évolution de l'endommagement et également thermographie et peut être utilisé avec succès pour déterminer la limite d'endurance (HCFS) et la courbe de Wöhler du matériau composite. Les résultats par CT scan ont mesurée avec succès les endommagements et l'état du matériau après essai de fatigue du matériau composite.

LIST OF FIGURES

Page

LIST OF TABLES

ACKNOWLEDGEMENTS

NOMENCLATURES

εe Elastic strain

εp Plastic strain

K   Stress concentration factor

a_o small fixed distance ahead of the hole boundary used in the average stress criterion

d_o Characteristic distance ahead of the hole boundary used in the point stress criterion

E_1 Modulus of elasticity of single ply in axis-1 direction or modulus of elasticity of anisotropic plate in axis-1 direction

E_2 Modulus of elasticity of single ply in axis-2 direction or modulus of elasticity of anisotropic plate in axis-2 direction

E_α Modulus sof elasticity of anisotropic plate in α direction

E_L Modulus of elasticity of single ply in fiber direction

E_T Modulus of elasticity of single ply transverse to fiber direction

G_{12} Shear modulus of single ply associated with {1,2} system

$K_{\pi/2}$ Stress concentration factor at $\alpha = \pi/2$

k $\sqrt{\dfrac{E_1}{E_2}}$

R   Radius of circular hole

x,y   rectangular cartesian coordinates

{1,2}   Rectangular coordinate system

α angular coordinate

v_{12} poisson's ratios

ξ_1 $R/(R+d_o)$

ξ_2 $R/(R+a_o)$

$\sigma 1$ Principal stress

$\sigma 2$ Principal stress

εx Elastic strain

εy	Elastic strain
τxy	Shear strain in-plane
νxy	Poisson's ratio in-plane
Ex	Longitudinal Young's modulus (fibre direction)
Ey	Transverse Young's modulus
Gxy	Shear modulus in-plane
σY	Yield strength
α_1,α_2	Coefficient of thermal expansion
C_p	Spesific heat at constant pressure
ρ	Density
$\Delta\sigma$	Change in stress
S	Detector signal
Δ_ϕ	Change of infrared emmitance
ΔT	Temperature changes at the surface of the loaded component, as follows :
K_1	$-3Bfe\alpha_1 T^3/\rho C_p$
K_2	Material coefficient $= \alpha_2 / \alpha_1$
Q	Stiffness
T	Transformation matrix relating the local material (1,2) and principal stress axes (x,y)
$\Delta\epsilon$	Change of the plane strain in the principal stress axes
E_d	Energy dissipation
ε_{max}	Strain maximum in hysteristic loading
ε_{min}	Strain minimum in hysteristic loading
Φ	Energy parameter
I	Intensity
b	Fatigue sensitivity coeffisient
Nf	Number of cycles
D	Damage evolution
E	Residual modulus
E_o	Initial modulus
W_f	Weight fraction
V_f	Volume fraction

Chapter I   INTRODUCTION

1.1   BACKGROUND

According to recent studies, the weight of an automobile largely effect on its energy consumption and weight saving technology in automobiles is crucial to reduce both the energy / fuel consumption and emissions substantially [1].

From the material use point of view, there is a need for developing new material that can be used to replace conventional material in automotive and aeronautic industry according to the weight reduction issues and environmental aspect. In this regard, there are six main issues that are driving material development in the automotive and aeronautic industry. The first four issues are the development and use of lighter weight material which correlates with the issue of fuel efficiency, reduce CO_2 emissions and save non renewable resources. Two other issues driving the automotive and aeronautic industry to seek new materials are cost effectiveness and the capability of material.

As a combination material that can be varied with respect to size, shape, orientation and content in order to obtain optimum properties for specific engineering applications, to date, the use of composite materials has increased progressively to substitute traditional materials, such as steel, aluminium or wood, due to its specific properties. The excellent stiffness to weight and strength ratios of polymeric matrix composite materials, particularly those reinforced with fiber, make it very attractive for certain manufacturing sectors. The properties of fiber reinforced composites depend on a number of parameters such as material parameters : volume fraction of the fibers, fiber matrix adhesion, orientation of fiber, etc and experimental parameters : specimen shape, the use of tabs for testing, the test velocity, and the loading conditions.

Glass fiber and carbon fiber are the most fiber-reinforced plastic composite materials are ideal for many engineering and structural applications owing to their attractive physical properties. Product developments for demanding applications have been achieved in different engineering sectors to take full advantage of the benefits of composite materials such as design versatility and parts consolidation. Fiber reinforcement material is popular because it is easily drawn into high

strength fibers, it is readily available and may be fabricated into fiber reinforced plastic economically, using a wide variety of composite manufacturing techniques. Fiber reinforced plastic composites have been widely used in many engineering structures due to their excellent mechanical properties especially in automotive industry that require high strength to weight ratios. Generally, in all application of composite, the CAGR (Compound Annual Growth Rate) value of global composite materials shipment market is estimated to increase about 7.4% of CAGR from 2011 – 2017. In automotive industry especially, global automotive composite material market is also estimated to grow about 7% of CAGR from 2.8 $ Billion in 2011 to 4.3 $ Billion in 2017 [2].

Unlike steel, the fabrication process of fiber reinforced plastic composite have multiple options with many variables, making it widely more challenging to select the most cost effective. Recent composite technology research and development efforts have focused on new low-cost material product forms, and automated processes that can markedly increase production efficiencies. In comparison with commercial systems and in application where the state of stress is known to be approximately equal in all directions, discontinuous fiber thermoplastics composite can significantly reduce cost and weight for medium or large volume production [3]. Discontinuous fiber thermoplastics are still predominantly used in non-structural and cosmetic elements, but over the last decade there has been significant progress for structural applications. Hexcel corporation has developed a high performance form of discontinuous fiber compounds that has been used for structural applications in industrial and recreational markets for about 12 years [4].

With the increasing use of composite materials comes an increasing need to understand their behaviour. Mechanical testing such as tensile static testing, can give many of important characteristic of material such as yield strength, tensile strength, elongation, etc which describe the global mechanical behaviour of material.

Regardless of how well an automotive component is maintained or how favorable the operation conditions are, many of the component will eventually fail from fatigue caused by the repeated flexing of loading and not be able to fulfill the

function as it should and it can cause damage. Hence, an understanding of fatigue and damage behaviour of is paramount importance for predicting the service (or fatigue) life of composite materials subjected to long-term cyclic loads to prevent the occurrence of failure and proving its capability to replace conventional steel component.

Composite materials exhibit very complex failure mechanisms under fatigue loading because of anisotropic characteristics in their strength and stiffness. There are four basic failure mechanisms in composite materials as a result of fatigue: matrix cracking, delamination, fiber breakage and interfacial debonding. In the practical use of the composite structure as an automotive component, Some geometrical discontinuities like cutouts and holes are an important machining operations to facilitate the assembly of composite component such as joining of riveted and bolted joints because composites cannot be welded directly like metal materials to ascertain the structural integrity of complex composite products. From mechanical point of view, the hole tends to cause stress concentration in areas adjacent to the hole's boundary, and reduce the load-carryring capacities of the products. Therefore, it is important to take note of this notch sensitivity when designing for bolt holes, joints or cut-out.

Many method have been applicated to monitoring and observed the damage mechanisms in composite materials which is compounded by the fact that damage is not visible to the naked eye and can occur in many different forms. Regarding to the exploitation safety of structures of composite made parts, the most important are the characteristics, describing the appearance and growth of the cracks under the impact of the static and dynamic loads. In general, the fatigue damage of polymer matrix composites occurs within the composite, without cracking macroscopic, with the exception of the final fracture. At the microscopic level, the fatigue damage of composites occurs invariably by microcracking of the resin, followed by microcracking interfaces and finally damage of the reinforcing fibers. Consequently, monitoring and diagnosis of the early detection of these different forms of damage growth requires the application of a contactless method in real-time operation,i.e non destructive method.

NDT (Non Destructive Testing) is a monitoring and observing method that widely used in composite field to understand how the damage initiate and grow until failure occurs. It is advantageous that the inspection is performed while the material is being tested as opposed to periodic removal of the material from a test fixture. This is more time efficient and removes the potential for handling induced damage.

Thermography is an experimental technique of non destructive testing that allows for the monitoring of surface while the equipment is online and running under full load. This contactless method is an excellent condition monitoring tool to assist in the reduction of maintenance costs on mechanical equipment and only need minimal surface preparation (i.e. coatings is not needed). This method based on infra-red thermography, basically includes a camera, equipped with a series of changeable optics, and a computer interface. The core of the camera is a high sensitive infrared focal plane array detector, which absorbs the infra red energy emitted by the object/surface temperature and converts it into electrical voltage or current then represented in the form of thermographic images. It is well known that when a material is subjected to a loading, heat transfer will occurs both in elastic and plastic regime under adiabatic conditions. Thermography investigation on composite material were conducted by several previous studies showed that thermography can indicate the zones of stress and strain on entire surface of the tested subject and succesfully detect the damage propagation based on the temperature changes because the inspection is nonintrusive. The benefit of infrared thermography is the viscosity of the matrix which is heated more than the metal. It helps find the first microscopic damage early, it should help to identify more individual degradation mechanisms; transverse cracks, interface cracks, fiber cracks, etc.

The other real-time NDT method of acoustic emission has the ability to detect and locate damage continuously in a non-destructive behaviour [4]. Failure mechanisms in composite material namely debonding, delamination, fiber cracking and/or matrix cracking also succeeded detectable by acoustic emission [5].

Post failure analysis of NDT method to inspect the inner structure of an object is computed tomography. X-ray computed tomography is a radiographic based inspection technique that produces cross-sectional and 3D volumetric images of the linear attenuation coefficient of a scanned object. These attenuation coefficients directly relate to the material densities present within the object under inspection. Due to its ability of exact three-dimensional cross sectional imaging of the entire part, x-ray computed tomography (CT) is the ideal technology to have complete material characteristic. Several previous studies of tomography observation on composite material conclude that x-ray computed tomography can be very well adapted to the non destructive evaluation of defect detection and characterisation for composite material.

From the previous combination background of damage behaviour and non destructive method on composite material, there is a demand of the ability to apply the combination of mechanical testing and NDT analysis of thermography that supported by acoustic emission and tomography in order to understand the damage behaviour of specific type of fiber composite material. Consequently, a further study is mandatory to investigate the damage observation of fiber composite material by NDT method.

Under this study, unidirectional glass fiber composite (GFRP) and discontinuous carbon fiber composite (DCFC) will be used as the specimen test. The use of these types of fiber composite and is driven by the fact that relatively low cost compared to others. Later, especially for discontinuous carbon fiber composite, analysis of discontinuous carbon fiber composite parts is a challenge since the material has limited information and different behaviour than traditional composites nor isotropic materials. The list of problem research that leads to the new challenges for this study are listed below:

1. Mechanical characteristic and damage behaviour of GFRP and DCFC
2. Develop a description of NDT method on damage characteristic of GFRP and DCFC materials

As a conclusion of this section, Fig.1.1 is presented as the framework of research background.
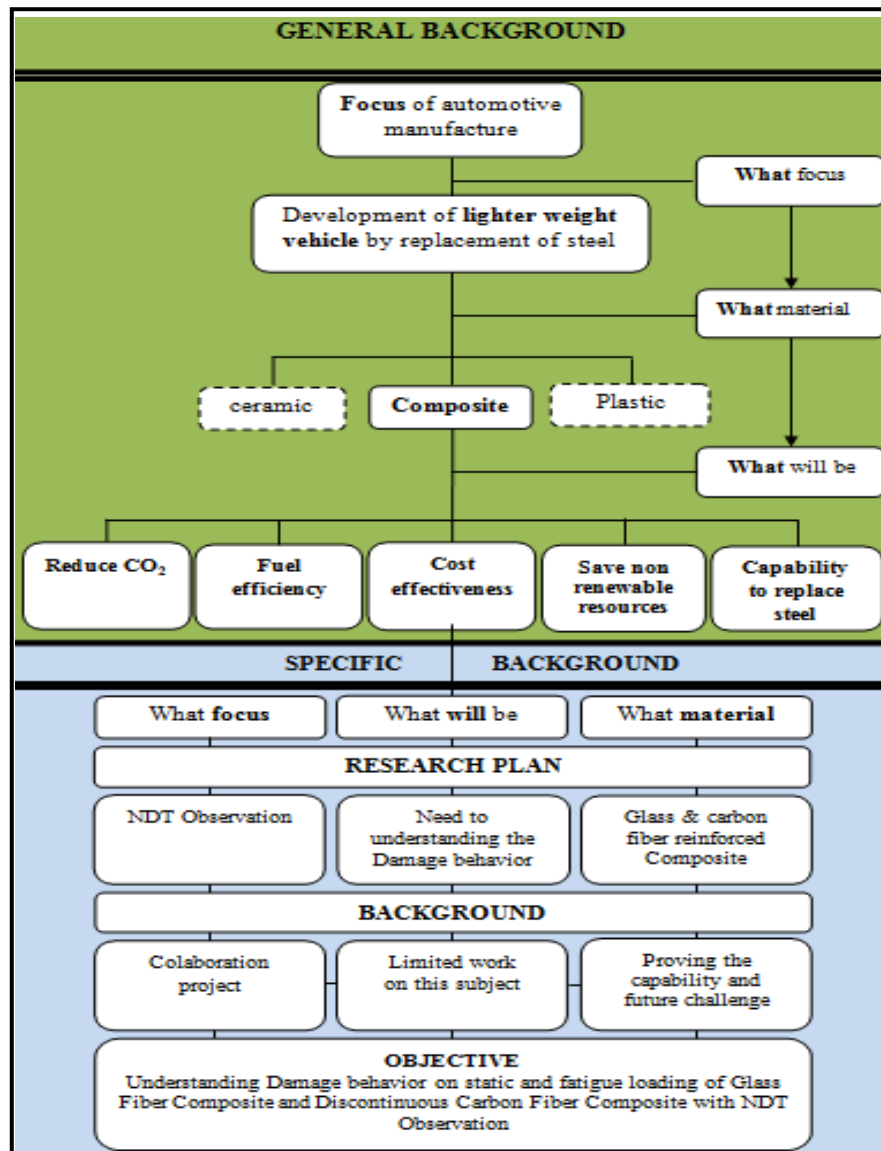
Figure 1.1 Framework of research background

1.2   OBJECTIVE RESEARCH

This research is part of collaboration project of PSA Peugeot Citroën in France with LEME laboratory of University of Paris Ouest Nanterre-La Défense. This project is a jointly funded industrial and academic research initiative to apply the NDT method on observe the damage behaviour of GFRP and DCFC. To achieve this aim, a series of experiments are conducted to examine the damage behaviour (appearance, type, location, evolution) of GFRP and DCFC under tensile (static and fatigue) loading. Generally, damage behaviour of fiber composite under static condition can be in the form of fiber fracture, fiber splitting, fiber pull out, fiber/matrix debonding, matrix cracking and

delaminations between layers of the laminate. Under fatigue loading, The damage evolution can be determined directly by using stiffness reduction that consists of the development of transverse matrix cracks dominates the stiffness reduction ascertained in this first stage, Predominant damage mechanisms that develope in delaminations and cracks propagation in intermediate stage, and as final stage, the occurance of fiber fractures lead to significant stiffness reduction and specimen completely failed [16].

Additionally, during all the tests, specimen surface was observed with NDT thermography supported by acoustic emission (AE) and post failure observation of tomography (CT scan) in order to characterize the damage behaviour through NDT observation.

As a result, this research studies have the objectives are as follows:

1. To obtain the NDT thermography characteristic and provide a combination with mechanical testing results of tensile static loading on damage behaviour and mechanical properties of GFRP and DCFC

2. To obtain the NDT thermography characteristic and provide a combination with mechanical testing results of tensile fatigue loading on damage behaviour and mechanical properties of GFRP and DCFC

3. To determine the NDT characteristics of the results support by acoustic emission (AE) under tensile static loading and tomography (CT-scan) on damage behaviour of GFRP and DCFC where produced by tensile fatigue loading.

1.3 RESEARCH CONTRIBUTION

After conducting a thorough literature review, it is evident that studies of the NDT method for damage analysis of fiber composite are limited. There is no prior work on NDT thermography and post failure observation of tomography on discontinuous carbon fiber composite (DCFC) material. Most studies are limited to continuous composite. It is also notable that in many cases of damage observation on unidirectional fiber composite (GFRP), a combination of NDT thermography and acoustic emission, fatigue strength analysis by thermography and tomography observation have not been fully conducted.

The work presented in this thesis concentrates on the application of NDT method of thermography supported by acoustic emission and tomography as observation tools on damage behaviour of DCFC and GFRP specimen under tensile (static and fatigue) loading condition. This approach aims to correlate all the results in order to obtain a more reliable and accurate representation of the damage behaviour of fiber composite. Moreover, determination of high cycle fatigue strength and the prediction of S-N curve based on thermography and energy dissipation approach also described in this study. To the knowledge of the author, all the results are significant contribution on damage characteristics of DCFC and GFRP composite material that used in this study.

Beside the gap or future work based on the previous studies and the research background, this research will open the opportunity to accomodate the interest in supporting maritime industry in Indonesia where generally using composite as a material for shipping industry due to an excellent corrosion resistance. This opportunity is directly related to the declaration of Indonesia as a maritime pivot by Indonesian President Joko Widodo in Summit East Asian Nations 2014 where the shipping industry to be one of the priority pillar.

For the future, through this research, the application of NDT observation in understanding the damage behaviour of composite component in shipping industry or others is highly expected and reliable for predicting the service (or fatigue) life of composite materials subjected to long-term cyclic loads to prevent the occurrence of failure.

1.4   CONTENT OF THESIS

Chapter 1 describes an introduction of this research. A clear description of background, problem statement, objective of the research and novelty are elaborated as a guideline in conducting this research.

Chapter 2, following the introduction, provides an overview of the state of the art in NDT study and damage analysis on composite material. The review comprehends of the composite, damage behaviour, and NDT method is provided. The observation results on each NDT method of thermography, acoustic emission and tomography associate with damage observation are highlighted in this

chapter. The justification of this work also described along with require further investigation as the novel results.

Chapter 3 explains on experimental method of mechanical testing and NDT observation. The specimen type, procedure of mechanical tensile loading under static and fatigue condition and NDT method of Thermography, acoustic emission, tomography are well documented based on experimental measurements.

Sequentially, Chapter 4 and Chapter 5 outlines the analysis of mechanical testing and NDT thermography observation on GFRP and DCFC. Analysis of static tensile loading along with thermography observation of GFRP and DCFC for specimen with and without hole, analysis of fatigue tensile loading along with thermography observation on GFRP and DCFC for specimen with hole, and rapid strength analysis of GFRP and DCFC under fatigue loading are presented.

Support analysis by acoustic emission and tomography on damage behaviour of fiber composite are given in chapter 6. The coupling between thermography and acoustic emission for damage observation of GFRP and post failure analysis of tomography are focused in this chapter. The correlation of damage behaviour and observation analysis is discussed based on temperature intensity from thermography, the energy - amplitude of acoustic emission signals, and gray value from tomography.

Chapter 7 contains overall conclusion and future work derived from this research work.

Chapter II   LITERATURE REVIEW

2.1   INTRODUCTION

The damage behaviour of composite materials has been widely investigated in recent years with a lot of works on damage mechanisms (section 2.3) and damage observation (section 2.4 - section 2.8)

This literature review is started by a general discussion on composite material (Section 2.2) and the damage behaviour of composite material in general (Section 2.3). Some aspects of the effect of loading type in composites are then briefly introduced (page 21-23). Following this, the composite with an open hole condition are also discussed (page 23-29).

Although they are not strictly speaking as a new type of reinforcement form in composite material, Discontinuous carbon fiber composite have only less coverage in the literature associates with NDT investigation. A limited number of works already exist regarding their mechanical properties and damage behaviour (page 47-51). However, glass fiber composites does not need a brief discussion and their behaviour is well documented.

NDT techniques of thermography, acoustic emission and tomography and details of these procedures for monitoring damage in composites are available in the literature (page 29-46). The application of these NDT method for damage observation in composite material are also described.

From the new focus from industrial point of view shown by background research and limited information on NDT method of thermography, acoustic emission and tomography for damage observation on fiber composite material thorough literature review, there is a need to conduct a research that concentrates on the application of NDT method as an observation tools of damage behaviour for composite material, as seen in Fig 2.1 as an ilustration of the state of the art of new research.

10
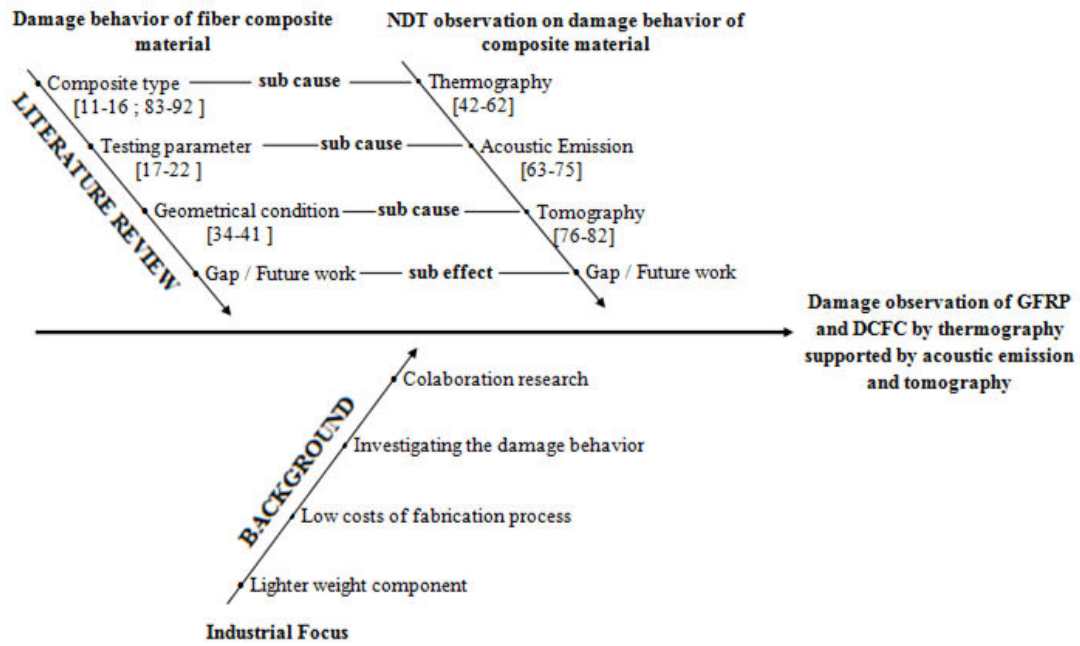
Figure 2.1 Ilustration of the state of the art

From the Fig. 2.1, the ilustration gives the new focus from industrial point of view shown by background research and the limitation from several topics of damage behaviour of fiber composite and the application of NDT thermography, acoustic emission, and tomography. This limitation then need to be identified as the future work or further investigation of NDT observation on damage behaviour of unidirectional glass fiber composite (GFRP) and discontinuous carbon fiber composite (DCFC) . The following descriptions have therefore been identified as requiring further investigation based on state of the art which is novel results for GFRP and DCFC material that used in this study, to the knowledge of author, i.e :

1. Damage observation of GFRP and DCFC by NDT thermography and supporting results by acoustic emission under tensile static loading

2. Damage observation of GFRP and DCFC by NDT thermography under tensile fatigue loading

3. The use of thermography approach coupled with energy dissipation approach for the determination of high cycle fatigue strength (HCFS) of GFRP and DCFC

4. The use of post failure NDT method of tomography for the observation of damage and material constituent of GFRP and DCFC under tensile fatigue loading

2.2 COMPOSITE MATERIAL

Composite materials are created by combining two material to achieve desired properties that usually processed separately and the bonded, resulting properties that are different from those of either of the component materials namely reinforcement and matrix.

Mohanty et.al. [6] very clearly that the composites should not be regarded simple as a combination of two materials. In the broader significance; the combination has its own distinctive properties. In terms of strength to resistance to heat or some other desirable quality, it is better than either of the components alone or radically different from either of them. Uzamani et.al. [7] defines as "The composites are compound materials which differ from alloys by the fact that the individual components retain their characteristics but are so incorporated into the composite as to take advantage only of their attributes and not of their short comings", in order to obtain improved materials. Bilba et.al. [8] explains composite materials as heterogeneous materials consisting of two or more solid phases, which are in intimate contact with each other on a microscopic scale. They can be also considered as homogeneous materials on a microscopic scale in the sense that any portion of it will have the same physical property.

Some advantages of composite materials over conventional ones are as follows [9]:

- Tensile strength of composites is four to six times greater than that of steel or aluminium (depending on the reinforcements).

- Higher fatigue endurance limit (up to 60% of ultimate tensile strength).

- 30% - 40% lighter for example any particular aluminium structures designed to the same functional requirements.

- Composites are more versatile than metals and can be tailored to meet performance needs and complex design requirements.

- Composites enjoy reduced life cycle cost compared to metals.

- Composites exhibit excellent corrosion resistance and fire retardancy.

- Composite parts can eliminate joints / fasteners, providing part simplification and integrated design compared to conventional metallic parts.

The reinforcement presents the strength and stiffness that more harder, stronger, and stiffer compared to the matrix. Fiber reinforced composites is one of reinforcement type besides particulate and structural that are available in three basic form :

- Continuous fibers are long, straight and layed-up parallel to each other.
- Chopped /Discontinuous fibers are short and randomly distributed
- Woven Fibers

Glass fiber and carbon fiber are the most common fiber reinforcement that typically used within the automotive industry for applications such as body panels, suspension, steering, brakes, and other accessories. Glass fibers are manufactured by drawing molten glass into very fine threads and then immediately protecting them from contact with the atmosphere or with hard surfaces in order to preserve the defect free structure that is created by the drawing process, known as E-glass [7]. The advantages of glass fiber are inexpensive, easy to manufacture and possess high strength and stiffness. Carbon fiber produced by oxidising and pyrolysing a highly drawn textile fiber such as polyacrylonitrile (PAN), preventing it from shrinking in the early stages of the degradation process, and subsequently hot-stretching it [7].

Matrix is the continuous phase and can be clasified into : polymer–matrix composites (PMC), metal–matrix composites (MMC), and ceramic–matrix composites (CMC). Polymer-matrix is the most commonly used matrix materials, because compared to metal and ceramic matrix composites, polymer composites are less costly to manufacture. In a composite material, the matrix material have the following critical functions [10]:

- Holds the fibers together
- Protects the fibers from environment
- Distributes the loads evenly between fibers so that all fibers are subjected to the same amount of strain.
- Enhances transverse properties of a laminate
- Helps to avoid propagation of crack growth through the fibers by providing alternate failure path along the interface between the fibers and the matrix.
- Carry interlaminar shear.

Overall, the clasification of composite materials based on its reinforcement and the matrix that generated by different fabrication process demonstrated by Fig.2.2 below
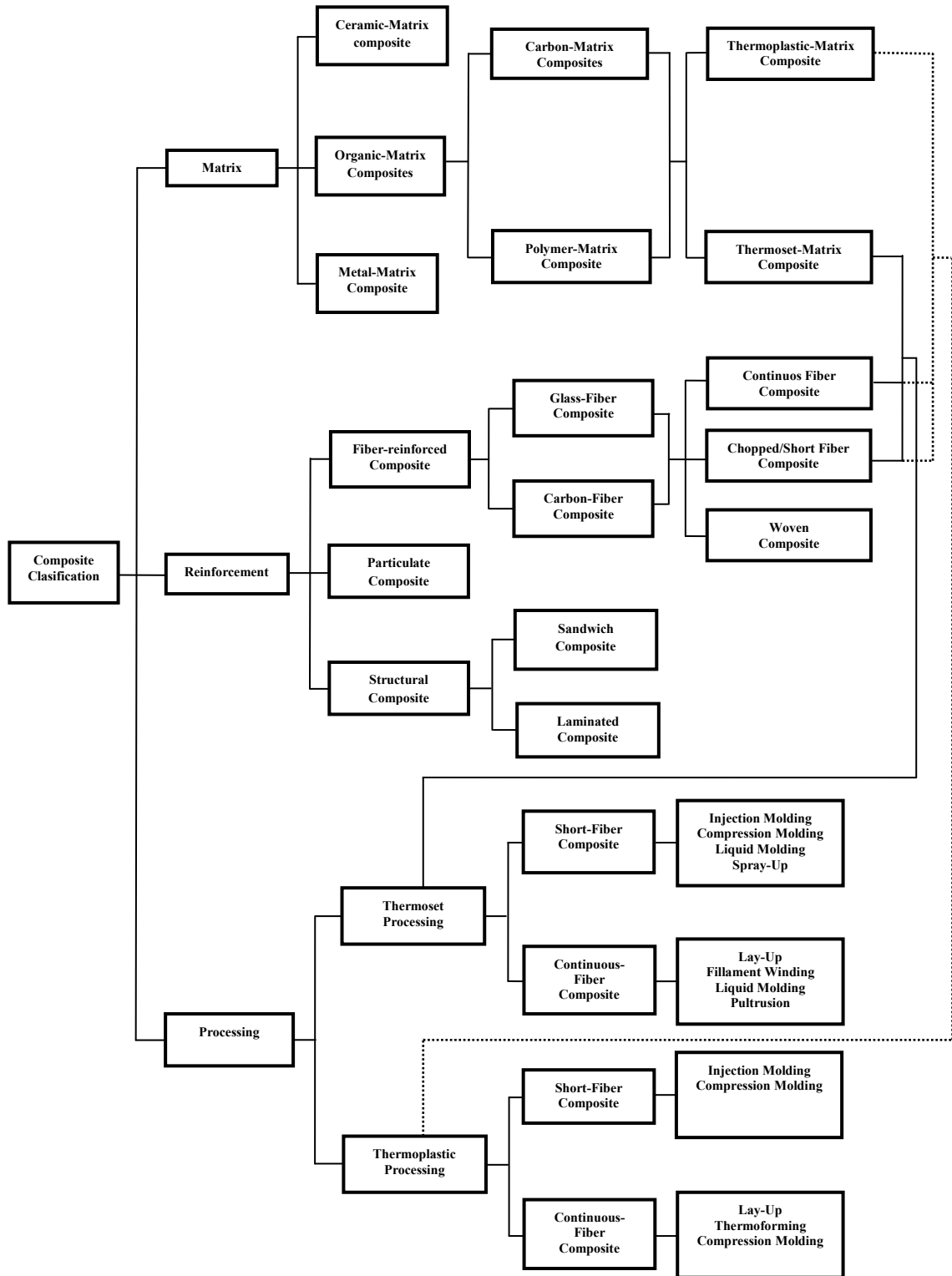
Figure 2.2 Classification of composite

2.3 DAMAGE BEHAVIOUR OF COMPOSITE MATERIAL

Understanding the characteristics of damage behaviour of composite material is very important part of performance evolution as the big picture of composite products like ilustrated in Fig.2.3.
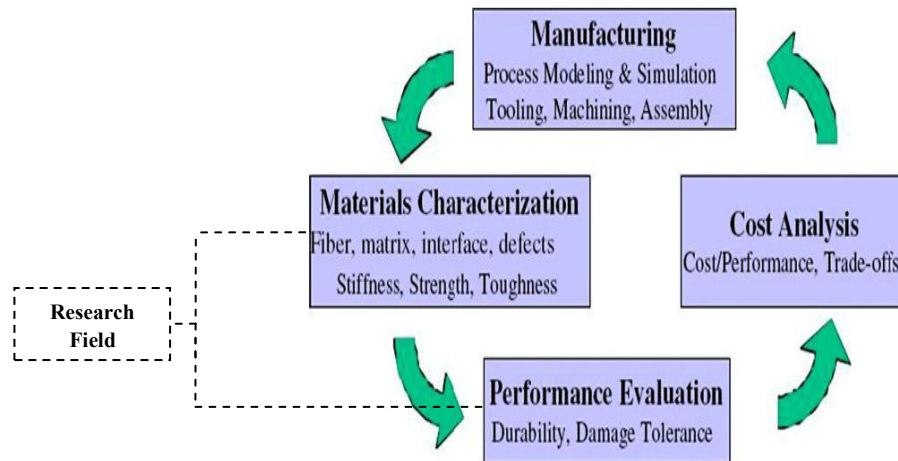
Figure 2.3 The "big picture" of composite products [11]

Several previous studies already investigated the failure behaviour of composite material under static and fatigue condition experimentally. In static condition, Boey [12] in his study about progressive failure under axial loading compression and tensile with varying strain rates noted that the composite is strain rate sensitive as the stress and strain increases with the strain rate. The results also shown the failure mechanism that the initial failure in compression load is matrix cracking, the matrix cracking leads to the fiber micro-buckling, delamination and fiber breaking as the load increases. After that, the next stage of failure propagation is an increasing of all failure modes culminating in a critical local state of stress which initiate fracture of the specimens by shear mode. In tension load, the specimen failure initiated by matrix cracking, followed by delamination and fiber breaking, coupled with interfacial debonding resulted in extensive matrix cracking. After, the final stage of the failure propagation is a rapid progressive of all failure modes which leads fracture of the specimen at critical zone of stress resulting by load and displacement increase.

Generally, failure mechanisms of fiber composite can be in the form of fiber fracture, fiber buckling, fiber splitting, fiber pull out, fiber/matrix debonding,

matrix cracking and delaminations between layers of the laminate that introduced by severe loading conditions, environmental attacks and defect within fiber and matrix. Table 2.1 below gives the type of failure mechanism of fiber composite.

Table 2.1 Type of failure mechanism of fiber composite [13]

Type of Failure	Mechanism
Fiber breakage	Damage usually occurs when the composite is subjected to tensile load. Maximum allowable axial tensile stress (or strain) of the fiber is exceeded.
Fiber pull out	Fiber fracture accompanied by fiber/matrix debonding or fiber/matrix separation
Matrix cracking	Strength of matrix is exceeded
Fiber buckling	Axial compressive stress causes fiber to buckle
Fiber splitting	Transverse in the fiber or interphase region between the fiber and the matrix reaches its ultimate value
Delamination	Interlaminar damage in fiber composite that cause considerable reduction in structural stiffness and leads to growth of the damage and final damage

Despite their excellent characteristics, composite are susceptible to the fatigue and damage phenomena when subjected to certain cyclic loads (static or dynamic) and/or environmental conditions. Failure processes may actually begin during fabrication or at a low applied stress level. Furthermore, failure may be catastrophic and unpredictable. Unlike metals, composite exhibit a peculiar behaviour in fatigue. The experience with the metal fatigue cannot be directly used for composite materials due to its inhomogeneous and anisotropic properties.

For example, after initiation, the propagation of the crack is responsible for final fatigue failure in metals, while accumulation of cracks leads to failure in composite material [14]. Even for unidirectional reinforced composite under the simple loading case, such as tension loading along the direction of fibers, fatigue cracks may initiate at different locations and in different directions [15]. Further more, the composite material experience relatively significant material degradation under fatigue loading. All these differences make it difficult to apply the same fatigue analysis methodology of metals to the composite materials.

Hence, an understanding and prediction of further propagation of such defects is importance for predicting the service (or fatigue) life of composite materials subjected to long-term cyclic loads.

2.3.1 Damage behaviour of fiber composite under fatigue loading

Early study about fatigue failure development of fiber reinforced plastic was conduct by Schulte [16] by analyze the stiffness reduction. The stiffness reduction can be used directly to monitor failure development by grouping into three distinctive stages of damage development [16] :

- The initial region (stage I) with a rapid stiffness reduction of 2-5%. The development of transverse matrix cracks dominates the stiffness reduction ascertained in this first stage,

- An intermediate region (stage II), in which an additional 1–5% stiffness reduction occurs in an approximately linear fashion with respect to the number of cycles. Predominant damage mechanisms are the development of edge delaminations and additional longitudinal cracks along the 0° fibers,

- and a final region (stage III), in which stiffness reduction occurs in abrupt steps ending in specimen fracture. In stage III, a transfer to local damage progression occurs, when the first initial fiber fractures lead to strand failures. These damages evolution as seen in Fig.2.4 below.
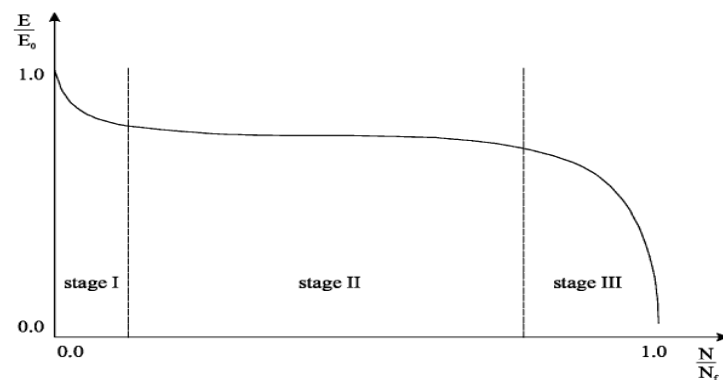
Figure 2.4 Stiffness degradation of fiber reinforced composite materials [13]

In relation with fatigue life of composite, Talreja [11] also divided into three region of composite failure by fatigue. Based on his explanation, First region is the composite failure strain in tension, represents the non-progressive fiber breakage regime in which random fiber failure mechanism governs, Second region is the regime of progressive fiber-bridged matrix cracking in which interfacial debonding plays a role and the final region is the region of matrix cracking, which is effectively arrested by fibers, assisted possibly by interfacial debonding, such that composite failure is not reached within specified large

number of cycles. The boundary between Region II and Region III is the so-called fatigue limit.

Other differences of fatigue damage behaviour between composite and metals was explained by Bathias [17]. In composite, fatigue damage is not related to plasticity, which is very different behaviour compared to metals that its fatigue damage is strongly related to the cyclic plasticity. Due to complex behaviour of composite, further studies has been undertaken to gain more understanding of fatigue failure behaviour in glass fiber reinforced plastics (GFRP) experimentally.

Dyer and Isaac [15] studied about the fatigue behaviour of continuous glass fiber reinforced plastics to evaluate the micromechanisms that occurred during fatigue and how damage accumulated throughout the sample lifetime. It was found that damage accumulation during fatigue has a patern characterised by matrix cracking, delamination and fiber failure. These cracks were seen to have penetrated the fiber bundles before failure, and propagated by debonding of the fiber/matrix interfaces. The observation using SEM shown that both the fibers and the resins failed in a brittle manner.

Fatigue mechanisms in unidirectional glass fiber reinforced plastic was investigated by Gamstedt et.al [18]. The fatigue life performance, stifness degradation and micro mechanisms have been investigated for glass fiber reinforced polypropylene. From microscopic observations, it could be concluded that the better fatigue resistance of glass fiber reinforced plastic can be attributed to the greater interfacial strength and the resistance to debond propagation.

In [19-22],. The effect of lay-up design and the rise of the temperature of the specimens on fatigue perfomance were investigated. The results shows that the fatigue strength is strongly influenced by the layer design and the temperature rise on the surface of the specimens reaches a maximum value at failure or the damage parameter E present a nearly linear relationship with te rise of temperature.

Fatigue crack propagation of GFRP was investigated by Pegoretti and Ricco [23]. The aim of the study is to investigate how the fatigue-crack propagation is affected by the test frequency and the amount of reinforcing fibers. It was found that, at a fixed stress intensity factor amplitude (ΔK), the fatigue crack

propagation (FCP) rate per cycle (da/dN) is reduced when the fiber content is increased. When the effects of the loading frequency were investigated, it was found that the higher the frequency the lower the FCP rate at any fixed ΔK value.

Gagel et.al [24] investigated the relation between crack densities, stiffness degradation, and surface temperature distribution of fatigue behaviour of glass fiber reinforced epoxy. The results shows that in the case of cyclic loading, the stiffness decreases with an increase in Crack Density (CD) until the end of the steady stage of fatigue life. Then, the loss in stiffness turns to be progressive until failure that contrast to the CD development, which continues to grow degressively. It was observed that the location of final failure coincides with the region of the highest surface temperature and cannot be related to the local CD.

In order to avoid large safety factors being applied, failure accumulation during the component lifetime must be monitored. So, it is possible to replace components before final failure. Undergoing different failure types, such as matrix cracking, fiber–matrix debonding, delamination, fiber breakage, quite evenly distributed within the entire material volume [11,17]. The failure behaviour composite under fatigue is ilustrated by the damage progression-time diagram in Fig.2.5.
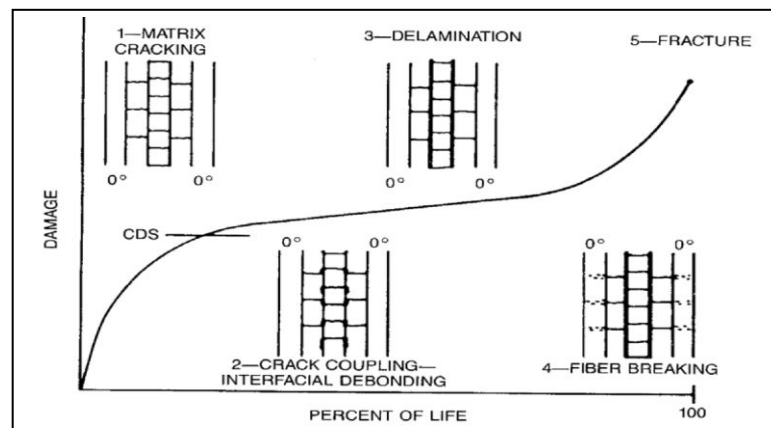
Figure 2.5 Development of damage in composite under fatigue [11]

There are several types of failure stage behaviour in the failure diagram. In the initial stage matrix crack will form and increase with the number of load cycles and will eventually form macroscopic cracks. These macroscopic cracks will show a classical crack propagation patern. The matrix cracks will generally run through the ply thickness and also ply width. These cracks will initiate

microcracks in adjacent plies. In the plies interfaces close to the macroscopic and microscopic cracks strong interlaminar stresses develop which lead to separation between the plies locally. At this state the rate of damage progression increase rapidly and will soon lead to an area where the local stresses reaches a level above the critical and a fracture is initiated. Two dominating stages can be clearly identified : the formation of local, independent matrix micro cracks and a second stage where various types and orientations of cracks interact with increasing rates which finally lead to failure. Wang and Chung [25] also studied about the evolution of fiber breakage of glass fiber composite. It was found that fiber breakage to occur involves 1000 fibers or more and started at about half of the fatigue life during fatigue testing and at least 18% of the fibers were broken before fatigue failure. This Fig.2.6 below also shows the damage type of composite from several investigated by previous authors.
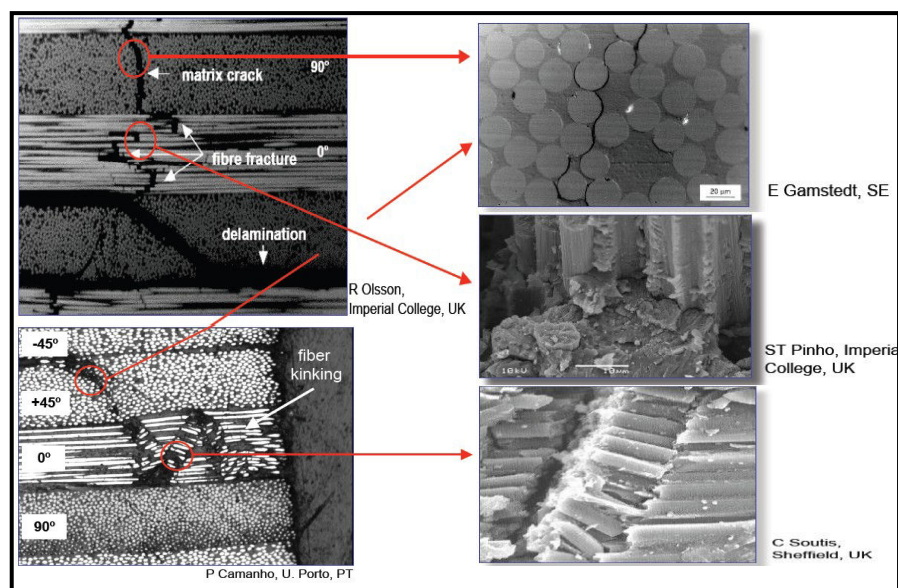
Figure 2.6 Damage type of fiber reinforced plastic [27]

Between the macroscopic and microscopic levels, there exists a very important middle domain, typical of composite materials, which is treated at the mesoscopic level: that of transverse cracking, distribution of the reinforcements and of porosity, that is, the domain of sequential cells [28]. At the mesoscopic level, the fatigue damage is multidirectional and the damage zone, much larger than the plastic zone, is related to the complex morphology of the fracture as reported by Bathias [17].

2.3.2 Effect of loading type on fatigue of fiber composite

Fatigue in materials is caused by repeated loading and unloading cycles to maximum stresses below the ultimate strength of a material. This cyclic loading causes a progressive degradation of the material properties and eventual failure. In many constant amplitude load controlled fatigue experiments, a specimen is loaded sinusoidally in time with the stress:

$$\sigma(t) = \sigma_m + \sigma_a \sin\left(\frac{2\pi t}{f}\right) \qquad (1)$$

Common parameters for describing cycling loading are shown in Fig.2.7.
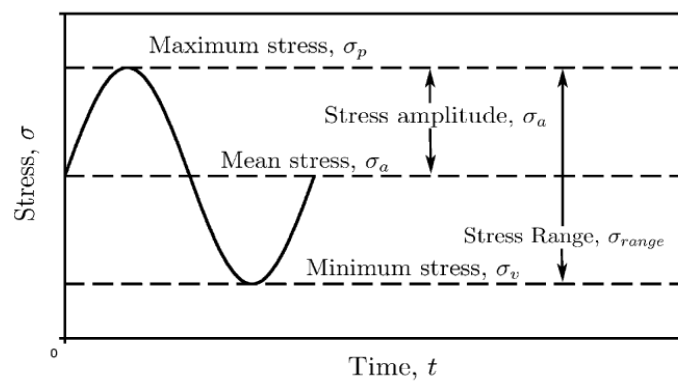
Figure 2.7 Illustration of sinusoidal loading

Different loading regimes characterized by R-ratio are shown graphically in Fig.2.8.
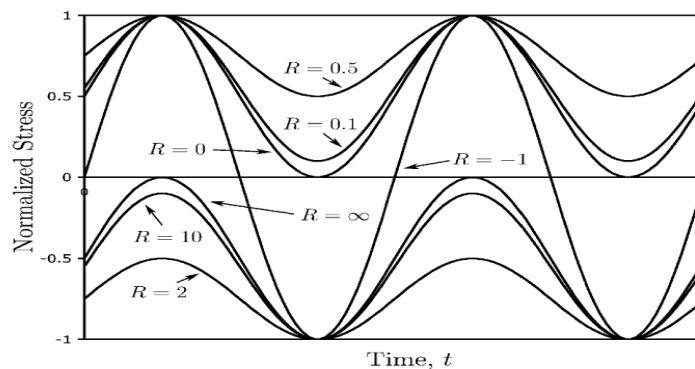
Figure 2.8 Different loading ratios to a maximum absolute value stress of 1.0

R ratio and loading type have not the same effect on fatigue behaviour of glass fiber reinforced plastic (GFRP). Fiber Composite especially in laminates service are submitted to loading, including cyclic loading, which leads to the formation of internal damages, such as matrix fissures, fiber rupture, delamination and microbuckling [15]. These damages will bring their negative effect on the

mechanical performance of laminates, which reduces the useful life of the material. Many previous study has been undertaken to investigated the effect of loading on fatigue of GFRP.

Bathias [17] in his point of view about damage in composite reported that under monotonic loading all composite materials present a compressive strength inferior to the ultimate tensile strength and decreasing as a function of the reinforcement type (boron, carbon, glass, and kevlar). Under cyclic loading the fatigue behaviour is the same. At the limit, when the fatigue cycle is entirely in compression, fracture can occur. For practical applications, it is very important to notice that in compression loading the ratio SD/UTS can be as low as 0.3 for certain composites.

Fatigue Damage, mechanism and failure prevention in fiberglass reinforced composite under different stress ratio were researched by Freire and Aquino [26]. The tests were performed under stress ratios, R (= $\sigma_{min}/\sigma_{max}$), of 0.1, -1 and 10. The results shows that for R = 0.1 laminates experienced fatigue damage according to: formation and saturation of transversal cracks, formation and propagation of delamination, fiber rupture and ultimate composite fracture. For R = -1 the order of the events leading to fracture of both laminates slightly changed to: transversal cracking, formation and propagation of delamination, saturation of transversal cracks, continued formation and propagation of delamination, fiber rupture and ultimate composite fracture. For R = 10 fracture was restricted to delamination, fiber rupture and ultimate composite fracture.

Investigation about the effect of stress ratio on the fatigue of unidirectional fiber glass epoxy composite has been done by Kadi and Ellin [29]. The test was performed under tension-tension and tension-compression loading and variation of stress ratio (R = 0.5 , 0, and -1). The experiment data were obtained for several fiber orientation. It is shown that, in general, tensile and compressive parts of the stress do not contribute equally to the damage.

About the type of loading, Bathias [17] also said that each type has the specific effect on composite materials. The analysis of bending behaviour is more difficult compared to tension or compression because several types of damage could occur in bending such as tension, shear and compression simultaneously.

And for the compression loading, impact damage is plays important role to predict fatigue endurance because of the involved of low energy impacts on the initiation of fatigue fracture which has the same role with machining grooved on the surface of metals. This behaviour be a concern because the low energy could instigates delamination which can propagate under cyclic loading. One of the previous study about fatigue behaviour of behaviour of glass fiber reinforced plastic under bending with different fiber orientation on cantilever beam specimens was studied by Paepegem and Degrieck [18]. Experiments show that these two specimen types based on fiber orientation (0° and 45°) have a quite different damage behaviour and that the stiffness degradation follows a different path. The results show that the outermost layers which have been subjected to the largest tensile stresses, are severely damaged, ,while the outer layer on the compression side showed no signs of damage were observed. This brings about an important result: due to the growth of damage and the degradation of the bending stiffness, there is a continuous redistribution of the stresses in the cross-section, especially near the fixation where damage growth is dominant. The position of the 'neutral fiber' (according to its definition in the classical beam theory) does not remain in the middle of the cross-section, but tends to move towards the compression side and transfers the load to that zone.

2.3.3 Stress concentration of composite with the open hole condition

The stress concentration effect that caused by the open hole on mechanical properties of component is an important issue in failure reliability evaluation for example the component life of joining application in automotive industry especially with composite material. Joining structure that containing the hole in mechanical fastener joints such as pinned joints are very useful and inevitable in complex structure because of their low cost, simplicity for assemble and facilitation of disassembly for repair [34]. The natural behaviour of anisotropic and heterogeneous makes composite material is more complicate and to analyze than isotropic material in the joint application which contains the hole. In the presence of a hole, crack, or other discontinuity, the strength reduction of a

composite from is often the critical design driver and therefore failure prediction is of significant practical importtance [35].

Previous studies about the effect of the hole on the stress concentration and failure mechanism of composite material under static and fatigue loading will be defined below. Awerbuch and Madhukar [36] noted that local damage on the microscopic level in the highly stressed region with cutouts occurs in the form of fiber pull-out, matrix micro-cracking, fiber-matrix interfacial failure, matrix serrations and/or cleavage, and fiber breakage. Ochoa and Reddy [37] ilustrated the failure of discontinuity and their interactions at different scales as seen in Fig.2.9.
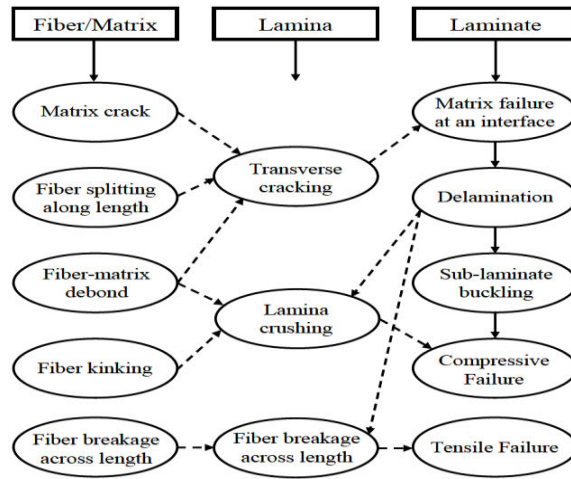
Figure 2.9 Failure mode at different scales

William [38] studied the stress concentration around a small hole in composite plate based on tangensial stress around a circular hole by Lekhnitskii et.al [39] and hole size effect by Nuismer and Whitney [40]. The tangential stress,σ_α (or tangential stress concentration factor, $K = \sigma_\alpha \,/\, \sigma_\infty$) along the hole boundary may be expressed as :

$$K = \frac{\sigma_\alpha}{\sigma_\infty} = \frac{E_\alpha}{E_1} \{[-cos^2\phi + (k + n)sin^2\phi]k\ cos^2\alpha +\ [(1 + n)cos^2\phi - k\ sin2\phi\ sin2\alpha - n\ 1+k+n sin\phi cos\phi sin\alpha cos\alpha \qquad (2)$$

where E_α is the modulus of elasticity in the α direction (Fig.2.12) given by :

$$\frac{E_\alpha}{E_1} = 1\Big/\Big[sin^4\alpha + \frac{E_1}{E_2}\ cos^4\alpha + \frac{1}{4}\Big(\frac{E_1}{G_{12}} - 2v_{12}\Big) sin^2 2\alpha\Big] \qquad (3)$$

where k and n are defined by

$$k = \sqrt{\frac{E_1}{E_2}} \qquad (4)$$

$$n = \sqrt{2\left(\frac{E_1}{E_2} - \nu_{12}\right) + \frac{E_1}{G_{12}}} \qquad (5)$$
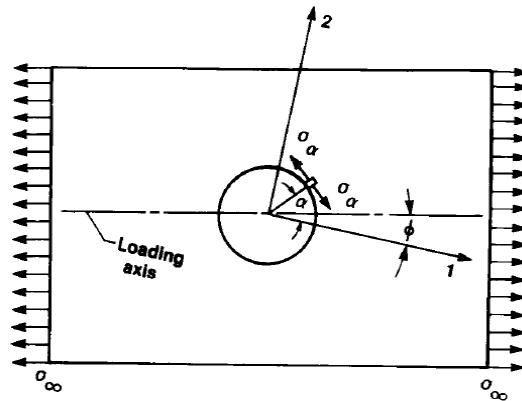
Figure 2.10 Tension at an angle to a principal elastic axis 1 of an isotropic plate with a hole [38]

The ilustration of tangensial stress distribution around the hole for composite plate with different fiber orientation (pararel and perpendicular to loading direction) given by Fig.2.11 below.

Figure 2.11 Tangensial stress distribtuion around a hole [38]

Whitney and Nuismer [40] proposed two failure criteria to consider the hole size effect in composites. These models were called the point stress (PSC) and average stress failure criteria (ASC). Consider a circular hole of radius R (Fig.2.12), if the remote uniform stress σ_∞ is applied in the y-axis direction, then the normal stress σ_y in the y-axis direction at a point on the x-axis in front of the hole may be approximated by :

$$\sigma_y(x,0) = \frac{\sigma^\infty}{2}\left\{2 + \left(\frac{R}{x}\right)^2 + 3\left(\frac{R}{x}\right)^4 - [(1+n) - 3]\left[5\left(\frac{R}{x}\right)^6 - 7\left(\frac{R}{x}\right)^8\right]\right\} \quad (6)$$
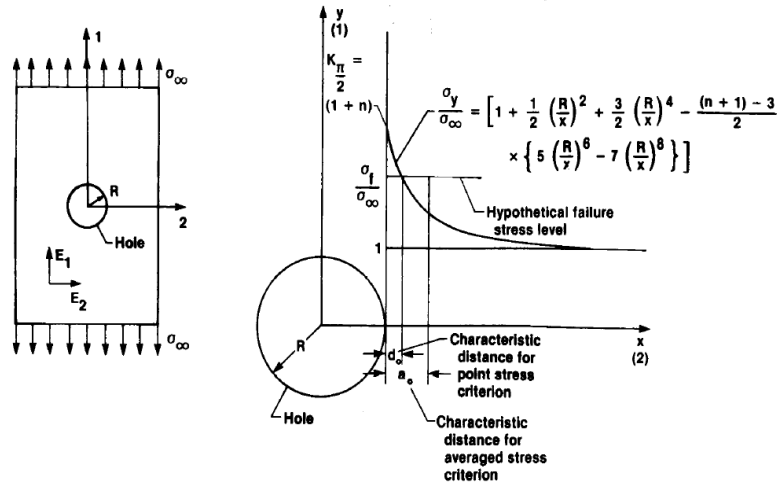
Figure 2.12 Failure hypothesis [38]

At the hole boundary (x=R), the normal stress in the y-direction (σ_y/σ_∞) give the stress concentration factor $K_{\pi/2}$

$$K_{\pi/2} = \frac{\sigma_y(R,0)}{\sigma_\infty} = \frac{\sigma_\alpha\big|_{\alpha=\frac{\pi}{2},\emptyset=0}}{\sigma_\infty} = 1 + n \tag{7}$$

$$K_{\pi/2} = 1 + \left[2\left(\frac{E_1}{E_2} - \nu_{12}\right) + \frac{E_1}{G_{12}}\right]^{1/2} \tag{8}$$

which agree with equation (4) by setting $\alpha = \pi/2$ and $\emptyset = 0$. To account the hole-size effect in equation (8), point stress criterion and average stress criterion were proposed for predicting circular holes and straight cracks.

The point stress criterion assumes that the failure will occur when the stress σ_y (x,0) at a certain small fixed distance (or charateristic distance) d_o ahead of the hole boundary first reaches the tensile strength σ_f of the material (or tensile strength of the plate without a hole) (Fig.2.12). The stress σ_y is described in the following equation :

$$\sigma_y\,(x,0)\big|_{x=R+d_0} = \sigma_f \tag{9}$$

Using Eqs. (6) and (9), the stress concentration factor, $K_{\pi/2}$, can be written as

$$K_{\pi/2}^{PSC} = \frac{\sigma_y(x)}{\sigma_\infty} = 1 + \frac{1}{2}\,\xi_1{}^2 + \frac{3}{2}\xi_1{}^4 - \frac{(1+n)-3}{2}\left(5\,\xi_1{}^6 - 7\,\xi_1{}^8\right) \tag{10}$$

where,

$$\xi_1 = \frac{R}{R+d_0} \tag{11}$$

The average stress criterion assumes that the failure will occur when the average value of stress σ_y (x,0) over some small fixed distance a_o ahead of the hole

boundary first reaches the tensile strength σ_f of the material (or tensile strength of the plate without a hole) (Fig.2.12). It is described in the following equation :

$$\frac{1}{a_0} \int_{R}^{R+a_0} \sigma_y \,(x,0)dx = \sigma_f \tag{12}$$

Using Eqs. (6) and (12), the stress concentration factor, $K_{\pi/2}$, can be written as

$$K_{\pi/2}^{ASC} = \frac{\sigma_y(x)}{\sigma_\infty} = \frac{1}{2(1-\xi_2)} \left\{2 - \xi_2{}^2 - \xi_2{}^4 + [(1+n)-3](\xi_2{}^6 - \xi_2{}^8)\right\} \tag{13}$$

where,

$$\xi_2 = \frac{R}{R+d_0} \tag{14}$$

Based on Neismar and Whitney criterion, William [38] examined the effect of hole size on stress concentration factor for composite plate as seen in Fig.2.13 below.
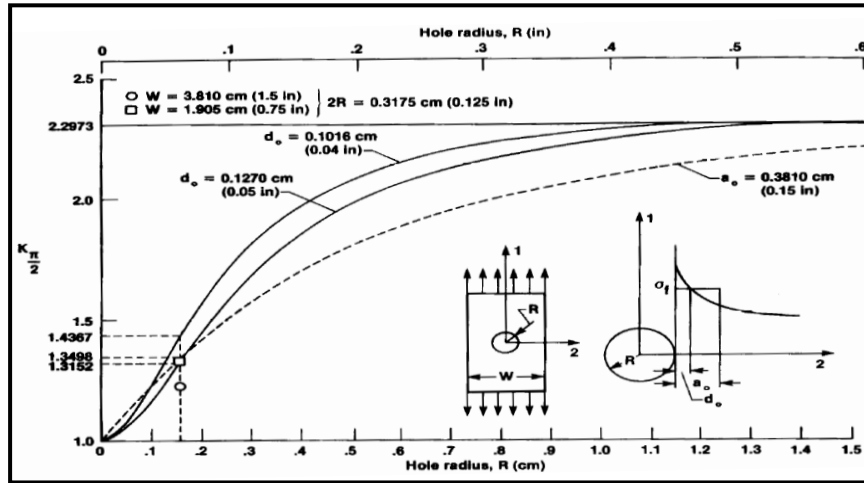
Figure 2.13 Stress concentration factor $K_{\pi/2}$ as a function of hole size

Arslan et.al [41] in similar study, investigated the effect of fiber orientations and various E1/E2 values in composite plate contain a circular hole. A four-layered glass-epoxy composite is chosen, starting from the top, the glass fibers make with the x-axis the following angles, respectively, 0^0, 45^0, -45^0, and 90^0. Results (Fig.2.14) shown that the stress concentration value reaches a maximum at $\theta=90^0$ for layer 1 (fiber orientation angle is 0^0).
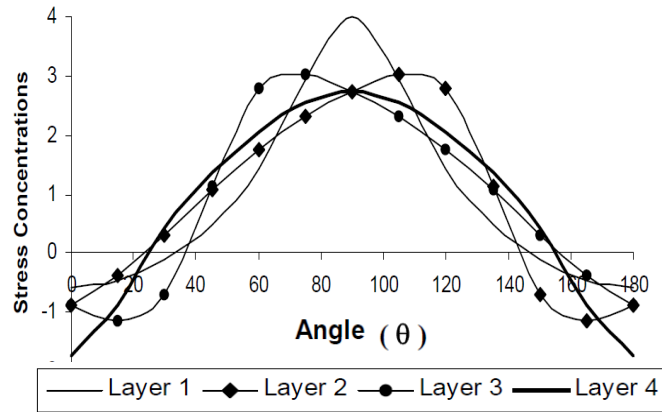
Figure 2.14 Stress concentration factor versus θ for glass-epoxy composite

Furthermore, the stress concentration values change also, depending on the ratio of the elasticity modulus of the fiber direction to the transverse one (*E1/E2*). In Fig.2.15, the effect of the *E1/E2* ratio is shown for 0^0 and 90^0 fiber orientation angles. For 0^0 fiber orientation, when the circumferential stress is parallel to the fiber direction, causing more of the force transfer to take place through the fibers and when the circumferential stress is perpendicular to the fiber direction and force transfer takes place through the matrix material that don't undergoes change significantly near the points where θ equals 0^0 and 180^0 caused by matrix's weakness and low elasticity modulus. The vice versa condition occurs for 90^0 fiber direction which very little change when the loading is in the transverse direction to the fibers where θ equals 90^0.
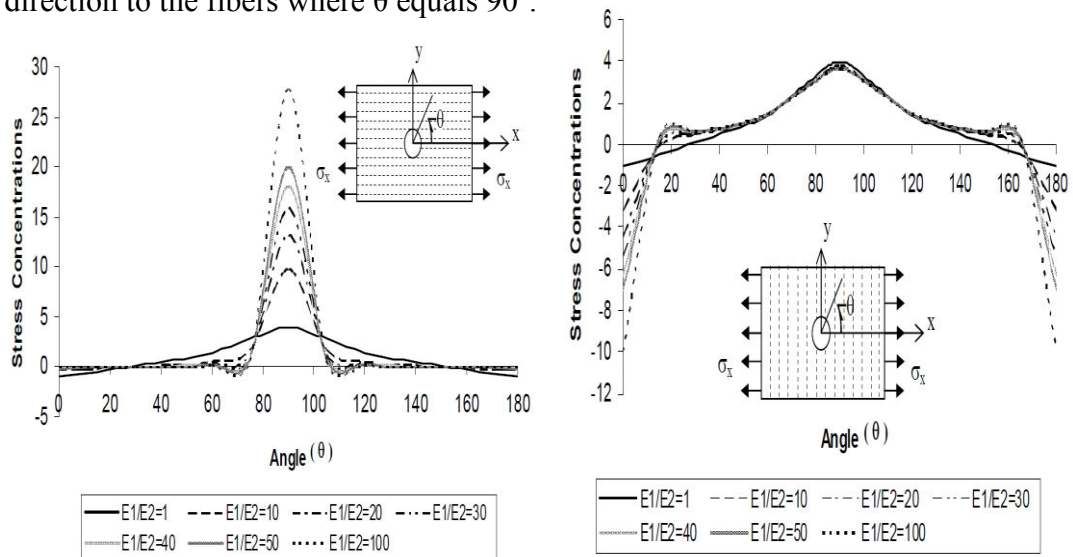
Figure 2.15 Stress concentration versus θ for various elasticity modulus ratio [41]

In design under fatigue loading, stress concentration factor is used in modifying the values of endurance limit while in design under static loading it simply acts as stress modifier. Cracks generally occur in an area where stress is at its maximum, thus, they are most likely to nucleate at a stress concentration. In analysis or design work, fatigue stress concentration can be calculated using the relation with static concentration, defined as :

$$K_f = 1 + q \ (K_t - 1) \tag{15}$$

where, q as notch sensitivity can be written by :

$$q = \frac{K_f - 1}{K_t - 1} \tag{16}$$

where K_f is fatigue stress consentration and K_t is static stress concentration.

For DCFC material, the notch sensitivy can be applied as characteristic dimension d_o that found by ferabolli et.al [87]. Both, q and d_o have same perspective that such a large value signifies that this material is much more tolerant to open holes or full norch sensitivy. On the contrary, if these values have a value close to 0, the material has no sensitivity to notches at all.

2.4   THERMOGRAPHY ON COMPOSITE MATERIAL

During the last few years, the industrial interest has been oriented towards the development of new non-destructive testing techniques in order to achieve high accuracy, cost effectiveness and more efficient testing methods. In a wide range of different NDT techniques, thermography was until recently considered as an emerging technology and nowadays is widely used in characterization of composite materials. The use of infrared thermography is recommended whenever a fast inspection method, involving no contact with tested part is required. Thermography nondestructive testing has been shown to be an effective technique for detecting damage in composites during load testing because the inspection is nonintrusive. In the case of polymer composite materials, it is applicable to the detection of cracks, impact damages and fatigue degradation [42-44].

The basic idea of thermography is to apply infrared frequency range of electromagnetic radiation emitted by object under research to obtain information concerning its selected physical properties or processes taking place within this

object. The camera thermograpy will absorbs the IR energy emitted by the object and it transforms the amount of infrared energy into the temperature then represented in the form of thermographic images. Fig.2.16 shows the ilustration of thermography process.

Thermography is a well-established experimental technique that has been used in a wide range of engineering applications including in composite field. Thermography is one of non destructive testing (NDT) that allows for the monitoring of temperatures and thermal patterns based on the measurement of the temperature changes when an external load is applied to a component as a result of a reversible effect while the equipment is online and running under full load. The temperature distribution behaviour on the surface of scanned or process of surface temperature changes is very important to understand the material properties and structural characteristic of experimentally tested material that influence temperature distribution of scanned surface.
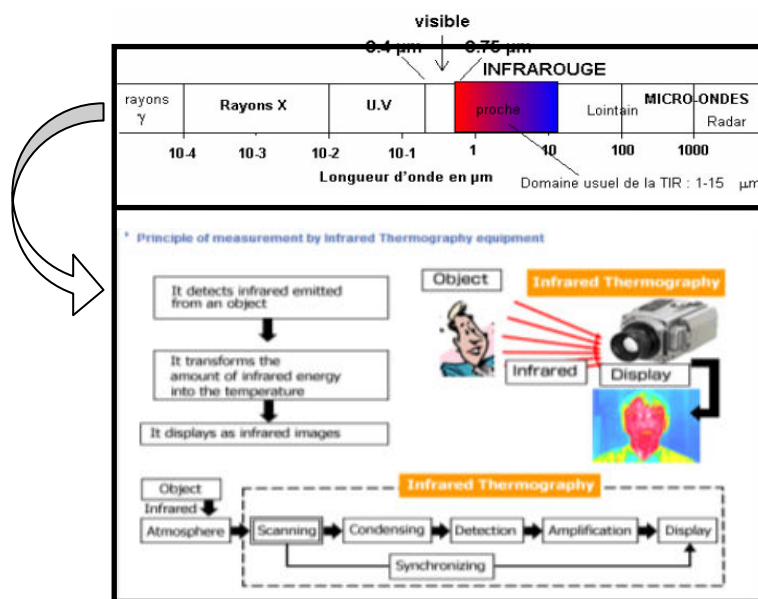
Figure 2.16 Thermography ilustration

The thermoelastic response from composite differs significantly from homogeneous isotropic materials, as composite is non-homogeneous in its mechanical and physical properties. Stanley and Chan [45] presented the relationship between temperature changes and applied stress on the surface of composite material with plane stress conditions, as follows :

$$\Delta T = -\frac{T}{\rho C_p}\left(\alpha_1 \Delta\sigma_1 + \alpha_2 \Delta\sigma_2\right) \tag{17}$$

where :

α_1 and α_2 are the coefficient of thermal expansion (μm/m^{o}C)

C_p is the spesific heat at constant pressure (J/g ^{o}C); ρ density (g/cc)

$\Delta\sigma$ is the change in stress (N/m^2) ; Subscripts 1 and 2 denote the longitudinal and transverse to fiber directions.

Feng et.al [46] presented the relationship from detector signal S and the amplitude of the stress which is according to the change of infrared emmitance Δ_ϕ produced by temperature changes ΔT at the surface of the loaded component, as follows :

$$S = \Delta_\phi = 3e\text{BFT}^2\Delta T \tag{18}$$

by subsituting eq (17) into eq (18) we obtain the relationship between S and the amplitude of the stress, as follows :

$$S = K_1 \left(\Delta\sigma_1 + K_2 \Delta\sigma_2\right) \tag{19}$$

where :

$$K_1 = -3Bfe\alpha_1 T^3/\rho C_p \tag{20}$$

$$K_2 = \text{material coefficient} = \alpha_2 / \alpha_1 \tag{21}$$

For determining K_1 and K_2, Feng et.al [46] demonstrate a case of a unidirectional composite with off-axis fiber direction subjected to the a stress amplitude condition $\Delta\sigma_y$, as shown in Fig.2.17.
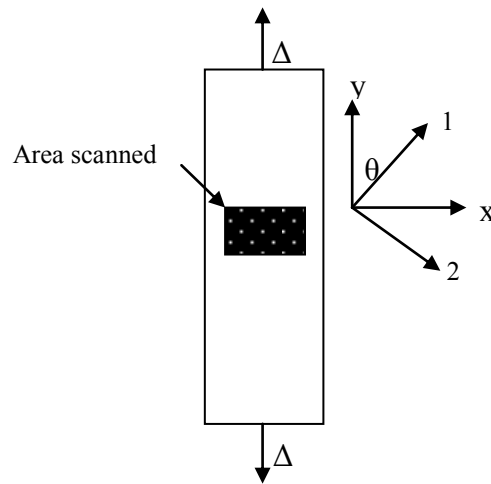
Figure 2.17 Case ilustration of unidirectional composite with off-axis direction

the stress condition for $\Delta\sigma_1$ and $\Delta\sigma_2$ by presence of θ can be expressed as :

$$\Delta\sigma_1 = \Delta\sigma_y \cos^2 \theta \qquad (22)$$

$$\Delta\sigma_2 = \Delta\sigma_y \sin^2 \theta \qquad (23)$$

by combining eqs (19), (22), and (23), gives the expression to determine coeffisients K_1 and K_2 that depends on angle θ between loading direction and fiber orientation :

$$S = K_1 \Delta\sigma_y \left(cos^2\theta + K_2 \, sin^2\theta\right) \qquad (24)$$

Reformulation of equation (17) to described the temperature changes in terms of strain based on the principal material directions was given as [47] :

$$\Delta T = -\frac{T}{\rho C_p} [\alpha]_{1,2}^T Q_{1,2}[T][\Delta\in]_{x,y} \qquad (25)$$

where :

Q : the stiffness

T : transformation matrix relating the local material (1,2) and principal stress axes (x,y)

$\Delta\epsilon$: the change is the plane strain in the principal stress axes

2.4.1 Thermography study on composite material

Several studies already performed on composite material to understand its mechanical behaviour by means of thermography.

Under static loading condition, thermography was found successfully detected the damage mechanism on the surface of composite specimen. The application of NDT thermography in damage analysis of fiber glass composite under static tensile loading conditions was conducted by previous authors. Libonatti [48] investigated the evolution of composite damage under static tensile tests by using thermography method with different of fiber orientation respect to the loading direction . The results showed that the types of failure is dependent on fiber orientation by suddenly increase of temperature indicate the location of the failure due to the rupture of fiber. Thermography method for characterizing tensile deformation of glass/epoxy composite specimens also studied by Kutin et.al [43]. The temperature is monitored simultaneously as seen in Fig.2.18.
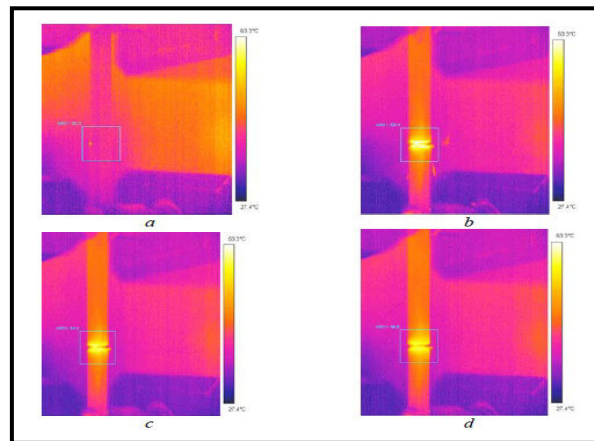
Figure 2.18 Temperature distribution during extension [43].

Based on temperature changes of test results, thermography can indicate the zones of stress and strain on the entire surface of the tested object and obtained results confirm that thermography is very useful for early diagnostics of structures under the real conditions.

Muneer et.al [42] also studied about thermomechanical behaviour of glass fiber composite under static tensile loading. The results shows that in all the cases, temperature decreases linearly in the elastic region along with increased stress due to the thermo-elastic effect and then the specimens show non-linear behaviour in temperature response that related to the physical damages (e.g., matrix cracking, interfacial debonding and delaminations). Colombo et.al [49] in their study about mechanical characteristics of GFRP by thermography categorized thermal behaviour of fiber composite into four stages : completely elastic behaviour, globally elastic behaviour, non elastic behaviour and final breakage. In elastic periode, temperature shows a decrease trend since the input energy from mechanical testing is stored and absorbed by composite material. In non elastic behaviour and final breakage periode, the temperature increases in non-linear and suddenly condition due to the energy released that caused the final failure of the specimen characterized by delamination or fiber breakage.

Others studies develop the thermography method to study glass fiber composite in fatigue condition and also for the effect of an open hole specimen [50-52]. EMSE [50] investigated applicability of thermography method in damage evalution of glass fiber composite with an open hole specimen. The results shows

that the last three images acquired (Fig.2.19) successfully detect damage that make obvious progress final damage.
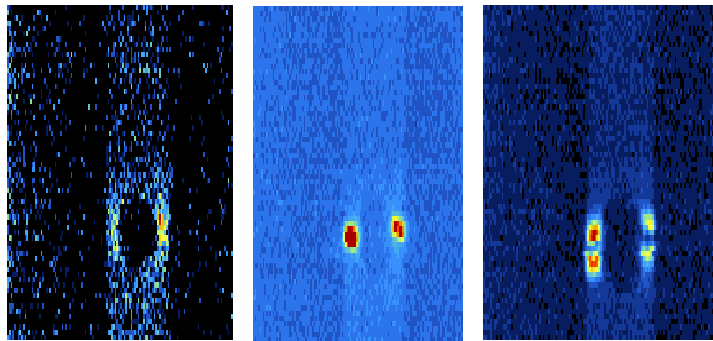
Figure 2.19 Thermography images of damage mechanism on composite [34]

Toubal et al.[51] also investigated the damage mechanism of composite material with thermography analysis under fatigue loading. The evolution of the temperature consists to three stages. In the first part, the variation in the temperature is due to frictions (fibres/fibres and fibres/matrix) and to the damages which start and are propagated during the fatigue test. In the second part the temperature reaches a balance that is due a saturation in the damage, then leads to suddenly increase of temperature corresponding to the rupture. The damage evolution that detects by thermography is relate with damage grows in during fatigue, i.e first damage stage due to the occurence of multiple damage, second steadily and slowly increase of damage, and rapidly grows of damage due to the fracture of fibres. Fig.2.20 below ilustrates the comparison between temperature and damage evolution on their results for fatigue testing.

Toubal et al.[51] concluded that the temperature analysis on specimen surface can be used to predict damage evolution of composite material.
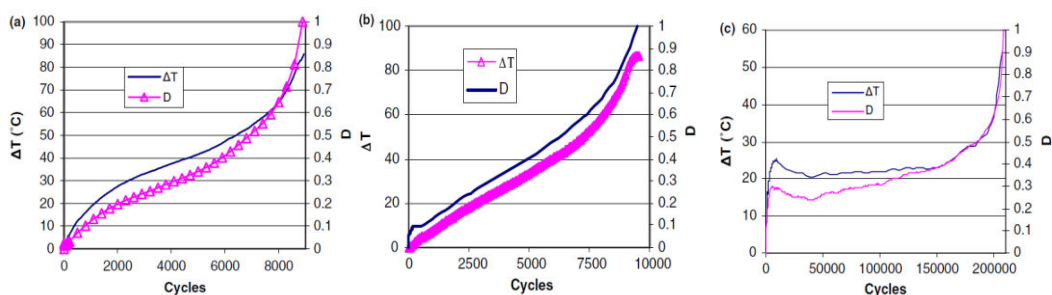
Figure 2.20 Comparison between the change of temperature and the damage evolution: (a) 70% level of loading, (b) 67.5% level of loading, (c) 60% level of loading [51]

Beside glass fiber composite, thermography method also conducted by previous study by EMSE [50] on carbon fiber composite and show sensitive behaviour in detect temperature changes in stress concentration area where the damage process actually takes place for tension compression fatigue loading as shown in Fig.2.21. Damage detection in carbon fiber composite also presented by Rossignol et.al [52]. Thermography successfully observed damage location on the surface of carbon specimen and thermography can detect different damage mechanism on the matrix and on the fiber of carbon fibers plastic reinforced materials under flexural static loading (Fig.2.24).

1500 N   **2000 N**   **2500 N**   **3000 N**
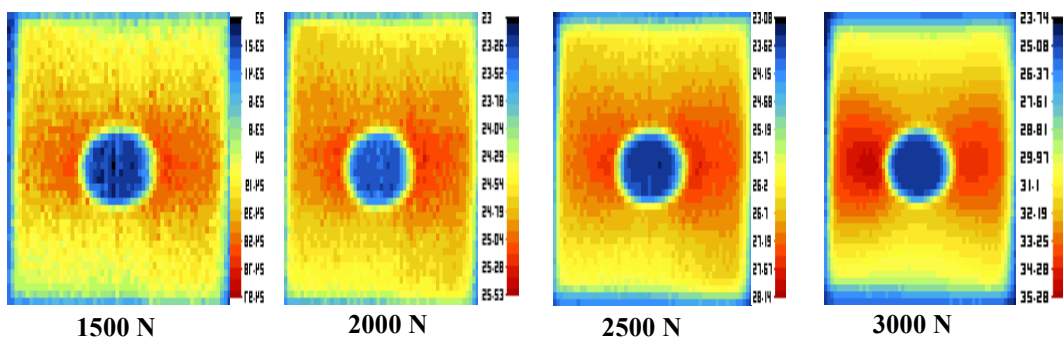
Figure 2.21 Temperature changes as increase of stress around the hole on CFC under tension compression fatigue loading [50]

Damage located by thermography   Different damage mechanisms by thermography

Damage propagation by thermography
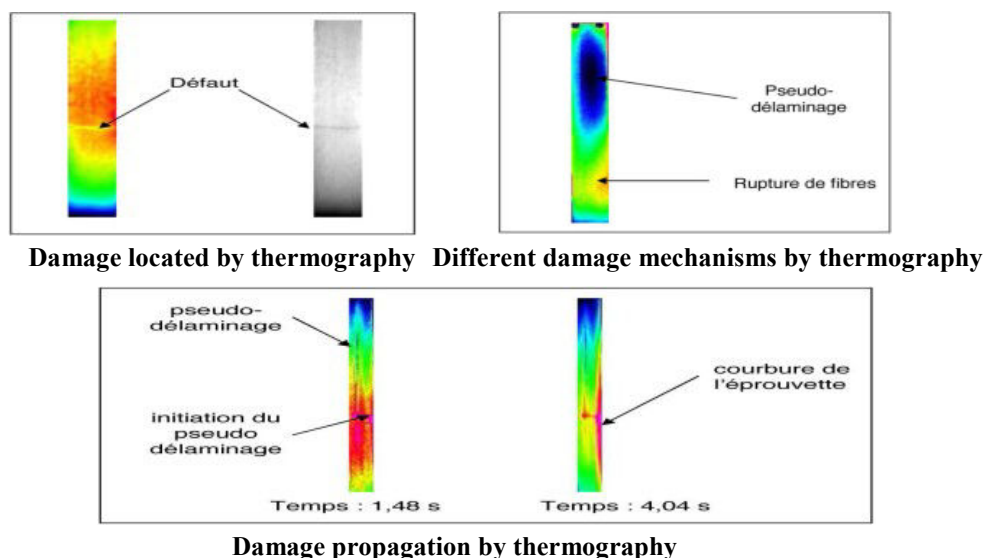
Figure 2.22 Damage observation by thermography on carbon fiber composite [52]

2.4.2 Thermography approach to determine high cycle fatigue strength

Beside the ability to detect the damage appearance and damage evolution, themography method also successfully use for determine the high cycle fatigue

strength for steel and also composite material [53-56,59-62]. Risitano et al. [53-54], was the first time that developed a thermography approach based on thermal maps over a surface of a specimen to determine the fatigue limit then known as Risitano method. They proposed that the fatigue limit could be determined by plotting the stabilization temperature (in a few thousand cycles) against the applied stress and finding the value of the fatigue limit as the intercept of the curve on the stresses axis , as ilustrated in Fig.2.23b. In the case of composite material, friction between fiber and matrix, the different damage mechanisms of fiber breaking, fiber-matrix debonding, matrix cracking, etc associated to the visco-elasto-plastic behaviour of matrix generate a significant amount of heat which is converted in significant temperature increase for low and high stress level [55-58]. Since it is not necessary to run the fatigue test up to failure in order to achieve the stationary temperature increase, the thermography approach was presented as a rapid tool able to estimate the fatigue limit. Compare to the traditional Wöhler S-N curve, the Risitano method is not necessary to use the large number of specimens and very efficient time-consuming procedure, and consequently offers a considerable saving in cost [56].
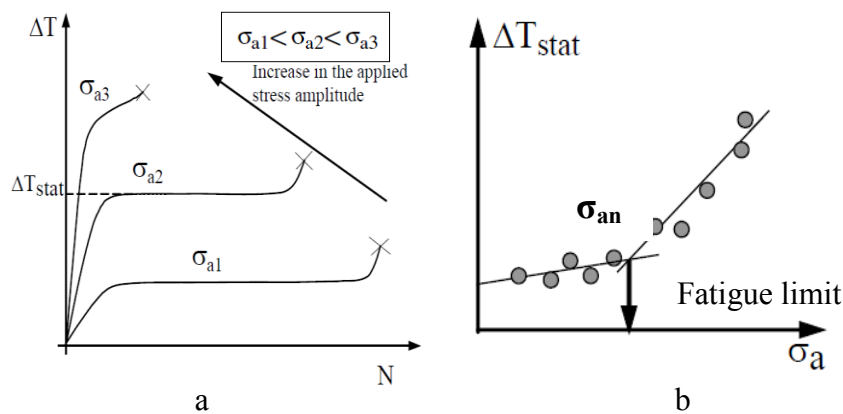
Figure 2.23 (a) Stabilisation temperature during fatigue test
(b) Determine the fatigue limit for composite material

Recently, Toubal et al and Montesano et al. [60-61] was several authors that applied the thermography approach to determine the high cycle fatigue strength (HCFS) on fatigue life for composite material. They combined the calculation of energy dissipation from experimental fatigue data during stabilization periode of temperature increase to determine the HCFS with the thermography results for the validation.

The linear relationship between stabilization temperature (Δt_{stab}) and energy dissipation for each load level (Fig.2.26c) means that the energy dissipation (Ed) directly correlates to the temperature increase during fatigue loading due to the intrinsic energy dissipation of the material [61]. The main mechanisms causing energy dissipation for the composite material may be attributed to the viscoleastic behaviour of matrix, matrix cracking, fiber fracture, and interface cracking/friction among others [56].

The calculation of energy dissipation per unit volume is measured by the following equation :

$$E_d = \int_{\varepsilon_{min}}^{\varepsilon_{max}} \sigma_{load}\,(\varepsilon)d\varepsilon - \int_{\varepsilon_{min}}^{\varepsilon_{max}} \sigma_{unload}\,(\varepsilon)d\varepsilon \qquad (26)$$

In [59,61-62], thermography approach also applied to predict the fatigue life that has a good agreement with the S-N curve from experimental data. The approach for the purpose of estimating fatigue life of materials under cyclic loading using an energy parameter, Φ, defined as :

$$\Phi = \Delta T_{stab}\, Log\, Nf = constant \qquad (27)$$

2.5 ACOUSTIC EMISSION ON COMPOSITE MATERIAL

Acoustic emission is a well-known technique for the detection of a wide range of micro-structural failures in different materials [63]. When a failure mechanism is activated and cause microstructural changes, part of the total strain energy is dissipated as a wave that propagates from the failure source through the medium [63]. When these wave reach to the surface, they cause it to vibrate and these waves are also kown as acoustic emission (AE) [64].

AE signals are obtained by measuring the surface activities with transducers that very sensitive and can be potentially make an earlier detection of failure. In polymer-matrix composite several different failure mechanisms that can be identified, i.e. delamination fiber breakage, matrix cracking, fiber matrix debonding, and fiber pull-out [63, 65-69] by AE technique. The ilustration of Acoustic emission set up for experimental testing and the schematic description of typical acoustic emission signals in waveform that plotted as voltage against time

including mainly three features: energy, counting and amplitude shown by Fig.2.24 below.
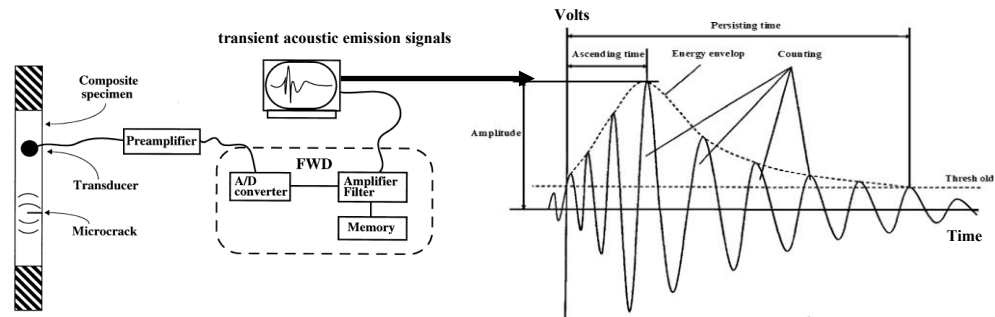
.Figure 2.24 Acoustic Emission Ilustration [69]

According to the different size of acoustic emission sources, the frequency domain of acoustic emission phenomena varies from the infrasonic range to the ultrasonic region and in composite material, the frequency of acoustic emission can detect different type of damage mechanism as concluded by several previous authors shown by Fig.2.25.
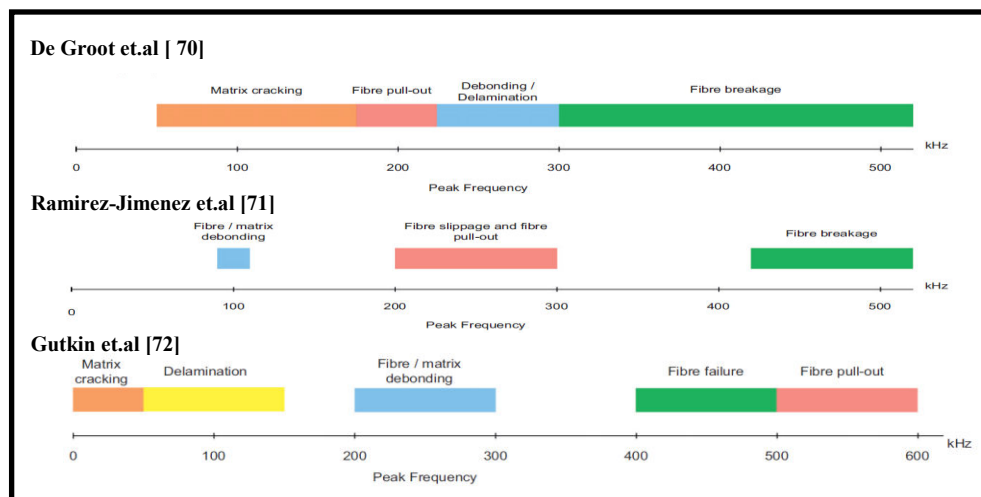
Figure 2.25 Frequency domain of acoustic emission of composite damage

The most popular methods to identify damage mechanism are identification by signal frequency and/or amplitude distribution (signal strength) [73].

Others studies also presented the results of acoustic emission in composite material related to the amplitude distribution of acoustic emission response that shows different type of failure modes. For instance, as concluded by Mechraoui et.al [73] as seen in Fig.2.26.
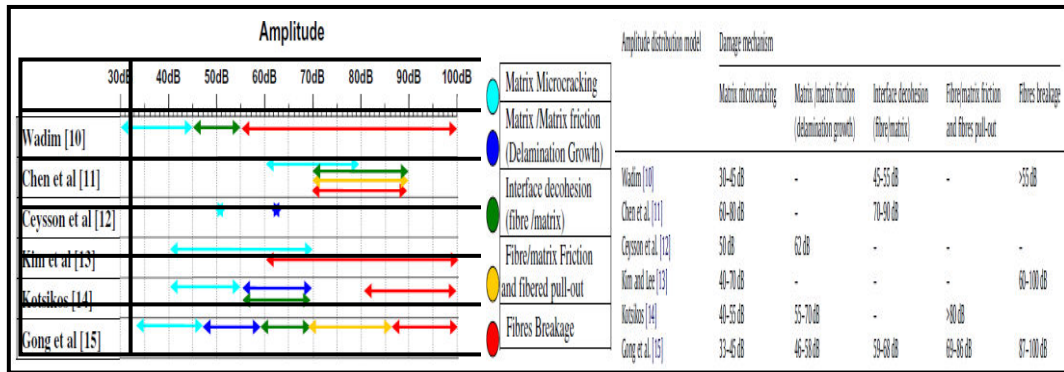
Figure 2.26 Amplitude distribution according to damage in composite [73]

Kharoubi et.al [74] in their study, gave the amplitude and energy response for different type of damage of glass fiber composite (Fig 2.27).

[(0)]$_8$	Fissuration matricielle	Décohésion	Rupture de fibres
	Classe 2	Classe 0	Classe 1
Nombre de coups cumulés	2,0 E+6	1,1 E+6	2,5 E+6
Log Energie (aJ)	1-200	10-5000	600-100 000
Amplitude (dB)	40-90	55-100	75-100

[(0/90)s]$_2$	Fissuration matricielle	Décohésion	Rupture de fibres
	Classe 2	Classe 0	Classe 1
Nombre de coups cumulés	8 E+5	3 E+5	0,6 E+5
Log Energie (aJ)	1-100	2-2500	5000-50 000
Amplitude (dB)	40-90	45-90	> 90

[(0/90)2]$_s$	Fissuration matricielle	Décohésion	Rupture de fibres
	Classe 1	Classe 2	Classe 0
Nombre de coups cumulés	> 6 E+5	1,0 E+5	1,8 E+5
Log Energie	1-900	100-5000	1000-50000
Amplitude (dB)	40-90	65-90	> 90

[(0$_2$/90$_2$)]$_s$	Fissuration matricielle	Décohésion	Rupture de fibres
	Classe 0	Classe 1	Classe 2
Nombre de coups cumulés	1,2 E+6	2,5 E+5	1,7 E+6
Log Energie (aJ)	1-1000	200-2000	1000-50000
Amplitude (dB)	40-90	65-90	80-100

A. AE signal of damage mode under tensile static loading [74]

[(0)]$_8$	Fissuration matricielle	Décohésion	Rupture de fibres
	Classe 2	Classe 1	Classe 0
Nombre de coups cumulés	18,0 E+5	5,0 E+5	17,0 E+5
Log Energie (aJ)	1-1000	100-10 000	1000-70 000
Amplitude (dB)	40-100	60-100	75-100

[(0/90)s]$_2$	Fissuration matricielle	Décohésion	Rupture de fibres
	Classe 2	Classe 1	Classe 0
Nombre de coups cumulés	15,0 E+5	2,5 E+5	5,0 E+5
Log Energie (aJ)	1-2000	50-6000	1000-50 000
Amplitude (dB)	40-100	55-100	80-100

(0/90)2]$_s$	Fissuration matricielle	Décohésion	Rupture de fibres
	Classe 2	Classe 0	Classe 1
Nombre de coups cumulés	9,0 E+5	1,5 E+5	2,2 E+5
Log Energie (aJ)	1-1000	100-2000	1000-50 000
Amplitude (dB)	40-100	55-100	78-100

[(0$_2$/90$_2$)]$_s$	Fissuration matricielle	Décohésion	Rupture de fibres
	Classe 0	Classe 1	Classe 2
Nombre de coups cumulés	34,0 E+5	11,0E+5	27,0 E+5
Log Energie (aJ)	1-1000	90-4000	500-50 000
Amplitude (dB)	40-100	60-100	75-100

B. AE signal of damage mode under tensile cyclic loading [74]

Figure 2.27 AE signal of damage mode under tensile cyclic loading [74]

Li et.al [75] in their study also classify damage in fiber composite based on amplitude distribution of acoustic emission response under tensile static loading for unidirectional glass fiber composite. The results confirmed that acoustic emission successfully detects different type of damage mechanism in composite material by producing different characteristics of acoustic emission signals as seen in Fig.2.28.

	40~60dB	60~80dB	80~90dB	90~95dB
First stage	100%	0%	0%	0%
Second stage	66.7%	32.3%	0%	0%
Third stage	50%	35.7%	0%	14.2%
Percentage of total	64%	28%	0%	8%

a. Amplitude distribution of 90° specimen in each tensile stage

	40-60 dB	60-70 dB	70-80 dB	80-90 dB	90-100 dB
First stage	83.8%	16.2%	0%	0%	0%
Second stage	50.9%	34.2%	14.9%	0%	0%
Third stage	82.3%	13.7%	2.7%	0.63%	0.67%
Forth stage	50%	12.8%	3.2%	1.3%	2.9%
Percentage of total	79.9%	14.7%	3.5%	0.7%	1.2%

b. Amplitude distribution of 0° specimen in each tensile stage

Figure 2.28 Amplitude distribution in tension of glass fiber composite [75]

Recently, study about acoustic emission observation on damage mechanisms of glass fiber composite material is conducted by Toumi et.al [76]. Based on the cumulative acoustic emission event count and cumulative acoustic emission energy, the damage evolution can be detected under static and fatigue loading.

2.6   TOMOGRAPHY ON COMPOSITE MATERIAL

Within last years, the proportion of used fiber composite materials in various areas of industrial production rose steadily. Beside aviation industry also automobile manufacturer realized the advantages of light weight design and identified it as a key feature to vehicle production of tomorrow. Fiber composite materials are characterized by several advantageous properties like high specific stiffness and strength which make them ideal for lightweight applications.

Testing methods which allow complete material characterization and non-destructive troubleshooting with adequate effort are still a field of current research. Due to its ability of exact three-dimensional cross sectional imaging of the entire part, X-ray computed tomography (CT) is the ideal technology for that purpose.

X-ray computed tomography is a radiographic based inspection technique that produces cross-sectional and 3D volumetric images of the linear attenuation coefficient of a scanned object. These attenuation coefficients directly relate to the material densities present within the object under inspection.

Computed tomography is use non-destructively to inspect the inner structure of an object by transmission measurements using X-rays. A large number of projection images are obtained by rotating the sample. After a reconstruction process, the volume rendering of the external and internal geometries of the part is created (Fig.2.29).
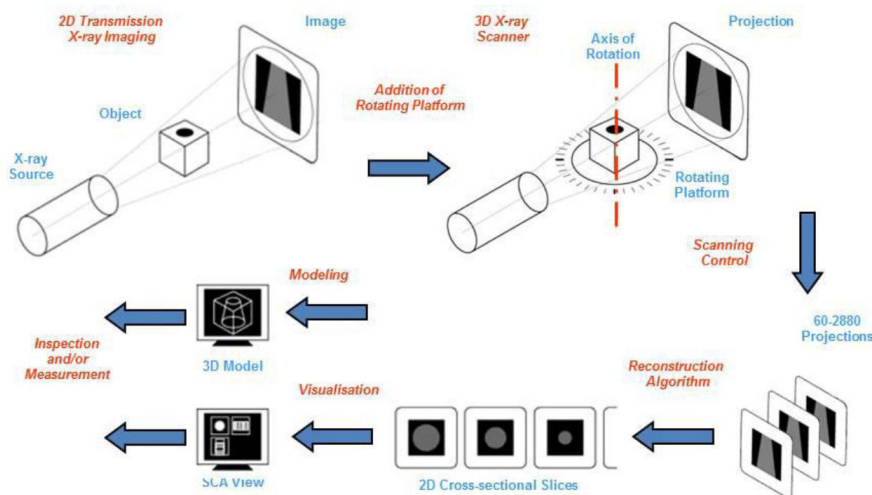
Figure 2.29 Overview of CT scan and measurement process [77]

The main advantage of CT over conventional radiography is that it removes the inherent superimposition; improving the subject contrast and the probability of detection. Furthermore, the many angles of X-ray projections used in the CT reconstruction means that planar defects become detectable due to the increased probability of the X-ray beam being well orientated to them. These beneficial properties have proven to be very effective for inspection of FRP composite materials [78-81]. Similar to radiography, CT is excellent for detecting volumetric

flaws such as porosity, inclusions and thickness changes. Its high penetrating power means it is able to inspect the full thickness of most composite structures and the use of micro-focus sources allows very high spatial resolutions to be achieved; resulting in defect detectability on a micron scale. Unlike radiography, CT is able to reliably detect planar defects such as delaminations and cracks. Plus accurate depth measurements are easily attainable from the cross sectional images.

The CT image values (grey-levels) provide information on the material's X-ray attenuation coefficient at each point in the image which would allow the CT grey levels to be converted to values which are directly proportional to the local material density. For every sensitive pixel of the detector, this intensity is given by the Beer-Lambert law as follows :

$$I = I_o . \exp\left(- \int_L f(x,y)dL \right) \tag{28}$$

$$\ln\left(\frac{I_0}{I}\right) = - \int_L f(x,y)dL \tag{29}$$

where the function $f(x,y)$ represents the value of linear attenuation coefficient of the inspected material,μ, at the point (x,y) all along the X-ray beam as shown in Fig. 2.30 below.
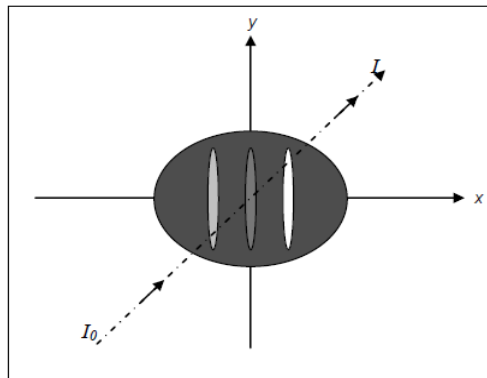
Figure 2.30 An X-ray beam passing through an object with different four linear attenuation coefficients [78]

Due to its ability of exact three-dimensional cross sectional imaging of the entire part, X-ray computed tomography (CT) is the ideal technology for determination and visualization of relevant material properties and

characterization of defects and damage. Figure below show the example of 3D visualization of asphalt concrete sample obtain from a series of gray image slices that stacked together to created a 3D visualization of the specimen (Fig.2.31).
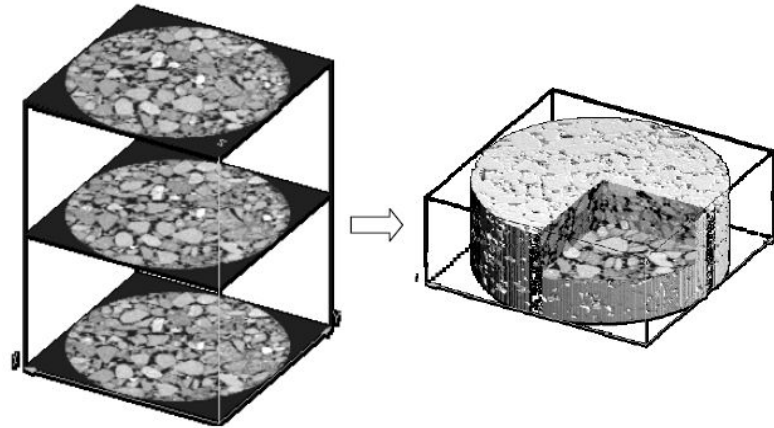
Figure 2.31 3D internal microstructure of a testing sample is reconstructed from series of x-ray tomography images [79].

Table 2.2 below summarises the capabilities of CT scan, when applied to FRP composite structures.

Table 2.2 Summary table for CT scan on FRP composite material [78]

Advantages	Disadvantages	Type of defects
• Very effective for determining nature and size of volumetric defects. • High penetrating power. • No contact or surface preparation required. • Defect detectability in the micron range with contrast sensitivity between 1-2% of the total through thickness. • Cross sectional imaging so superimposition of features is removed and contrast is improved. • Planar defects are detectable.	• Object size is limited to that which fits within the FOV of the detector. • Geometric magnification and thus spatial resolution is also limited by the object fitting within the detector FOV. • Difficult to obtain sufficient contrast between the fibers and epoxy resin due to the similarities in density.	As with radiography, CT inspection is very good for volumetric flaws, such as voids, inclusions and thickness changes. It also has increased probability of detection (compared to radiography) for planar type defects such as delaminations and cracks. CT is also capable of detecting BVID, fiber breakage and fiber/ply orientation.

Wright et al [80] investigated notch tip damage of carbon fiber-epxy composites under uniaxial tension using Computed tomography. Fig.2.32 below shows the typical reconstruction of 3D tomography image for split and transverse

ply crack of carbon fiber composite under 40% of ultimate tension failure stress. these first damage mechanisms can initiate and interact in a complex manner which can cause the laminate damage.
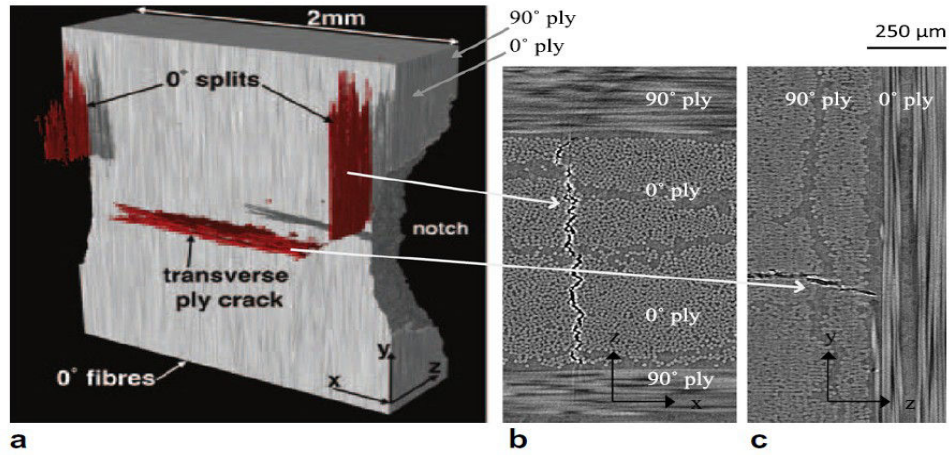
Figure 2.32 Tomography 3D visualization of damage on composite material [80]

Other defect of porosity on carbon fiber-reinforced composite material also observed by Kastner et al [81] using computed tomography. this study deals with the application of CT scan to characterize the size, shape and position of all indivudual pores. Fig.2.33 below shows several images of porosity inside the material.
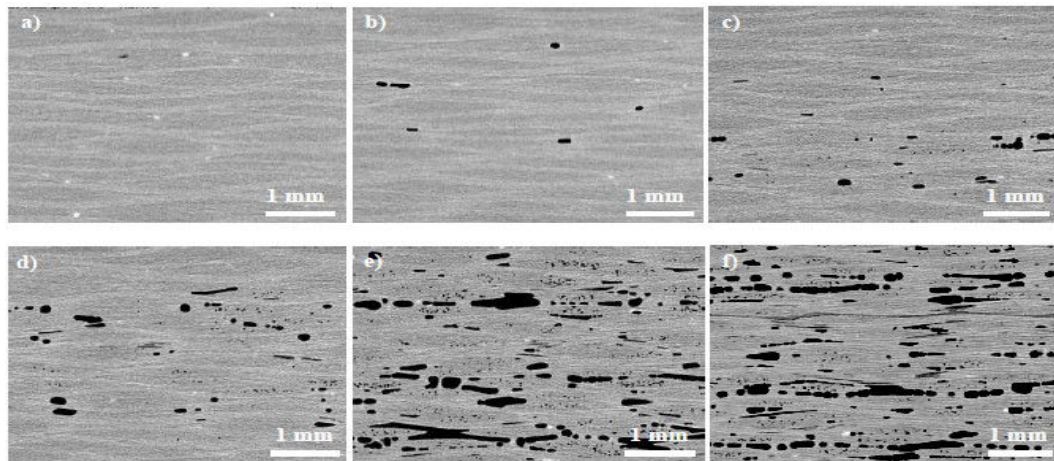
Figure 2.33 CT images of typical carbon reinforced composite [81]
(a: ~0 vol- %, b: ~0,15%, c: ~0.35 %, d: ~0.9 %, e: ~4.50 %, f: ~10 %)

The influence of the resolution/voxel size, on the obtained porosity also investigated. By improving the voxel size, it can be seen that the voxel size has an influence on the porosity content (Fig.2.34).
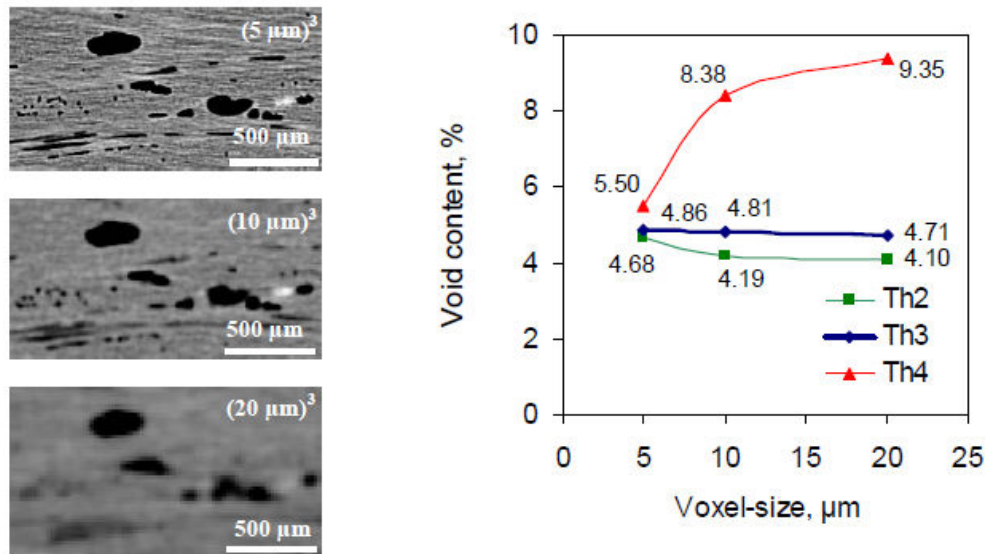
Figure 2.34 CT images of a sample measured with different voxel sizes   [81]

Damage evolution under fatigue for short glass fiber composite material was studied by Cosmi and Bernasconi [82]. The damage evolution is analyzed by means of computed tomography. By identify different segmentation threshold value for fiber phrase and microvoid phrase, tomography can informs about fiber and micro-void distributions based on grey value (Fig.2.35).
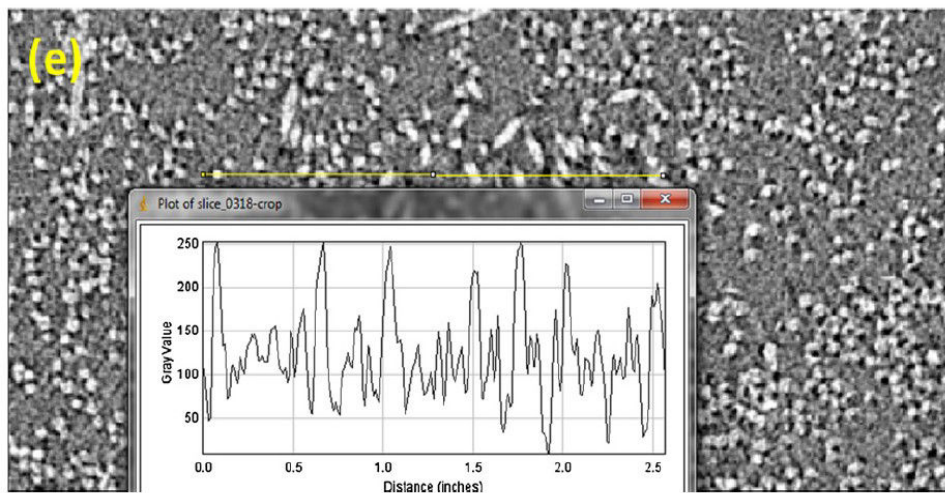
Figure 2.35 Grey value along the yellow line parameter with fibers are shown white and voids black [82]

Under different condition of fatigue loading, by observing the micro-voids percentage as damage evaluation, it is possible to have a relation curve between micro-voids and fatigue life (Fig.2.36).
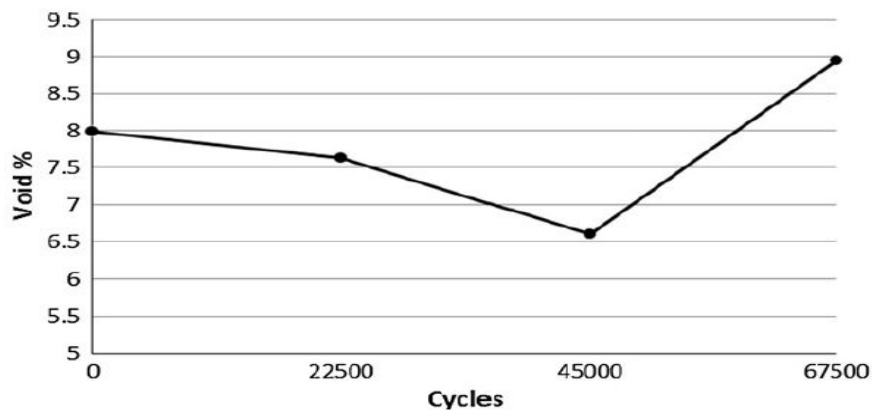
Figure 2.36 Micro-voids percentage in the entire samples as a function of the
fatigue life (number of cycles) [82].

Recently study about tomography observation on damage evolution of fiber composite material is conducted by Goedescu et al [83]. Carbon-epoxy laminates with lay-up $[0/90]_6$ (axis loading) and $[\pm45]_6$ (off-axis loading) are using as the specimen test under tensile monotonic tests for this study. With tomography, defects are observable through the contrast of grey levels. Fig.2.37 presents the results of tomography slice images (0.1 mm thickness) for both type of specimen on development of damage/voids within the laminate thickness at the middle depth of specimen.

(a) type A   (b) type B
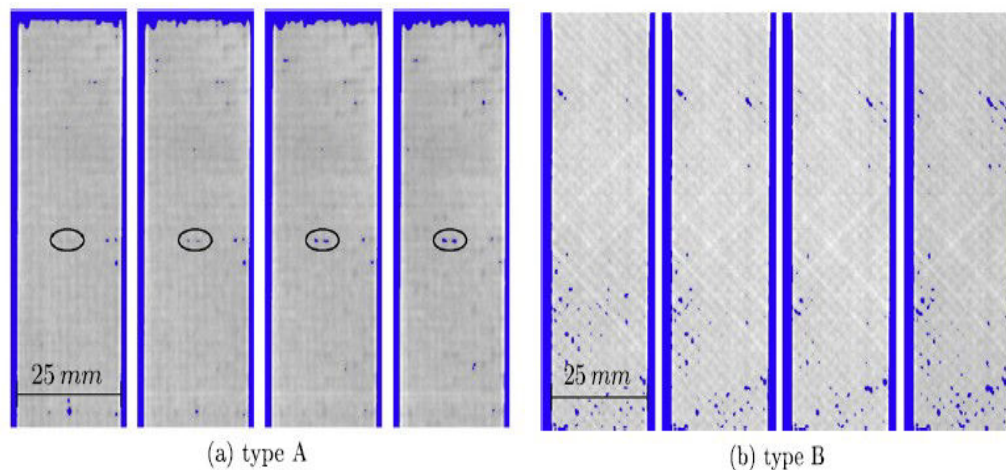
Figure 2.37 2D images of tomography result (material is depicted in grey and
void is depicted in blue) [83]

2.7   DISCONTINUOUS CARBON FIBER COMPOSITE (DCFC)

Recent composite technology research and development efforts have focused on new low-cost material product forms, and automated processes that can markedly increase production efficiencies [3]. Discontinuous Carbon Fiber Composite (DCFC) is a fully automated preforming solution that uses fibers in the raw and most inexpensive form (DCFC raw material costs are estimated to be only 16% of carbon prepreg, based on €14.00/kg for STS carbon fiber and €2.11/kg for epoxy) and shown to be cost effective between 400 and 10,000 parts per annum, when compared to a commercial semi-preg body panel system and steel respectively [3,84].The commercial application of this material form already exist, for example the window frames of the Boeing 787 Dreamliner as seen in Fig.2.38 below.

Figure 2.38 DFC product for windows frame of Boeing 787

DFC product forms such as sheet molding compound (SMC) or bulk molding compound (BMC) have long been used in industrial and automotive applications such as body panels [85]. The main advantages of this type of material is have a good suitability to be molded in complex geometries with lower manufacturing costs and at higher rates that justify their adoption to reduce overall part acquisition costs [85].

However, to use this material for other structural application such as joining parts in automotive or aircraft industry that containing holes, it should be have a good understanding about the hole-insensitivity behaviour of this material. DFC behave structurally is different compared to Continuous Fiber Composites (CFC) especially in hole/defect behaviour and its damage behaviour. For discontinuous carbon fiber composite, failure is a matrix-dominated event, which occurs by transverse chip cracking, longitudinal chip splitting, and chip disbonding, with

little fiber breakage [86]. Several studies also already performed on discontinuous carbon fiber composite to understand its mechanical behaviour under static loading.

Boursier and Lopez [85] investigated the failure initiation and effect of defects on structural discontinuous carbon fiber composite. It was found that DFC is relatively insensitive to holes compared to the CFC and the first crack of DFC do not indicate the final failure location. Fig.2.39 below shows the experiment results that indicate the behaviour of DFC material.
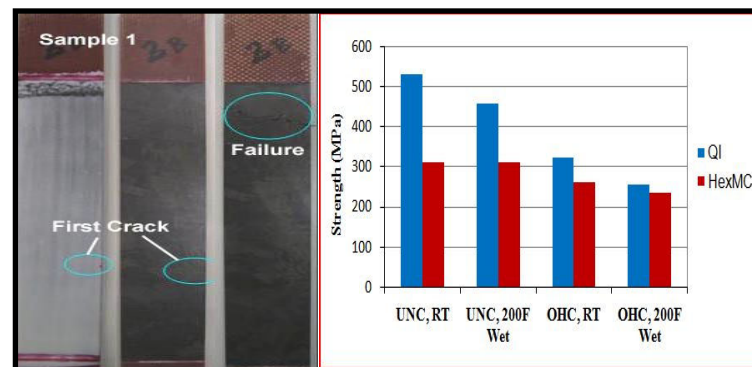
Figure 2.39 Failure and insensitive of DCFC [85]

Harper [3] studied about the effect of several microstructural parameter that effect the mechanical properties of the discontinuous carbon fiber composite. The results shows that fillament count, fiber length and areal density have an effect on its UTS (see table 2.3). From these parameters, laminate thickness that according to the global areal density is the most significant variable that affect the stiffness and the strength of DFC material. It is therefore essential that the DFC process is capable of producing thin (<3mm) laminates with a consistent areal density. Stiffness was reduced by 7.5% and strength by 18.8% when the areal density was reduced from $2.25kg/m^2$ to $0.75kg/m^2$ as a consequence of poor fiber coverage leading to unreinforced areas.

The several studies about mechanical behaviour of discontinuous carbon fiber composite were also performed by Ferabolli et.al. [86-88; 90-92]. In their research about the characterization of DFC for Aerospace application, the results of tensile test shown that the failure of DFC is the combination of two failure modes : cracking caused separation along the surface that perpendicular to the chip axis and delamination caused separation along the thickness that parallel to

the chip length. The comparison between flexural strength, compressive and tensile strength indicating the different behaviour from continuous fiber laminates. Flexural strength of DFC is the highest, followed by compressive , and then tensile strength which continuous quasi-istropic always have the lowest compressive strenth, and tensile and flexural strength are usually closer together. These static strength of DFC highly influenced by fiber/chip length. Fig.2.40 below shows the result of different static strength of DFC as function of chip length.

Table 2.3 The effect of microstructural on tensile modulus of DFC [3]

Tow size (K)	Fibre length (mm)	Areal density (kg/m²)	Volume fraction (%)	Modulus (GPa)	COV (%)	Rel. Error (%)	UTS (MPa)	COV (%)	Rel. Error (%)
6	25	0.75	27.6	22.2	10.8	6.8	164.5	13.4	8.5
6	25	1.5	27.6	21.5	12.2	7.7	182.1	11.9	7.5
6	25	2.25	31.1	25.9	7.3	4.6	207.0	10.2	6.5
6	50	0.75	27.6	21.7	11.7	7.4	155.1	11.8	7.5
6	50	1.5	27.6	22.2	13.1	8.3	169.2	11.2	7.1
6	50	2.25	31.1	24.5	13.4	8.5	221.0	8.9	5.6
6	75	0.75	27.6	20.0	16.3	10.3	130.1	25.8	16.3
6	75	1.5	27.6	21.1	21.0	13.3	161.2	18.6	11.8
6	75	2.25	31.1	24.9	13.4	8.5	189.7	14.2	9.0
12	25	0.75	27.6	22.0	6.8	4.3	176.8	1.8	1.1
12	25	1.5	27.6	23.2	10.6	6.7	203.0	9.3	5.9
12	25	2.25	31.1	25.5	15.5	9.8	208.0	14.3	9.0
12	50	0.75	27.6	21.1	12.8	8.1	158.3	19.1	12.1
12	50	1.5	27.6	24.6	14.4	9.1	189.9	16.8	10.6
12	50	2.25	31.1	26.8	12.6	8.0	215.5	15.4	9.7
12	75	0.75	27.6	20.0	11.0	7.0	130.7	24.7	15.6
12	75	1.5	27.6	22.2	25.8	16.3	181.9	20.2	12.8
12	75	2.25	31.1	24.5	9.8	6.2	206.6	16.5	10.4
24	25	0.75	27.6	23.3	13.2	8.3	141.0	26.2	16.6
24	25	1.5	27.6	24.3	12.1	7.7	214.2	12.4	7.8
24	25	2.25	31.1	23.3	11.8	7.5	174.7	26.2	16.6
24	50	0.75	27.6	19.2	16.0	10.1	145.1	22.5	14.2
24	50	1.5	27.6	21.6	10.0	6.3	183.7	11.5	7.3
24	50	2.25	31.1	26.3	11.7	7.4	214.3	15.0	5.9
24	75	0.75	27.6	20.8	14.7	9.3	79.3	24.1	15.2
24	75	1.5	27.6	20.5	16.3	10.3	150.9	18.5	11.7
24	75	2.25	31.1	24.5	12.7	8.0	184.3	17.7	11.2
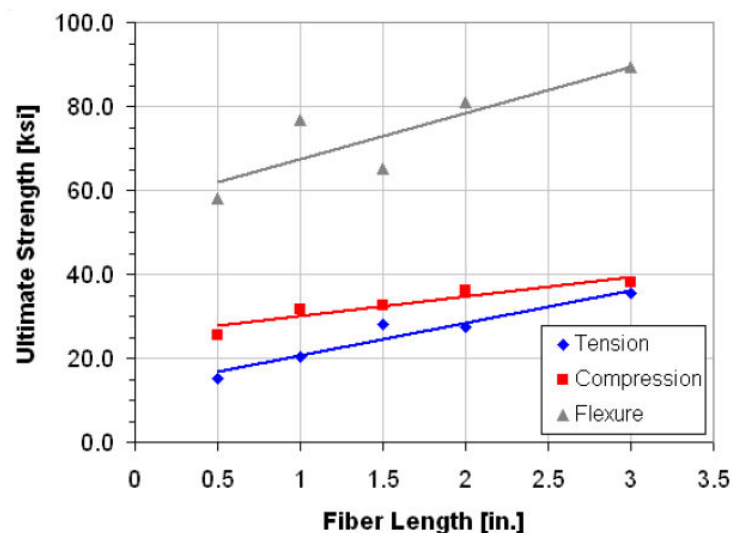
Figure 2.40 UTS of DFC for different static condition [86]

The effect of specimen condition (with and without hole) on elastic tensile behaviour and failure response for this DFC material also investigated by Feraboli et.al [87]. For Unnotched specimen, under tensile loading, the specimen fails in a combination of chip disbonding (matrix shearing between the chips) and fiber failure as shown in Fig.2.41.
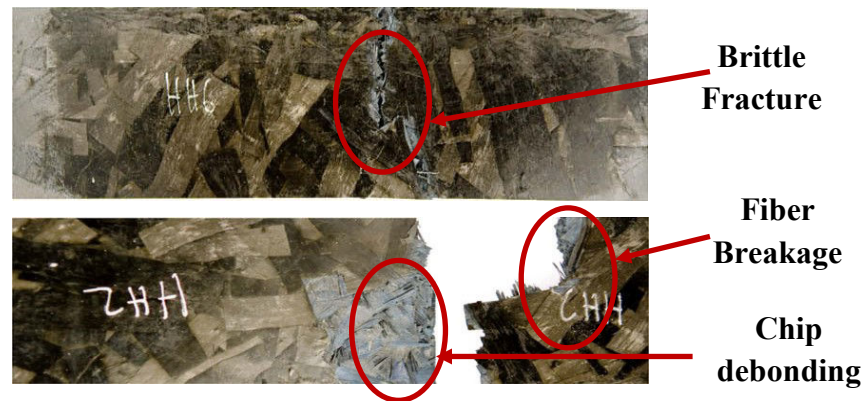
Figure 2.41 Failure of DCFC [87]

For an open hole specimen of DCFC, under tensile loading, the failure behaviour shows different failure behaviour compared to the composite material in general. The specimen shows insensitive behaviour due to an open hole condition. The failure of specimen occured in gross area of the surface for certain test with a small hole specimen (Fig.2.42a). The results also confirm that the strength of this DCFC does not decrease with the presence of the hole (Fig.2.42b).
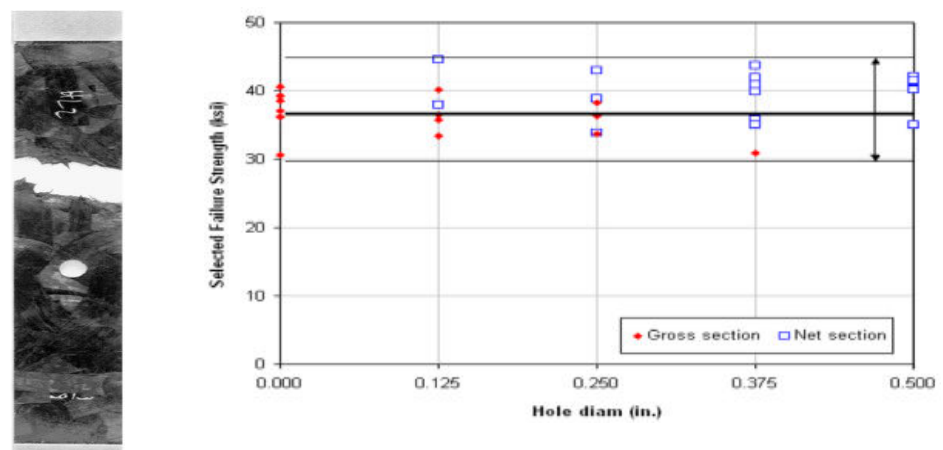
a. Failure in gross section   b. Variation of notch strength with hole diameter

Figure 2.42 Failure of DCFC in gross section [87]

This uncommon behaviour of DCFC possibly due to the internal stress concentration arising from the heterogeneous nature of meso-structure [87,93]. Inspection of this damage behaviour also presented by Feraboli et.al [88] using ultrasonic c-scan, Bale et.al using thermography [89] and Bond et.al [93] with digital image correlation (DIC). The observation results shows that, the specimen fail away from the hole by the presence of 'delta-T spots' by Ultrasonic C-scan and DIC shows that gross section ('A') experiences greater strain than the region that surrounds the hole as seen in Fig.2.43 below.
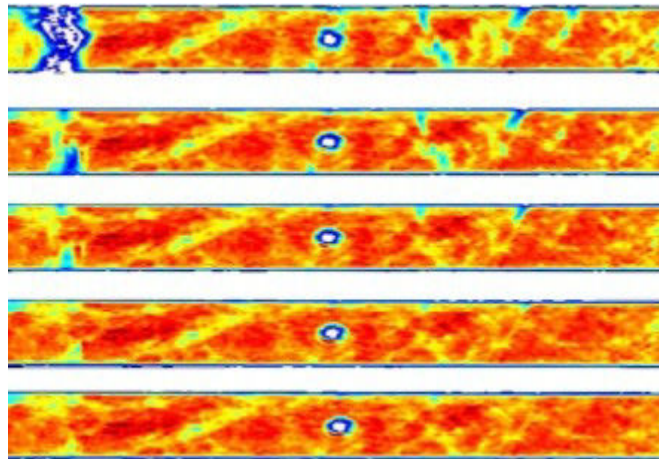
Ultrasonic C-Scan Observation [88]
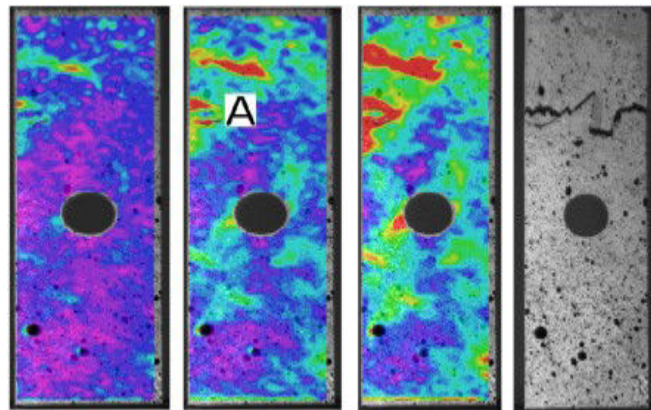
DIC observation [93]

Figure 2.43 Damage observation of DCFC

From several previous studies, results on prepreg-based discontinuous carbon fiber/epoxy composites show that the macroscopic response is virtually notch-insensitive, possibly due to the internal stress concentration arising from the heterogeneous nature of the meso-structure [87,94].

Chapter III.   EXPERIMENTAL METHODS

3.1   INTRODUCTION

This chapter describes the detail of materials used and experimental prosedure of the mechanical testing under tensile (static and fatigue) loading and also NDT observation of thermography supported by acoustic emission and post failure observation of computed tomography (CT) scan. All the important of expected results from mechanical testing and NDT observation also describe. At the end of this chapter, the flowchart of this experimental procedure is given.

3.2   MATERIAL

The material used for the study are unidirectional glass fiber composite (GFRP) and discontinuous carbon fiber composite (DCFC).

3.2.1 Unidirectional glass fiber composite (GFRP)

The GFRP specimen that used in this study was produced by resin transfer molding (RTM). In order to facilitate the wetting of fibers, epoxy resin is selected. The composite laminate consisted of 10 layers of unidirectional glass fiber (0.24 thickness of layer) that contains 60% of nominal fiber volume throughout the thickness as the reinforcement and epoxy resin was employed as the matrix. The orientation of fiber is 97% parallel and 3% perpendicular againts each other.

The specimens are rectangular specimen with dimensions 200 mm x 25 mm x 4 mm and bonded with glass/epoxy tabs of 50 mm to prevent the premature failure in the grip area and ensure that the specimen will clamped well into the machine during the tests. There are two types of GFRP specimen that use in this study, i.e :
1.   Rectangular specimen without hole
2.   Rectangular specimen with 5 mm of hole diameter in the center.

Fig.3.1 below shows the dimension and the size of the GFRP specimen.

Dimension : Lo : 200 mm;   T : 4 mm ;   L : 100 mm   W : 25 mm
             t : 2 mm;   d : 100 mm; L_1 : 50 mm   D : 5 mm
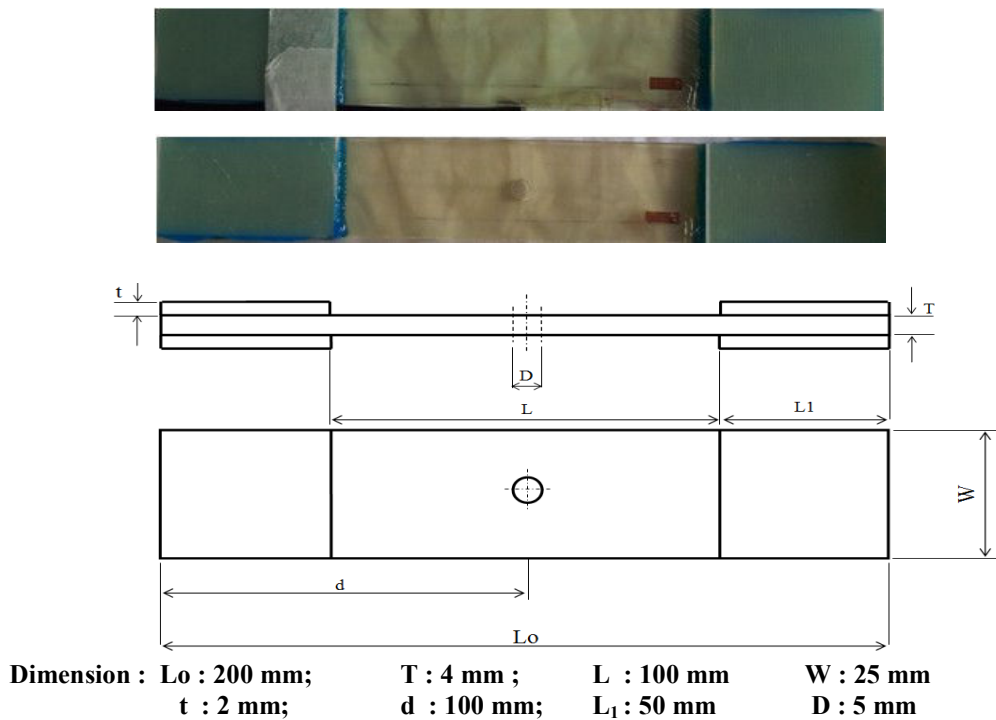
Figure 3.1 GFRP specimen

3.2.2 Discontinuous carbon fiber composite (DCFC)

This composite specimen is discontinuous (chip form) carbon fiber as the reinforcement and epoxy was employed as the matrix. The chip dimensions on which this study focuses is 50 mm in long and 8 mm in wide that gives a good compromise between mechanical performance and manufacturing ability [87]. The random stack of chips is then press molded in an aluminum tool for 1 hour at 120° C) under 80 bar (MPa) of pressure and has a fiber content of 57 % by volume. Material density is 1.55 g/m^3.

The raw laminate then cut into rectangular shape. There are two types of DCFC specimen that use in this study, i.e :

1. Rectangular specimen without hole
2. Rectangular specimen with hole (5 mm and 10 mm of hole diameter).

All of three specimens have the same rectangular dimension of 200 mm x 25 mm x 4 mm. Glass/epoxy tabs of 50 mm each are bonded to the specimen at the end length side to prevent the premature failure in the grip area and ensure that the specimen will clamped well into the machine during the tests. The tabs are

bonding using Redux 609 scotch weld film by cured at 130° C for 30 minutes to obtain optimum properties. Fig.3.2 shows the specimen of DCFC.

prepeg chips in random distribution   raw laminate

Dimension : Lo : 200 mm   T : 4 mm   L : 100 mm   W : 25 mm
t : 2 mm   d : 100 mm   L$_1$: 50 mm   D : 10 mm
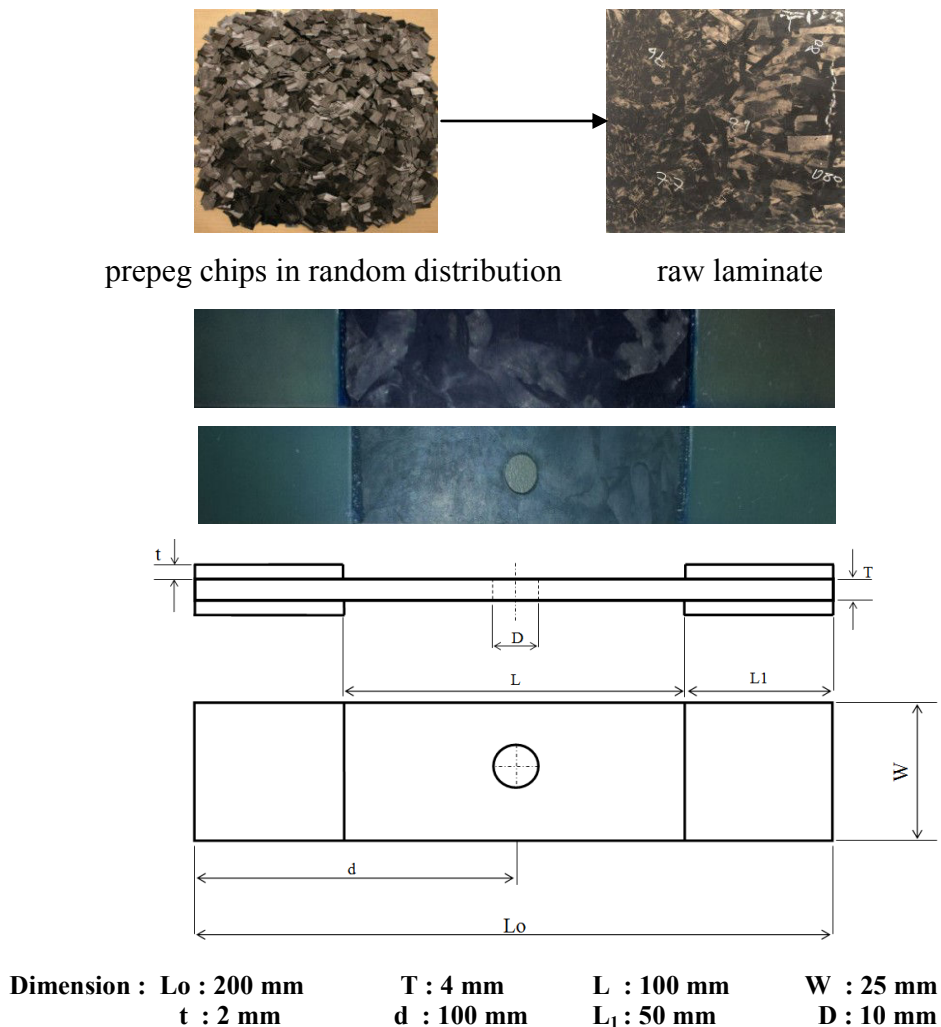
Figure 3.2 DCFC specimen

Since all specimens are fully given material that supplied by PSA Peugeot Citroen Company, Post analysis of surface roughness from machining process on drilling of hole specimen was also conducted. This test was conducted in order to measure the surface of the hole and its effect in creating local stress concentration due to fabrication process [Appendix A.2]. General information of machining parameters on the drilling of fiber-reinforced composites that influencing surface roughness is reffered from previous study [Appendix A.3]

3.3   Experimental

This research aimed at investigating the problem through the following steps: Mechanical testing, Monitoring of the evolution of damage under static/fatigue and loading conditions by thermography supported by acoustic emission and observed the post failure analysis with computed tomography (CT) scan. The tests were monitored and conducted at room temperature. The experiments and the observation will stopped when the composite specimens failed. Note that only no more than 3 specimens were used for each stage in this experimental test.

This experimental divides into seven stages :

1.   Preparation test to ensure the test in a good condition [Appendix A.1]

2.   Tensile static testing on GFRP with and without circular notches (hole) and observed with IR camera and supported by acoustic emission

3.   Tensile static testing on DCFC specimens with and without circular notches (hole) and observed with IR camera

4.   Tensile fatigue testing on GFRP specimens with circular notches (hole) and observed with IR camera

5.   Tensile fatigue testing on DCFC specimens with circular notches (hole) and observed with IR camera

6.   Rapid tensile fatigue testing on GFRP and DCFC specimen with an open hole and observed with IR camera

7.   Tomography observation on GFRP and DCFC specimens with circular notches (hole) resulted from fatigue tensile testing

3.3.1 Tensile (static and fatigue) testing

Test was carried out with a servo-hydraulic testing machine of INSTRON Machine 8501 with a capacity of 100 kN. The machine was equipped with a standar load cell and hydraulic grips. The global longitudinal strain of the specimen was measured based on crosshead displacement and local longitudinal strain were measured using an electric uni-axial strain gauge with a gauge length of 5 mm where attached on specific position of specimen surface. Fig.3.3 below

shows the experiment condition. All tests were done following the ASTM D 5766 standard test method.
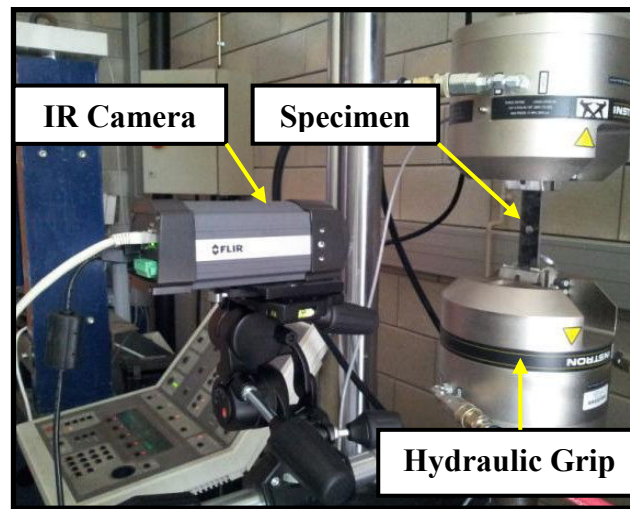
Figure 3.3 INSTRON Machine and IR camera

Either static or fatigue, specimens were aligned and mounted first in the lower and afterwards in the upper grips of the test station. Previously, strain gauge already installed on the surface of the specimen. After mounting the specimens, any loading due to the gripping was minimized through Instron controller panel. A unit of computer with an external data acquisition (Labview software) was used to record all the test results such as load, strain and displacement. During the recording, all the data stored in a computer hard disk. Then, the tests was considered to begin. Static tensile tests were performed under a constant cross-head speed of 1 mm/min. Fatigue tests were performed under load control, at a stress ratio, R, equal to 0.1, i.e., tension tension loading and constant 3 Hz of frequency (ASTM D3479). Various maximum stresses were used for the fatigue tests. The test specimens were allowed to cycle until failure occurred or until a predetermined number of cycles was reached. Moreover, rapid test of fatigue loading with same parameter also conducted to determine the high cycle fatigue strength and fatigue life utilizing IR camera that referred to the Risitano's method. This rapid fatigue test was used one specimen for each test of maximum stress until certain cycle of 10000 cycles. Once this 10000 cycles are reached, the test was stopped, then continue with the next maximum stress.

3.3.2 NDT Thermography

For follow the temperature changes on the specimen surface, an infra-red camera of FLIR A325sc was used for the tests. Control of the camera and data recording are done with the FLIR R&D software. The FLIR R&D software is able to measure temperature change in various shape and dimensions such as spots, lines, and area as well as of using several various palette of colours and shades. The camera resolution is 320 x 240 pixels with detector type of uncooled microbolometer. Camera spectral range is 7.5 to 13 μm, whereas the temperature range is from -20°C to +120°C with accuracy $\pm$ 2°C or $\pm$ 2% of reading. The camera is provided with the automatic correction of emissivity and atmospheric transmission based on distance, atmospheric and relative humidity. IR camera was placed approximately 30 cm of fix distance in front of the specimen surface; therefore, it was possible to obtain full-field thermal maps of the specimens during the tests. This thermography observation did not use an externally applied heat source. In this case, the thermal images acquisition were set at 30 Hz.

3.3.3 NDT Acoustic Emission

During the tensile tests, Acoustic emission was continuously monitored by using a Mistras monitoring system. AE measurements were achieved by using two transducers which coupled on the surface of the samples with silicon grease. The transducers were held in place with a clamp mechanical device. The amplitude distribution covers the range 0–100 dB. The nominal distance between the sensors was around 60 mm. After the installation of the transducers, a pencil lead break procedure was used to simulate AE signals in the calibration of each test. Furthermore each waveform was digitized and stored. After storage and before processing the signals were subjected to a linear location procedure to determine the location of AE signal source. In the analysis of AE results, only events located between the sensors were used. The acoustic emission analysis is performed by the NOESIS software in particular to have the parameter value of energy and amplitude associated with damage appearance. The illustration of the experimental condition using acoustic emission system as seen in Fig.3.4 below.
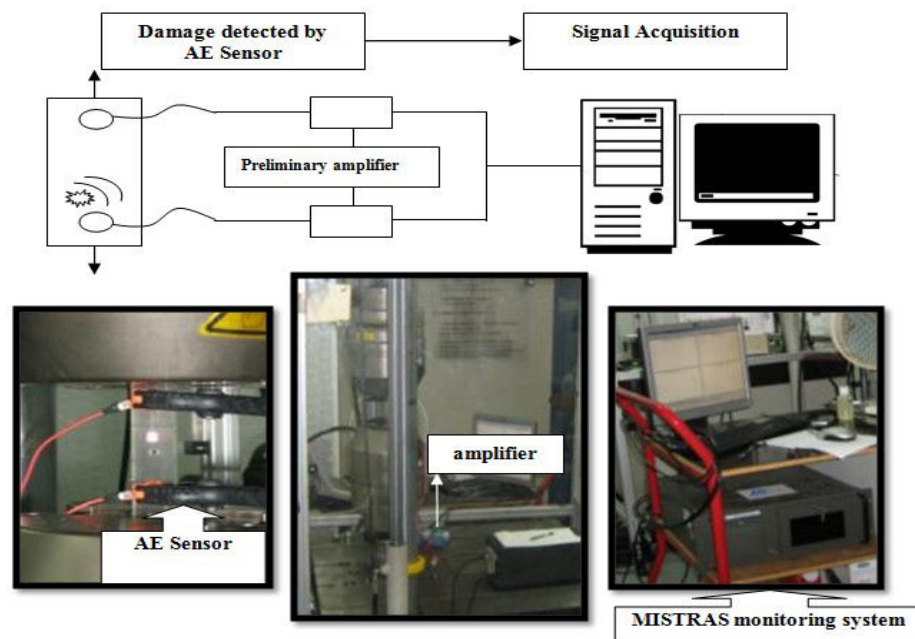
Figure 3.4 Acoustic Emission set up

3.3.4 NDT Tomography

After certain cycles of tensile fatigue loading, the tests were stopped and observed the specimen under CT-Scan. This observation using two condition, i.e :

1. GFRP 0° specimen under tensile fatigue condition with σ_{max} : 150 MPa until 500 cycles without macro damage.

2. GFRP 0° specimen under tensile fatigue condition with σ_{max} : 150 MPa until 1500 cycles without macro damage.

3. DCFC specimen under tensile fatigue condition with σ_{max} : 250 MPa until 3100 cycles without macro damage.

4. DCFC specimen under tensile fatigue condition with σ_{max} : 250 MPa until 200 cycles without macro damage.

The specimen for each condition mounted facing each other. CT-scan machine is connected to a computer using a software for visualization the rotating observation and also a software of image post processing to have images sequences during the test. The turn table will rotating 360° for around 1 hour. All images of CT-scan then analyze based on image pixel and grey value using Image-J software. Fig.3.5 shows the CT-scan machine and the experimental description.
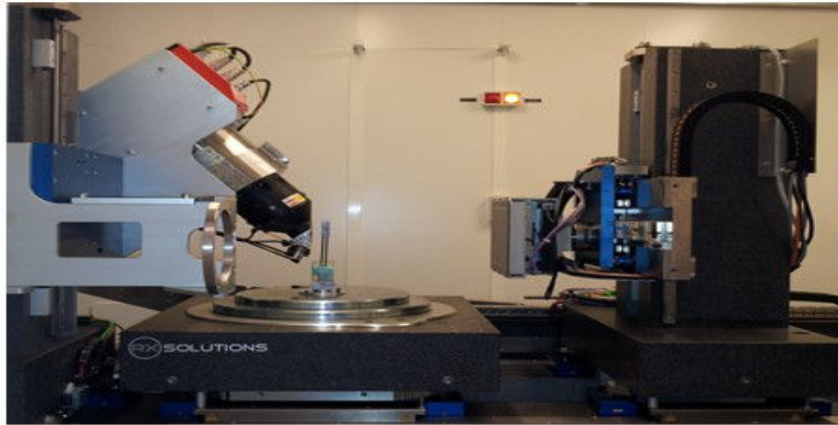
Parameter	Value
Current	199 µA
Voltage	80 KV
Resolution	17 µm
Number of slices	1121 Images
Time	1 hour (0.1° / s of rotation)
Power	14 W

Figure 3.5 CT-scan machine

3.4 Analysis

The test data shall be assessed on the basis only of test specimens undergoing failure in the test portion and specimens taking the prescribed number of repetitions. In cases where tensile failure or slippage has clearly taken place at the anchorage portion, the data shall be disregarded and additional specimens shall be tested until the number of test specimens failing in the test portion exceeds the prescribed number. An analysis will undertaken to evaluate the damage behaviour that occured during static and fatigue test and how damage accumulated throughout the specimens. For the static tensile test, the UTS for each type of specimen will obtained using the same displacement rate of the test. For the fatigue test, the S-N curves will obtained for each load level of UTS. Damage evolutions during test observed using thermography camera and also acoustic emission (AE), then tomography to confirm the observation results as a post failure analysis. The temperature behaviour according to the thermal detects and sound detects by AE will obtained during the test. Microscopic study of specimens will obtained to study the damage type for each test. All the results will discussed to have a good understanding and correlation of mechanical behaviour and damage observation of fiber composite material by NDT method.

Some expected results are :

1. Mechanical testing of tensile (static and fatigue) loading :

    - Tensile Curve.

    Tensile curve shows the relationship between the load and the cross head displacement. The Stress-strain curve also can be obtained fom tensile tests by dividing the measured load by average cross section of the specimens and the cross-head displacement by nominal gage length of the specimens. Elastic Modulus, E will determined by linear interpolation of the stress-strain curves. The same curve also can be obtained using the local strain results from strain gages

    - S-N Curve.

    The S-N curve shows the relationship between the maximum repeated stress, the stress range or the stress amplitude and the number of repetitions. When some test results come at the same point in the S-N diagram, the number of data shall be noted. Right-facing arrows shall be used to indicate that the test specimen did not fracture at that number of repetitions

    - E/E_o - n/N_f curve.

    The E/E_o - n/N_f curve shows the stiffness degradation during the test until failure. This curve is used to create damage evolution curve during the fatigue test (D - n/N_f curve)

    - E_d - load level curve

    The E_d - load level curve shows the energy dissipation for a cycle in stabilization periode for each maximum stress of rapid fatigue test. This curve is created to determine the high cycle fatigue strength (HCFS) based on tensile fatigue test

2. NDT thermography observation :

    - ΔT - Time curve.

    This curve shows the variation of temperature profile on obervation area of specimen surface during the tensile static test until catastrophic failure or rupture. This temperature variation is resulted by $\Delta T = T - T_o$, swith T is the temperature surface at t time and T_o the initial temperature surface at $t = 0$. This curve also compared with strain result from tensile static test results to

having a comparison of damage appearance that detected by strain gage and an IR camera.

- ΔT - n/N_f Curve.

This curve shows the increasing of temperature on several point at specimen surface during the test. This curve then used to compared with damage evolution (D - n/N_f curve) of particular maximum stress from tensile fatigue testing. Both curve of D - n/N_f curve and ΔT - n/N_f Curve are compared to have a correlation between the increase of temperature and the evolution of the damage in this material.

- *ΔT* - load level Curve

The *ΔT* - load level curve shows the temperature profile in stabilization period for each level of maximum stress during rapid fatigue test. This curve is created to determine the high cycle of fatigue strength (HCFS) based on thermography observation. Each value of HCFS from mechanical testing and NDT thermography observation are used to create Ed - *ΔT* curve. This Ed - *ΔT* curve is created to have a relation between dissipated heat measured by IR camera and the intrinsic energy dissipation of the material produced by tensile fatigue test.

3. NDT Acoustic Emission (AE) observation :

- Amplitude - Energy curve.

This curve shows the value of the amplitude and the energy of AE signal corresponds with the appearance of damage in composite material that can be used to categorize typical damage mechanism based on both value. These results are compared with themography observation and damage appearance from mechanical testing to have a good description of damage mechanisms.

4. Post failure analysis of NDT tomography observation :

- Gray value - pixel curve.

The Gray value - pixel curve shows the different gray level and the number of pixel related to damage and inner structure of the material after particular cycle of tensile fatigue test. These results are compared with the slice image of observation area to have a good description of damage appearance and each constituent of GFRP and DCFC material.

3.5 Experimental Flowchart

As a closure to this chapter, the flowchart of this experimental method shown in Fig.3.6.
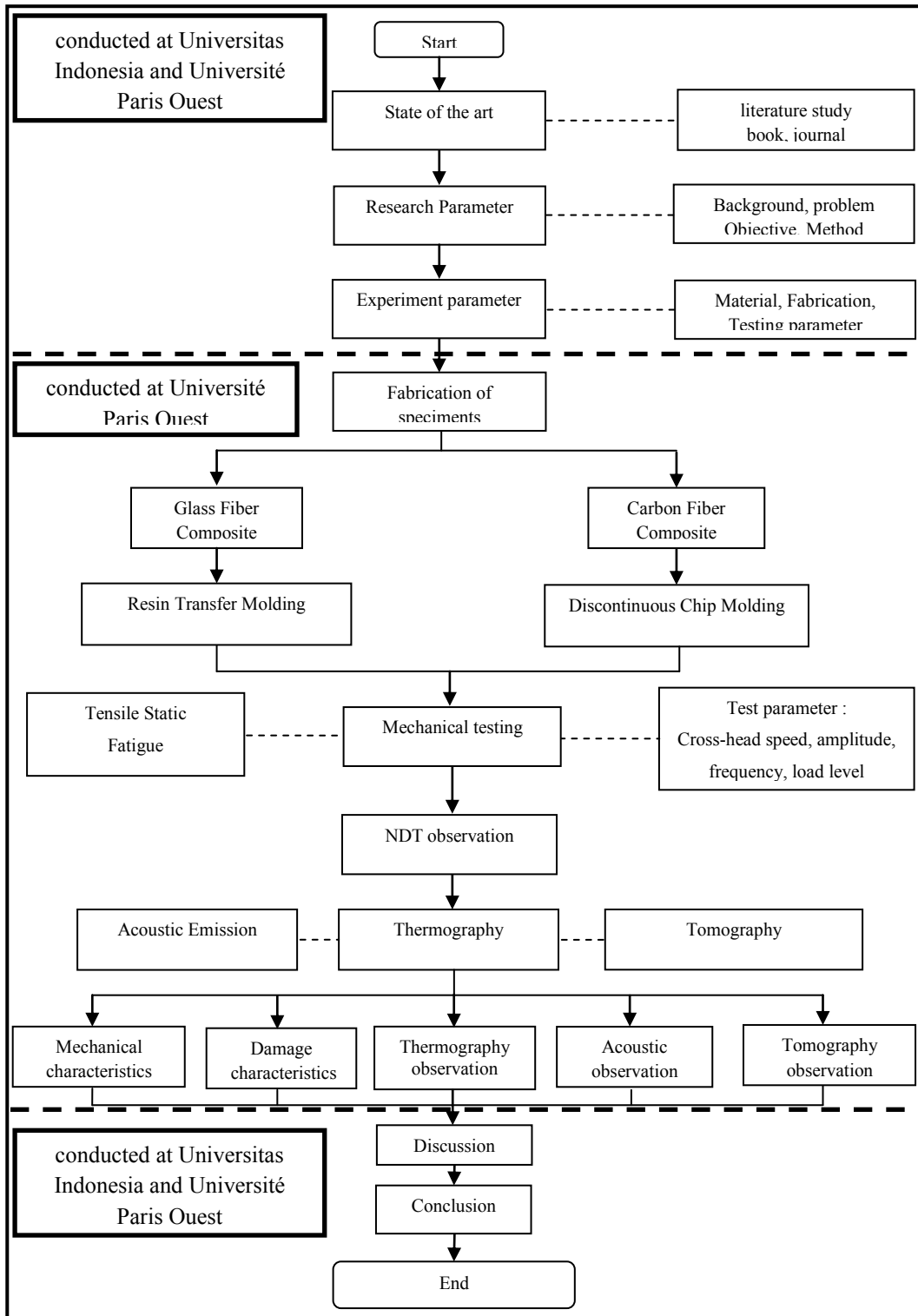
Figure 3.6 Flowchart of research method

Chapter IV. TENSILE (STATIC AND FATIGUE) TESTING AND DAMAGE OBSERVATION OF UNIDIRECTIONAL GLASS FIBER COMPOSITE (GFRP) BY THERMOGRAPHY

4.1 Tensile static testing and damage observation of GFRP by thermography

The experimental results of tensile static testing and the damage observation analysis by thermography will now presented. All the results will be outlined and discussed for both type of specimen (GFRP 90° and GFRP 0°). Detailed discussions of the relevant experimental results will be presented within each corresponding section.

4.1.1 Tensile static testing of GFRP 90° specimen without hole and damage observation by thermography

The tensile test on GFRP 90° specimen was conducted until failure with the aim to have the strain propagation, ultimate tensile strength (UTS), elastic modulus and damage behaviour of the specimen. In order to follow the damage mechanism, single strain gage installed on the specimen surface to give the information about strain evolution and also IR camera is used to assess the temperature evolution during the test. Fig.4.1 shows the stress-strain curve of GFRP 90° without hole under tensile static testing .
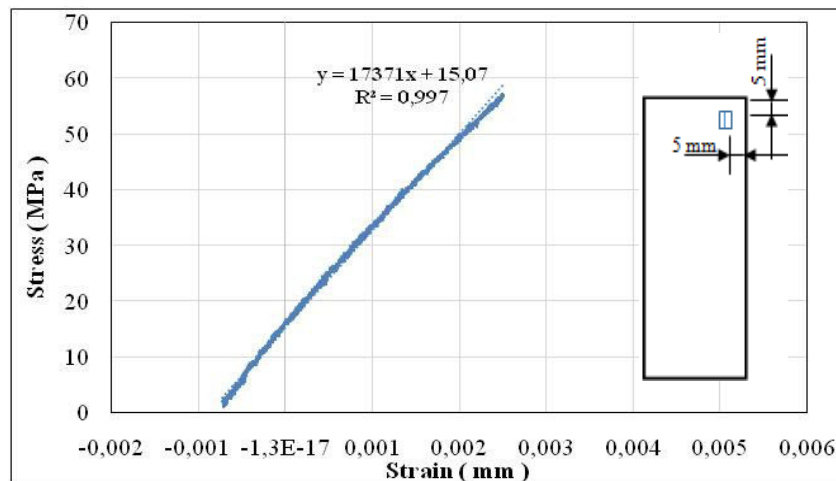
Figure 4.1 Stress-strain curve of GFRP 90° without hole

In Fig.4.1, the curve indicates the stress versus strain curve obtained from tensile test which stress is resulting from given load and strain derived from strain

gage. The stress - strain curve represents linear relationship that clearly indicates the typical brittle behaviour with the sudden failure of composite material under static tensile loading. There was no clear substantiation of non-linearity in the stress-strain curves, except at the beginning of the test that possibly caused by the realignment of the fibers and could be corresponding to grip movement. The UTS for this GFRP 90° specimen is around 58 MPa resulting modulus measurement of 17.4 GPa. This modulus measurement from experimental result is well predicted by micromechanical of rule of mixture (Appendix B). It means fabrication process succeeded made the appropriate contributions of fiber and matrix to their volume fractions in affecting the stiffness properties. This specimen of GFRP 90° without hole fails in a brittle type as seen in Fig.4.2.

Loading direction
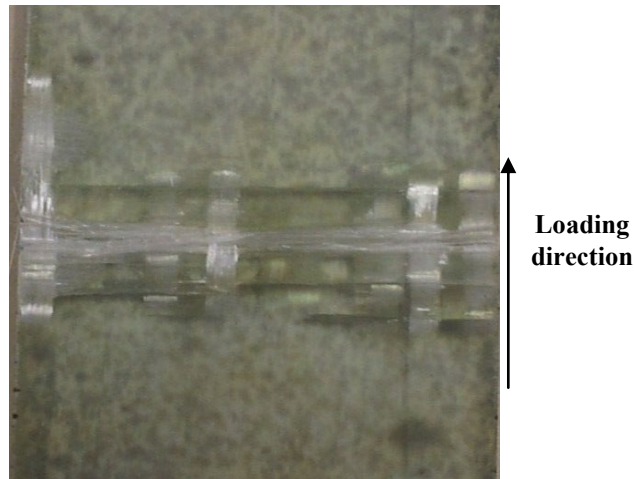
Figure 4.2 Macroscopic of catastrophic damage form of GFRP 90° without hole

The damage GFRP 90° specimen in tension is fairly straight in a brittle facture behaviour with a transverse fracture surface perpendicular to the direction of the applied load. Consequently, at the final failure of the specimen there is no permanent change in original rectangular shape of the specimen during the test, and hence no ductility. The initiation damage occurs in the form of cracking emanating due to matrix cracking that aligned with fiber direction. This first damage of matrix cracking occurs due to the higher load is distributed more on matrix which exceed the ultimate strength of the matrix. Since in this fiber orientation which mostly perpendicular with loading direction, the fibers are carrying very little or no load at all and the matrix dominantly carries the load.

It has been observed that after initial damage, the specimens continued to sustain the load under increasing displacements. Subsequently, matrix cracking then penetrates the interface between fiber and matrix and provokes another damage appearance of fiber/matrix debonding. Debonding usually happens when the fiber/matrix has not been distributed evenly throughout the laminates and could be due to the weak interface between fiber and matrix. From observation of specimen failure, it was confirmed the emergence of damage mechanisms of splitting or interfacial failure that spread and seen in the damage area until the end of width side of the specimen. This damage mechanism caused by matrix cracking propagation and the presence of fiber orientation in parallel with loading direction. It has previously been observed that during the second stage, a matrix crack met a fiber can propagate along the interface, if the fiber is parallel to the tensile axis [15]. The combination of these damage mechanisms could reduce the stiffness and capability of the laminates in carrying or transfer load. In the final stage of damage propagation, when the critical point was reached, damage area reaches to the end of width side of the specimen and specimen ultimately failed mainly due to the fiber breakage. It means that fiber in the laminates no longer able to hold or carry the increasing of given load and damage has occurred completely.

During the test, specimen surface also observed by the IR camera to follow the evolution of temperature. Fig.4.3 shows the thermal images up to final failure.

Load increase
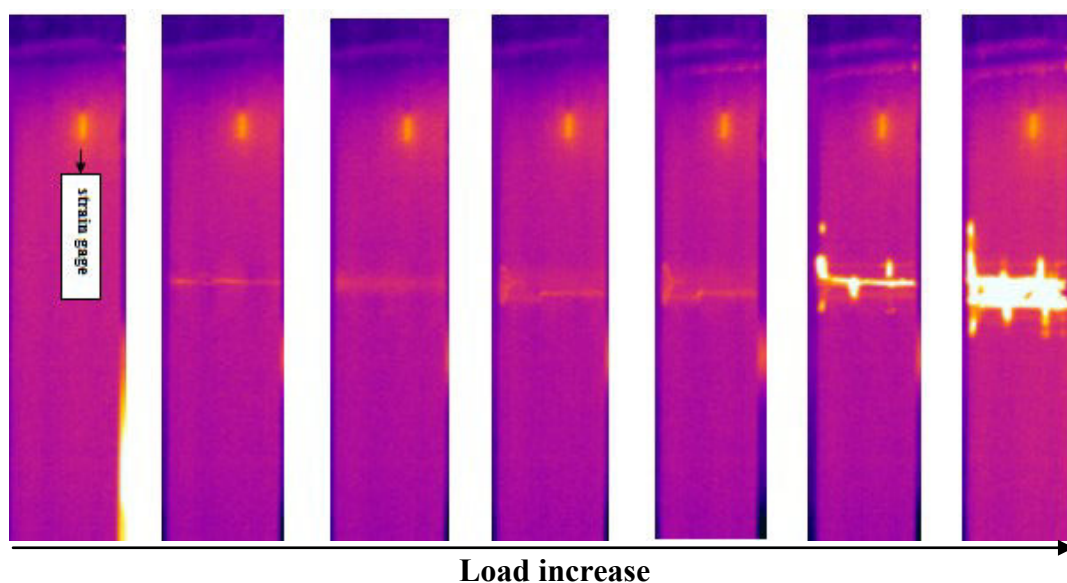
Figure 4.3 Thermography images of GFRP 90° without hole

In order to follow the evolution of temperature during the test, the area profile is used at several areas of specimen surface to have all change of the maximum temperature until final failure. Fig.4.4 below shows the area profile and temperature change on specimen surface before and until final or catastrophic failure period.

a. Before final failure

b. Until final failure
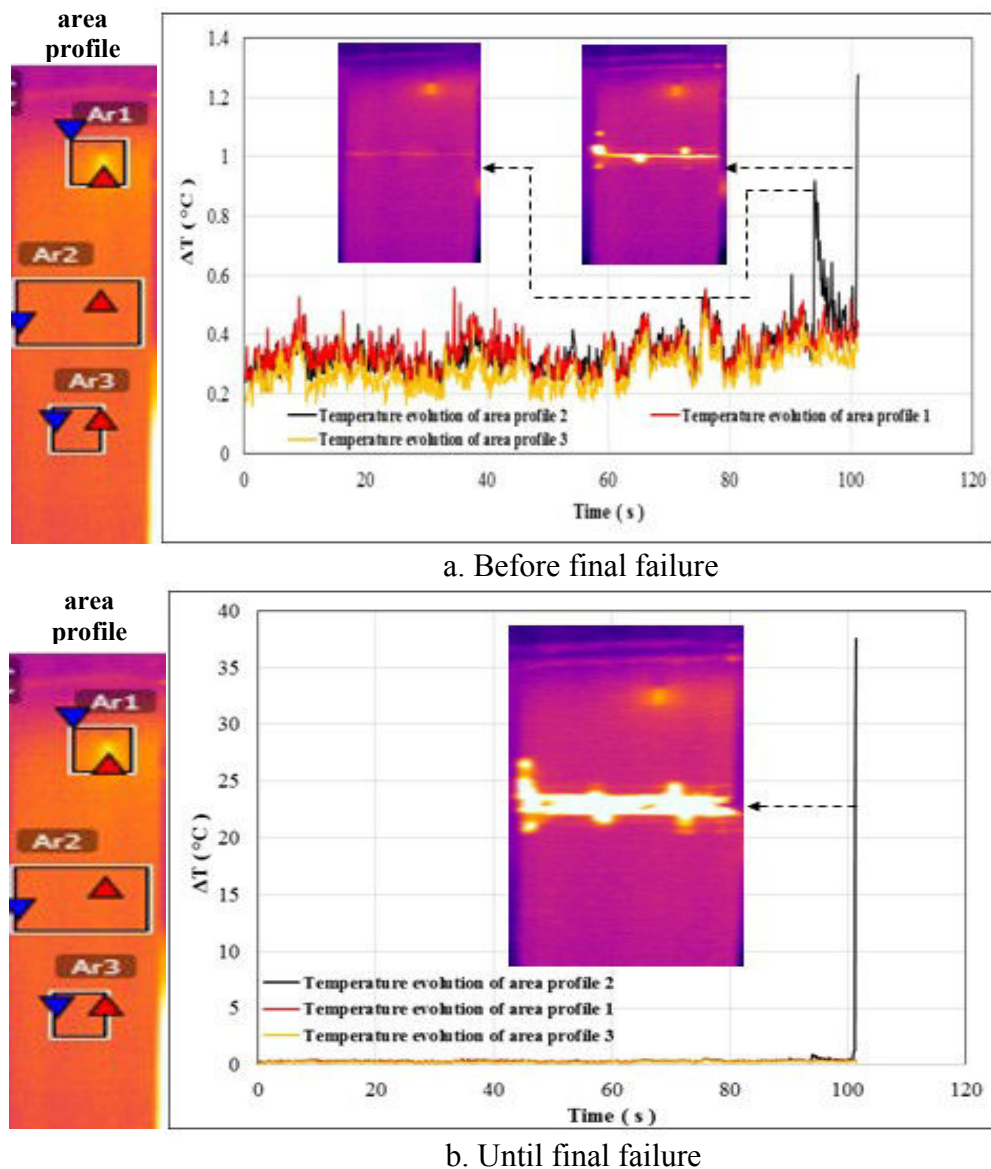
Figure 4.4 Temperature evolution of GFRP 90° without hole

From Fig.4.4 above, all the temperature surface (ΔT) that detect by the IR camera vary between 0.2 – 1.3 °C. From the comparison between thermal images and temperature change during the test before the final failure, ΔT above 0.6 °C that's clearly showing by several peaks of temperature profile are related to the

presence of macro damage. When damage occurs, it represents the energy which gradually released. The energy that has been absorbed is sufficient to create macro-crack, enlarging the pre-existing ones, and also to create new inner and surface cracks. The heat generated from the energy release, then detected by the IR camera that showed an increase in temperature in the area of damage. Each of the peaks of temperature is indicate different type of initial macro damage. We found that $\Delta T \approx 0.9$ °C is directly associate with the appearance of first macro matrix cracking and $\Delta T \approx 1.3$°C is related to the appearance of interface failure or splitting. The higher temperature of splitting is in fact, due to absorb more energy of damage. From the temperature evolution during tensile test, the presence of macro damage indicates the area of final failure, which is exist and concentrate on the region of failure area. This value of ΔT profile between 0.9°C and 1.3°C then simply can be used as ΔT threshold or range temperature of critical period before final failure. In sum, initial macro damage provokes the occurrence of catastrophic or final failure of the specimen that induce the highest peak of temperature at $\Delta T \approx 37$ °C. Using the information of strain propagation that occurs when this initial of macro damage occurs, both from displacement and strain gage are showing the higher strain propagation compared to other propagation behaviour that generally linear as seen in Fig.4.5 below. It shows, both thermography and strain gage confirm the presence of initial macro damage which happens before catastrophic or final failure of the specimen.
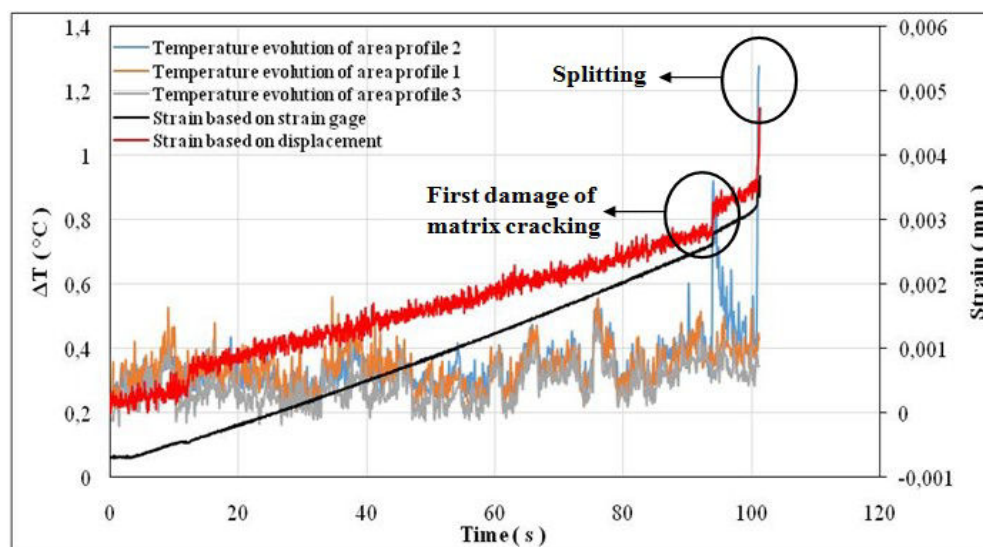
Figure 4.5 Strain and temperature evolution of GFRP 90° without hole

Fig.4.5 above shows the comparison of early detection on damage appearance first macro matrix cracking and interfacial failure (splitting) from strain gage and temperature change. The damage appearance shown with a small discontinuity in the strain curve and also a higher increase of temperature at the same time. This point was taken as damage due to the coupling effect of thermal and mechanical behaviour.

It can be noted that, thermography observation by IR camera can give a good local information about the early damage appearance and propagation, as well as damage type, damage location until rupture based on temperature profile. Thermography observation by IR camera also has excellent confirmation with strain gage detection on damage appearance for GFRP 90° without hole specimen under tensile static loading.

4.1.2 Tensile static testing of GFRP 90° specimen with hole and damage observation by thermography

The curve in Fig.4.6 is the stress versus strain curve obtained from tensile test which stress is resulting from given load and strain derived from the cross head displacement and strain gage that installed on the specimen surface. The specimen was GFRP 90° with hole.
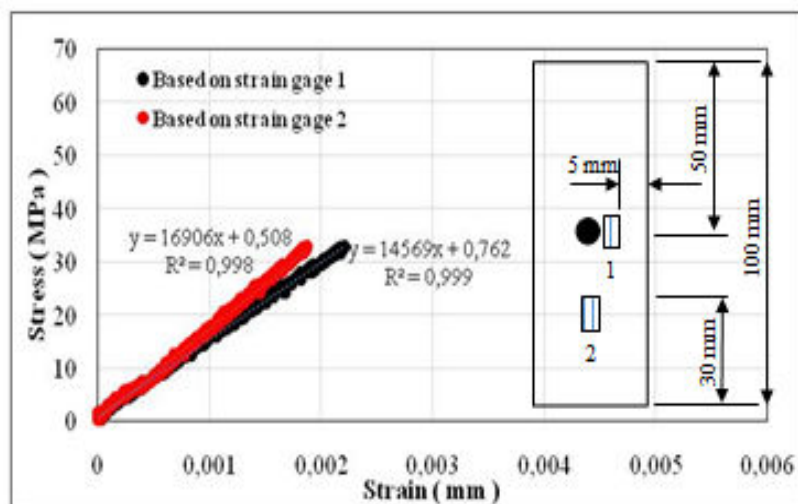
Figure 4.6 Stress-strain curve of GFRP 90° with hole

Stress - strain curve represents linier relationship that typical stress-strain curve of a unidirectional glass/epoxy specimen under static tensile loading. There

was no clear substantiation of non-linearity in the stress-strain curves. The UTS for this GFRP 90° specimen is around 54 MPa resulting modulus measurement approximetely 15 GPa. As a reference, UTS of unidirectional glass fiber composite with fiber orientation perpendicular with loading direction (GFRP 90°) without hole given by previous investigation is around 58 MPa where almost have the same UTS. The present of the small hole didn't significantly reduce the UTS of GFRP 90°, where only have around 15% of different. In addition, From local strain, we notice the presence of the hole produce a higher strain compare to area that contain no hole. This difference can be explained by the fact that, in the area where the contain no hole, the local area is bigger than area with hole, so that generate higher local stress concentration and become the location of final failure. This specimen of GFRP 90° with hole also fails in a brittle type, perpendicular with loading direction and at the edge of the hole as seen in Fig.4.7.
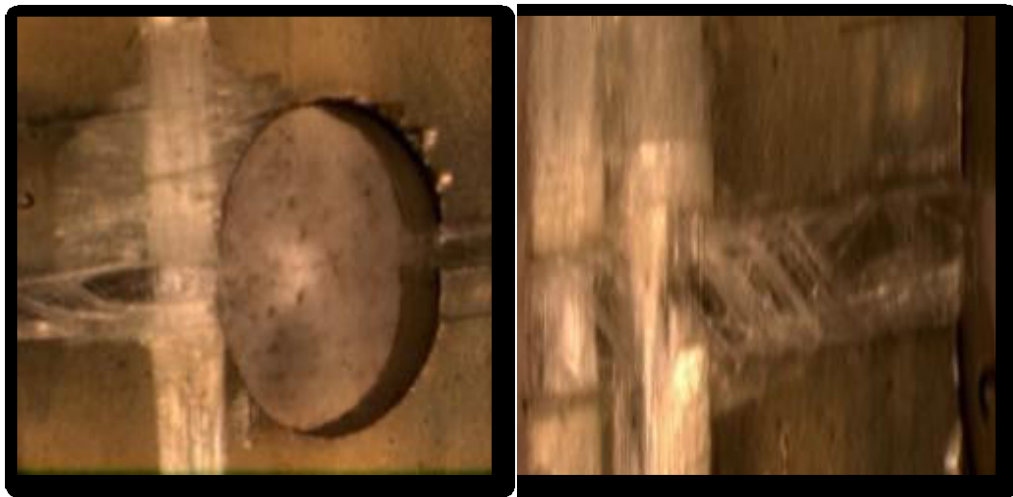
Figure 4.7 Microscopic observation on damage of GFRP 90° with hole

The damage of GFRP 90° specimen in tension is fairly straight and transverse to the loading axis. This behaviour is strongly infuenced by the matrix. The presence of the hole increases stress concentration that leads to strength degradation and initiate damage during the test. It was found that damage starts at the edge of the hole and propagated along the width where the highest stress concentration (three times higher) occurs (Appendix C). The initiation damage occurs in the form of cracking emanating due to matrix cracking. The damage area expanded by the debonding of the fiber and the matrix at the interface located at the edge of the hole and pararel with fiber orientation. It has been observed that

after initial damage, the specimens continued to sustain the load under increasing displacements. In this damage area, matrix cracking and splitting also occurs until the end of width side of specimen. The presence of interfacial failure or splitting in fact as a result of matrix cracking propagation and the presence of fiber orientation that parallel with loading direction. In the final stage of damage propagation, when the critical point was reached, damage area reaches to the end of width side of the specimen and specimen ultimately failed mainly due to the fiber breakage. It means that fiber in the laminates no longer able to hold or carry the increasing of given load and damage has occurred completely. In general, there is no different damage mechanisms between GFRP 90° specimen with and without hole.

During the test, specimen surface also observed by IR camera to follow the evolution of temperature. Fig.4.8 shows the thermal images up to final failure.
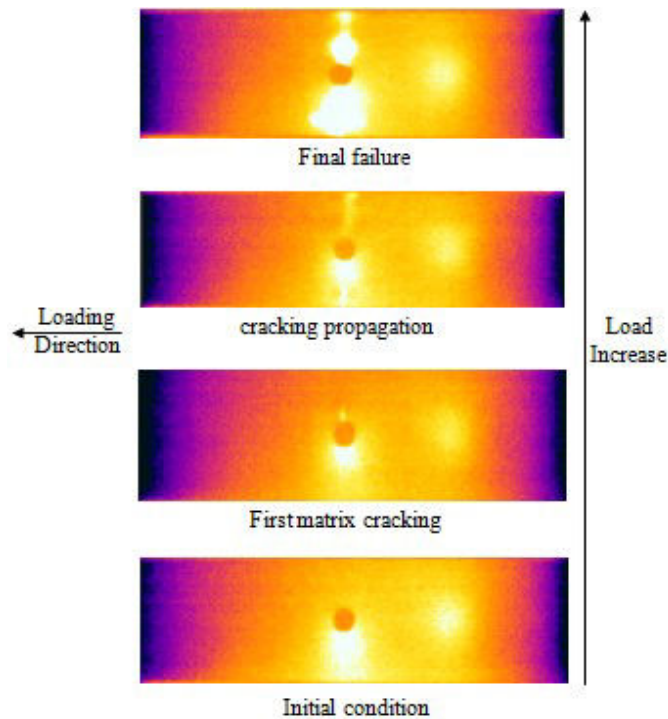
Figure 4.8 Thermography images of GFRP 90° with hole

In order to follow the evolution of temperature during the test, the area profile is using at several area of specimen surface to have all change of the maximum temperature until final failure. Fig.4.9 below shows the area profile and temperature change on specimen surface before catastrophic failure period.
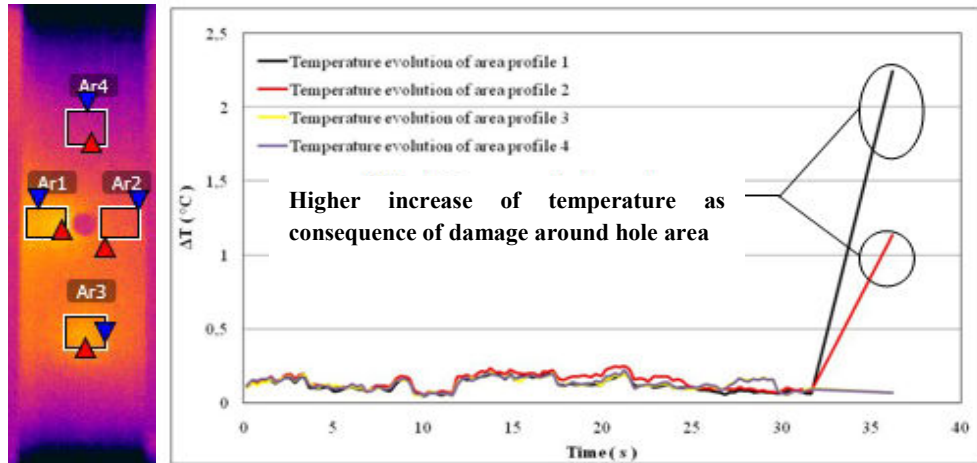
Figure 4.9 Temperature evolution of GFRP 90° with hole

All the temperature surface that detect by IR camera vary between 0.1 – 2.3 °C. The observation area at the edge of the hole clearly shows higher peak of temperature profile. The higher temperature is in fact due to the detection of heat generated by energy release when damage occurs. This temperature change confirms the initial damage appearance of matrix cracking and splitting at the edge of the hole. From the temperature evolution during tensile test, the presence of macro damage indicates the area of final failure, which is exist and concentrate on the region around the hole. The value of ΔT profile of $\approx 1.2^o$C then can be used as preliminary of ΔT threshold or temperature of critical point before final failure.

The temperature detection of damage, then compares with strain gage results as seen in Fig.4.10.
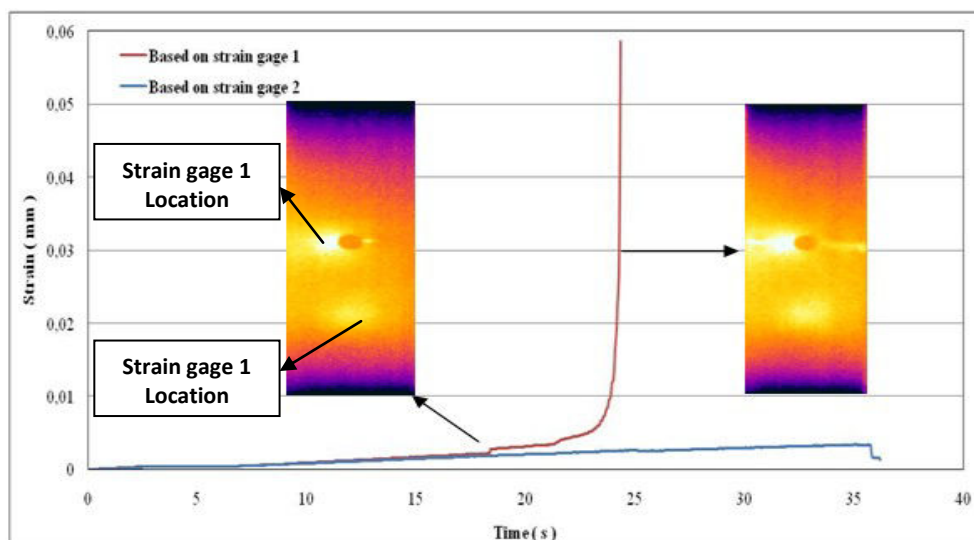
Figure 4.10 Macro damage detection by strain gage and thermography

Using the information of strain propagation that occurs when this initial of macro damage occurs, strain gage at the edge of the hole is showing the higher strain propagation compared to other propagation behaviour by strain gage far from the hole as seen in Fig.4.10. It shows, both thermography image and strain gage confirm the presence of initial macro damage which happens before catastrophic or final failure of the specimen. The other area on specimen surface that contains no damage or failure propagation, temperature profile and strain gage indicate there is no significant temperature and strain increase.

It can be concluded that, thermography and strain gage have a good relation on detecting the damage appearance and propagation for GFRP 90° with a hole under tensile static loading.

4.1.3 Tensile static testing of GFRP 0° specimen with hole and damage observation by thermography

The unidirectional glass fiber composite (GFRP 0°) also tested in this study under the same test condition of tensile static loading using specimen with an open hole condition. Figure 4.11 below shows a typical stress-strain curves for GFRP 0° under tensile static loading.
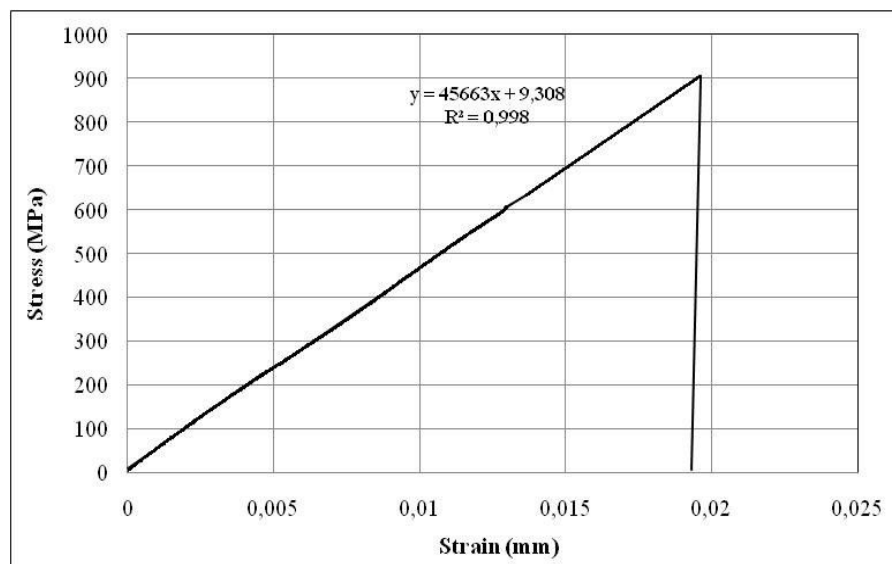
Figure 4.11 Tensile curves of GFRP 0° with hole

The stress - strain curve obtained from given load of tensile test and strain based on strain gage at the edge of the hole. Here, final failure took place at

ultimate tensile strength (UTS) of 900 MPa and strain values around 0.019. The elastic modulus (E) around 45 GPa is exhibited by linear interpolation from stress-strain curves where similar by the result of rule of mixture (Appendix B). This similar results between experimental and analytical indicate that the contributions of fiber and matrix to their volume fractions in influencing the modulus properties is suitable produced by good fabrication process.

A significant higher of UTS for GFRP 0° compared with GFRP 90° shows different effect of fiber direction on a GFRP specimen for different fiber orientation. As a reference, UTS of unidirectional glass fiber composite with fiber orientation perpendicular with loading direction (GFRP 90°) given by previous investigation is around 54 MPa where 16 times lower for the same specimen dimension. Fiber direction has profound impact on the tensile properties of composites as already known in general. The reason is GFRP 0° specimen that parallel with the loading direction has a very good ability and higher tensile strength to accommodate the stress resulting from the tensile loading. This cannot be separated from the nature of composite which is a function of fiber orientation direction (anisotropic). Simply, this comparison between two different fiber direction can be explained by *iso-strain condition* (fiber aligned with the loading direction) and *iso-stress condition* (fiber perpendicular with the loading direction) from Voigt and Reussmodel. The fiber direction also has an effect on the damage mechanism on the specimen surface. The damage mode of each fiber direction for GFRP with hole specimen was found differently.

From Fig.4.11 it is clearly shown that GFRP exhibited a typical brittle behaviour with sudden failure. In order to have more understanding about the damage appearance of GFRP 0° with an open hole condition under tensile test, the other tensile test was also conducted to get local information about stress-strain behaviour in the area at the edge of the hole and at the gross area corresponding to damage appearance. This tensile test was not conducted until the failure of the specimen. Tensile test was carried out until 20 kN of tensile load with the same displacement rate of 1 mm/min. Several strain gages were placed at the edge of the hole and at gross area on the specimen surface.

From the test results with strain gages as seen in Fig.4.12, indicate that local strains on the specimen surface were different. Area that along the line with hole (strain gage 4) has the lower strain compare to area on the side of the hole (strain gage 3). Tensile curve also shows that higher strain occured at at the edge of the hole (strain gage 1 and 2). It can be noted that GFRP 0° orientation has the region that carry lower load result in small strain and the region that carry higher load provoke large strain.
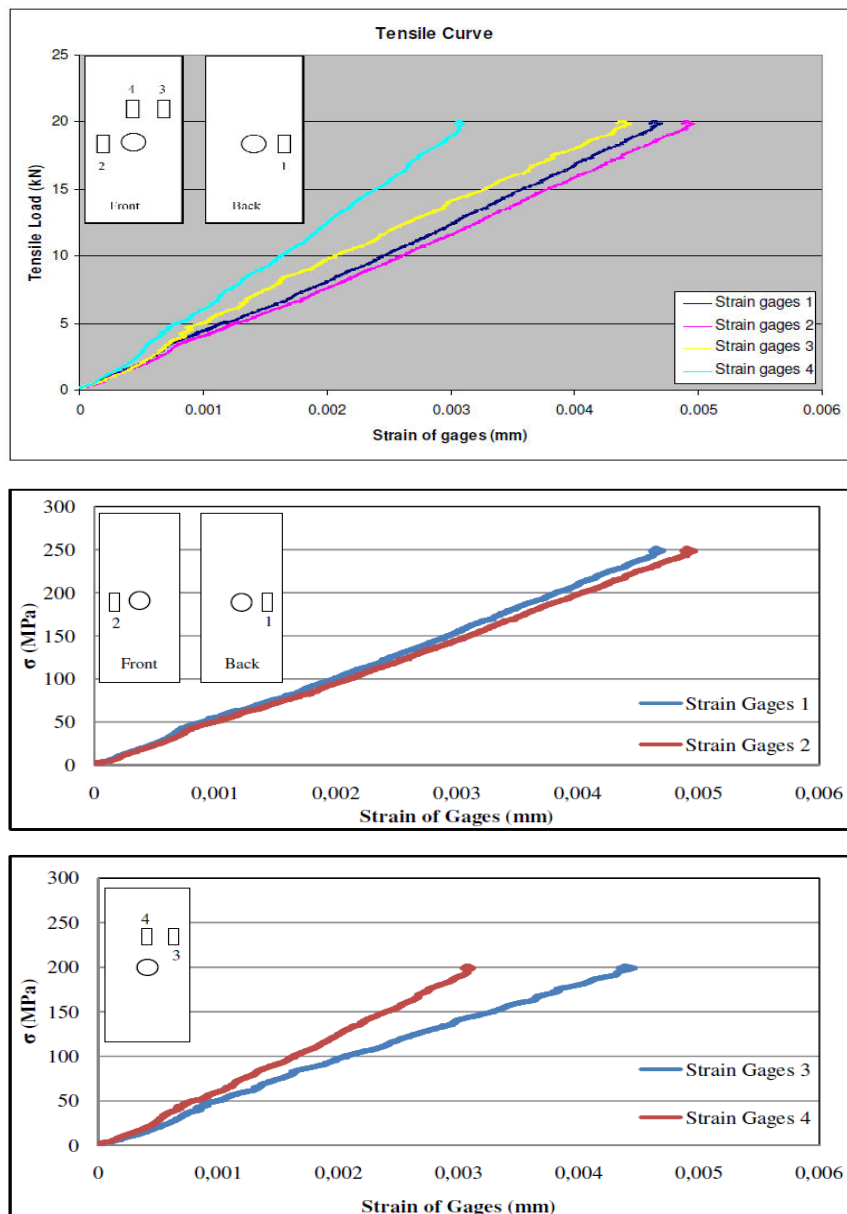
Figure 4.12 Tensile test of GFRP 0° with strain gage

From this condition, we can assume that area at the edge of the hole and side area of the hole will experience higher stress concentration and can be a catastrophic failure area. These results then will be compared with specimen that have been damaged due to the tensile load to prove the earlier assumptions based on results obtained from strain gage.

From previous study [41], the investigation on the stress concentration around the hole for glass epoxy found that the stress distribution resulting lowest stress concentration at the area along the hole for tensile loading testing pararell with fiber direction on composite. For this GFRP 0° with hole specimen, the presence of an open hole will be redistributing also the force at the edge of the hole resulting the highest stress concentration around four times higher at this area (Appendix D). There is no stress pass through the hole and result in the lowest stress at the area along the hole location,as seen the ilustration in Fig.4.13.
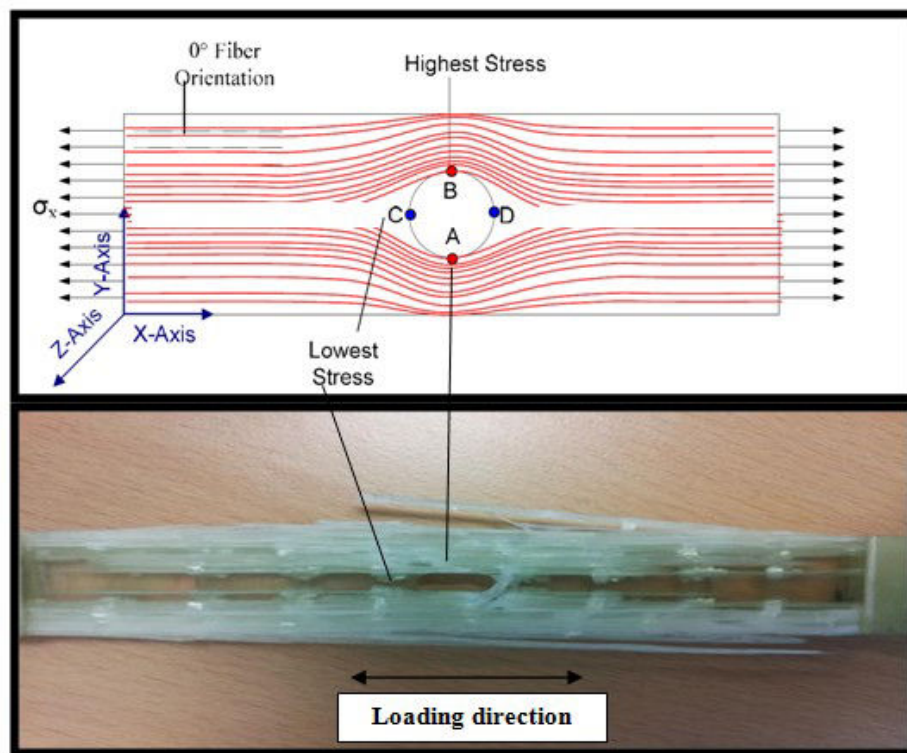
Figure 4.13 Ilustration of stress distribution and final failure of GFRP 0°

The damage mechanism of GFRP 0° with hole specimen may be attributed to the combination of matrix damage, fiber-matrix debonding and fiber breakage (Fig.4.14). From the observation results, the first damage of matrix macro-cracking is in splitting form and also indicates by cracking sound. After the first

failure of matrix that take place at the edge of the hole, the failure was developed into other damage mechanism until the width side of specimen. The further failure of the matrix macro-cracking may resulted by fiber-matrix debonding and then the failure may propagate along the fiber-matrix interface and showing 'brush like' failure that indicate the weak interface. This damage appearance confirms the strain detection in Fig.4.12. The other details of damage mechanisms of bundle fiber matrix decohesion in transverse direction also found almost in all surface area of the specimen until both sides of tab area, as seen in Fig.4.14. The bundle of fiber failure in transverse direction or interfacial failure occurs on brittle model showing the existence of fiber in this direction. The final failure cause changes in the shape of the hole into the more stretching hole in the direction of tensile loading.
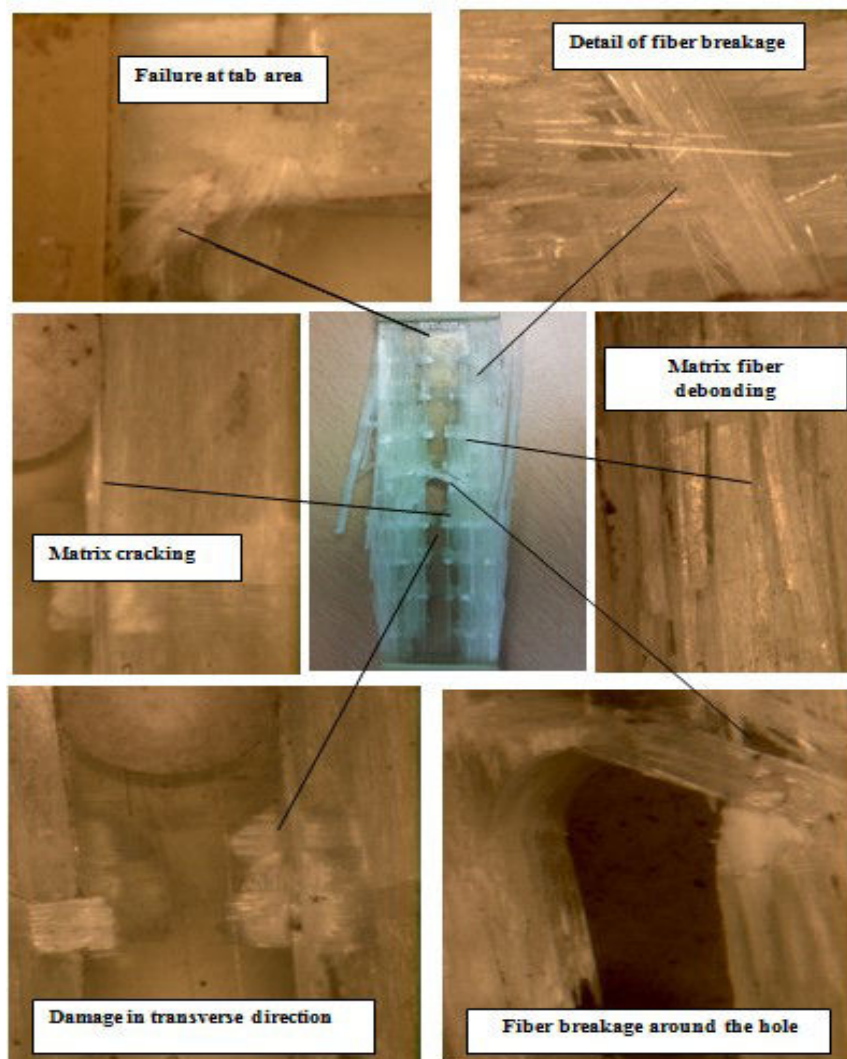
Figure 4.14 Damage types of GFRP 0° with hole

This damage appearance confirms that the strain detection (Fig.4.12) does not have the same strain propagation on specimen surface. Fig.4.13 and Fig.4.14 show that the area along the line with the hole indicate the area with no damage occurs or area with lowest stress concentration. This behaviour also confirms by strain propagation of strain gage that placed at the same area. The area along the line with the hole sustains lower strain compare to other area on the specimen surface (area around the hole and side area of the hole). With the same perspective of damage appearance and strain propagation, we also found that area around the hole and side area of the hole have a bigger strain propagation that of course will lead to an area that experience damage mechanisms until catastrophic failure. It can be noted that, strain gage has an excellent ability to detect damage propagation and final failure location before it occurs for this fiber composite material (GFRP 0°) that contains an open hole condition.

During the test, specimen surface also observed by IR camera to follow the evolution of temperature. Fig.4.15 below shows the IR camera detection on specimen surface during tensile test until final failure. From tensile test and thermography observation, it was found that the failure occurred parallel to fiber direction in brittle model and dominated by fiber matrix debonding and fiber pull out.
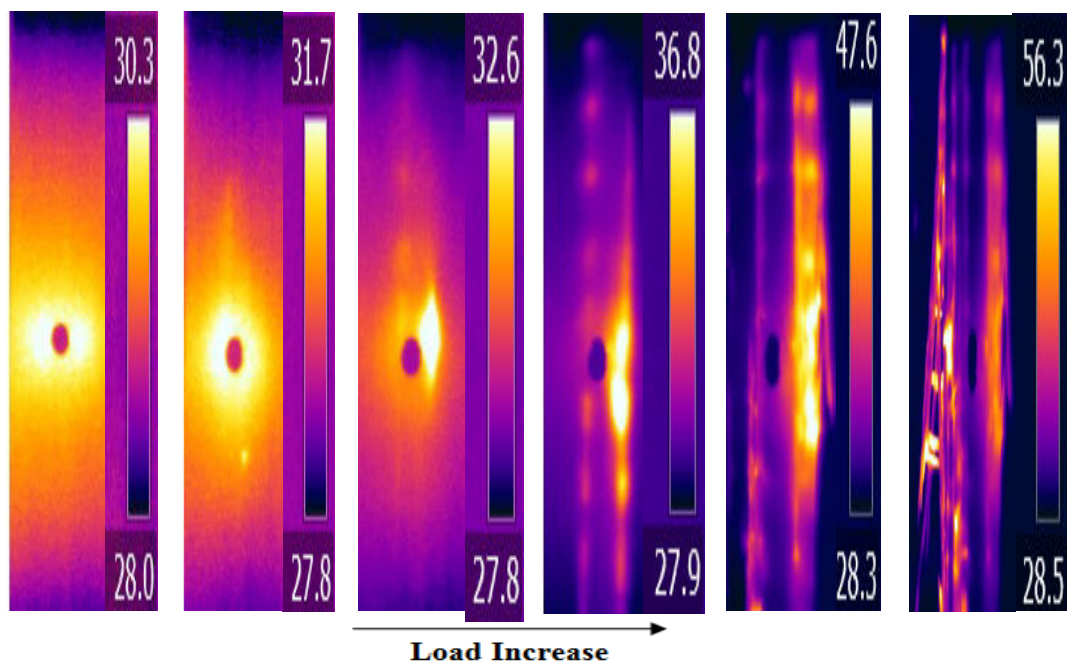
Figure 4.15 Thermography images of GFRP 0° with hole

In order to follow the evolution of temperature during the test, the point profile is used at several areas of specimen surface to have all change of the maximum temperature until final failure, as seen in Fig.4.16.
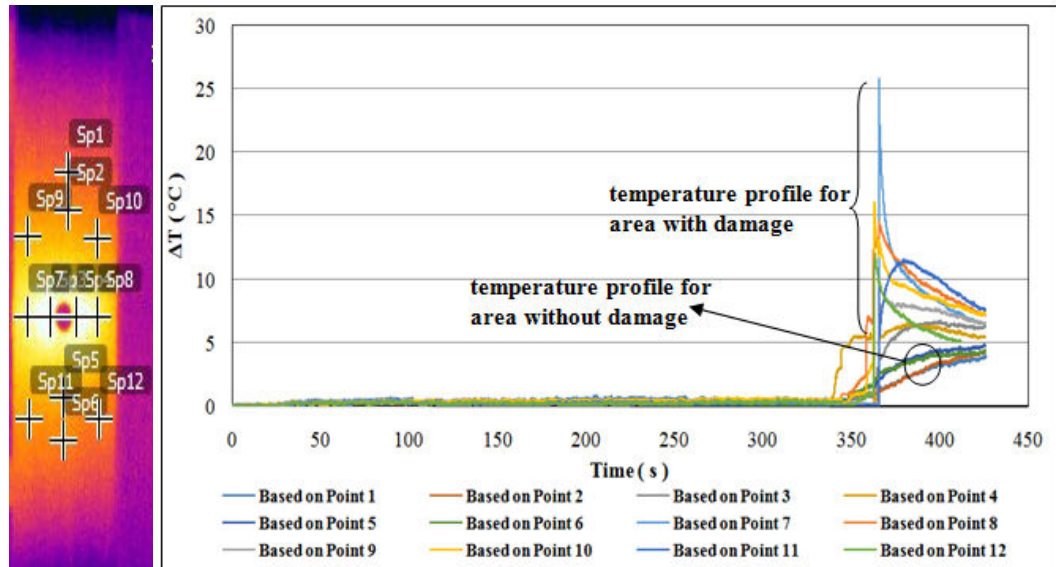
Figure 4.16 Temperature evolution of GFRP 0° with hole

From Fig.4.16 above, all the temperature surface (ΔT) that detect by IR camera vary between 0.2 – 26 °C. Temperature profiles for area without damage or area that sustained lower strain propagation has no characteristic of suddenly temperature increase as known as damage identity. The area with damage and damage propagation experiences suddenly increase of temperature and reaches higher point of ΔT. From the comparison between thermal images and temperature change during the test before the final failure, ΔT above ≈ 2°C relates to the presence and propagation of macro damage. When damage occurs, it represents the energy which gradually released. The heat generated from the energy release, then detected by the IR camera that showed an increase in temperature in the area of damage. During a tensile test, the formation of cracks in matrix and fiber breakage leads to a pulse of heat that can be measured at the surface. Each of the peaks of temperature is indicate different type of initial macro damage. We found that ΔT ≈ 2°C - 7°C is associate with the appearance and propagation of macro matrix cracking and interface failure or splitting in the traverse direction. ΔT above ≈ 10°C is related to the appearance of fiber breakage and fiber pullout interfacial failure at final period of damage propagation. This

value of ΔT profile between 2°C and 10°C then simply can be used as ΔT threshold or range temperature of critical period in terms of macro damage appearance before final failure. It can be concluded that, thermography successfully follows the damage propagation for GFRP 0° with hole under tensile static loading.

4.2 Tensile fatigue testing and damage observation by thermography of GFRP

This section describes the experimental investigation on the fatigue behaviour of GFRP 90° with hole. Thermography observation applies to detect temperature distribution on specimen surface during the tests. The aim is to determine the damage evolution with respect to the number of cycles by varying the stress level applied. In practice, damages are observed by two systems. The first consists in a damage evolution during the test by strain gage and/or displacement to follow the stiffness degradation by controlling the continuous decay of the elastic properties. The second system consists in an analysis under thermography observation. The change of temperature will be monitoring to have temperature profile according to damage appearance and propagation. In this way it is possible to determine the relationship of damage evolution between experimental results and thermography analysis.

The constant amplitude load controlled tension-tension fatigue tests were performed with other fatigue test parameters selected were sinusoidal waveform, 3 Hz frequency, and the stress ratio of 0.1. Fatigue loads were applied as percentages of ultimate tensile strength (UTS). The fatigue load, where specimens survived 1 million cycles is referred as a high cycle fatigue strength (HCFS) in this report.

Fatigue tests were conducted for several stress levels based on UTS with the range of 40%-65% of UTS. The initial maximum stress level was taken as about 65% of the UTS. Maximum stress levels were then chosen to give a range of lifetimes (Nf) between 10^3 and 10^6 cycles. The S-N curve of GFRP 90° based on normalized stress (maximum fatigue tensile stress divided by ultimate static

tensile strength as the ordinate) and cycles to failure under stress control mode is shown in Fig.4.17.
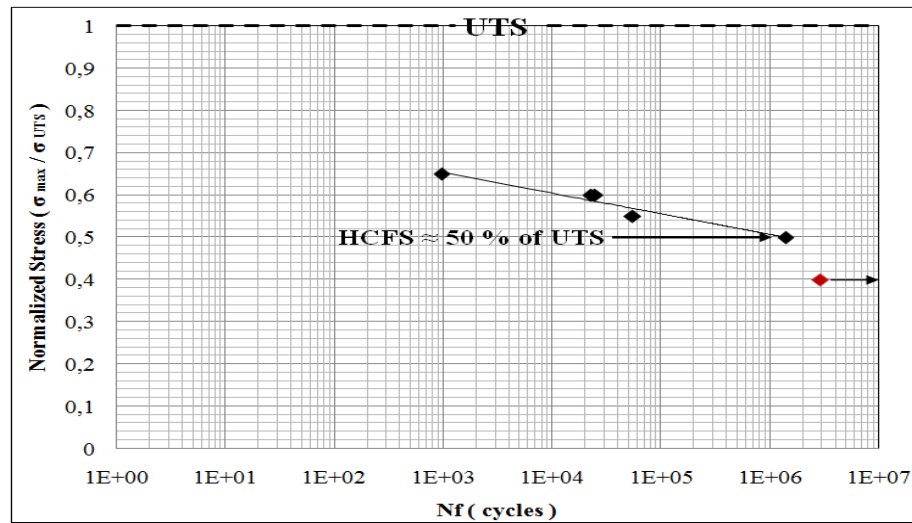
Figure 4.17 S-N curve for GFRP 90° with hole

The plot is linear and there is no failure after a run-off of 2.900.000 cycles for 40% of UTS. The S-N curve shows gradual decline in fatigue strength with an increase in the number of fatigue cycles. The trendline line predicts a high cycle fatigue strength (HCFS) of about ≈ 0.5 of normalized stress for the GFRP 90° with hole, means that Nf reaches one million cycles when the maximum stress value is around 50% of UTS. Hence a normalised stress level of up to about 0.5 (approximately 29 MPa) can be taken as a safe value for high cycle fatigue strength (i.e. the stress correspondent to a life of $5 \cdot 10^6$ cycles) for this GFRP 90° material. The normalized S-N curve is presented by the equation :

$$y \, (Nf) = \, 0.802 - b \, \ln(Nf) \tag{30}$$

where y is $\sigma_{max} / \sigma_{UTS}$, Nf is number of cycles, and the constant b, that represents the slope of normalised S-N curve, is called fatigue sensitivity coefficient. The value b was found to be 0.02 for this GFRP 90° with an open hole condition. Fig.5.2 below shows strain propagation of GFRP 90° under tensile fatigue loading with 65 % of UTS load level until first failure based on crosshead displacement and also strain gages.

First macro damage of matrix cracking at the initial period of the test was detected by strain gage at the edge of the hole and also by global strain based on the displacement of the actuator. In Fig.4.18 (top), the matrix cracking breaks the

strain gage by showing the significant strain increase and strain gage then stops to record the strain propagation. Globally, after the first matrix cracking, strain propagation shows to have an increasing trend until rupture. The other strain gage that placed far from the hole didn't indicate the strain increasing when the first appearance of macro damage.
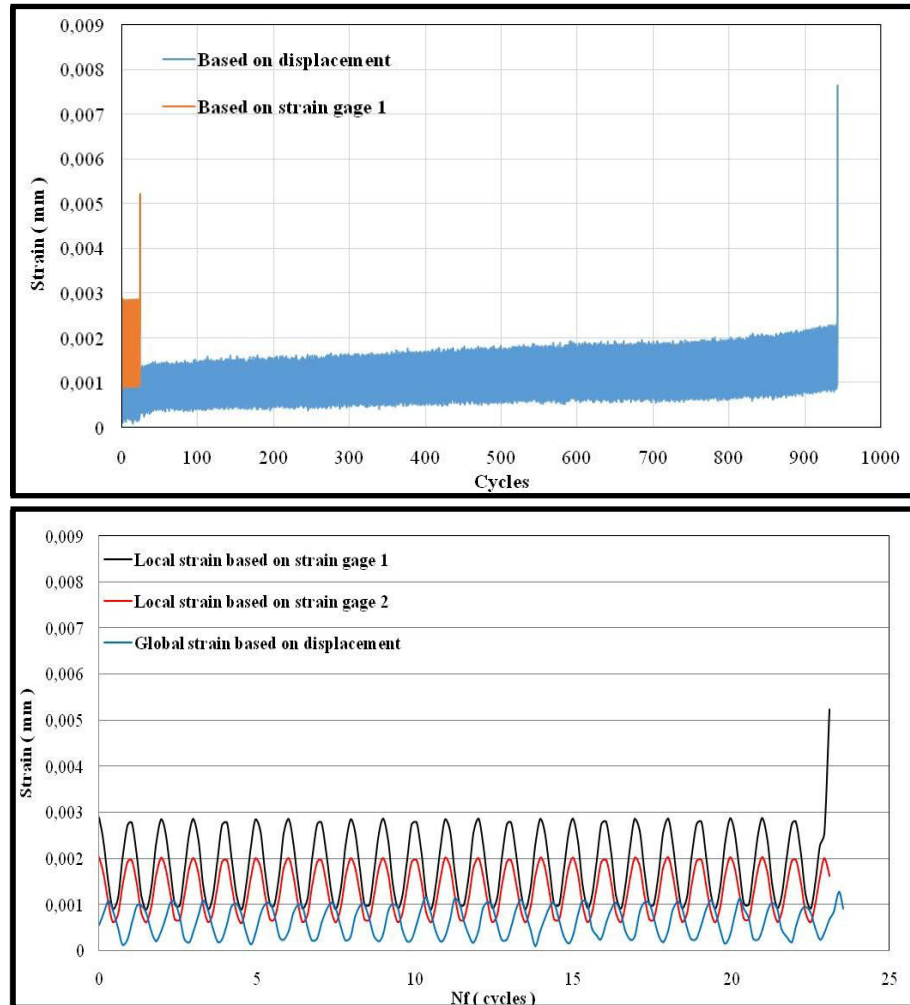
Figure 4.18 Strain propagation of GFRP 90° during the test

From an experimental point of view, it can be noted that global strain by displacement and replacement of strain at the edge of the hole by considered the new position around the hole are sufficient to follow the strain propagation. The placement of strain gage far from the hole isn't necessary since it can't follows the strain propagation compare to the global displacement and strain gage at the edge of the hole. In this report, damage propagation of load level 65% will be explained together with the temperature changes on the specimen surface to represent the

analysis method on this fatigue testing of GFRP 90°. The stiffness degradation based on displacement actuator and strain gage at the edge of the hole is shown by Fig.4.19 below.
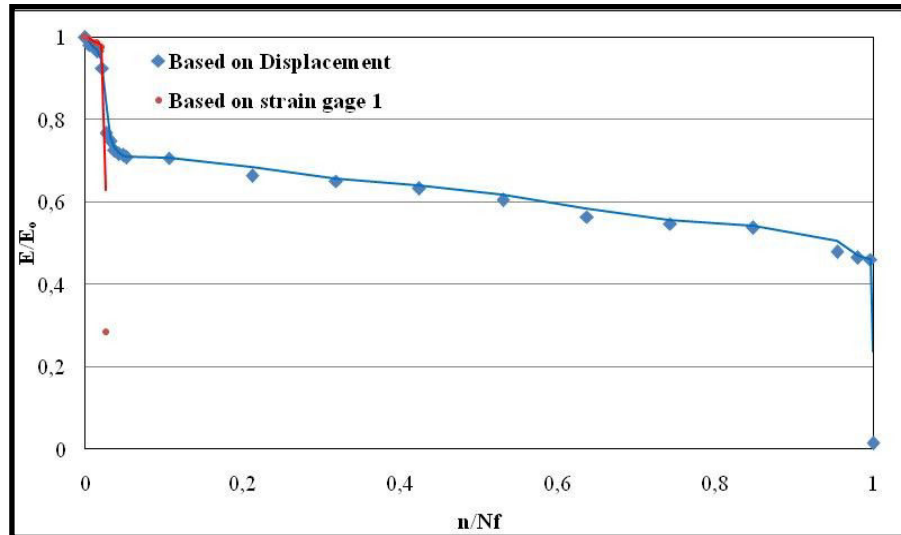
Figure 4.19 Normalized Stiffness degradation at 65% UTS tests of GFRP 90°

From the stiffness degradation curve of the change in material modulus has been commonly used to express the state of damage in polymer composite material. We can have cumulative damage, D as a function of loading cycles where defined as :

$$D = 1 - \frac{E}{E_0} \qquad (31)$$

where E and E_0 are the residual and initial modulus, respectively. Fig.4.20 shows the cumulative damage as a function of loading cycles for GFRP 90°

$$D = \frac{E_0 - E}{E_0}$$
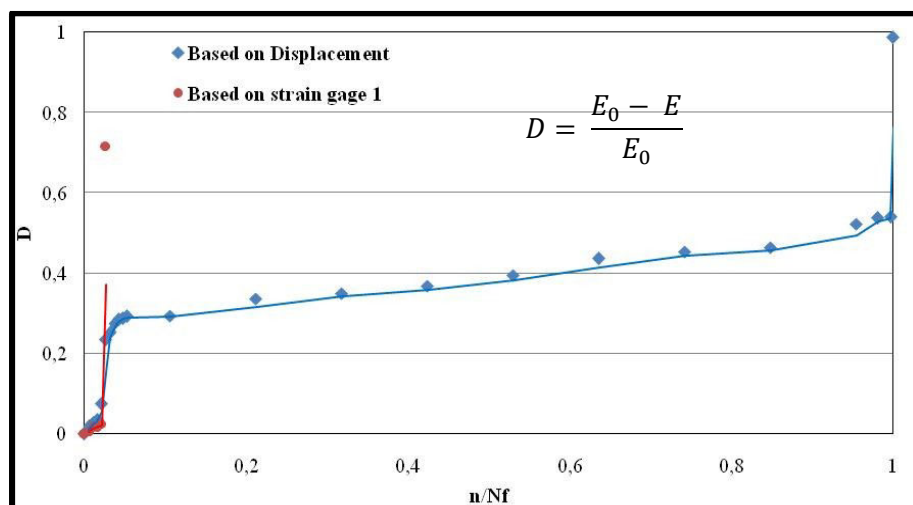
Figure 4.20 Damage evolution of GFRP 90° with 65% of UTS

From stiffness degradation and damage evolution, indicate that there are three stages of damage evolution in GFRP 90° specimen. This damage behaviour is categorized as brittle mode. The first stage of damage evolution could be caused by initial micro matrix cracking. For the second stage, it is 'saturation level' where the damage growth of matrix cracking becomes relatively stable. In the third stage, matrix and fiber breakage take place which caused a rupture by separation along the width that parallel to the fiber orientation.

Under fatigue condition, damage of this GFRP specimen also fails in brittle type as it happens under static test that strongly influenced by the matrix. The matrix cracking in perpendicular direction which start at the edge of the hole as the highest stress concentration area then leads to other damage mechanism of fiber/matrix debonding, longitudinal splitting, and fiber fracture. The final damage of specimen seems to occur when the damage area reaches a certain distance to the end of the width side of specimen, as seen in Fig.4.21.
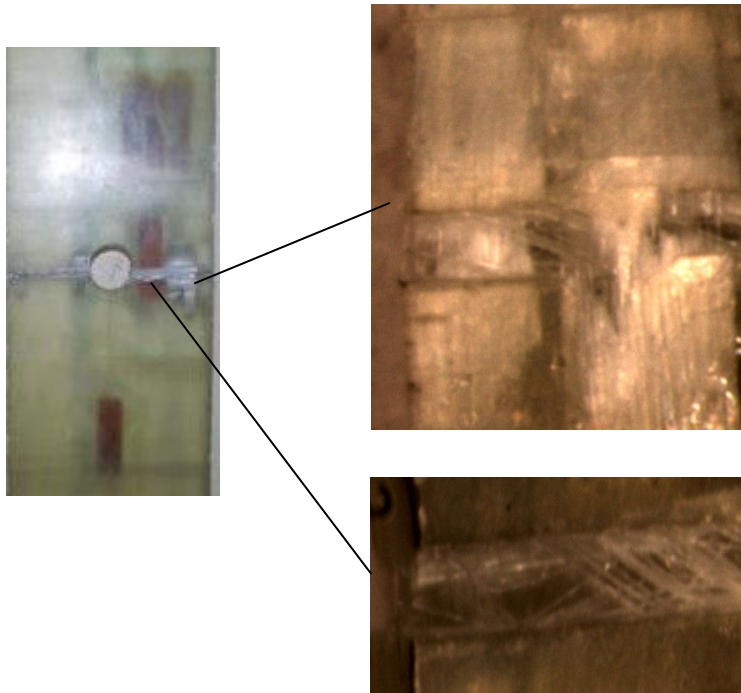
Figure 4.21 Final failure of GFRP 90° wiht hole under fatigue loading

This specimen of GFRP 90° with hole also fails in a brittle type, perpendicular with loading direction and at the edge of the hole as seen in

Fig.4.21. The damage of GFRP 90° specimen in tension is fairly straight and transverse to the loading axis. This behaviour is strongly infuenced by the matrix.

During the fatigue tests, IR camera was used to follow the temperature changes on the specimen surface. Fig.4.22 represents the temperature changes at the edge of the hole during the fatigue test with 65% of UTS.
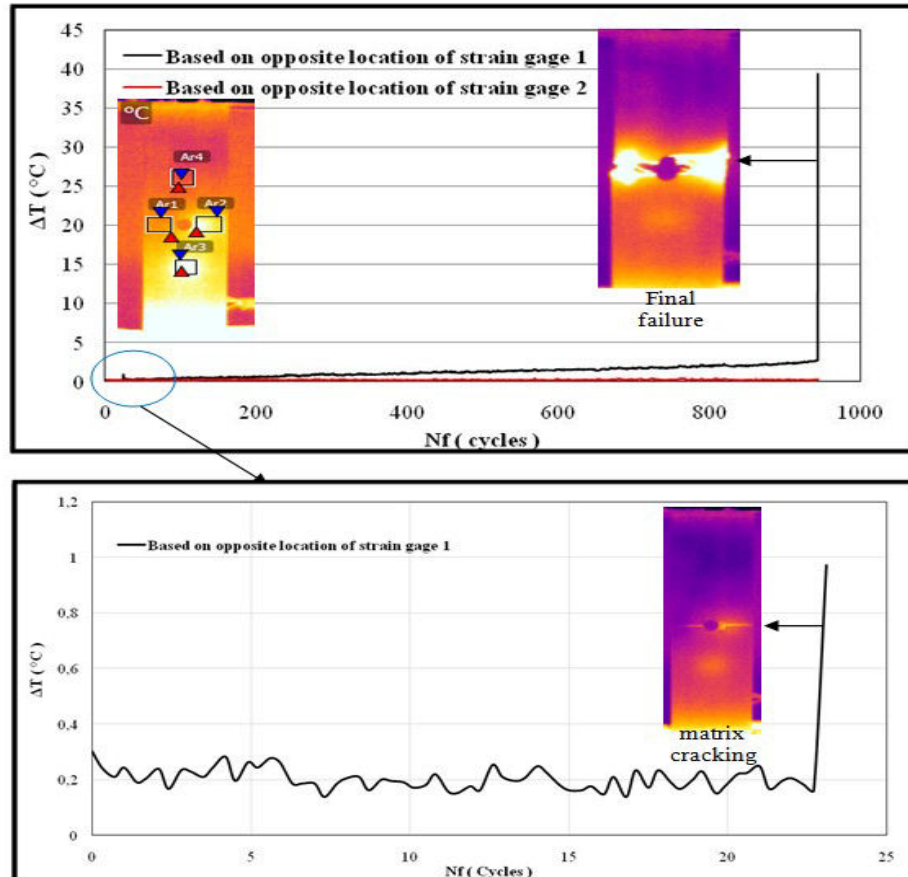
Figure 4.22 Evolution of surface temperature of GFRP 90$^{\text{o}}$

From Fig.4.22 above, all the temperature surface (ΔT) that detect by IR camera vary between 0.2 – 39 °C. From the comparison between thermal images and temperature change during the test before the final failure (Fig.4.4), ΔT ≈ 0.9 °C that's clearly showing by peak of temperature profile are related to the presence of first macro damage of matrix cracking. After that, the temperature showed to reach a stable period of an increase trend. The temperature profile had a gradual increase trend with the slope ≈ 0.001 $^{\text{o}}$C/cycle until around 200 cycles and continue to increase with a slightly higher of slope ≈ 0.002 $^{\text{o}}$C/cycle the increasing temperature becomes until around 800 cycles. The trend of temperature

experienced a significant increase at the final period with three times higher of slope, at 0.006 ^{o}C/cycle until reaching the rupture where ΔT suddenly increases and reaches the highest $\Delta T \approx 39^o$C at one cycle.

The temperature evolution then compares with damage evolution as seen in Fig.4.23.
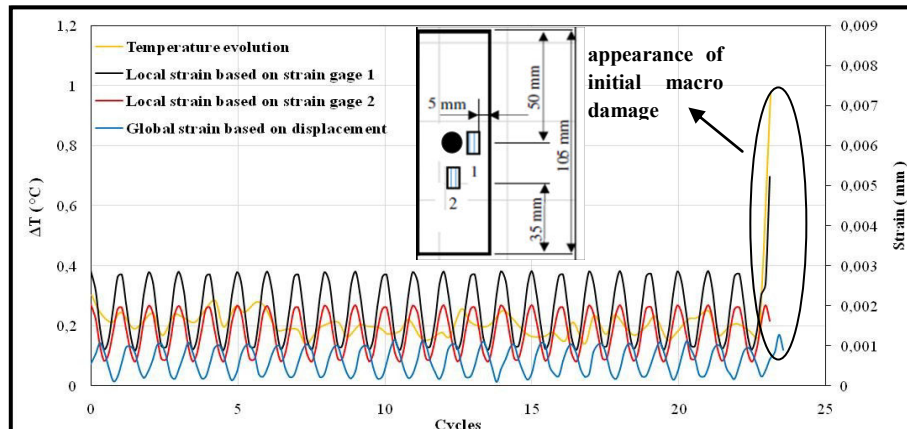
a. Temperature and strain gage detection on first macro matrix cracking
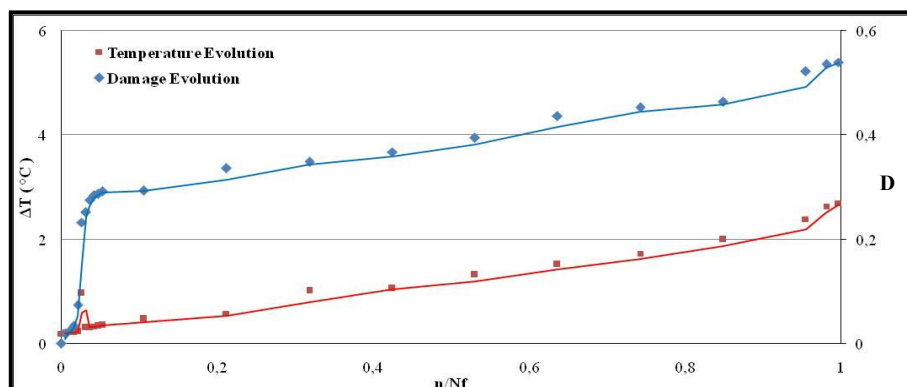
b. Temperature and damage evolution of before rupture
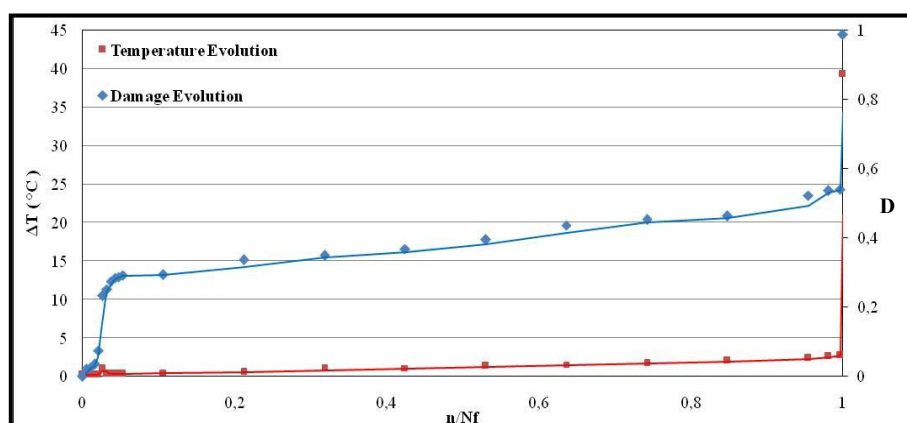
c. Temperature and damage evolution until rupture

Figure 4.23 Temperature and damage evolution of GFRP 90° with 60% of UTS

From the temperature and damage evolution during tensile fatigue test (Fig.4.22 and 4.23), the presence of damage was indicated by temperature change on specimen surface during the test that exist and concentrate at the hole. Meanwhile, the temperature evolution at another area of specimen surface that far from the hole didn't show an increase of temperature or relatively to have the same temperature from the beginning of the test until rupture of the specimen. When damage occurs, it represents the energy which gradually released. The heat generated from the energy release then detected by the IR camera that showed an increase in temperature in the area of damage. The evolution of the temperature can be categorized in four stages. In the first part, the initial increase of temperature is possibly due to the micro cracking in matrix. In the second part, a sudden increase in temperature caused by first appearance of macro matrix cracking. After that, the temperature reaches a slowly increasing trend due to the stable growth of matrix cracking as part of the third stage. The final part, a significant trend increase of temperature could be due to fiber/matrix debonding as the interfacial failure in splitting form and finally provokes the occurrence of fiber fracture which dealing with the rupture of the specimen.

It can be noted that, thermography observation by IR camera gives a good confirmation with strain gage detection on damage appearance and evolution for GFRP 90° with hole specimen under tensile fatigue loading.

4.3 Rapid analysis of fatigue strength based on thermography and energy dissipation of GFRP

The purpose of this analysis is to determine the fatigue strength based on experimental results by means of IR camera and energy dissipated in a unit volume of material. Thermographic approach that relies on the use of an IR camera, as originally called the Risitano method [53] has shown to be useful for the determination of high cycle fatigue strength (HCFS) of composite material [60]. The main advantage of this method is provide a rapid determination of HCFS that is very efficient time-consuming procedures.

This tests were conducted using GFRP 90^0 with hole specimen and under the loading frequency of 3Hz and R = 0.1 as discussed in Section 3.3. Using the IR camera, we had a temperature profile for specimen surface as a function of number of cycles for a test with different load level. The fatigue tests were conducted until 10000 cycles to have a stable or plateau profile of temperature evolution as seen in Fig.4.24. The same area observation at the edge of the hole was used for all tests which was the failure area to obtain the temperature profile.
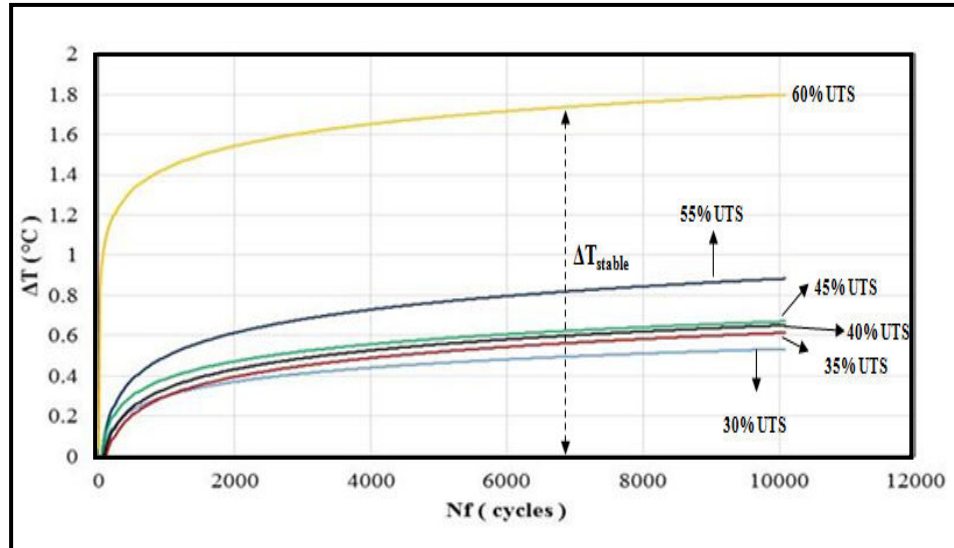
Figure 4.24 Temperature profile of GFRP 90° for each load level

According to Risitano method [53], the high cycle fatigue strength (HCFS) of material can be determined from the intersection of temperature profile ΔT_{stable} of different stress level obtained by separately fitting the experimental data for low and high stress amplitudes on the x -axis, respectively (that is for stress levels

below and above the expected fatigue limit). From Fig.4.24, there is a significant or higher increase of ΔT_{stable} around $\geq$ 10 times (0.2^oC-0.8^oC) at above 55% of UTS compare to increase of ΔT_{stable} around $0.02\ ^oC$-0.07^oC under 50% of load level. This load level then used to categorize the stress level of below and above, which shows the characteristic bilinear profile used for this method. Fig.4.25 shows how the HCFS is determined using a graphical procedure based on thermography method. It is noted that this method is a true in situ measurement technique.
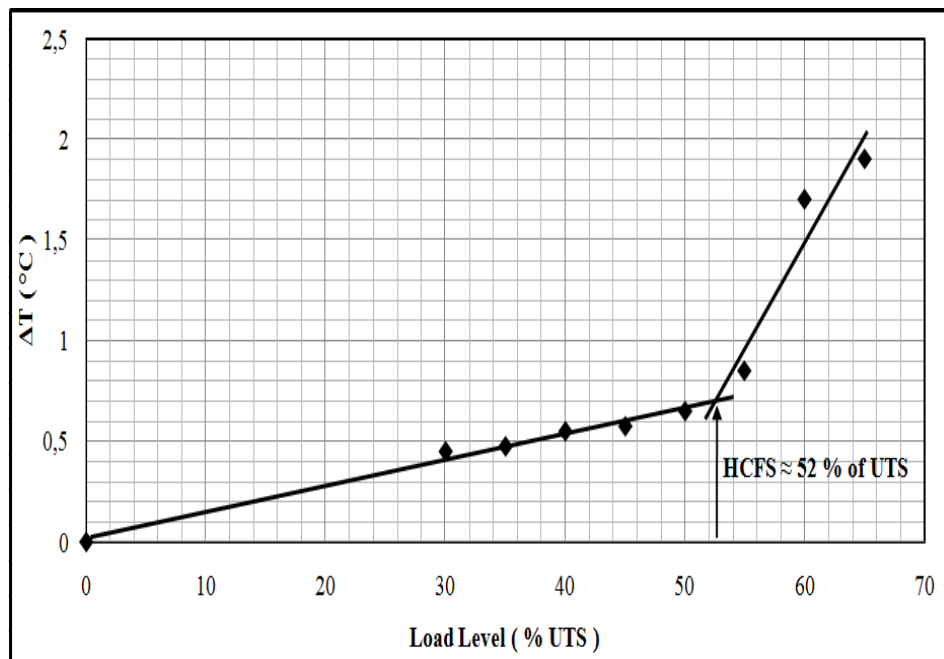
Figure 4.25 HCFS of GFRP 90° by thermography method

Fig.4.25 confirms the HCFS of 52 % of UTS, which is the similar results with 4% of error that obtained by plotting the Wöhler S-N curve in Fig.4.17. It is confirm that, ΔT_{stable} on specimen surface under fatigue loading for each load level is in fact the representative of dissipation of heat which may be due to the appearance and propagation of different damage mechanisms occurs inside the material. The shorter of fatigue life (in cycles) from Wöhler S-N curve and the significant increase of temperature from thermography method after the HCFS point or fatigue threshold, represents a transition in the damage state, or perhaps a change in damage propagation on different size scales from micro scale to

macro scale [61]. It can be noted that HCFS determined by thermography approach successfully applied for GFRP 90° material.

Further, an investigation for a quantitative characterization based on intrinsic energy dissipation was presented to validate and to coorelate the results of thermography approach. Three fundamental mechanisms are identified to be responsible for energy dissipation in fiber-matrix composites [55-57]:

- Fracture and failure of the fibers;
- Frictional sliding that takes place in the fiber matrix interphase
- Viscoelastic nature of polymer matrix

Under cyclic loading, it is known that intrinsic energy dissipation in composites could be due to different modes of cracking or local matrix deformation, results in a corresponding dissipation of heat every cycle [56]. The energy dissipation is identified as the area enclosed by a hysteresis loop for one particular cycle and several cycle according to cycle in ΔT_{stable} period, as ilustrated in Fig.4.26.
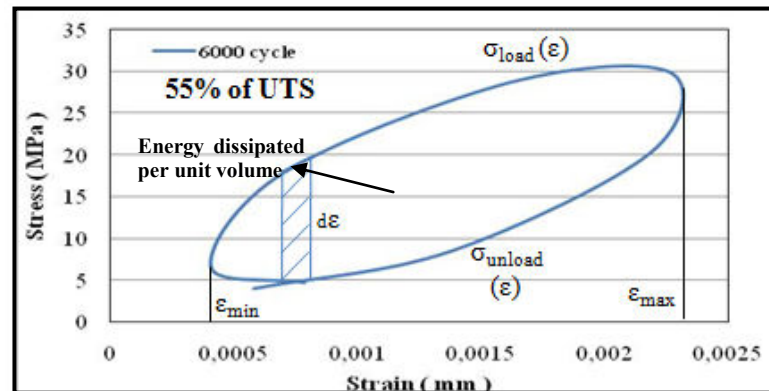
a. One cycle
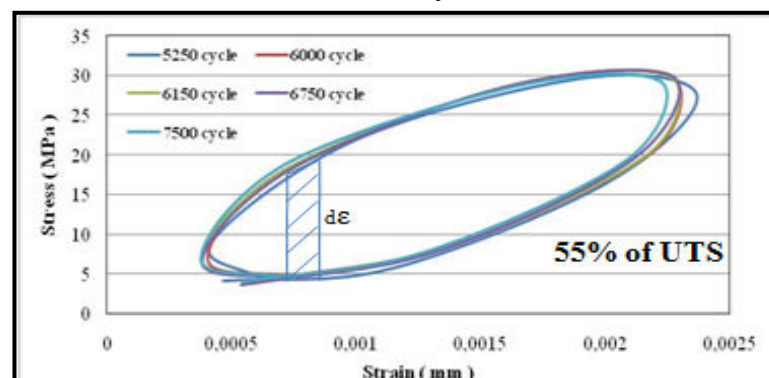
b. Several cycles

Figure 4.26 Ilustration of energy dissipation under 55% of UTS fatigue loading for GFRP 90°

From Fig.4.26 above, it found that there is no significant different of energy dissipation during the period of ΔT_{stable} under fatigue loading. The energy dissipated (E_d) was measured on the area of hysteris loops by the equation (40). By comparing the energy dissipated during a particular cycle in the fatigue tests during which temperature is stable (e.g., cycle 6000 or between 5750 cycle and 7500) for each load level, a correlation between the energy dissipation and the load level was created. A plot of the energy dissipation per unit volume as a function of the load level is shown in Fig.4.27.
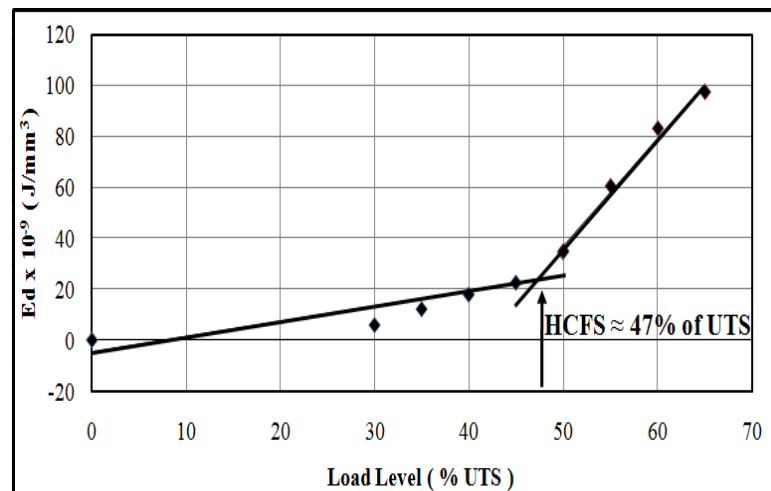
a. based on one particular cycle (i.e., 6000 cycle)
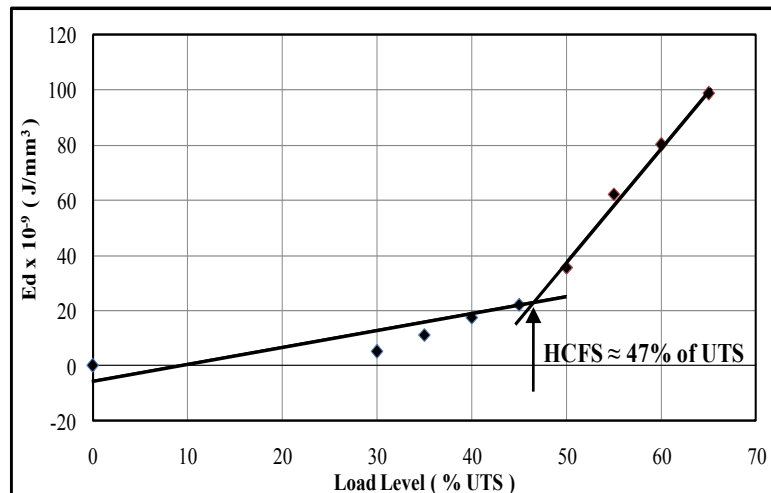
b. based on several cycles between 5750 cycle and 7500 cycle

Figure 4.27 HCFS of GFRP 90° by energy dissipation

Fig.4.27 shows how the HCFS is determined using a graphical procedure based on in situ measurement technique of energy dissipation. The HCFS of ≈ 47% of UTS obtained by energy dissipation was found no significant different to

that obtained using thermography method (Fig.4.25) and also from Wöhler S-N curve (Fig.4.17). It can be statedthat the thermography method is suitable for in situ characterization of HCFS with an error less than 10% respect to Wöhler S-N curve and energy dissipation approach.

Furthermore, a plot between energy dissipation per unit volume and ΔT_{stable} for each load level of fatigue test to have the relationship between thermal dissipated detected by IR camera and energy dissipated from the hysteritic heating was established, as seen in Fig.4.28.
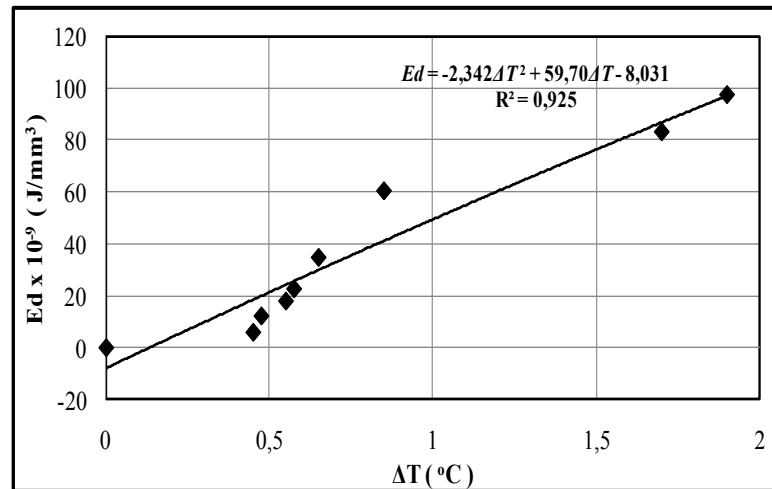
a. based on one particular cycle (i.e., 6000 cycle)
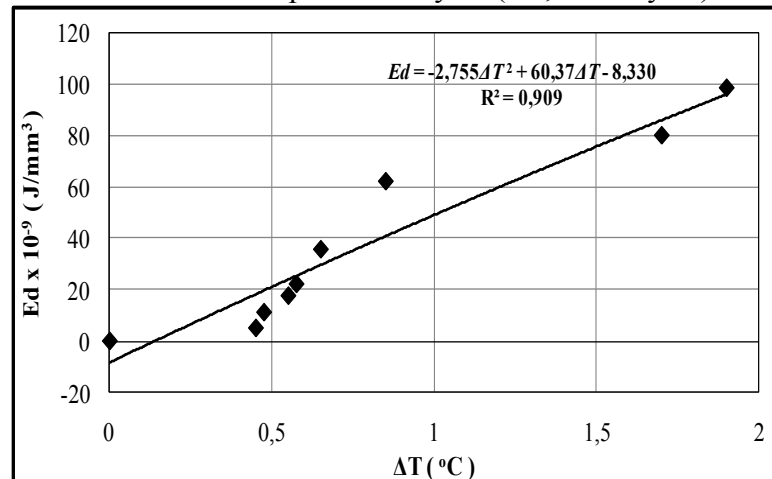
b. based on several cycle between 5750 cycle and 7500 cycle

Figure 4.28 Energy dissipation versus ΔT_{stable} of GFRP 90° for different load level

The relation between stabilization temperature profile and the energy dissipation during fatigue test can be approximated by a polynomial function with a data correlation factor, R^2 close to 1. It can be said that the increasing of temperature detected by IR camera on specimen surface as a result of thermal

dissipated is in fact due to energy dissipation of the material. The main damage mechanisms of GFRP 90° causing energy dissipation could be attributed to the damage appearance and propagation of matrix cracking, interface cracking/friction among others, and fiber fracture.

Thermography method that determined the S-N curve based on previous study [59,61] also presented for GFRP 90°. The S-N curve according to parameter Φ as a function of the stabilization temperature and the number of cycles to failure. The value for the parameter Φ for unidirectional glass fiber composite (GFRP 90°) was approximately Φ_{avg} = 4.1 °C log(cycle). Using Φ_{avg} , the S-N curve is created as shown in Fig.4.29.
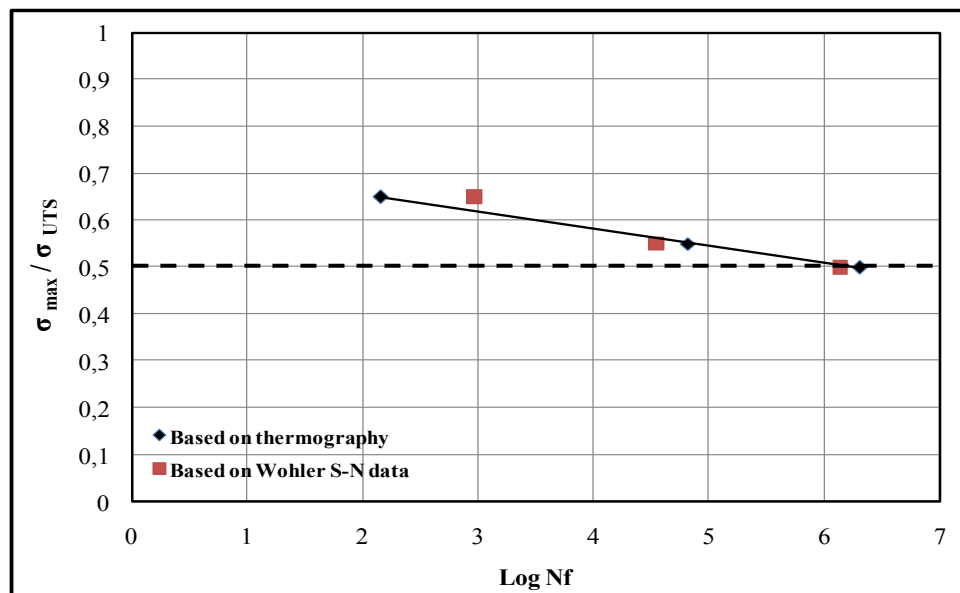
Figure 4.29 S-N curve based on thermography approach using Φ parameter

Figure 4.29 shows that the S-N curve obtained with thermography approach has a good agreement with the experimental data of Wöhler S-N curve (Fig.4.17). As a section conclusion, it proves that thermography and energy dissipation approaches can be successfully used to determine high cycle fatigue strength of GFRP 90° material. Or in other words a passive thermography method exists where the damage is characterized by the temparature increase during fatigue testing due to the hysteritic heating [56].Thermography approach also can be used to determine the S-N curve for GFRP 90°. The results found by these fairly quick approaches are in good accordance with those issued from the traditional Wöhler S-N curve which is therefore longer to obtain.

Chapter V.   TENSILE (STATIC AND FATIGUE) TESTING AND DAMAGE OBSERVATION OF DISCONTINUOUS CARBON FIBER COMPOSITE (DCFC) BY THERMOGRAPHY

5.1   Tensile static testing and damage observation of DCFC by thermography

In this section, a detailed analysis of DCFC specimen with and without hole will discussed. The following classes are of practical interest :

- Mechanical and damage characteristic
- Thermography observation on damage behaviour

Detailed discussions of the relevant experimental results will be presented within each corresponding section.

5.1.1 Tensile static testing of DCFC specimen without hole and damage observation by thermography

As mentioned before in literature review from several previous studies [84-94], DCFC has a natural non-homogenous behaviour coming from random chip form as reinforcement. In order to investigate its effect on stiffnes characteristic of the material, a series of tensile tests is conducted while systematically varying strain gage location. Six of single strain gages with 5 mm of length were placed on specimen surface, of which three were on the front face and three were on the back face. Based on strain propagation for each strain gage, stress-strain curve can be obtained. Fig.5.1 shows the result of stress -strain curve from tensile loading.
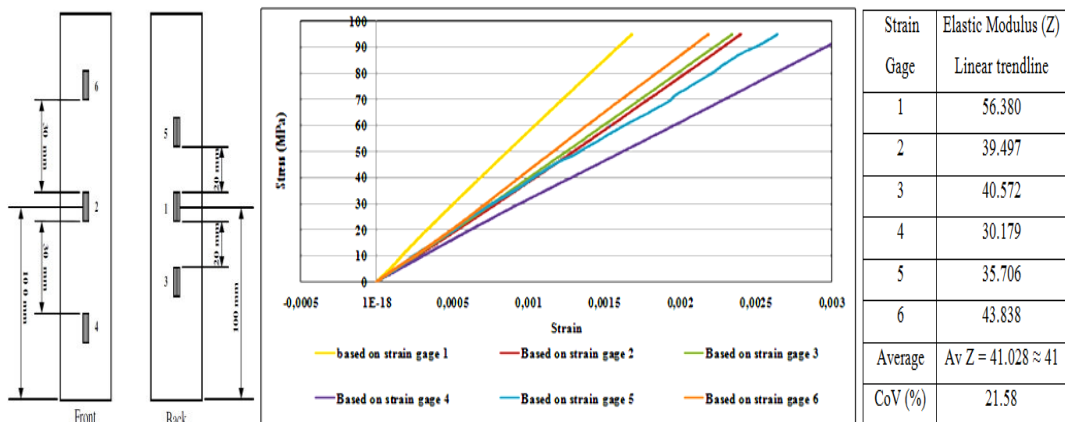
Figure 5.1 Stress-strain curve of DCFC without hole

The test conducted not until failure in order to have the modulus measurement and make the comparison for each value. Result shows that this form of discontinuous fiber composite specimens, exhibit high surface strain variations, along the length of a typical tensile specimen. It appears that the surface strain is the result of the whole underlying laminate meso-structure, which in turn means that the orientation of the chips through the entire thickness of the specimen dictates the surface strain behaviour [71]. These in turn lead to variation in modulus measurements by as much as 26.4 % and a CoV of variation as high as around 22 %. This variation of modulus measurement characterized by a highly non-homogenous substructure derived from fabrication process using random chip fiber of reinforcement form. In order to characterize the non-homogeneous behaviuor of DCFC, it could be considered to apply NDT method of DIC / digital image correlation (Appendix B) compared to strain gage as also recommended by previous study [92].

Further investigation for DCFC specimen without hole is tensile test until failure the observed the specimen surface with IR camera. Typical tensile test results of discontinuous carbon fiber composite (DCFC) is shown in Fig.5.2.

| a. Tensile curve | b. Modulus measurement |
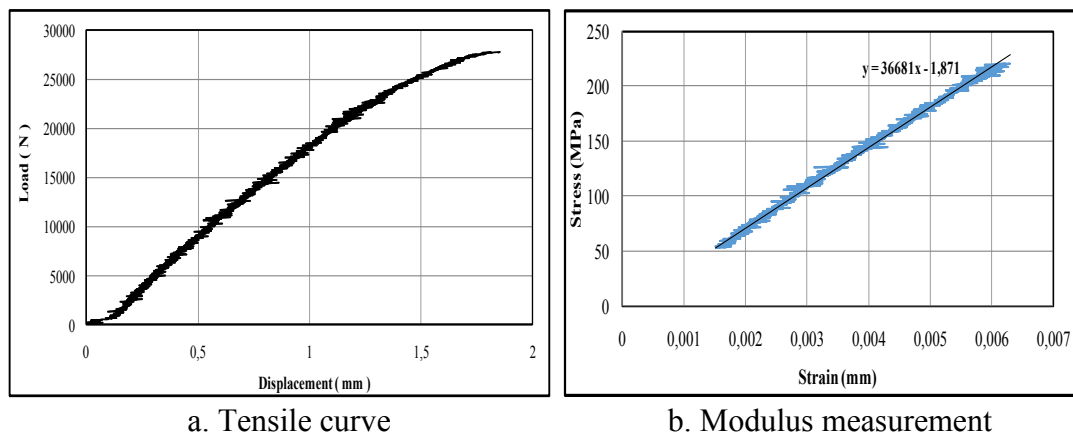
Figure 5.2 Tensile curve of DCFC

The tensile curve exhibits some non-linearity with the ultimate tensile load is 27. 8 KN resulting 278 MPa of ultimate tensile strength (UTS) at 1.85 mm of cross-head displacement. As a reference, UTS of discontinuous carbon fiber specimen without hole given by previous study [87] was vary between 231 MPa – 284 MPa depend on specimen width and hole diameter. For the modulus measurement, only counts the linear relationship between stress and strain in

order to ensure the behaviour remains in the purely elastic region. Stress increase calculates from the given load and strain based on cross head displacement that resulting 36.67 GPa of global modulus elastic. This global modulus elastic has slightly higher with micromechanical analysis of rule of mixture (Appendix C).

This specimen of DCFC without hole was failed in a brittle type and perpendicular with loading direction as seen in Fig.5.3. It was found that the specimen failed as a combination of two failure modes as also described by previous study [91] :

1. Cracking, or separation along the surface (chip /matrix debonding) and chip cracking that perpendicular to the chip axis.

2. Delamination caused separation along the thickness that parallel to the chip length
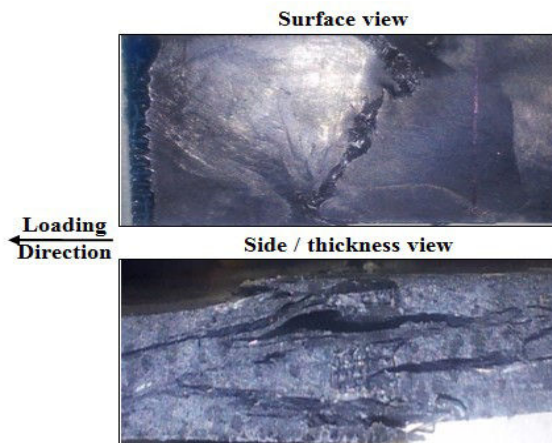
Figure 5.3 Catastrophic damage form of DCFC under tensile loading

Using the information comes from uniaxial strain gages of 5 mm located at two different location at specimen surface, Fig.5.4 shows the stress-strain curve and modulus measurement.
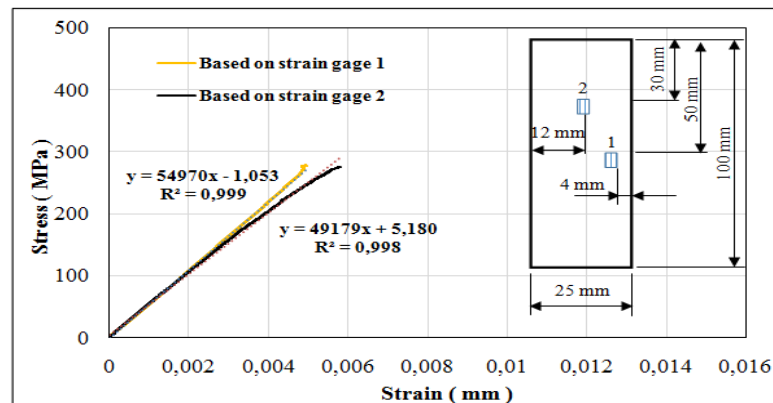
Figure 5.4 Stress-strain curve of DCFC specimen

There was a different of linearity behaviour of modulus measurement which clearly shows modulus measurement based on strain gage 1 perfectly linear until failure and modulus measurement based on strain gage 2 has an initial non linearity behaviour after reach a certain level of stress-strain until failure. Fig.5.5 below shows the illustration of modulus change of linearity behaviour.
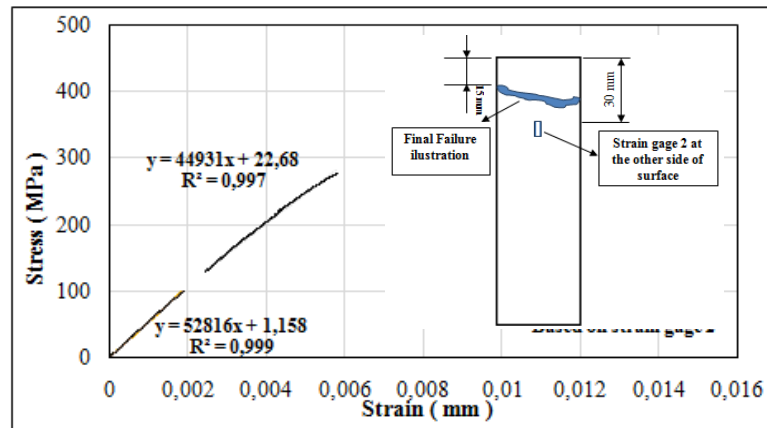
Figure 5.5 Change of modulus measurement of DCFC

This change of linearity behaviour of modulus measurement could be caused by micro damage/defect due to micro cracking in substructure between chips that occurs around the gage area that has an effect on strain detection and finally resulting larger strain compare to strain level that detects by other gage. This initial damage provokes the damage propagation and leads to catastrophic failure around the gage that located near to failure area. The other possibility of this non linearity behaviour is because of non-homogeneous nature of chip distribution and orientation in mesoscopic level in material. It is possible to consider that the distribution of chips affect the macroscopic modulus measurement may be responsible for producing locally lower mechanical properties than create local high strain and affect the local load distribution to accelerate damage. These possibilities then confirmed by location of final failure that close to the position of strain gage that used to measure the non-linear modulus behaviour.

It is reasonable to concluded that the decreasing of modulus measurement resulted by strain evolution of strain gage is due to the damage propagation of the failure area, compare to other gage at area without failure that resulting linear modulus measurement or clearly there is no decreasing of modulus measurement.

During the test, specimen surface also observed by IR camera to follow the evolution of temperature, as seen in Fig.5.6.
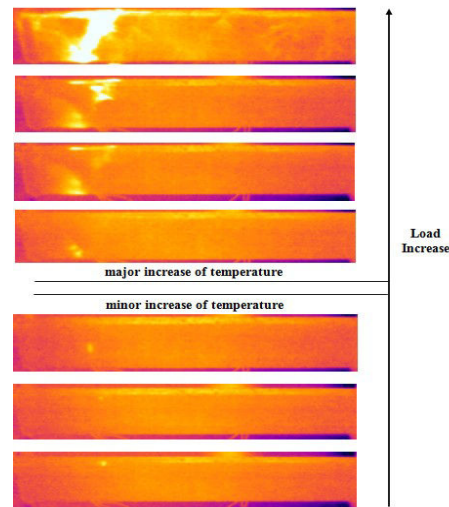
Figure 5.6 Thermography images of DCFC without hole

The area profile is used around failure area location to have all change of the maximum temperature. Fig 5.7 below shows the temperature change as a part of minor increase of temperature.
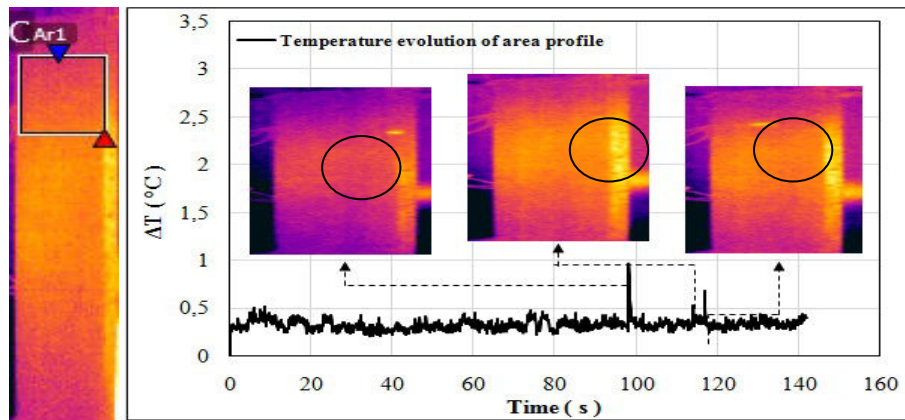
Figure 5.7 Delta-T spots of DCFC specimen during tensile loading

Several small increases of temperature on specimen surface are able to detect by IR camera at different time which occurs before final failure. Using terms of 'delta-T spots' by previous author [90], the delta-T spots (black circle) that detected by IR camera vary between 0.3 – 0.9 °C. ΔT above 0.5 °C was clearly showing by several peak of delta-T spots as seen in Fig.5.7. These delta-T spots had characteristic features like flashes of lighting and visible for a few seconds only by means of the IR camera.

The presence of temperature increase as known as delta-T spot possibly appears due to initial micro damage coming from lower mechanical properties as a result of manufacturing defects of non-homogeneous nature. This phenomenon also confirmed by previous study [91] explained that delta-T spots captured by ultrasonic c-scan in discontinuous carbon fiber composite likely correspond to swirls defect (regions of fiber kinking resulting from high flow) or resin-rich pockets. The level of these temperature increases depend on the intensity of the damage and its position in the material thickness. Furthermore, delta-T spots which located at the edges of the specimen could be possibility of other typical micro defect due to the cutting process of the specimen. Previously [85], this similar condition concluded that most cracks detected at the edge by optical observation can induce microscopic defects since the specimen is more easy to early crack due to cutting process. The value of ΔT profile around $0.5 \leq \Delta T \leq 1^{\circ}C$ shows the safety increasing of temperature or as a ΔT threshold due to the presence of the damage of DCFC under static tensile loading.

The obserevation by IR camera then compared with strain gage to confim the appearance of initial micro damage as seen in Fig 5.8. This figure indicates damage occurs that detect by higher peak of delta-T spots and strain gage results. For DCFC specimen without hole, it is observed a good agreement between the two measuring technique. Damage that detected by higher increasing of temperature also confirms by strain gage with a small discontinuity in the strain-time curve at the same time and damage area. In other words, the damage of DCFC affects the measurement taken by thermography and strain gage.
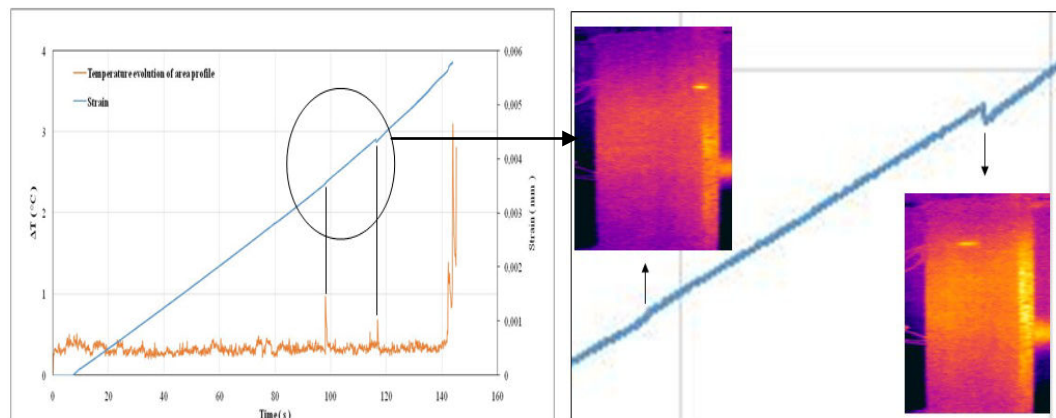
Figure 5.8 Strain and temperature evolution of micro damage of DCFC

After the emergence of delta-T spot, temperature changes to have a higher increase of temperature that confirmed the appearance of macro damage. It was found that, after the appearance of several delta around 66 % - 80% of UTS (184 MPa-221 MPa), specimen then continue to sustained the tensile load until specimen seems to suffer first macro damage. Fig 5.9 shows the temperature evolution and stress for micro and macro damage appearance.
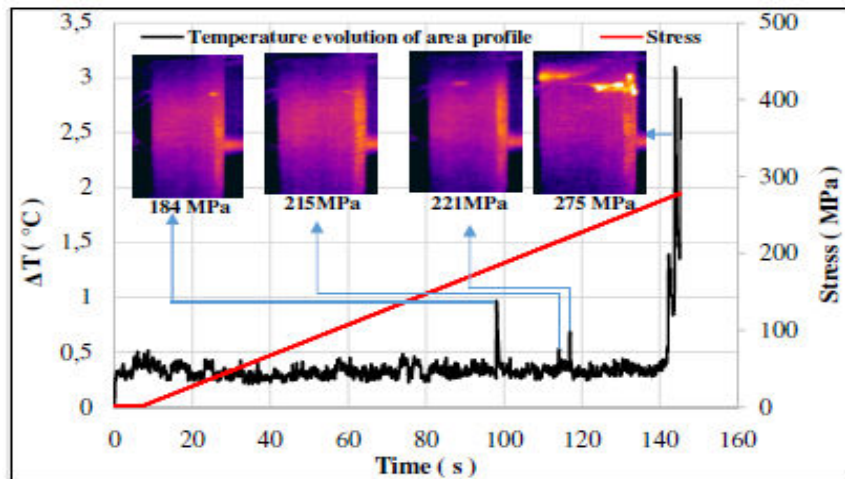
Figure 5.9 Stress and temperature evolution of DCFC

In sum, initial macro damage shown by $\Delta T \approx 1.38$ °C - 3.07°C provokes the occurrence of catastrophic or final failure of the specimen that induce the highest peak of temperature at $\Delta T = 27.2$ °C. Fig.5.10 shows the temperature evolution on specimen surface where all the three images indicate thermography image of final failure period of tensile test .
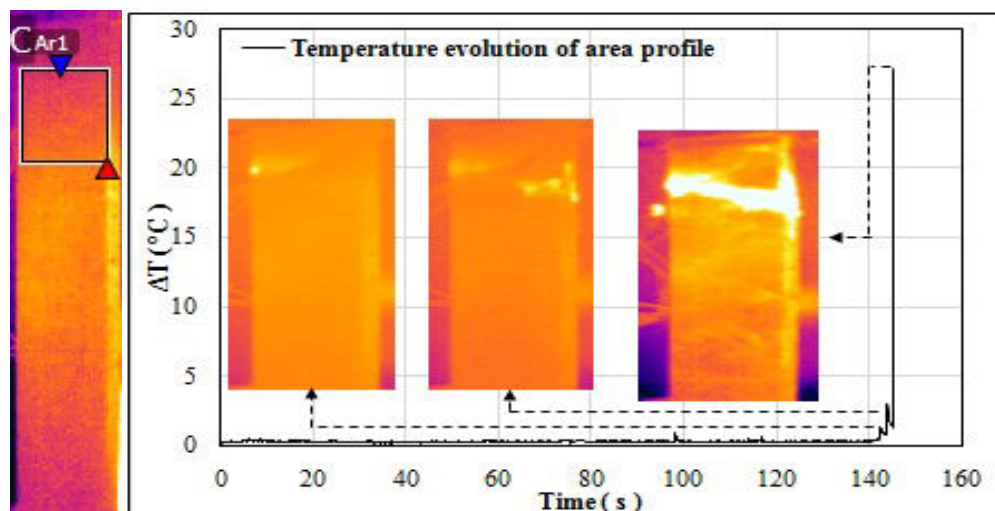
Figure 5.10 Temperature evolution at final failure period

From the temperature evolution during tensile test, the presence of several delta-T spots could be possible to indicate the area of final failure which are exist and concentrate in the region of failure area. Meanwhile, as the initial micro damage that detected by IR camera, these delta-T spots do not show as the beginning of damage propagation or the initial damage of macro damage. From thermography images, clearly show that initial macro damage occurs not propagate or start in the location at one of delta-T spots that detect by IR camera. The delta-T spot with more intense and less intense does not grow significantly during the test and eventually does not affect the initial presence of macro damage that leads to the catastrophic failure. This behaviour of DCFC under tensile loading is not the same as for continuous fiber composite (CFC). In CFC, the crack initiation or delta-T spot as it is known here, is often defined as failure or we can say that micro defect can dictates the propagation and the location of macro defect. This phenomenon also confirmed by previous study [91] explained that damage detected by C-scan as delta-T spot does not come and grow from pre-existing defects of manufacturing defects due to varying nature substructure although it appears in their nearness.

It can be stated that, non-destructive observation of thermography can be used to characterize the defects referred to increase of temperature or as 'delta-T spot' which minor increase of temperature due to manufacturing defect and major increase of temperature caused by macro damage under tensile loading [90]. There is no clear relation between both type of temperature increase since the initial macro damage does not propagate from earlier delta-T spot with minor increase of temperature even locate around the final failure area.

5.1.2 Tensile static testing on DCFC specimen with hole and thermography observation

This experimental test has the aim to observed the damage behaviour of DCFC due to the presence of circular notches (hole) by thermography. First experimental was used specimens with 0.2 of ratio between hole diameter and specimen width (d/w = 0.2).

Fig.5.11 below shows the relation between force from given load of the machine and cross-head displacement as the results of tensile test. The tensile curve exhibits some non-linearity with the ultimate tensile load is 32 KN resulting 400 MPa of ultimate tensile strength (UTS) at around 2.5 mm of cross-head displacement.
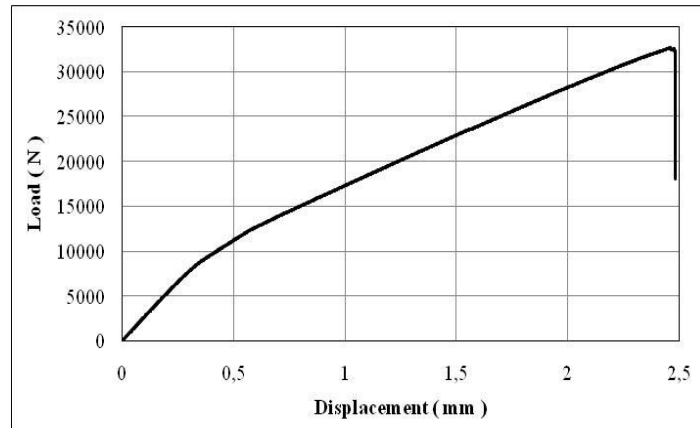
Figure 5.11 Tensile curve of DCFC with hole

As a comparison, the ultimate tensile load is slightly higher than with DCFC without hole. It means that, no decrease in gross section strength (regardless the presence of the hole section) or it can be described that DCFC has insensitive behaviour due to the presence of the hole as well explained from previous studies [87,94]. For the modulus measurement (Fig.5.12), only counts the linear relationship between stress and strain in order to ensure the behaviour remains in the purely elastic region. Stress increase calculates from the given load and strain based on cross head displacement that resulting 27.25 GPa of modulus measured.
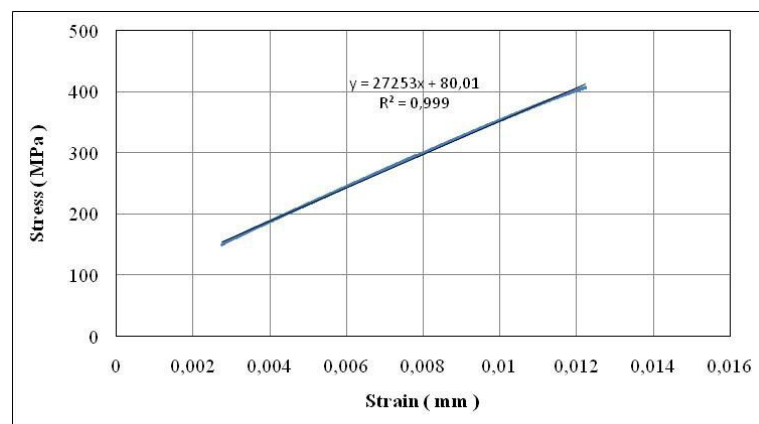
Figure 5.12 Stress - strain curve of DCFC specimen

From the final failure appearance as seen in Fig.5.13 , it was found that the specimen failed in a brittle model and position of the failure were not at the tip of the hole of far from the hole and perpendicular against loading direction.

No failure around the hole   **Chip/matrix debonding**

Fiber fracture   **Delamination**
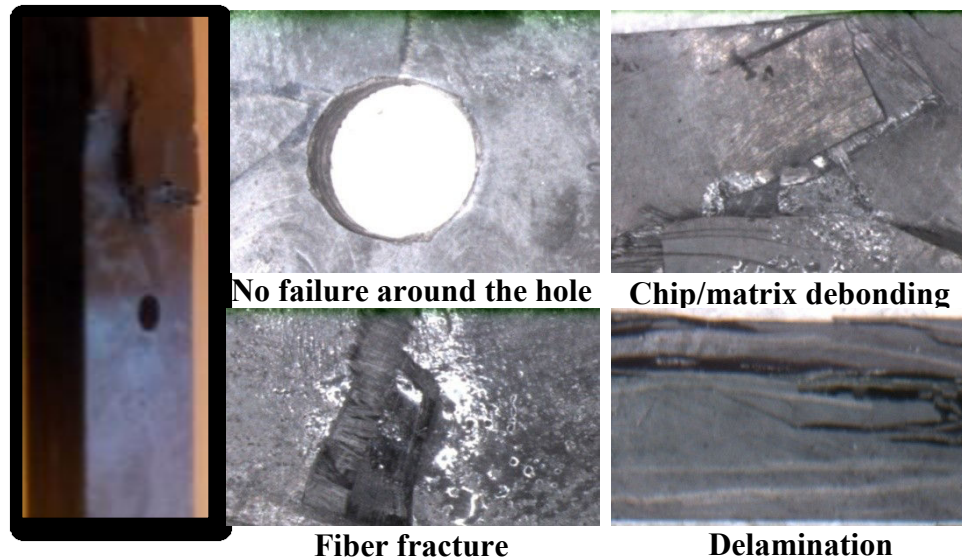
Figure 5.13 Damage tipe of DCFC under tensile loading

From Fig.5.13 above, it was found that the specimen with and without hole have similar failure type where failed as a combination of two failure modes as also described by previous study [91] :

1.   Cracking, or separation along the surface (chip /matrix debonding) and chip cracking that perpendicular to the chip axis.

2.   Delamination caused separation along the thickness that parallel to the chip length.

Damage evolution of this DCFC composite seems to start toward the surface as a typical of brittle fracture shown by chip/matrix debonding and chip cracking. Then propagated through a few chips the transform into delamination at the thickness side of the specimen until reaches the final failure. The presence of final failure that far from the hole is in fact an artefact of insensitive behaviour of DCFC material, as also explained by previous authors [87-94].

This test was also observed by IR camera to detect the temperature evolution on specimen surface associate with the presence and location of damage is likely to occurs. From the result of thermography observation in Fig.5.14, the

IR camera was detected several random location of delta-T spots (red circle) mostly in gross area (far from the hole) and vary between 0.2^{o}C – 1.5^{o}C.
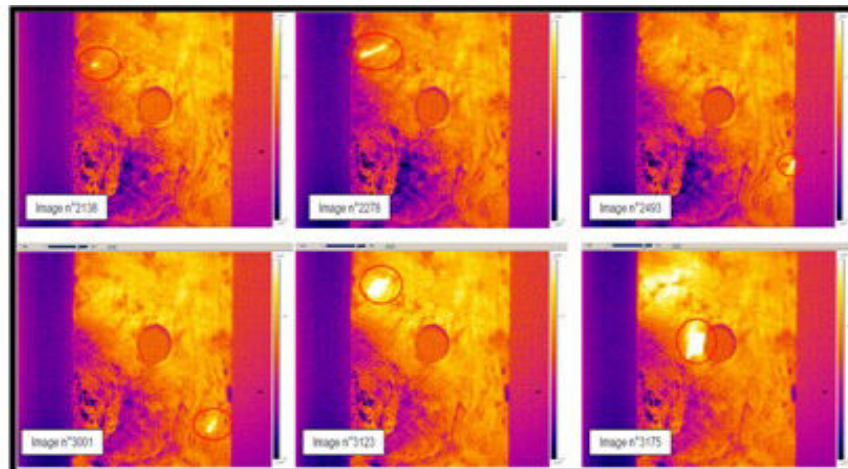
Figure 5.14 Delta-T spots of DCFC with an open hole specimen

This appearance of several delta-T spots could be correspond to micro damage mechanisms caused by manufacturing process which seem to indicate the real defects, such as resin-rich area, swirl defect (region of fiber kinking resulting from high flow, and also porosity due to the presence of void. As well as DCFC specimen without hole and also described from previous study [85], delta-T spots at the edge of the specimen width are related to micro defects as a result of early cracks since the specimen was cut,as ilustrated in Fig.5.15. This could be other possibility of first defect can induces microscopic damage, which are initiators as many micro damage inspected at the edge.
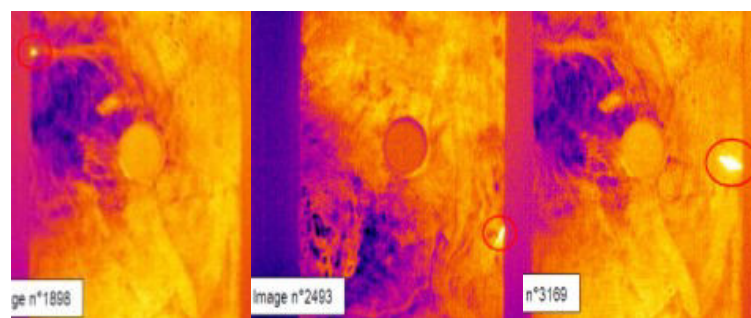
Figure 5.15 Micro defects at the edge of the specimen of DCFC

Those initials damage locations do not indicated the position of final failure sometimes delta-T spots occured at the tip of the hole like image no.3175 in Fig.5.14. The observation results on thermography give a good detection on insensitive behaviour of DCFC, with delta-T spots mostly occur in the gross

section away from the hole. The presence of delta-T spots can't precise in determining or predicting the final failure area, since the presence of delta-T spots have no good indication as initiators of macro damage appearance then leads to final failure, as same as found in DCFC specimen without hole. Although, delta T-spots of DCFC specimen can be seen around final failure location. In addition to previous explanation, this DCFC specimen is not repeatable, hence the material state can be vary dramatically between specimens due to the local meso-structre and can lead to different results related with micro damage and final failure appearance. This behaviour is not commonly to occur like traditional fiber composite nor isotropic materials where the damage is typically initiate by stress concentration around the hole. The contradiction of damage behaviour of this material is likely caused by non-homogeneous of material form which have large stress concentration at the end of chip plate form and also may due to large disparity in stiffness between the epoxy and carbon fiber which may lead to have a local stress as explained by previous authors [3,87,89-92,94]. The other reasonable explanation for this uncommon behaviour is porosity caused by void from molding process. This void effect on surface crack of discontinuous carbon fiber composite was also described by Boursier and Lopez [85]. From micrograph results, they found a shallow surface crack that likely started at the surface voids. Fig 5.16 shows the ilustration of critical area of non-homogeneous form resulted by manufacturing process compared with microscopic observation of final failure.
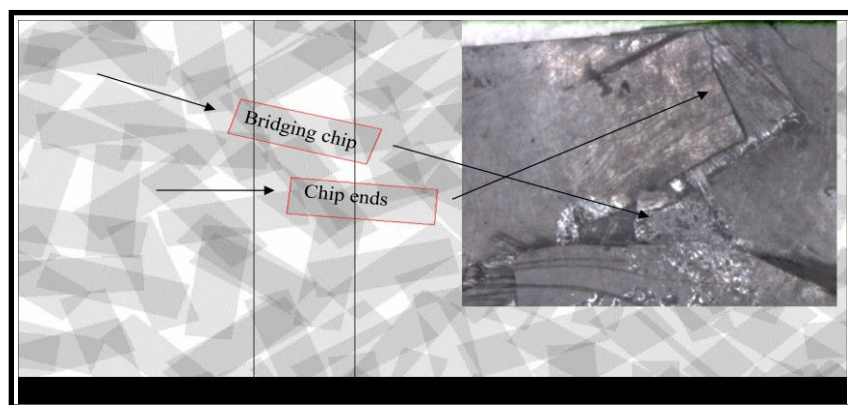
Figure 5.16 Critical area of DCFC

From Fig.5.16, shown that final failure occurs due to bridging chip and chip ends as the critical area. It means that the chip plate of material form has greater

stress concentration a the chip ends compare to the stress concentration of an open hole, and can therefore a reasonable effect for initiating damage not at the tip of the hole or away from the hole. Or in other words, the stress concentration of inherent material produced by non-homogeneous form of local meso-structure was found higher than the geometrical stress concentration due to the presence of the hole.

Based on tensile test results and thermography observation, It can be concluded that thermography successfully detects insensitive behaviour of DCFC due to an open hole condition. However, thermography itself has no good ability in locate the final failure area due to the limitation to observe the local meso structure in non-homogeneous form that can indicate the critical area as a cause of macro damage and final failure.

In [94], to ensure damage at the edge of the hole by isolate the effects of the internal stress concentration due to heterogeneous nature of material from the geometrical stress concentration of the hole, it is possible to use a constant ratio of hole diameter and width of the specimen (d/w ratio). The different d/w ratio were selected according to [94] which using a hole-to-width ratio of ≥ 0.375 to have fail at the hole.

As the second experiment using DCFC specimen with hole, next investigation conducts with d/w ratio of 0.4 for rectangular specimen of DCFC in order to have fail within the net section area at the edge of the hole. Fig.5.17 below shows the final failure location at the edge of the hole.

Figure 5.17 Rupture of DCFC with D/W ratio of 0.4

From result above, it can be seen that damage location occurs at net area or at the edge of the hole for hole diameter (d) of 10 mm and specimen's width (w) of 25 mm. This damage behaviour means that the hole insensitive of DCFC has been

shown to be sensitive for a critical d/w ratio of 0.4. This D/W ratio of 0.4 then use as specimen configuration of DCFC for next investigation of damage behaviour under static and fatigue loading and also observed by NDT methods. The tensile curve of discontinuous carbon fiber composite with hole is shown in Fig.5.18.
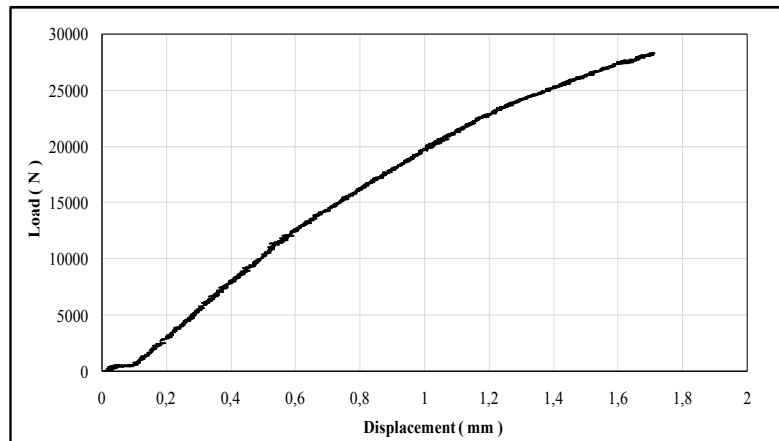
Figure 5.18 Tensile curve of DCFC with hole

The tensile curve exhibits some non-linearity with the ultimate tensile load is 28. 2 KN resulting 470 MPa of ultimate tensile strength (UTS) at 1.7 mm of cross-head displacement. As a comparison, the ultimate tensile load is slightly higher than with DCFC without hole. It means that, no decrease in gross section strength (regardless the presence of the hole section) or it can be described that DCFC has insensitive behaviour due to the presence of the hole as well explained from previous studies [87,94]. This specimen of DCFC with hole also failed in a brittle type and perpendicular with loading direction at both edges of the hole as seen in Fig.5.19.
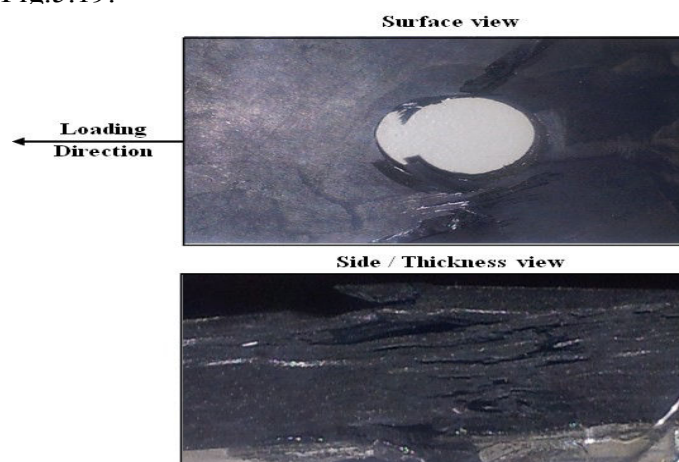
Figure 5.19 Damage form of DCFC with an open hole

From Fig.5.19 above, similar damage form reported in [91], shows the same kind of failure mode with the specimen without hole which consists of cracking and delamination form, The cracking form was found in combination of chip debonding cracking that perpendicular to the load axis. Further, delamination caused separation along the thickness that parallel to the load axis and chip length.

Using the information comes from uniaxial strain gages of 5 mm located at two different location at specimen surface, Fig.5.20 shows the stress-strain curve and modulus measurement. To calculate the open hole strength of composite materials, two approaches can be used that reported by previous study [86]. The first calculates the net strength defined as :

$$\sigma_{OHT} = \frac{P}{(w-d)\,t} \tag{32}$$

And second calculates that negligible the presence of the hole defined as :

$$\sigma_{UHT} = \frac{P}{w\,.\,t} \tag{33}$$

where σ_{OHT} is the stress of open hole specimen and σ_{UNT} is the stress of unnotched specimen, while w is the width of the specimen, d is the hole diameter and t is the specimen thickness.
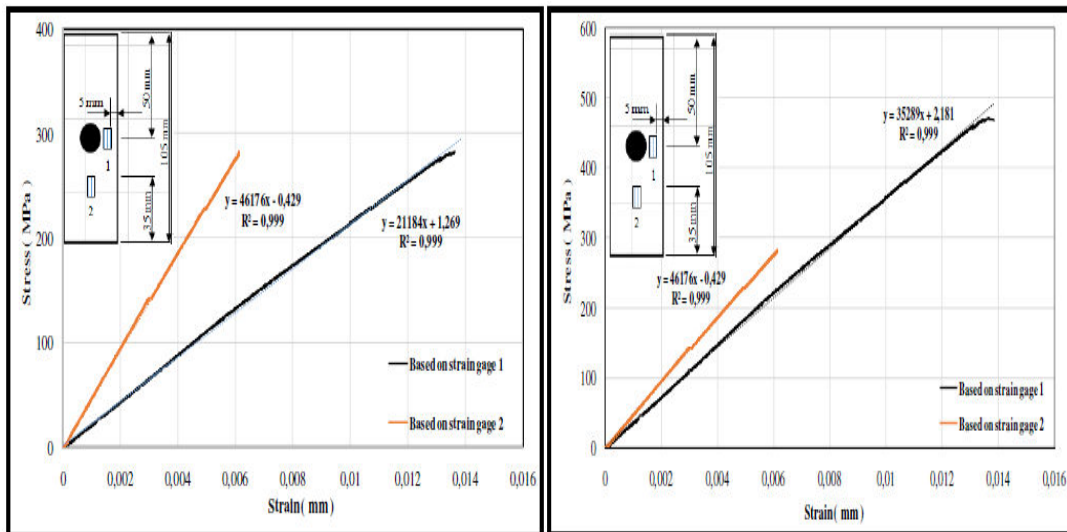
a. Stress-strain curve of DCFC   **b. Local stress-strain curve of DCFC**

Figure 5.20 Stress-strain curve of DCFC specimen with an open hole

Fig.5.20(a) above shows the stress -strain curve using equation of unnotched specimen (eq.33) for both local area (around and far from the hole) since for this

DCFC specimen, the presence of the hole has no significant effect on strength properties. In [87], also explained that, for such a small hole there is no decrease in gross section strength for DCFC specimen. Meanwhile, locally, at the edge of the hole, higher strain occurs due to the presence of the hole. Consequently, modulus measurement for both local area have a significant different as seen in Fig.5.20(a). Further, stress-strain curve and modulus measurement are presented, which counts the local area for each strain gage for the same value of given load until final failure, as seen in Fig.5.20(b).

Fig.5.20(b) shows the results based on the stress calculation using Eq.(32) and Eq.(33) related with local area contains hole and without hole. It was found that higher local stress concentration occurs at the the hole area due to presence of the hole (indicate by strain gage 1) compared to local stress concentration at area far from hole (indicate by strain gage 2) at the same value of given load. The different result on modulus measurement was caused by different propagation of stress and strain and also possibly due to non homogeneous form of local meso structure as found before for DCFC specimen without hole where modulus can vary as high as around 22%.

Combine these two approaches to calculate strength, locally, the presence of the hole gives the lower area on specimen around the hole area so that increasing the strength calculation. At the same time and loading period, the area that contains no hole, is resulting larger area thus reducing the calculate strength. This is clearly shown by Fig.5.22 that there is a different local stress concentration level between both area with and without hole even at the same time of loading period. The local stress concentration for local area at the edge of the hole was found around ≈ 1.7 times compared with area far from hole. This experimental results has no significant different with analytical results of local stress concentration at hole area, where found around ≈ 1.86 times (Appendix D). As a result, specific area without hole experiences small strain propagation due to the lower stress compared with specific area with hole that sustains large strain propagation due to the higher stress. These different condition of stress-strain for both specific area, ultimately has an effect of modulus measurement. It shows that this form of discontinuous fiber composite specimens, exhibit different surface

strain variations, along the length of a typical tensile specimen. It appears that the surface strain is the result of the whole underlying laminate meso-structure, which in turn means that the orientation of the chips through the entire thickness of the specimen dictates the surface strain behaviour [92].

It can be noted that, this variation of stiffness possibly characterized by a highly non-homogenous substructure derived from fabrication process using random chip fiber of reinforcement form. This variety nature form then predisposes the different strain that detected by strain gage and in the end resulting different value of elastic modulus measurement. In our previous investigation, similar result on elastic modulus variation also occurs at different location on specimen surface which leads to have a COV as high as around 22 %. During the test, specimen surface also observed by IR camera to detect the evolution of temperature that associated with damage appears and also the location were the damage is likely to occurs. Fig.5.21 below shows the thermal images up to final failure for DCFC specimen with an open hole.
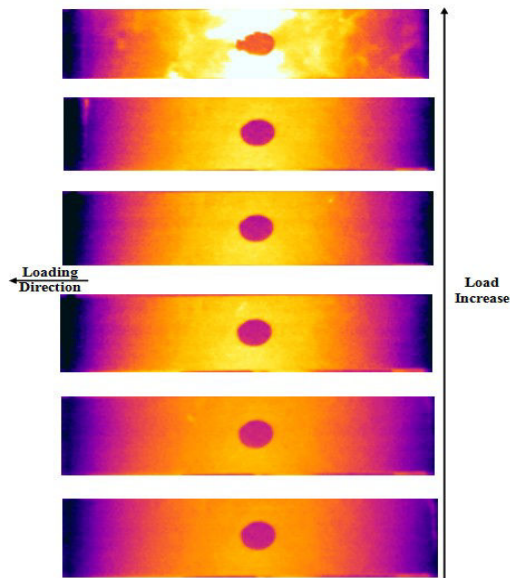
Figure 5.21 Thermography images of DCFC specimen with open hole

Several small increase of temperature on specimen surface are able to detect by IR camera at different time which occurs at random area on specimen surface before catastrophic or final failure. Using terms of 'delta-T spots', the temperature increase varies in intensity as seen in Fig.5.22 below that are of high intensity and low intense that affect the increasing of temperature.

a. Delta-T spots on DCFC   **b. High intense of Delta-T spots**
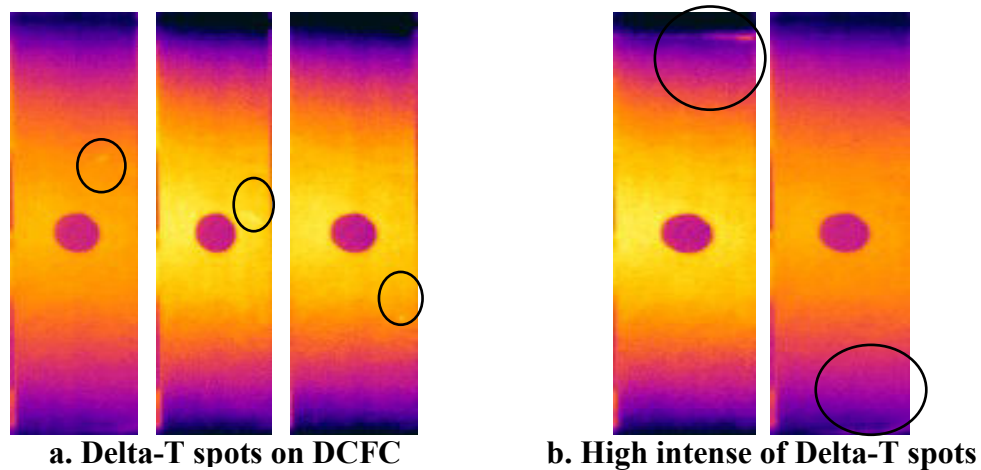
Figure 5.22 Delta-T spots on DCFC with an open hole during tensile loading

From Fig.5.22 above the delta-T spots vary in location, size and intensity. All the delta-T spot in Fig. 5.23(a) categorize as low intense or small increasing of temperature which have the ΔT between 0.4 – 0.6 °C. Apart from this low intense of delta-T spots, IR camera also detects high intense or larger increasing of temperature which locate around at the tabs, as seen in Fig.5.22(b).

Considering the local delta-T spots evolution, Fig.5.21 dan Fig.5.22 clearly indicated that most of the delta-T spots do not leading to determine the final failure location. The presence of early delta-T spots possibly brings out lower mechanical properties coming from manufacturing defects or from the non-homogeneous chips nature. As a consequence, these early hot-spots seem to represent only sporadic local damages, which do not grow nor coalesce to form macro damage. In order to follow the evolution of temperature during the test, four subdomains defined on the specimen are shown in Fig.5.23 (left) : one at each edge of the hole and the other closed to the clamps.
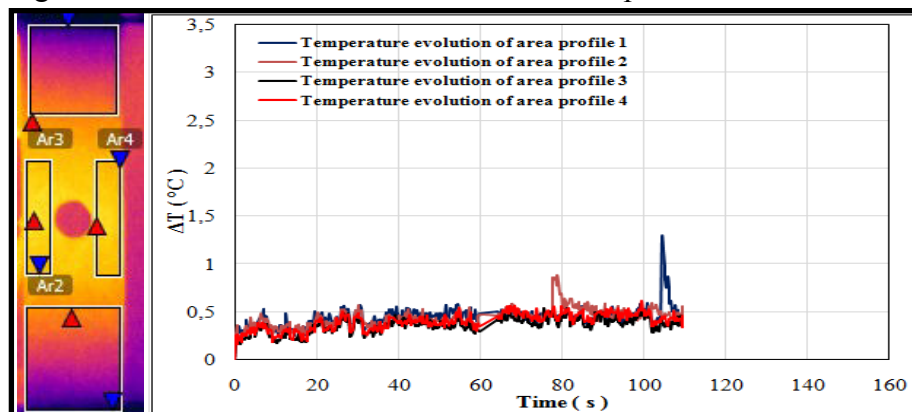
Figure 5.23 Area profile on specimen surface

During the test, all the maximum temperature change includes all those delta-T spots appear before final failure for all area observation on specimen surface will detect by IR camera. All the temperature surface that detect by IR camera vary between 0.3 – 1.4 °C. ΔT above 0.7 °C are clearly showing by several peak of delta-T spot before final or catastrophic failure. When the catastrophic or final failure occurs, suddenly ΔT reaches until the highest point of 28 °C at failure location (Fig.5.24).
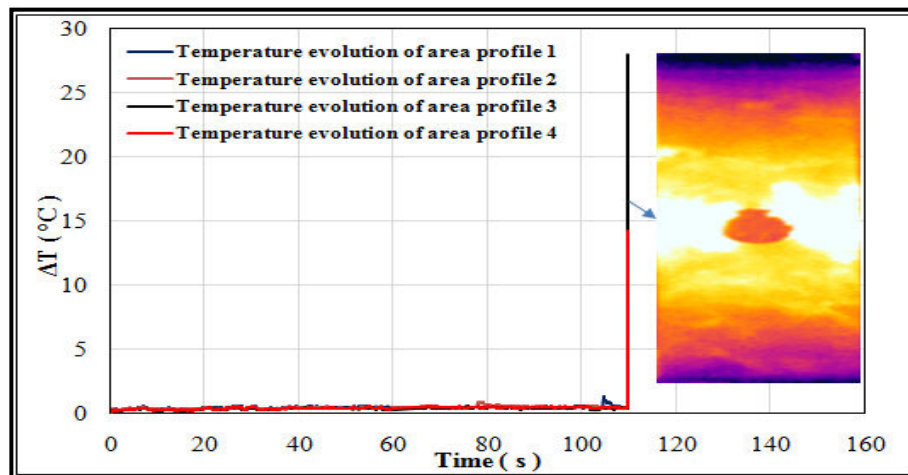
Figure 5.24 Temperature evolution on specimen surface until final failure

The increase in temperature followed by failure represents the energy which released at failure period. The energy was absorbed to deform the material before the failure. In other observation area that occurs no failure, temperature does not show the significant increase. In other words, it can be noted that failure of DCFC was characterized with a suddenly increase in temperature by releasing the strain energy. The final failure occurs at the edge of the hole which demonstrates that the hole diameter used for this study is large enough to produce such a stress concentration that the stresses in region away from the hole can be neglected. Thermography observation also confirms that all micro defects giving early delta-T spots have less effect than the hole triggering the critical damage.

As a conclusion for this section, Thermography successfully indicates damage appearence of DCFC specimen under tensile static loading. This results also confirm by relationship between stress and strain that given from mechanical test and strain gage. A small discontinuity in the stress and strain curve during the test due to the damage appearance associates with higher increase of temperature.

Fig.5.25 presents the relationship between temperature behaviour and stress-strain associates with damage appearance during the test.
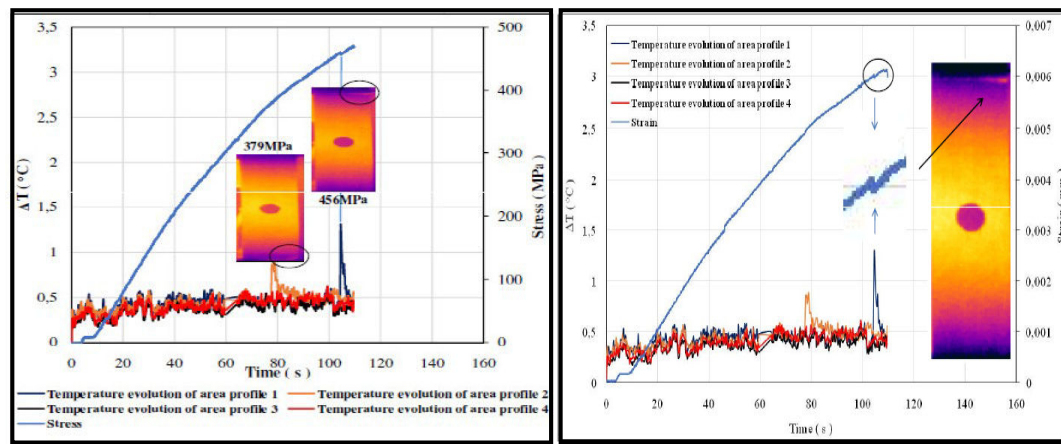
Figure 5.25 Temperature and stress-strain evolution during the test

5.2 Tensile fatigue testing and damage observation of DCFC by thermography

This section describes the experimental investigation on the fatigue behaviour of DCFC. Thermography observation applies to detect temperature distribution on specimen surface during the tests. The aim is to determine the damage evolution with respect to the number of cycles by varying the stress level applied. In practice, damages are observed by two systems. The first consist in a damage evolution during the test by strain gage and/or displacement to follow the stiffness degradation by controling the continuous decay of the elastic properties. The second system consist in an analysis under thermography observation. The change of temperature will be monitoring to have temperature profile according to damage appearance and propagation. In this way it is possible to determine the relationship of damage evolution between experimental results and thermography analysis.

Static test was initially conducted to determine the ultimate tensile strength (UTS) of this DCFC specimen with an open hole condition, which used as the maximum stress amplitude in terms of a percentage of the UTS for fatigue tests. For each value of the normalized stress $\sigma_{max}/\sigma_{UTS}$, the number of cycles Nf at which the specimen fails is reported in the S-N curve, as exemplarity shown in Fig.5.26 below.
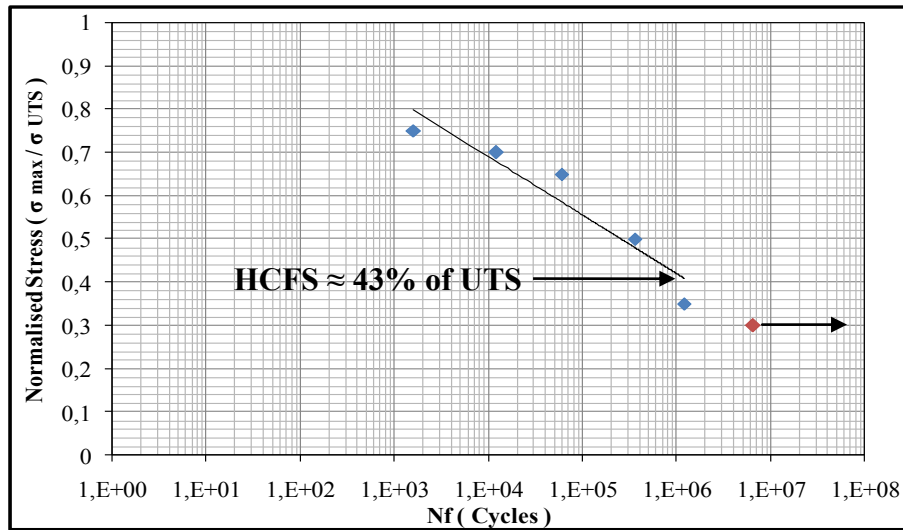
Figure 5.26 S-N curve of DCFC

The plot of S-N curve is nearly linear and there is no failure after a run-off of 7.500.000 cycles for 30% of UTS. The S-N curve shows gradual decline in fatigue strength with increase in the number of fatigue cycles. The trendline line predicts a high cycle fatigue strength (HCFS) of about ≈ 0.43, that is to say that Nf reaches 10^6 cycles when the maximum stress value is around 43% of UTS. Hence for this DCFC material, a normalised stress level of up to about 0.43 (approximately 200 MPa) can be taken as a safe value for high cycle fatigue strength (i.e. the stress correspondent to a life of more than 10^6 cycles).

The normalised S-N curve is represented by the equation,

$$\frac{\sigma_{max}}{\sigma_{UTS}} = 1.23 - b\ln(Nf) \tag{34}$$

where Nf is number of cycles, and the constant b, that represents the slope of normalised S-N curve, is called fatigue sensitivity coefficient. The value b was found to be 0.05 for this DCFC material.

Typical cumulative damage as a function of loading cycles generally described by the curve given in Fig.5.27. In these curves, D represents the cumulative damage or damage evolution defined as :

$$D = 1 - \frac{E}{E_0} \tag{35}$$

where E and E_0 are the stiffness modulus at any given loading cycle n and the intial stiffness modulus, respectively. Fig.5.27 below shows that similar behaviour occurs in damage evolution for different load level (80% and 85% of UTS).

During the first fatigue cycles, it occurs an intial rapid increase in damage evolution (an average increase about of 10 % during the first 20 % of the fatigue life). Thereafter, the damage increases slowly until being close to final failure. For the last 5% of fatigue life the damage increases suddenly and strongly as a consequence of final catastrophic failure. Damage evolution indicates that there are three stage of damage evolution in DCFC specimen. Initial micro matrix cracking damage growth of matrix cracking, chip/matrix debonding and chip cracking becomes stable. In the third stage, chip breakage take place and which caused separation along the thickness until the final failure.

a. Damage evolution for 85% of UTS (Nf = 470 cycles)   b. Damage evolution for 80% of UTS (Nf = 1580 cycles)
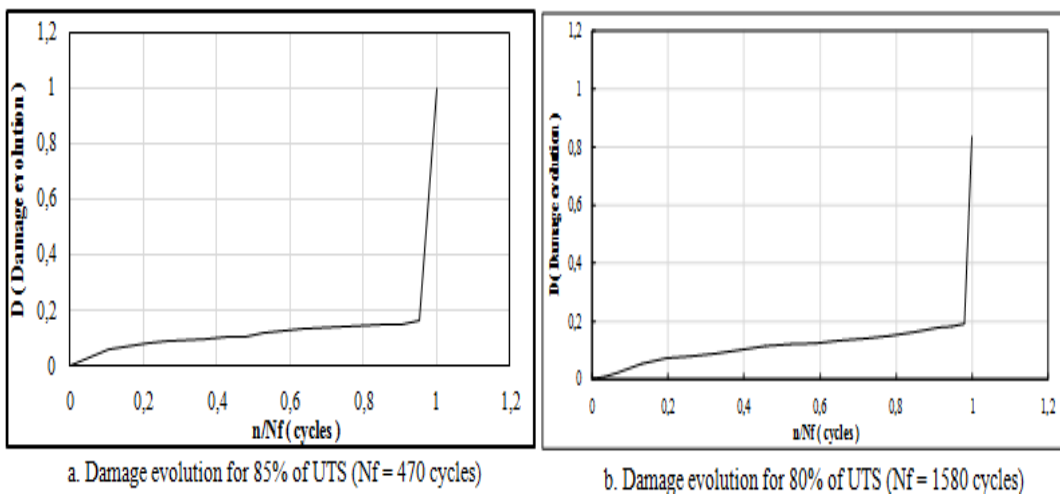
Figure 5.27 Damage evolution of DCFC

In the present study, the surface temperature (ΔT) of the specimen is evaluated by the IR camera as a function of the number of cycles as seen in Fig.5.28.
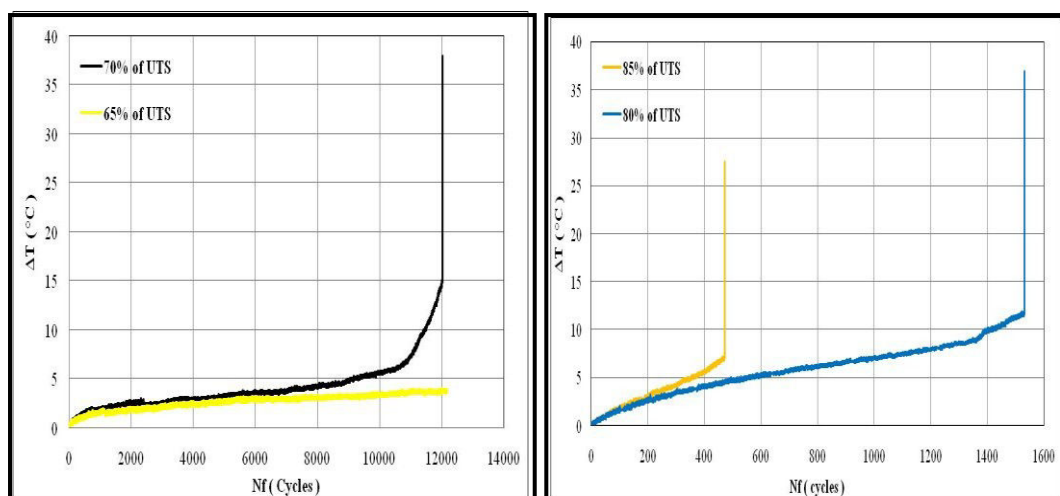
Figure 5.28 Temperature profile during fatigue test for each different load level

The observation surface was used the same location at the edge of the hole, which was at the eventual failure location of the specimen. The ΔT curves increase during fatigue testing for all the stress level, but not at the same pace. The specimen with the 65% load level shows an initial temperature increase until it reaches a slowly increase or kindly of stable thermal state (the slope being only of 0.0002°C/cycle), start at N_f around 1000 cycles and this state remains until at Nf = 12000 cycles without indication of temperature increase which different with temperature profile for 70% of load level. At the beginning, it shows to have same behaviour of temperature increase that consist of initial temperature increase and kindly of stable thermal state (with a slope of 0.0005°C/cycle from 1000 to 10500 cycles). After around 105000 cycles, temperature profile for 70% of load level starts to show a higher increase of temperature until reaches $\Delta T \approx 15°C$ (the slope being here 10 times higher, at 0.005°C/cycle) then suddenly lead to the highest $\Delta T \approx 37°C$ as a consequence of rupture of the specimen. The typical behaviour of temperature evolution globally has the same behaviour for higher stress level of fatigue testing. . After a rapid increase of a few degrees at the beginning of the test, ΔT changes with a constant rate (respectively 0:0066°C/cycle for 80% of UTS and 0:014°C/cycle for 85% of UTS) until reaching the final failure where ΔT suddenly increases a lot. Fig.5.29 below shows the hot zone, which localizes the damage area at the edge of the hole.
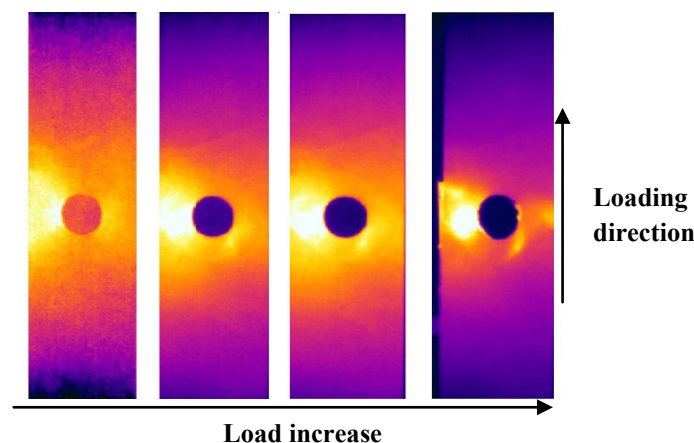
Figure 5.29 Thermography images of DCFC under fatigue test with 80% of UTS

From Fig.5.29 above, initial damage that detects by increasing of temperature occurs at the edge of the hole (left image). This damage then propagates in perpendicular direction against loading direction until catastrophic

or final failure of the specimen (right image). All the images are testing under 80 % of UTS. This specimen of DCFC with hole fails in a brittle type as seen in failure under static tests. The typical damage as seen in Fig.5.30 was found that the specimen failed as in static tensile loading that consists of two failure brittle modes of cracking and delamination as also described by previous study [91].
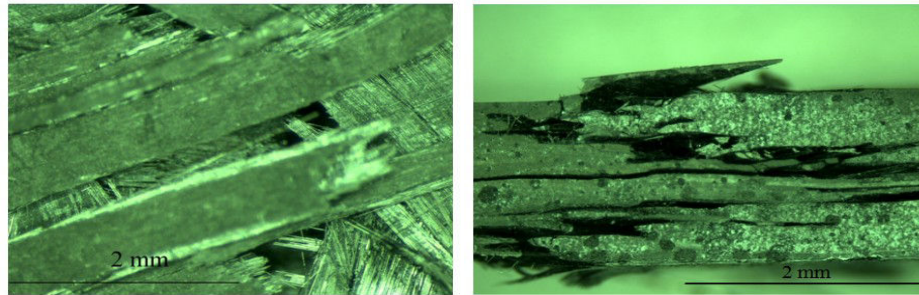
Figure 5.30 Rupture of DCFC specimen under fatigue loading

One of the main objectives of this study is to obtain a correlation between ΔT increase and damage evolution in DCFC material. Two examples of superposition of ΔT measurements and results of the damage propagation obtained from Young modulus evolution (see Eq. (31)) are given in Fig.5.31.
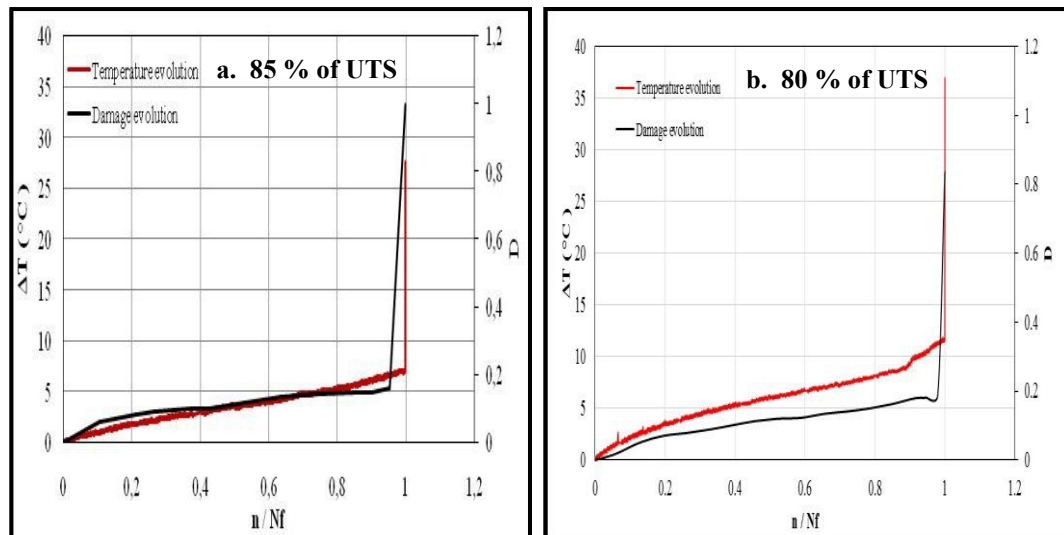
Figure 5.31 Comparison between the temperature and the damage evolution

This one well confirms that ΔT is strongly related to D for this composite material. Based on these above experimental results, it can be stated that the ΔT response can effectively used as a simple method to characterize and estimate the damage evolution of DCFC components subjected to fatigue loading.

5.3 Rapid analysis of fatigue strength based on thermography and energy dissipation of DCFC

The purpose of this analysis is to determine the fatigue strength based on experimental results by means of IR camera and consideration about the energy dissipated in a unit volume of material. Thermographic approach that relies on the use of an IR camera, as originally called the Risitano method [53] has shown to be useful for the determination of high cycle fatigue strength (HCFS) of composite material [60-61]. The main advantage of this method is provide a rapid determination of HCFS that is very efficient time-consuming procedures.

This tests were conducted under the loading frequency of 3Hz and R = 0.1 as discussed in Section 3.3. Using the IR camera, we have a temperature profile for specimen surface as a function of number of cycles for a test with different load level (Fig.5.32). Each test is stopped when ΔT grows with a constant slope, or is even constant over several thousand of cycles which corresponds to approximatively 10^4 cycles for all tests. The same area observation at the edge of the hole was used for all tests which is the failure area.
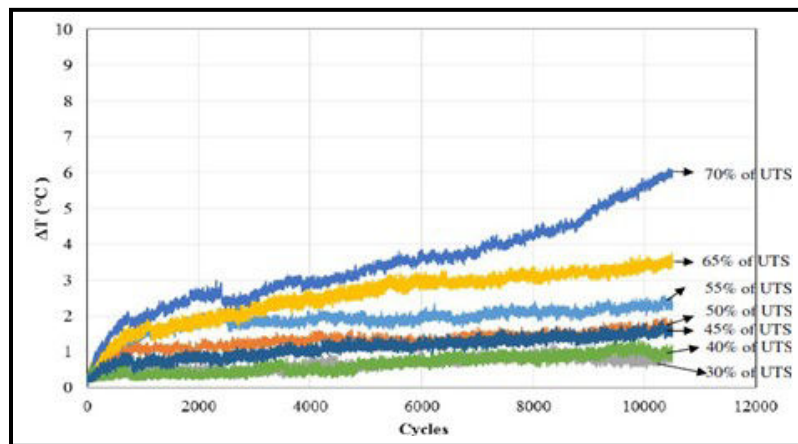
Figure 5.32 Temperature profile of DCFC for each load level

Once again, HCFS of material then determined from the intersection of temperature profile ΔT_{stable} of different stress level. From Fig.5.32, after 45% of load level, a significant increase of ΔT_{stable} around 0.4^{o}C - 1°C occured compare to small increase around 0.05^{o}C-0.2^{o}C under 45% of load level. This 45% of UTS then choose as a point of load level for splitting the stress value to categorize the stress level of below and above, which shows the characteristic bilinear profile

used for this method. Fig.5.33 shows how the HCFS of DCFC material is determined using a graphical procedure based on thermography method.
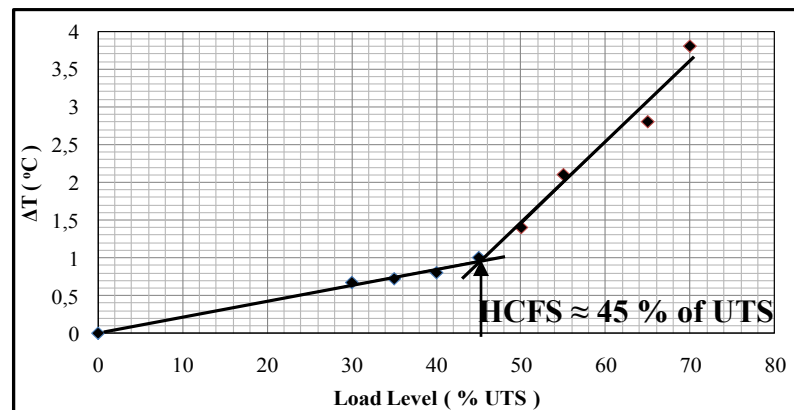
Figure 5.33 HCFS of DCFC by thermography method

Fig.5.33 confirms the HCFS of 45 % of UTS, which is similar results with 4% of error that obtained by plotting the S-N curve in Fig.5.26. It can be noted that HCFS determination by thermography approach can be applied for DCFC material. It is noted that this method is a true in situ measurement technique. Further, a result for a quantitative characterization based on intrinsic energy dissipation was presented to validate the accuracy of thermography approach. The energy dissipation is identified as the area enclosed by a hysteresis loop for one particular cycle and several cycle according to cycle in ΔT_{stable} period, as ilustrated in Fig.5.34.

| a one cycle | b several cycles |
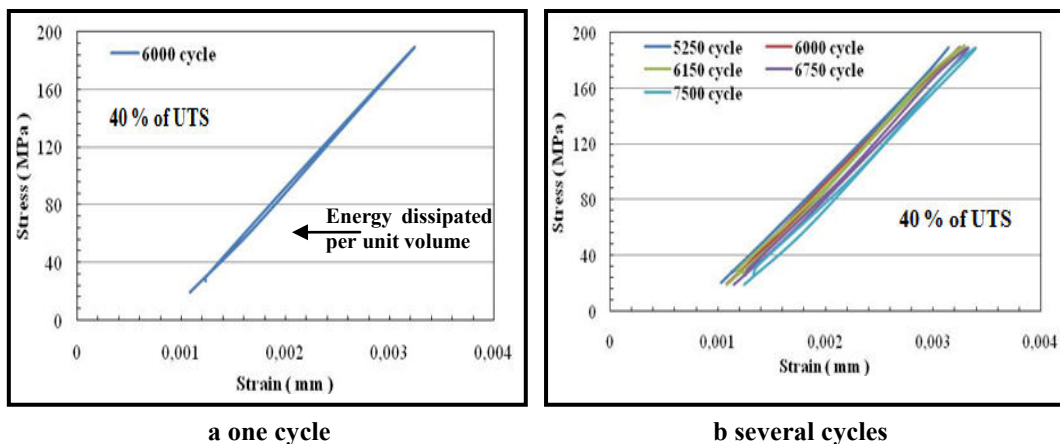
Figure 5.34 Energy dissipation under 40% of UTS fatigue loading of DCFC

From Fig.5.34 above, it can be noted that there is no significant different of energy dissipation during the period of ΔT_{stable} under fatigue loading. By comparing the energy dissipated during a particular cycle in the fatigue tests

during which temperature is stable (e.g., cycle 6000 or between 5750 cycle and 7500) for each load level, a correlation between the energy dissipation and the load level was created. An ilustration of energy dissipation (*Ed*) and a plot of the energy dissipation per unit volume as a function of the load level is shown in Fig.5.35.

| a. based on one particular cycle (6000 cycles) | b. based on several cycles (between 5750 and 7500 cycles) |
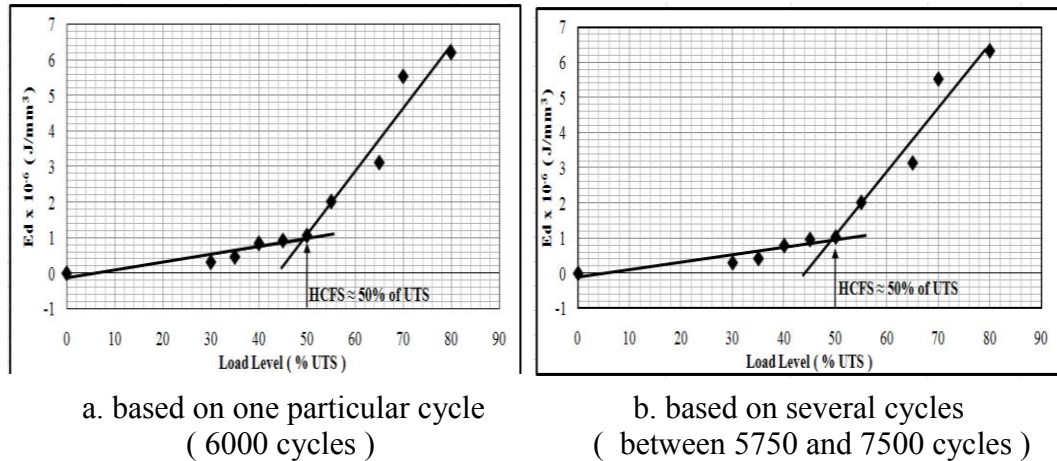
Figure 5.35 HCFS of DCFC by energy dissipation

Fig.5.35 shows the HCFS of DCFC material is determined using a graphical procedure based on energy dissipation approach. The HCFS of $\approx 50\%$ of UTS obtained by energy dissipation was found only a slight different to that obtained using thermography method (Fig.5.33). Hence quite similar HCFS values for DCFC are found with three different approaches : traditional Wöhler S-N curve (Fig.5.26), thermography (5.33) and energy dissipation analysis (5.35).

Furthermore, a plot between energy dissipation per unit volume and ΔT_{stable} for each load level of fatigue test was established, as seen in Fig.5.36.

| a. Based on one particular 6000 cycles | b Based on cycles between 5750 cycles and 7500 cycles |
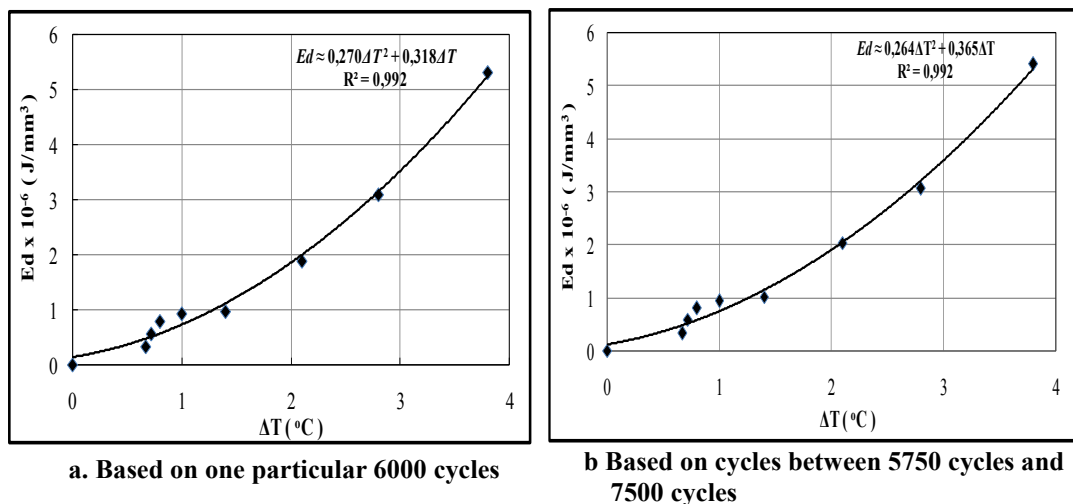
Figure 5.36 Energy dissipation versus ΔT_{stable} of DCFC for different load level

Finally, The relationship between ΔT_{stable} and Ed can be approximated by a polynomial function with a data correlation factor, R^2 close to 1, as indicated by Fig.5.36. This relationship means that the dissipated heat measured by IR camera is in fact due to the intrinsic energy dissipation of the material which be possibly caused by microscopic damage [61]. The main mechanisms causing energy dissipation maybe attributed to, among others, the viscoelastic nature of the matrix material, matrix cracking, fiber fracture, interface cracking/friction as reported in [55, 56]. In a DCFC material, the intrinsic energy dissipation could be reasonable produced by the mechanisms of inherent material stress concentration of non-homogeneous behaviour and microscopic damage, such as chip cracking, matrix cracking, and interface cracking between chip and matrix.

Thermography method that determined the S-N curve based on previous study [59,61] also presented for DCFC. The S-N curve according to parameter Φ as a function of the stabilization temperature and the number of cycles to failure. The value for the parameter Φ for DCFC was approximately $\Phi_{avg} \approx 12$ °C log(cycle) with a standar deviation of $\pm$ 2%. Using Φ_{avg}, the S-N curve is created as shown in Fig.5.37, where it has a less different with Wöhler S-N curve.
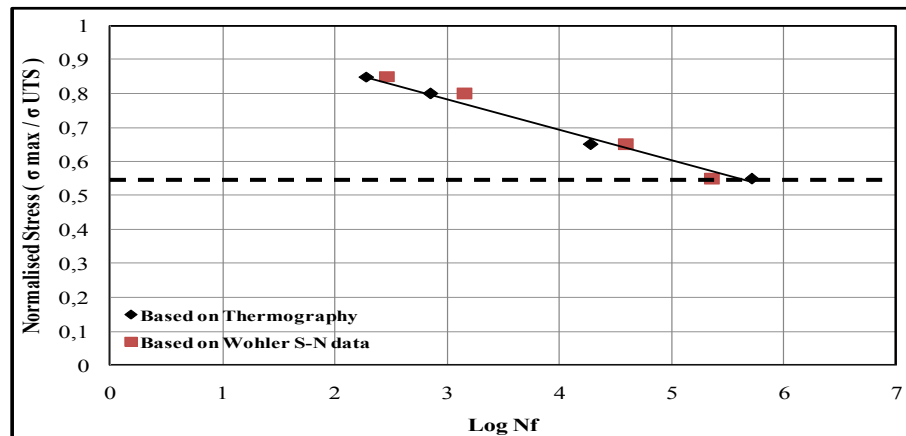
Figure 5.37 S-N curve of DCFC based on thermography approach using Φ parameter

As a section conclusion, rapid method based on thermography approach and supported by energy dissipation approach was successfully determined the HCFS of discontinuous carbon fiber composite (DCFS) material. The results found by these fairly quick approaches are in good accordance with those issued from the traditional Wöhler S-N curve (Fig.5.26) which is therefore longer to obtain.

Chapter VI.   SUPPORTING ANALYSIS ON DAMAGE BEHAVIOUR OF GFRP AND DCFC BY ACOUSTIC EMISSION AND TOMOGRAPHY

This chapter describes the experimental investigation on static and fatigue loading of GFRP and DCFC through NDT observation using different method applies to detect the damage mechanisms during the test. The aim is to coupling the NDT characterization with respect to the different parameter for each method accoring to the damage appearance during the test.

6.1   Coupling between thermography and acoustic emission for damage observation of GFRP 0° under tensile static loading

This investigation conducts with GFRP 0° with an open hole condition and has the aim to determined damage parameter based on thermography and acoustic emission as an observation results. Fig.6.1 shows the thermography images during the test.
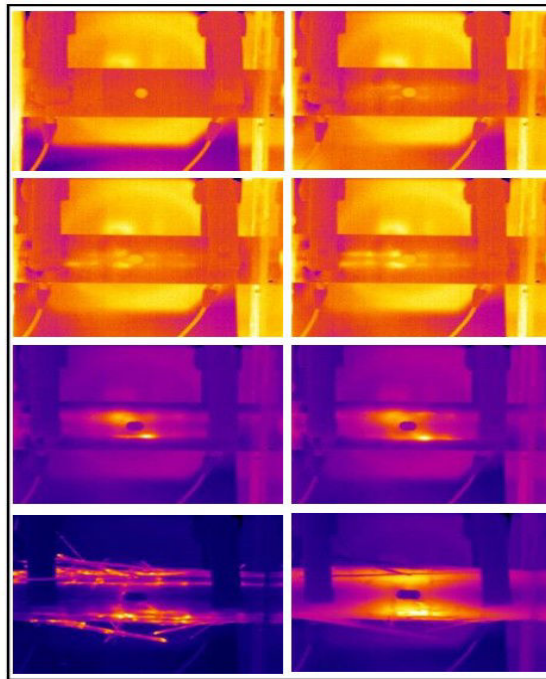
Figure 6.1 Thermography images of GFRP 0°

The changes of temperature with an increasing trend is very low at the beginning of the tensile test. The different temperature response due to the intensity of the damage and different mechanism on the specimen surface start

from micro matrix damage until the final failure of the specimen. From the images above, different contrast for each images were adjusted to obtain optimum contrast continuously. In the presence of thermography as a visual methods, the failure evolution can be followed visually that very usefull to categorize failure mechanism during the test and also can avoid removing the specimen to observe the failure that may induce misalignment in regripping the specimen and may cause premature cracking of the matrix.

The acoustic emission also performed. The accurate analysis of the acoustic emission plays an important role in explaining the failure mechanisms and damage evolution of composites. In this experiment, after the acquisition process with AE win software, post processing of Acoustic emission signal performed by NOESIS software to have the correspondance between failure mechanism of composite material in static tensile loading and clasification of acoustic emission signal based on the variation and the relationship between amplitude and energy. In [95], to have an accurate results of observations, analysis of acoustic emissions then validated with the failure evolution caused by temperature changes as the recording results of IR camera, as seen in Fig 6.2-6.4 below.

In Fig.6.2, it shows the damage detection by thermography and also acoustic emission for the first macro damage of matrix cracking.

Observation parameter	Macro matrix cracking
Visually	Splitting mode
Loading	Around 46 kN
Temperature	Small increase ($\Delta T = 2°C$)
Amplitude (dB)	78 - 84
Energy (aJ)	5 – 50
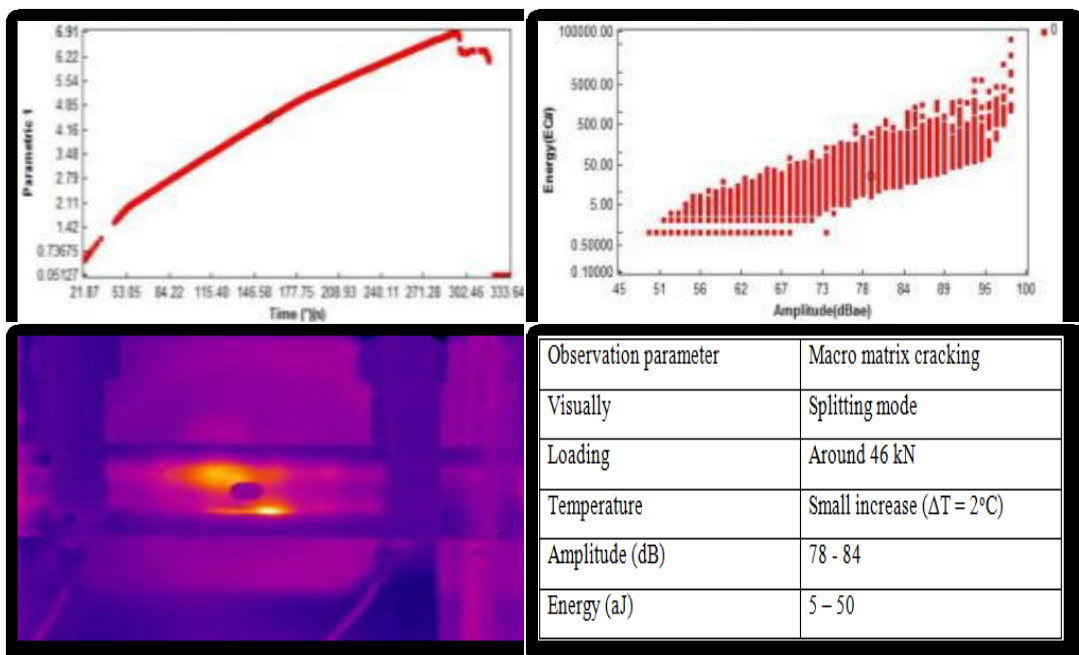
Figure 6.2 Thermography and AE results of first damage under tensile test of GFRP 0° [95]

From the Fig.6.2 above, at about 46 kN tensile loading (black circle), the first macro damage of matrix cracking in splitting mode occurs on specimen surface is detected by the change in temperature through changing the color of the thermography image. Acoustic emission also detects energy and amplitude at this condition (black circle) that induced by the damage mechanism. Fig.6.3 shows the damage propagation by thermography and also acoustic emission for the first macro damage of matrix cracking.
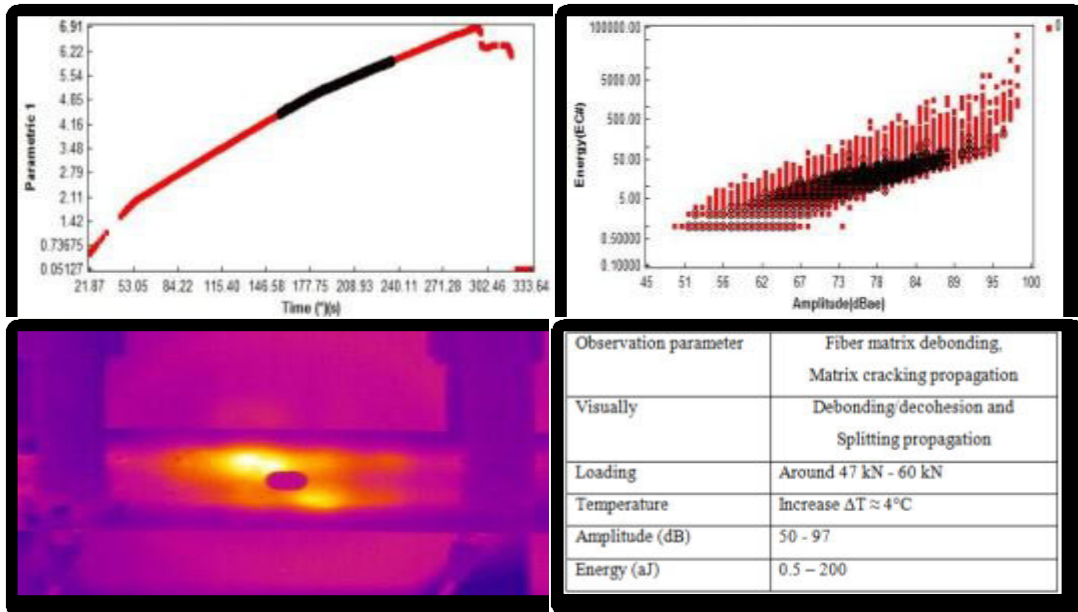
Figure 6.3 Fiber matrix debonding recorded by thermography and AE of GFRP 0° [95]

After the first macro damage of matrix cracking, with the increasing of tensile loading, the damage progagate in almost of the specimen area. From Figure above, loading increases in range 47 kN – 60 kN cause other damage mechanism that can be recognized from temperature change and the clasification of energy-amplitude in this damage condition. This form of damage could be fiber matrix debonding and matric cracking propagation that showing distribution of temperature change on the specimen surface and also energy-amplitude correlation as the results of AE signal (Fig.6.3). When the load reaches to the maximum force, fiber breakage occured in some areas of the specimen and also at the hole side and change the hole form into an elliptical hole or streching hole. Both of this damage mechanism lead to the end life of the specimen marked by black area from maximum force (UTS) until failure force.

From observation results of thermography camera and AE signal, it was found that temperature had a large increases change compared to other damage mechanism especially in some area that fiber breakage and fiber pullout occurs (Fig.6.4). This increasing of temperature could be related to the fracture energy of composite material that represents the energy which gradually released at fiber breakage and fiber pullout. This results also confirmed by AE signal that showing a large range of energy parameter. The amplitude-energy correlation indicating damage mechanism of fiber breakage and fiber pullout (Fig.6.4).

Observation parameter	Fiber breakage
Visually	Breakage and pull out
Loading	F max and F failure
Temperature	Large increase ($\Delta T = 38^{\circ}C$)
Amplitude (dB)	90 - 100
Energy (aJ)	2000 – 100000
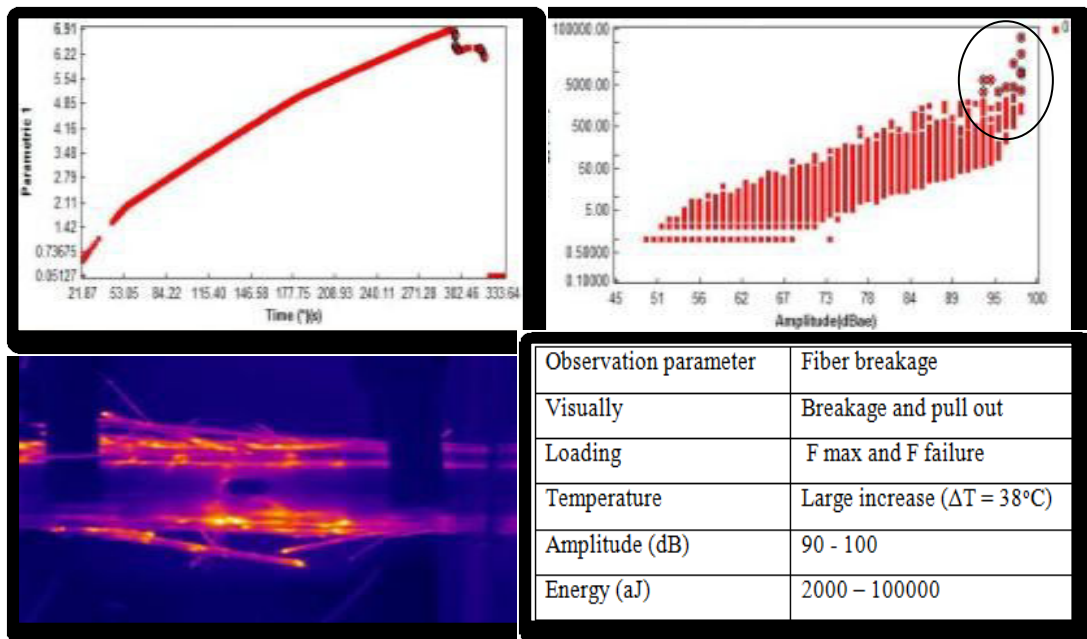
Figure 6.4 Observation results of fiber breakage and fiber pull out of GFRP 0° [95]

From Figure above, it can be noted that both of these observation method indicating the same evolution behaviour of damage process on the specimen.

As a section conclusion, these two methods give an accurate correlation of damage appearance and damage propagation obtained by thermography monitoring and acoustic emission parameters that non-instrusively measured under tensile test or glass fiber composite (GFRP 0°).

6.2 Post failure analysis of tomography for damage observation under tensile fatigue test

The results of CT-Scan post processing are a large number of projection images / slice images of the specimens through-thickness that obtained by

rotating the sample and focus on area around the hole (25 mm x 19 mm). Fig. 6.5 shows the ilustration of focus area and scanning process.

a. Ilustration of rotating image   b. Ilustration of post processing
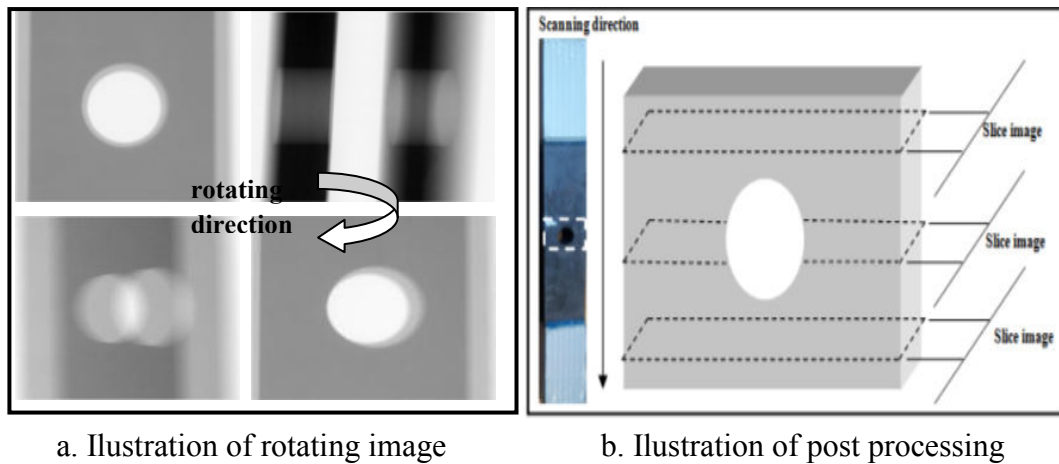
Figure 6.5 Ilustration of CT scanning process

6.2.1 Tomography observation of DCFC with hole

The tomography allows the investigation of the damage and the localization and quantification of the damage by checking the gray levels/values intensity. For the observation analysis, we use image J software. Fig.6.6 shows the example images of DCFC after post processing by CT-scan.
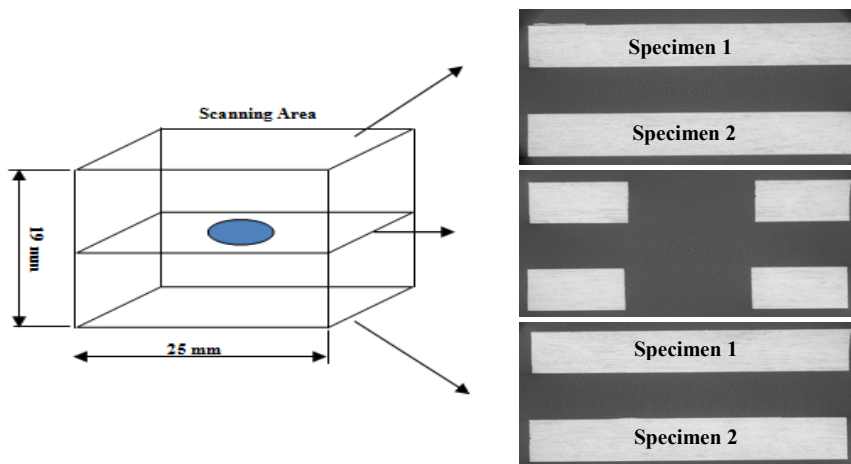
Figure 6.6 Example of slice image of DCFC resulting by CT-Scan around the hole

For image analysis, first step is cut out the gray value of artefacts that found from the tomography recording then working with colour as our preferences and to have better visual image as seen in Fig.6.7. In this observation anlysis, profile

and histogram analyze parameter will use to obtain gray level that related to the density of the material.

| Ring Artefact | Cut out of artefact | Working with colour |
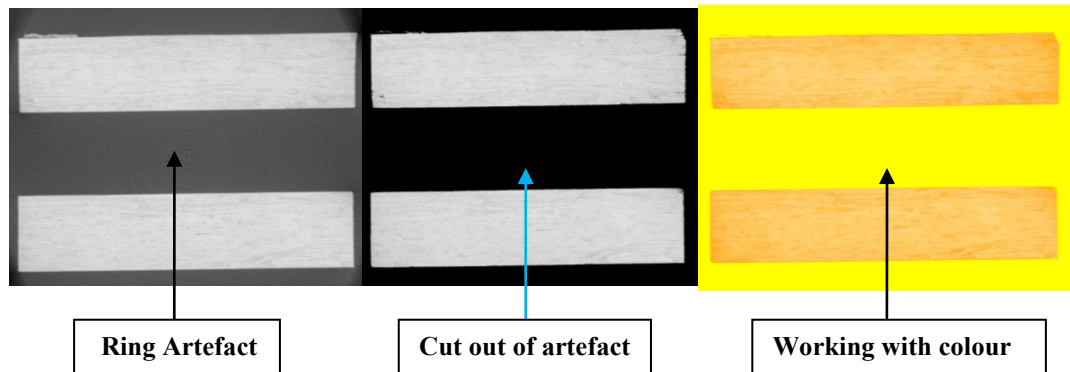
Figure 6.7 Example of slice image before and after colour treatment of DCFC

Cutout the artefact process has changed the gray value scale that we remove all the gray value of area without specimen. Fig.6.8 presents the ilustration of cutout gray value process of the artefact.

a. Gray value before cut out process

b. Gray value after cut out process
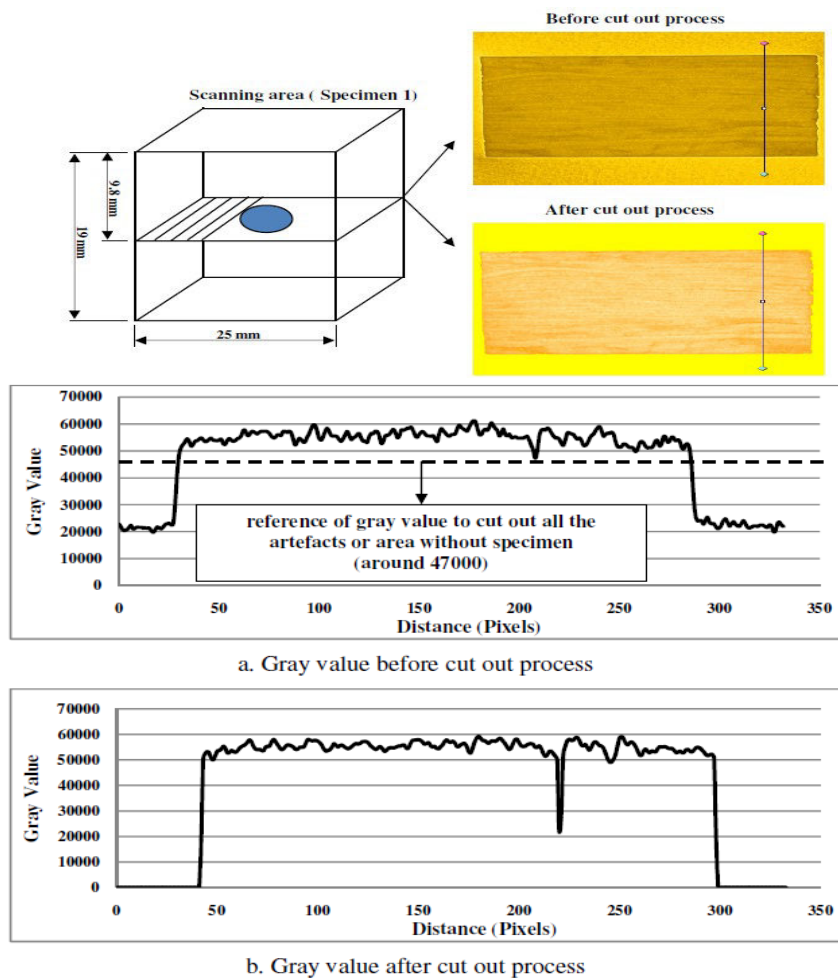
Figure 6.8 Cut out of gray value process of DCFC

Using this Image J software, a series of slide images can the be used to characterize the object volume, with the data reformatted to display or to present 3D reconstruction of the object, as seen in Fig.6.9.
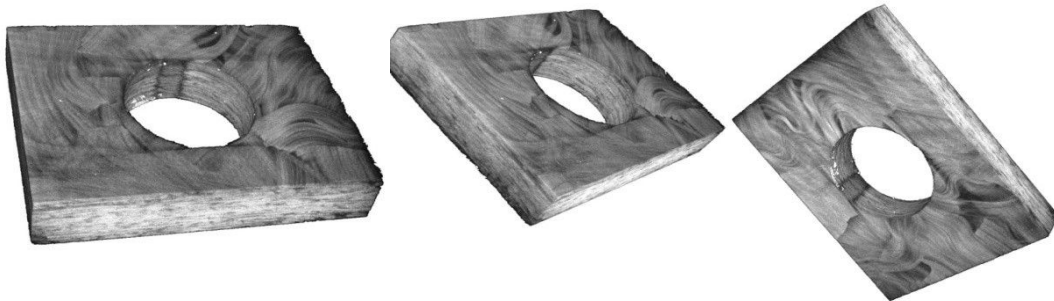
Figure 6.9 3D reconstruction of DCFC

The Observation area of the specimen can divide into 3 condition according to the gray value :

1.   Area without specimen that can be used to clasified possibly damage area.

2.   Matrix area

3.   Matrix + Fiber area

Based on line profile in Fig.6.10, we can categorize area using gray value. The observation analysis will focus at the slice images represent hole area.
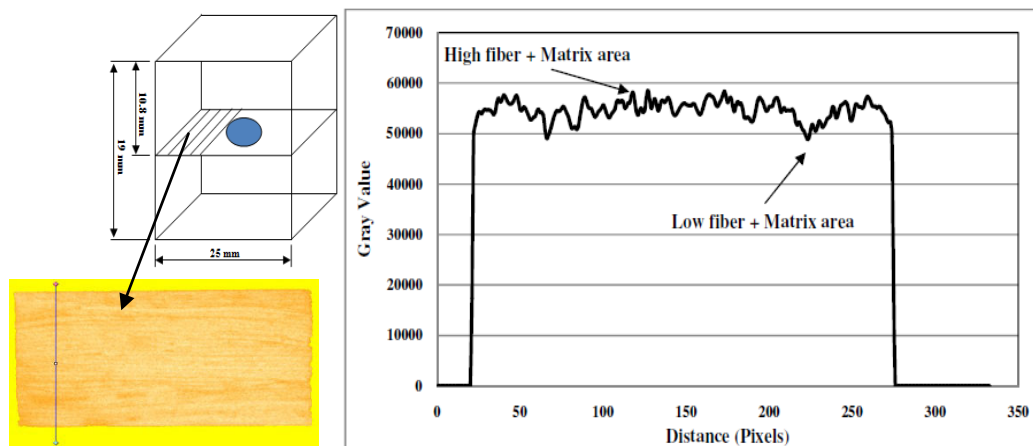
Figure 6.10   Gray level parameter of line profile for DCFC

From the cut out process of artefact on slice image, all the gray value under around 47000, we made in to zero value. CT can be used to not only distinguish between air (pores) and material, but also other inhomogeneities and features within the composite specimen are detectable. For example, different colour contrast on specimen's surface indicates the possibility of different amount

of fiber in fiber + matrix area. Figure 6.11 ilustrates the different contrast and gray value for one of image slice.
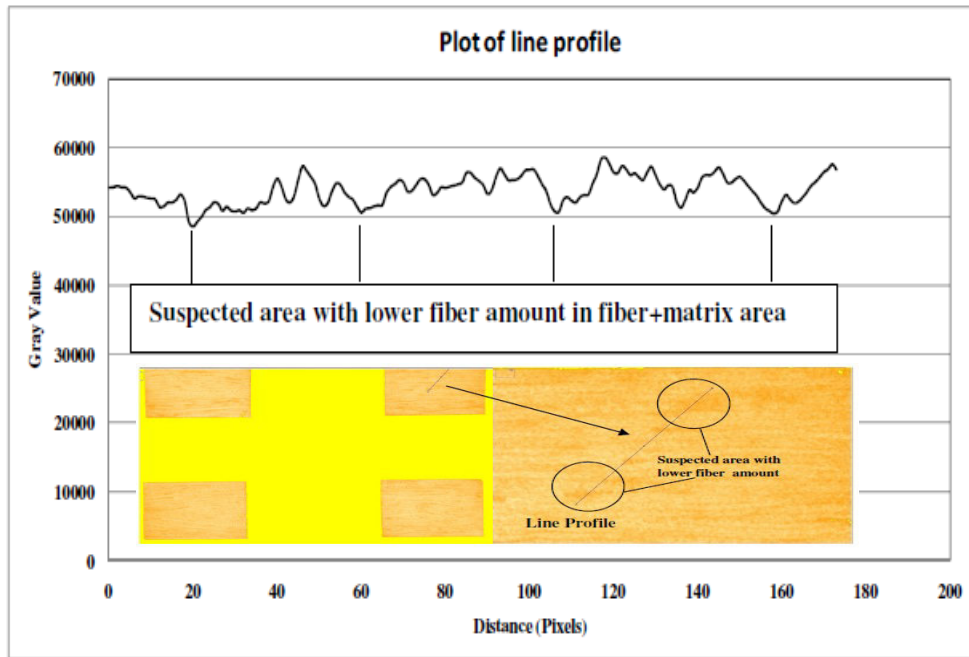
Figure 6.11 Gray value parameter of line profile for DCFC

From plot of line profile above, found that suspected area with lower fiber amount has lower gray value compare to other area along the line profile. Fig.6.12 shows line profile analysis of slice image of specimen with micro damage of cracking.

Area	Parameter Range (Gray Value)
Area without specimen	0
Micro cracking	0 - 20000
Low Fiber + Matrix	47000 - 53000
High Fiber + matrix	53000 - 60000
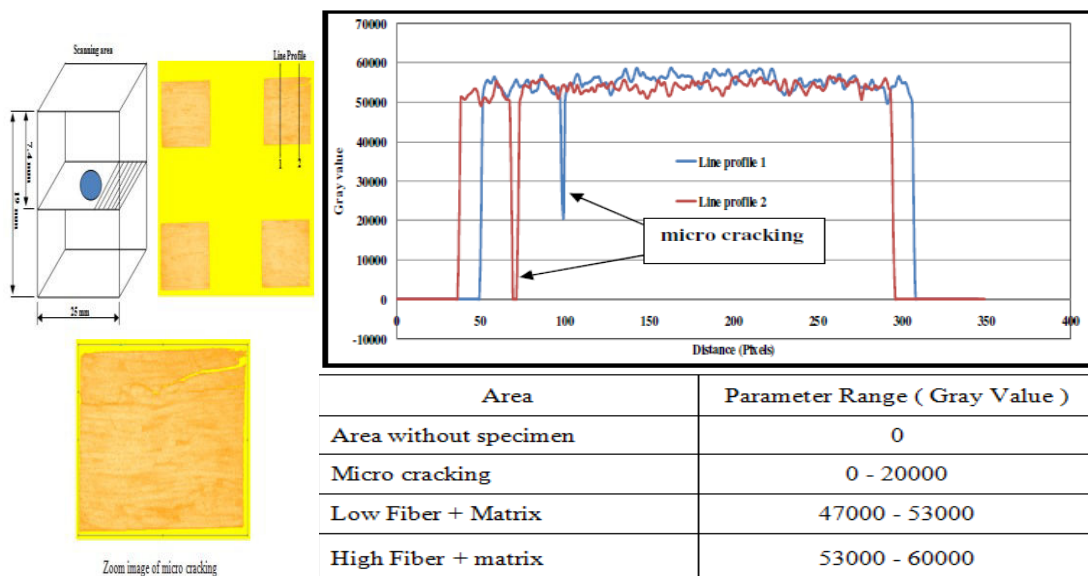
Figure 6.12 Gray value parameter of line profile for micro cracking on DCFC

From Fig.6.12 above, found that micro cracking or intra-chip cracks damage mechanism occurs based on gray value along the line profile and perpendicular to the loading direction. This crack is possibly typical of early stages of damage initiation and growth which caused by manufacturing defects or cutting process.

From other analysis of Image J using histograms, it can also gives information about the gray values and number of pixels found for each gray value from darkest (0) to brightest (65000) for 16 - bit type of images. Based on histogram result, is is possibly to categorize each area (precentage) and also possibly damage occurs inside the material. Fig.6.13 shows the histogram result of slice image of area around the hole that occurs micro cracking.

Area	Gray Value	Number of Pixels	Precentage
Damage	0 - 47000	893	0.78 %
Low Fiber + Matrix	47000 - 53000	32154	28.30 %
High Fiber + Matrix	53000 - 62000	80537	70.90 %
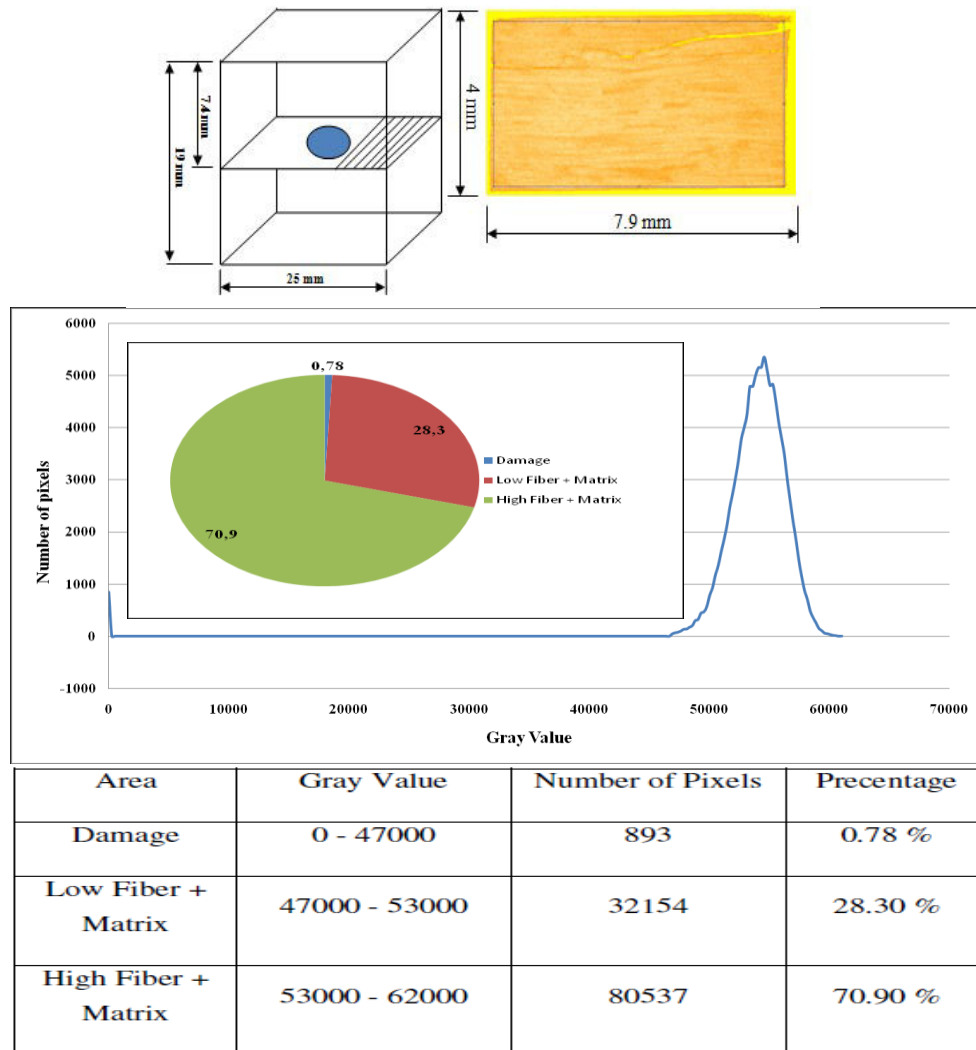
Figure 6.13   Histogram of slice image of DCFC

The specimen with this micro crack is in fact a result from fatigue testing with 65% of UTS at certain cycle of 3100 cycles in stage 2 period (stable state where damage is likely propagate). It means that tomography gives a good confirmation about damage existance in microscale under fatigue testing.

6.2.2 Tomography observation of GFRP 0° with hole

The observation conducts with the same condition with previous observation on DCFC. Fig.6.14 shows the ilustration of focus area and scanning process. The tomography allows the investigation of the damage and the localization and quantification of the damage by checking the gray levels / values intensity.
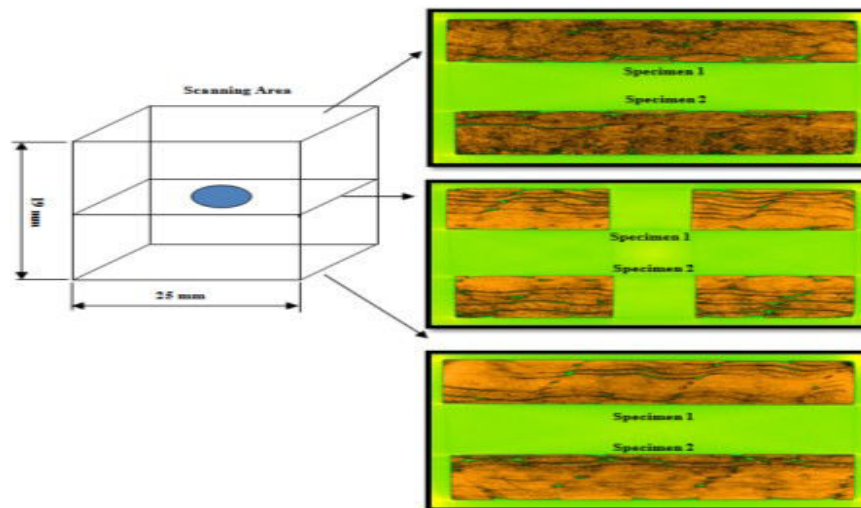
Figure 6.14 Example of slice image of GFRP 0° around the hole

Using this Image J software, a series of slide images can the be used to characterize the object volume, with the data reformatted to display or to present 3D reconstruction of the object. Fig.6.15 shows the 3D reconstruction of GFRP 0° specimen resulting fron CT-scan.
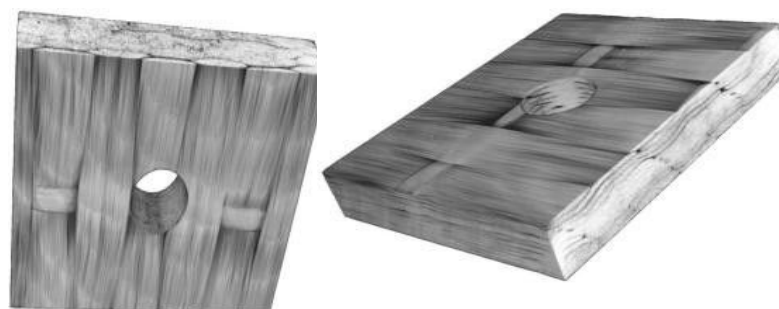
Figure 6.15 3D reconstruction of GFRP 0°

Based on line profile at the Fig.6.16 and Fig.6.17 below, observation area of the specimen can divide into 4 condition according to the gray value :

1. Matrix area

2. Low Fiber + Matrix area

3. High Fiber + Matrix area

4. Area without specimen that can be used to clasified possibly damage area

Observation area

Slice image of observation area
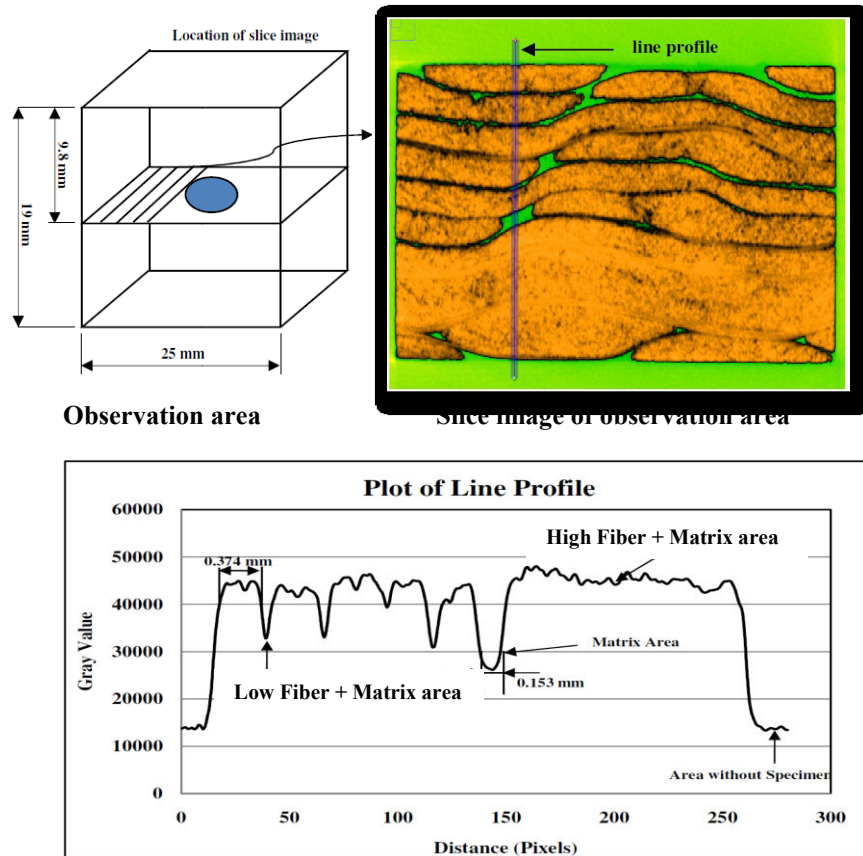
Area	Parameter Range (Gray Value)
Area without specimen	10000 - 20000
Matrix (Resin Area)	20000 - 30000
Low Fiber + Matrix area	30000 - 40000
High Fiber + Matrix area	40000 - 50000

Figure 6.16 Gray value parameter of line profile for GFRP 0°

From both observation in Fig.6.16 above according to the gray value, we can possibly say that there is no damage mechanism such as fiber breakage, delamination or matrix crack occur at the area around the hole. Simply, we can

use the gray value of region without specimen as the parameter of damage area that indicating lower gray value compare to other region. Nevertheless, the observation results show clearly other kind of phenomenon that develop inside the material, i.e wavy fiber laminate in perpendicular direction with given loading. Fig.6.17 shows the wavy fiber laminate at the area around the hole in perpendicular direction for both specimens.
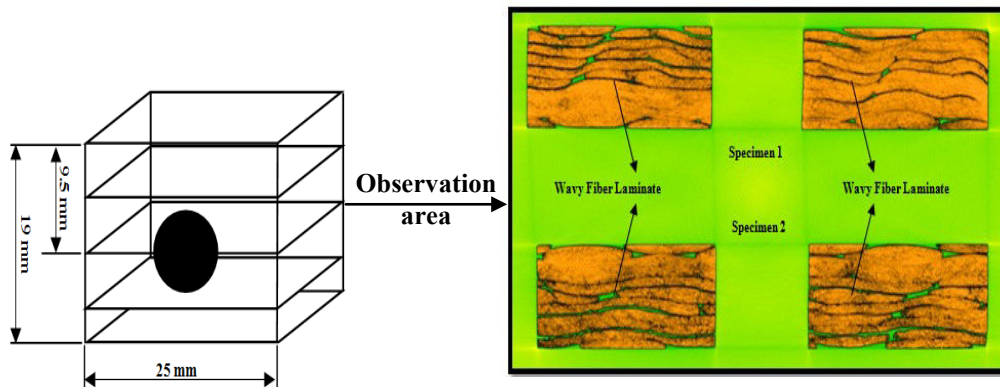
Figure 6.17 Wavy fiber laminate of GFRP 0°

From other analysis of Image J using histograms, it can also gives information about the gray values and number of pixels found for each gray value from darkest (0) to brightest (65000) for 16 - bit type of images. Based on histogram result, is is possibly to categorize each area (precentage) and also possibly damage occurs inside the material. Fig.6.18 represents the histogram result of one of slice image around the hole.
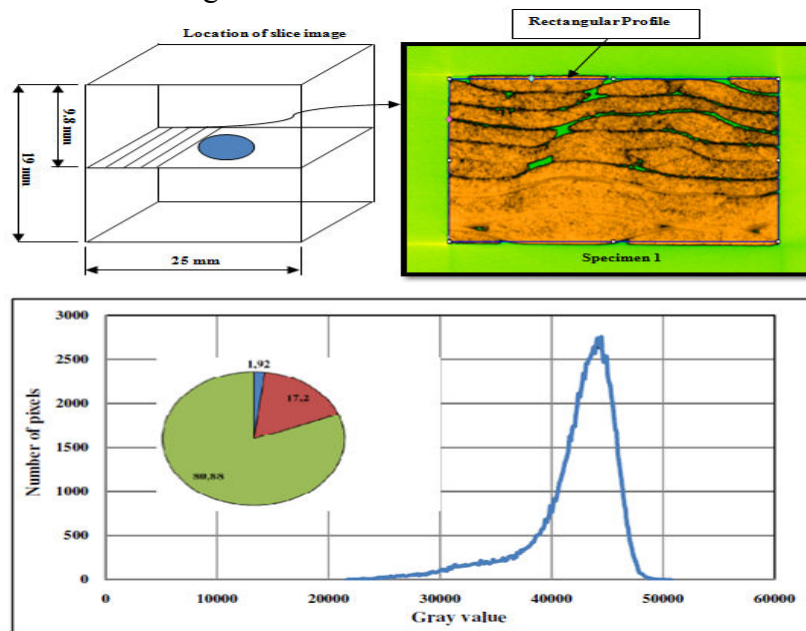
Figure 6.18 Histogram of slice image fro GFRP 0°

In accordance with the histogram result, we can classified the precentage of each area by range of gray value and number of pixels. Table 6.1 below shows the description of precentage area based on histogram.

Table 6.1 Description of Histogram for GFRP 0°

Area	Gray Value	Number of Pixels	Precentage
Matrix	20000 - 30000	2665	1.92 %
Low Fiber + Matrix area	30000 - 40000	23859	17.2 %
High Fiber + Matrix area	40000 - 50000	112228	80.88 %

Using this Histogram analysis, also observed in other areas of the specimen to obtain a clear description of the area classification based on gray value. Observation area performed at area not around the hole / area contains no hole that has difference appearance with the area around the hole. In Fig.6.19.below, the observation area has no kind of wavy fiber laminate.

Min : 23659   Max : 48797   Count : 97136   Mean : 40531.060   StdDev : 2503.824

Area	Gray Value	Number of Pixels	Precentage
Matrix	20000 - 30000	176	0.18 %
Low fiber + Matrix area	30000 - 40000	36153	37.21 %
High fiber + Matrix area	40000 - 50000	60807	62.59 %
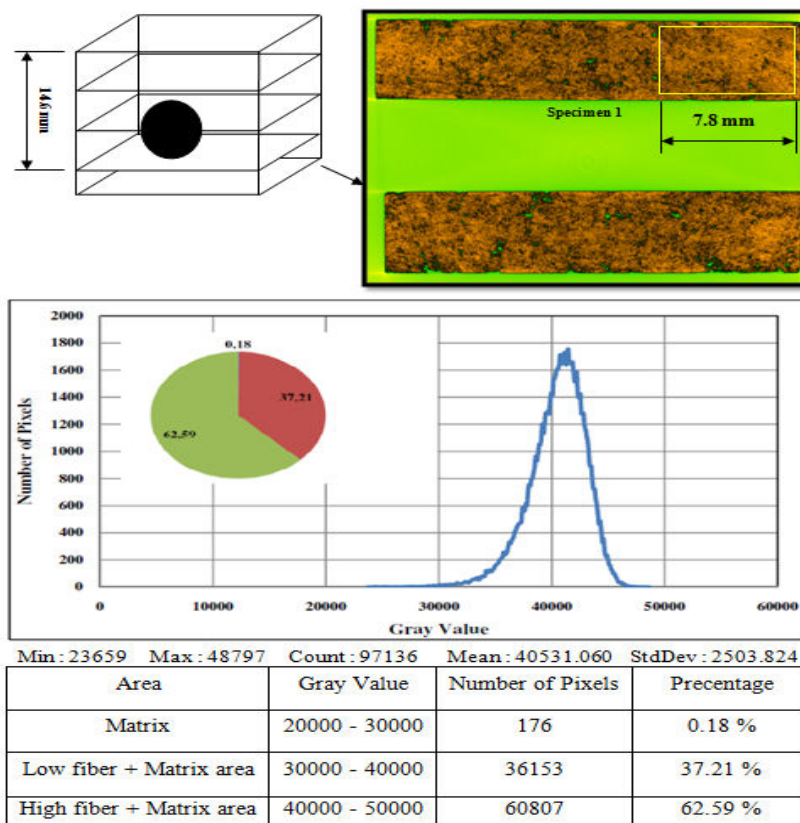
Figure 6.19 Histogram of slice image for GFRP 0°

Briefly, CT-scan analysis based on gray value segmentation method successfully measures and evaluates damage and material condition after fatigue test for discontinuous carbon fiber/epoxy composite (DCFC) and unidirectional glass fiber/epoxy composite (GFRP 0°).

Chapter VII. CONCLUSION AND FUTURE WORK

7.1 Conclusion

In the following section, several conclusions based on damage observation of GFRP and DCFC by NDT method are described below. The important finding in this chapter are:

1. **NDT thermography characteristic on damage behaviour under tensile static loading :**

- Thermography observation by IR camera can give a good local information about the early damage appearance and propagation, as well as damage type, critical point, damage location until rupture based on temperature profile.

- Thermography can be used to characterize the damage growth on DCFC specimen. The early detect by thermography on micro defect shows a flash lighting form of delta-T spot that has minor or small increase in temperature possibly due to manufacturing defect. Final failure or rupture of the DCFC specimen represents by suddenly increase of temperature that has major or the highest increase of temperature.

- The delta-T spots on DCFC material that possibly due to manufacturing defecr do not grow significantly during the test and eventually do not affect the initial presence of macro damage that leads to the catastrophic failure.

2. **NDT thermography characteristic on damage behaviour under tensile fatigue loading :**

- The evolution of the temperature of GFRP can be categorized in four stages. In the first part, the initial increase of temperature is possibly due to the micro cracking in matrix. In the second part, a sudden increase in temperature caused by first appearance of macro matrix cracking. After that, the temperature reaches a slowly increasing trend due to the stable growth of matrix cracking as part of the third stage. The final part, a significant trend increase of temperature could be due to fiber/matrix debonding as the

interfacial failure in splitting form and finally provokes the occurrence of fiber fracture which dealing with the rupture of the specimen represents by the highest increase of temperature.

- The typical behaviour of temperature evolution of DCFC has three stages of initial increase due to initial micro matrix cracking damage growth of matrix cracking, slowly increase due to stable propagation of chip/matrix debonding and chip cracking and suddenly increase caused by chip breakage and delamination until reaches the highest increase of temperature as a consequence of final failure.

- Thermography can be efficiently used as a simple method to characterize and estimate the damage evolution of GFRP and DCFC subjected to fatigue loading.

- Thermography can use accurately to predict the high cycle fatigue strength (HCFS) with 4% of error for GFRP and DCFC material

- Thermography method also can be used to determine the S-N curve for GFRP and DCFC material

3. Supporting analysis of Acoustic emission and tomography :

- The Acoustic emission can be used to determine damage propagation of GFRP under tensile static loading. Coupling with thermography, these two methods is satisfactory for giving information about damage propagation of matrix cracking, fiber matrix debonding, fiber breakage and fiber pullout for GFRP material.

- Tomography analysis based on gray value segmentation method successfully measures and evaluates damage and material condition after fatigue test for discontinuous carbon fiber/epoxy composite (DCFC) and unidirectional glass fiber/epoxy composite (GFRP).

7.2 Future work

Although several important finding were made in this study, additional work can be performed to further understanding based on this study. The following is a list of recommendations for future work :

- Develop an investigation on the effect of frequency on thermal response and energy dissipation for composite material.

- An experimental test for each constituent material (matrix, fiber) to understand the effect on the thermal response and energy dissipation associated with the thermal source of damage mechanisms.

- Further investigation on post failure analysis using tomography and also micro optic observation to understand the damage mechanisms of fiber composite material.

- A similar experimental test program can be conducted and developed with different fiber and matrix material

- Develop an analysis and simulation study to determine the damage constitutive model associate with temperature profile from NDT thermography.

REFERENCES

[1]   Y. Yang, R. Boom, B. Irion, D.J van Heerden, P.Kuiper, H.deWit, *Recycling of composite material*, Chem. Eng. Process, 2011.

[2]   C. Kazmierski, *Global composite market analysis–ACMA 2012 -* EducationalSession.http://www.lucintel.com/LucintelGlobalCompositeMarketAnalysis-ACMA2012-EducationalSession.pdf

[3]   L.T. Harper, *Discontinuous carbon fiber composite for automotive applications*. Thesis submitted to the University of Nottingham for the degree of Doctor of Philosophy. 2006.

[4]   P. Marin-Francha, T. Martin, D.C. Tunnicliffe, DK Das-Gupta, *PTCa/PEKK piezo-composites for acoustic emission detection*. Sensors and Actuators A 99. 2002. pp.236–243

[5]   Y. Yeun-Ho, C. Jin-Ho, K. Jin-Hwe, K. Dong-Hyun, *A study on the failure detection of composite materials using an acoustic emission*. Composite Structures 75. 2006. pp. 163–169

[6]   A. K. Mohanty, M.A. Khan, G. Hinrichsen, *Surface modification of jute and its influence on performance of biodegradable jute-fabric/Biopol composites*. Compos Sci Technol, Volume 60. 2000. pp. 1115–1124.

[7]   M.A. Usamani, O.I. Salyer, L.G. Ball, L.J. Schwendeman, *Bagasse-fiber-reinforced composites*. Journal of Elastomers and Plastics, Volume 13, No. 1. 1981. pp. 46-73.

[8]   K. Bilba, M.A. Arsene, A. Quensanga, *Sugar cane bagasse fiber reinforced cement composites. Part I. Influence of the botanical components of bagasse on the setting of bagasse/cement composite*. Cement and concrete composites, Volume 25. 2003. pp. 91-96.

[9]   P. Tudu, *Processing and characterization of natural Fiber reinforced polymer composites*. Thesis. Department of Mechanical Engineering National Institute of Technology Rourkela. 2009.

[10]   F.C. Campbell, *Structural composite material*. ASM International. 2010. www. asminternational.org

137

[11]   R. Talreja, *Damage and fatigue in composites – A personal account* Composites Science and Technology 68. 2008. pp. 2585–2591.

[12]   Y.K. Boey, *Study of progressive failure of composites under axial loading with varying strain rates*. Thesis. Naval Postgraduate School. 2011.

[13]   A. Yudhanto, *Effects of micromechanical factors in the strain in variant failure theory for composites*. Thesis. National University of Singapura. 2005.

[14]   B. Harris, *Fatigue in composites: Science and technology of the fatigue response of fiber-reinforced plastics*. Published by Woodhead Publishing Limited. 2003.

[15]   K.P. Dyer, D.H. Isaac, *Fatigue behaviour of continuous glass fiber reinforced composites*. Composites Part B 29B**.** 1998. pp.725–733.

[16]   K. Schulte, *Damage monitoring in polymer matrix structures*, Journal de Physique IV, Vol.3. 1993. pp. 1629– 1636.

[17]   C. Bathias. *An engineering point of view about fatigue of polymer matrix composite materials*. International Journal Fatigue 28. 2006. pp.   1094-1099.

[18]   E.K. Gamstedt, A. Lars, L.A. Berglund, T. Peijs, *Fatigue mechanisms in unidirectional glass-fiber-reinforced polypropylene* Composites Science and Technology 59. 1999. pp. 759-768.

[19]   J.A.M. Ferreira, J.D.M. Costa, P.N.B. Reis, M.O.W. Richardson, *Analysis of fatigue and damage in glass-fiber-reinforced polypropylene composite materials*. Composites Science and Technology 59. 1999. pp. 1461-1467.

[20]   P.T. Curtis, *A review of the fatigue of composite materials*. Royal Aircraft Establishment, Technical Report 87031. 1987.

[21]   B. Harris, H. Reiter, T. Adam, R.F. Dickson, G. Fernando, *Fatigue behaviour of carbon fiber reinforced plastics*. Composites 21. 1990. pp. 232-242.

[22]   A. Rotem, H.G. Nelson, *Fatigue behaviour of graphite-epoxy laminates at elevated temperatures*. Fatigue of Fibrous Composite Materials, ASTM STP 723. 1981. pp. 152-73.

[23]   A. Pegoretti, T. Ricco, *Fatigue crack propagation in polypropylene reinforced with short glass fibers*. Composites Science and Technology 59. 1999. pp.1055-1062.

[24]   A. Gagel, D. Lange, K. Schulte, *On the relation between crack densities, stiffness degradation and surface temperature distribution of tensile fatigue loaded glass-fiber reinforced epoxy*. Composites: Part A 37. 2006. pp. 222–228.

 [25]   X. Wang and D.D.L. Chung, *Fiber breakage in polymer matrix composite during static and fatigue loading*. Journal Material 14 no 11. 1999. pp. 4224-4229.

[26]   R. C. S. Freire Jr and E.M.Freire de Aquino, *Fatigue damage mechanism and failure prevention in fiberglass reinforced plastic*. Material Research, Vol. 8, No. 1. 2005. pp. 45-49.

[27]   C.G. Davila and C.A. Rose, *Progressive damage analysis of composite*, Aircraft Aging and Durability Project. www.eng.morgan.edu.

[28]   E. Bayraktar, S.D. Antolovich, C. Bathias, *New developments in non-destructive controls of the composite materials and applications in manufacturing engineering*. Journal of materials processing technology 206. 2008. pp. 30–44.

[29]   H.E. Kadi and F.Ellyin Reddy. *Effect of stress ratio on the fatigue of unidirectional glass/fiber epoxy composite laminae,* Composite, Vol 25, No.10.1994. pp. 917-924**.**

[30]   A. Puck and W. Schneider, *On failure mechanisms and failure criteria of filament wound glass-fibre/resin composites*, Plastics and Polymers. 1969. pp. 33–44.

[31]   L. Guangyan, *Damage progression in open-hole tension composite laminates by the element-failure method*. A thesis submitted for the degree of doctor of philosophy department of mechanical engineering National University of Singapore. 2007.

[32]   Z. Hashin, *Failure criteria for unidirectional fiber composites*, Journal of Applied Mechanics, vol. 47. 1980. pp. 329–334.

[33] R. M. Christensen, *The comparison and evaluation of three fiber composite failure criteria*, Annual Conference & Exposition on Experimental & Applied Mechanics. 2005.

[34] B. Okutan, *Stress and failure analysis of laminated composite pinned joints*, A Thesis Submitted to the Graduate School of Natural and Applied Sciences of Dokuz Eylul University In Partial Fulfillment of the Requirements for the Degree of Doctor of Philosophy in Mechanical Engineering, 2001.

[35] ESP. Brian, *Stress distribution and strength prediction of composite laminates with multiple holes,* Presented to the Faculty of the Graduate School of The University of Texas at Arlington in Partial Fulfillment of the Requirements for the Degree of Doctor of Philosophy the University of Texas at Arlington. 2007.

[36] J. Awerbuch and M.S. Madhukar, *Notched strength of composite laminates; predictions and experiments – A review*, Journal of Reinforced Plastic Composites. 4. 1985. pp. 3-159.

[37] O.O. Ochoa and J.N. Reddy, *Finite element analysis of composite laminates*, Kluwer Academic Publishers. Norwell. 1992.

[38] L.K. William, *Stress concentration around a small circular hole in the HIMAT composite plate*, NASA. 1985.

[39] S.G. Lekhnitskii, S.W. Tsai, T. Cheron, *Anisotropic plates*, Gordon and Breach Science Publishers. New York. 1968.

[40] R.J. Nuismer and J.M. Whitney, *Uniaxial failure of composite laminates containing stress concentrations*, Fracture Mechanics of Composites, ASTM STP 593, American Society for Testing and Materials. 1975. pp. 117-142.

[41] H.M. Arslan, M.Y. Kaltakci, H.R. Yerli, *Effect of circular holes on cross- ply laminated composite plates,* The Arabian Journal for Science and Engineering, Vol 34, Number 2. 2009. pp. 301-315.

[42] K.M.M. Muneer, R.V. Prakash, K. Balasubramaniam, *Thermomechanical studies in glass/epoxy composite specimen during tensile loading*. World

Academy of Science, Engineering and Technology 56. 2009. pp. 865-872.

[43]   M. Kutin, S. Ristic, M. Puharic, M. Vilotijevic, M. Krmar, *Thermographic testing of epoxy-glass composite tensile properties.* Contemporary Materials II. 2011. pp. 88-93.

[44]   C. Colombo, F. Libonati, F. Pezzani, A. Salerno L. Vergani, *Fatigue Behaviour of a GFRP Laminate by thermographic measurements.* Procedia Engineering 10. 2011. pp. 3518–3527.

[45]   P. Stanley and W.K. Chan, *Quantitative analysis by means of thermoelastic effect*, J. Strain Analysis 20. 1985. pp. 129-134.

[46]   Z. Feng, D. Zhang, R.E. Rowlands, B.I. Sandor, *Thermoelastic determination of individual stress components in loaded composites*, Experiment Mechanics. 1990. pp. 89-95.

[47]   S. Sambasivam, *Thermoelastic stress analysis of laminated composite materials*, Ph.D thesis, Faculty of Engineering, Science and Mathematics School of Engineering Sciences, UNIVERSITY OF SOUTHAMPTON. 2009.

[48]   F. Libonati, *Damage analysis of composite by means of thermography.* Symphosium on Experiment Solid Mechanics *ISBN 978-88-95940-30-4.* 2010.

[49]   C. Colombo, F. Libonati, L. Vergani, *Study of the mechanical characteristics of GFRP by thermography*, ICCS 16. 2011.

[50]   Ecole Des Mines de Saint Etienne (EMSE), *Suivi par thetmographie infrarouge sur composites carbon-epoxy.* 1996 http://www.carlosantulli.net/stetstage96.pdf

[51]   L. Toubal, M. Karama, and B. Lorrain, *Damage evoution and infrared thermography in woven composite laminates under fatigue loading. hermoelastic Stress Analysis of damage mechanisms in composite materials*, International Journal of fatigue 28 Composites. 2006.pp.1867–1872

[52]   J. Rossignola,   M.L .Pastor, A.Thionnet, *Détection d'endommagement dans les composites à l'aide d'une technologie utilisant des micro-ondes et par thermographie infrarouge*, Matériaux. 2010.

[53]   G. Curti, G. La Rosa, M. Orlando, and A Risitano, *Analisi tramite infrarosso termico della 'temperatura limite' in prove di fatica* (in Italian), 14th AIAS Italian National Conference, Catania, Italy. 1986:211-20.

[54]   G. La Rosa and A. Risitano, *Thermographic methodology for rapid determination of the fatigue limit of materials and mechanical components*,   International Journal of Fatigue 22. 2000. pp. 65-73.

[55]   G. Meneghetti, M. Quaresimin, M. De Monte, *fatigue strength assessment of a short fibre-reinforced plastic based on the energy dissipation* , 16th international conference on composite materials, 2007.

[56]   R. Steinberger , T.I. Valadas Leitaão , E. Ladstätter, G. Pinter, W. Bilinger, and R.W. Lang, *Infrared thermographic techniques for non-destructive damage characterization of carbon fibre reinforced polymersduring tensile fatigue testing*, International Journal of Fatigue 28. 2006. pp. 1340-1347.

[57]   T.P. Soemardi, *Etude du comportement mecanique et de l'endommagement de tube en composites verre/epoxy soumis a des sollicitations axiales et biaxees en statique et en fatigue*, Ph.D thesis, Formation Doctorale Mécanique et Matériaux, Ecole Centrale Paris. 1990.

[58]   T.P. Soemardi, D. Lai, C. Bathias, *Static and fatigue biaxial testing of fiber composite using thin walled tubular specimens*, IUTAM Symposium. New York-USA in Dvorak (ed). Springer Verlag, Germany. 1991.

[59]   G. Fargione ∗, A. Geraci, G. La Rosa, A. Risitano, *Rapid determination of the fatigue curve by the thermographic*, International Journal of Fatigue 24. 2002. pp. 11-19.

[60]   L Toubal, B. Lorrain, F. Peyruseigt, and M. Karama, *Détermination de la limite d'endurance d'un carbone/époxy par analyse thermographique* (in French), 17ème Congrès Français de Mécanique, Troyes, France, Septembre 2005.

[61]   J. Montesano, Z. Fawaz, and H. Bougherara, *Use of infrared thermography to investigate the fatigue behaviour of a carbon fiber reinforced polymer composite* , Composite Structure 97. 2013. pp. 76-83.

[62]   A. Risitano and G. Risitano, *Cumulative damage evaluation in multiple cycle fatigue tests taking into account energy parameters,* International Journal of Fatigue 48. 2013. pp.214-222.

[63]   M. Giordano, A. Calabro ,C. Esposito, A. D'Amore, L. Nicolais, *An acoustic-emission characterization of the failure modes in polymer-composite materials*, Composites Science and Technology 58. 1998. pp.1923-1928.

[64]   N. C. Shippen, D. F. Adams, *Acoustic emission monitoring of damage progression in graphite/epoxy laminates*, Journal of Reinforced Plastics and Composites, Vol. 4. July 1985. pp. 242-261.

[65]   J. M. Berthelot, *Relation between amplitudes and rupture mechanisms in composite materials*, Proceedings of Acoustic Emission from Composite Materials II, Montreal. 1986. pp. 126-133.

[66]   H. Otsuka, H. A. Scarton, *variations in acoustic emission between graphite- and glass-epoxy composites*, J. Composite Materials, Vol. 5. Nov.1981. pp. 591-597.

[67]   J. P. Favre, J. C. Laizet, *amplitude and counts per event analysis of acoustic emission generated by transverse cracking of cross-ply CFRP*, Composites Science and Technology, Vol. 36. 1989. pp. 27-43.

[68]   Favre, J. P., and J. C. Laizet, *Acoustic analysis of the accumulation of cracks in CFRP cross-ply composites under tensile loading*, Journal of Acoustic Emission, Vol 9. 1990. pp. 97-102.

[69]   M. Johnson, *Classification of AE transients based on numerical simulations of composite laminates*, NDT&E International 36. 2003. pp.319–329

[70]   P.J. de Groot, P.A.M.Wijnen, R.B.F. Janssen, *Real-time frequency determination of acoustic emission for different fracture mechanisms in carbon/epoxy composites*, Composites Science and Technology 55. 1995. pp.405–412.

[71]   C.R. Ramirez-Jimenez, N. Papadakis, N. Reynolds, T.H. Gan, P. Purnell, M. Pharaoh, *Identification of failure modes in glass/polypropylene composites by means of the primary frequency content of the acoustic emission event*, Composites Science and Technology 64. 2004. pp.1819–1827.

[72]   R. Gutkin, C.J.Green, S. Vangrattanachai, S.T. Pinho, P. Robinson, P.T. Curtis, *On acoustic emission for failure investigation in DCFC: Pattern recognition and peak frequency,* Mechanical Systems and Signal Processing 25. 2011. pp.1393–1407.

[73]   Mechraoui S.E, Laksimi A, and Benmedakhene S. *Reliability of damage mechanism localisation by acoustic emission on glass/epoxy composite material plate.* Composite Structures 94. 2012. pp. 1483-1494.

[74]   M. Kharoubi, L. Fatmi, A. El Mahi, R. EL Guerjouma, R. Berbaoui, *Identification du dommage par EA de stratifiés composites chargés en statique et cyclique*, 10ème Congrès Français d'Acoustique, *Lyon, 12-16 Avril 2010.*

[75]   W. Li, G. Dai, F. Long, P. Jiang, Y. Wang, *Study on FRP composite material damage based on the acoustic emission testing technology,* 18th World Conference on Non-destructive Testing. 2012.

[76]   R.B. Toumi. J. Renard, M. Monin, P. Nimdum, *Fatigue damage modelling of continuous E-glass fibre/epoxy composite*, Procedia Engineering 66. 2013. pp. 723-736.

[77]   A.A. Malcolm and T. Liu, *Case Studies in the use of computed tomography for non-destructive testing, failure analysis and performance evaluation* , Singapore International NDT Conference & Exhibition. 2011.

[78]   M. Amos, *Advanced industrial x-ray computed tomography for defect detection and characterisation of composite structures*, A thesis submitted to The University of Manchester for the degree of Doctor of Engineering in the Faculty of Engineering and Physical Sciences. 2010.

[79]   B. Zhang, *Digital test of composite material using x-ray   tomography and finite element simulation*, Dissertation submitted to the faculty of

Virginia Polytechnic Institute and State University in partial fulfillment of the requirements for the degree of Doctor of Philosophy. 2007.

[80]   P. Wright, A. Moffat, I. Sinclair, S.M. Spearing, *High resolution tomographic imaging and modelling of notch tip damage in a laminated composite*, Composites Science and Technology 70. 2010. pp.1444–1452.

[81]   J. Kastner, B. Plank, D. Salaberger, J. Sekelja, ASTNER*, *Defect and Porosity Determination of Fibre Reinforced Polymers by X-ray Computed Tomography*, 2nd International Symposium on NDT in Aerospace. 2010.

[82]   F. Cosmi and A. Bernasconi, *Micro-CT investigation on fatigue damage evolution in short fibre reinforced polymers*, Composites Science and Technology 79. 2013. pp.70–76.

[83]   C. Goidescu, H. Welemane, C. Garnier, M. Fazzini, R. Brault, E. Péronnet, S. Mistou, *Damage investigation in CFRP composites using full field measurement techniques: Combination of digital image stereo-correlation, infrared thermography and X-ray tomography*, Composites: Part B 48. 2013. pp. 95–105.

[84]   M. Turtle, T. Shifman and B. Boursier, *Simplifying certification of discontinuous composite material forms primary aircraft structures,* Hexcel Research and Technology. http://www.hexcel.com

[85]   B. Boursier and A. Lopez, *Failure initiation and effect of defects in structural discontinuous fiber composites*, Hexcel Research and Technology. 2010. http://www.hexcel.com

[86]   P. Feraboli, E. Peitso, F. Deleo, T. Cleveland, M. Graves, P. Stickler, *Characterization of discontinuous carbon fiber/epoxy systems for aerospaceapplications*.http://www.aa.washington.edu/research/structures/pubs/208.pdf

[87]   P. Feraboli, E. Peitso, T. Cleveland, P. Stickler B, C.J. Halpin, *Notched behaviour of prepeg-based discontinuous carbon fiber/epoxy systems*. Composites : Part A 40. 2009. pp. 289-299.

[88]   P. Feraboli, T. Cleveland, P. Stickler, J. Halpin, *Stochastic laminate analogy for simulating the variability in modulus of discontinuous composite materials*, Composites : Part A 41. 2010. pp. 557-570.

[89]   J. Bale, E. Valot, M. Monin, P. Laloue, O. Polit, C. Bathias, T.P. Soemardi, *Thermography observation on damage behaviour of discontinuous carbon fiber composite*, The 13th Japanese-European Symposium on Composite Materials, Bougenais, France. 2013.

[90]   P. Feraboli, T. Cleveland, M. Ciccu, P. Stickler, L. DeOto, *Defect and damage analysis of advanced discontinuous carbon/epoxy composite materials,* Composites : Part A 41. 2010. pp. 888-901. http://www.aa.washington.edu/research/structures/pubs/208.pdf

[91]   P. Feraboli, E. Peitso, F. Deleo, T. Cleveland, M. Graves, P. Stickler, *Characterization of discontinuous carbon fiber/epoxy systems for aerospace applications.*

[92]   P. Feraboli, E. Peitso and T. Cleveland, *Modulus measurement for prepeg-based discontinuous carbon fiber/epoxy systems,* Journal of composite materials Vol 43 No.19. 2009. pp. 1947-1965.

[93]   M.D. Bond, L.T. Harper, T.A. Turner, N.A. Warrior, *Full - field strain measurement of notched discontinuous carbon fiber composites,* ICCM 17 Proceeding. http://www.iccm-central.org

[94]   C. Qian, L.T. Harper, T.A. Turner, N.A. Warrior, *Notched behaviour of discontinuous carbon fiber composites: Comparison with quasi-isotropic non-crimp fabric,* Composites: Part A 42. 2011. pp. 293–302.

[95]   J. Bale, E. Valot, M. Monin, P. Laloue, O. Polit, C. Bathias, T.P. Soemardi, *Damage observation of glass fiber epoxy composites using thermography and supported by acoustic emission*, Applied Mechanics and Materials Journal Vol. 627. 2014. pp.187-190.

[96]   S.H. Najem, *Methodology for Assessment of factors influencing surface roughness on the drilling of carbon-reinforced composite,* Journal of Babylon University/ENgineering Science 2 Vol.21. 2013. pp.604-615.

APPENDIX A

A.1. Tensile test using rossette strain gage to ensure the test in a good condition.

A flat specimen of GFRP 90° without hole is used as specimen of this tensile test. At the center of the specimen for both surface, pinned strain gage rosette (Fig.A.1).
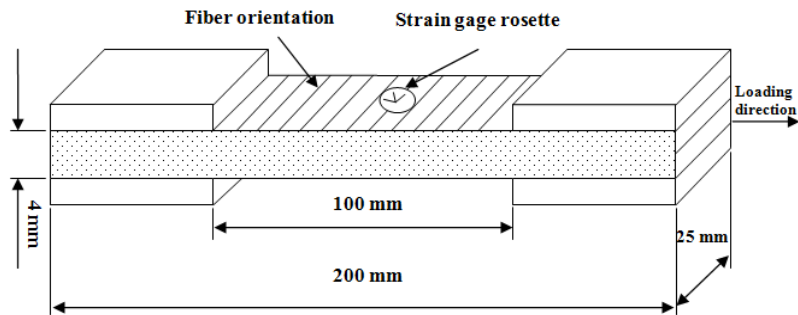
Figure A.1 Specimen of GFRP 90° and placement of strain gage rosette

This tensile test is conducted with the aim to isolate possible eccentricities in the specimen loading to have a good test condition. Fig.A.2 below shows the tensile test result on strain propagation during the test. Strain values were coming directly from strain gage. The test conducted with constant displacement rate of 1 mm/minute until F $_{tensile}$ = 3500 N and no macro failure occurs .
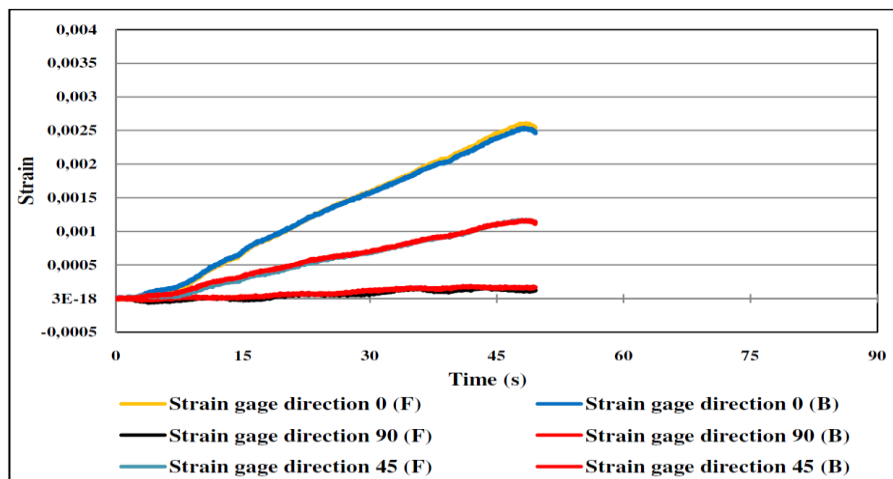
Figure A.2 Strain propagation of GFRP 90° during tensile test

From the result above, showing that the larger strain of the specimen occurs in pararel direction with tensile loading or perpendicular with fiber orientation. Strain result (curve coincide) comes from both surface (front and back) indicate that the test run in good condition without experiencing other type of loading such as bending.

1

A.2. Surface roughness test

This test is conducted in order to measure the surface of the hole and its effect in creating local stress concentration due to fabrication process. Fig.A.3 shows the results of surface roughness test.

Rmax	18.1731 µm
Rz	14.2393 µm
Sm	181.8751 µm
Da	0.4577
Dq	0.7285
La	29.0414 µm
Lq	23.4883 µm
Tilt A	-0.6104 °
lr	117.0330
Rsk	-0.9321
Rku	3.9186
AVH	2.4587 µm
Hmax	5.5285 µm
Hmin	1.0033 µm
AREA	2537.3856 µm2
Ra	1.9702 µm
Rq	2.5301 µm
Rp	4.8567 µm
Rv	11.8345 µm

Roughness Curve
C1   = 0.000000 mm 0.774 µm
C2   = 0.000000 mm 0.774 µm
C1 - C2 = 0.000000 mm 0.000 µm

—— Roughness Curve
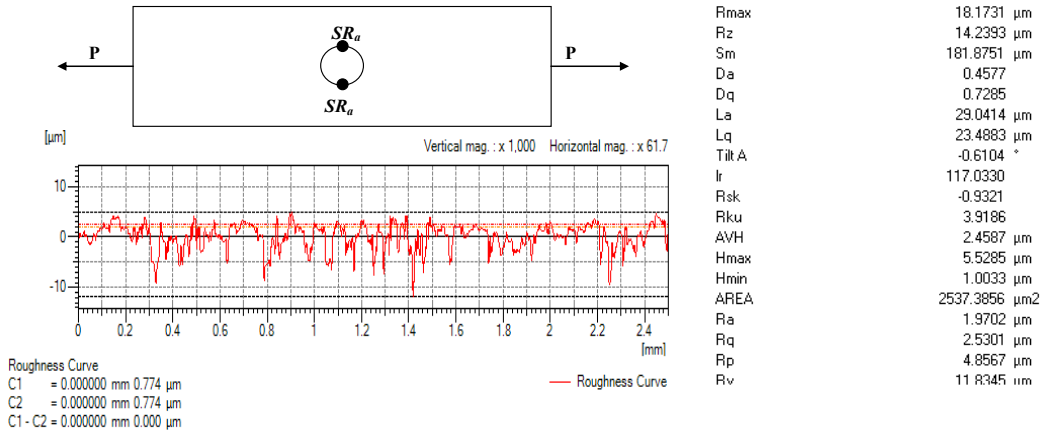
a. Surface roughness results of hole surface perpendicular with loading direction

Rmax	20.4574 µm
Rz	12.6852 µm
Sm	348.7372 µm
Da	0.3776
Dq	0.5695
La	47.5828 µm
Lq	37.7116 µm
Tilt A	3.3832 °
lr	111.8358
Rsk	-0.0492
Rku	2.5195
AVH	3.4405 µm
Hmax	10.5088 µm
Hmin	1.0059 µm
AREA	3515.5592 µm2
Ra	1.7306 µm
Rq	2.2279 µm
Rp	6.9043 µm
Rv	9.7794 µm

Roughness Curve
C1   = 0.000000 mm 1.793 µm
C2   = 0.000000 mm 1.793 µm
C1 - C2 = 0.000000 mm 0.000 µm

—— Roughness Curve
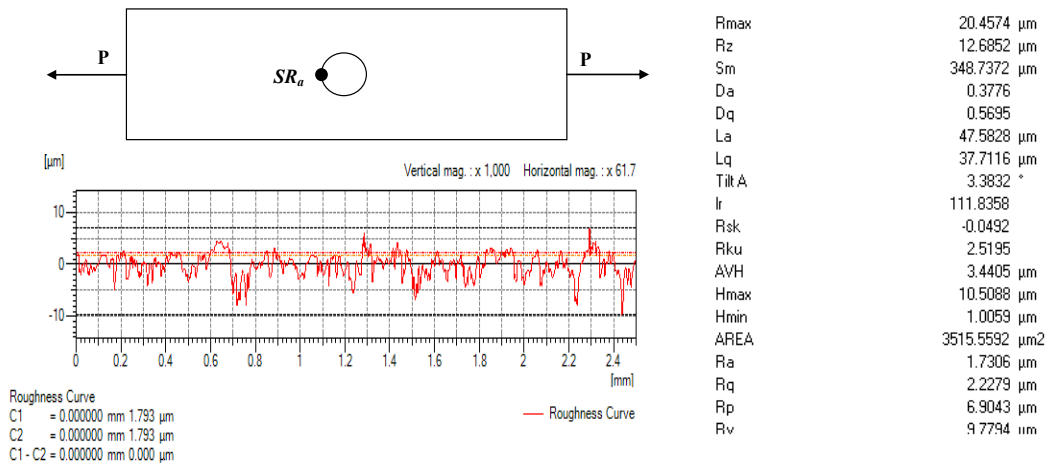
b. Surface roughness results of hole surface paralell with loading direction
where : P = tensile loading direction ; SR_a = surface roughness area

R_a = Average of surface roughess from surface roughness area

Figure A.3 Surface roughess test

From the result above, showing that the surface roughness at hole surface has no different between area that parallel with loading direction known as area with lower stress concentration area ($SR_a \approx 1.73$µm) and area that perpendicular with loading direction known as area with higher concentration area ($SR_a \approx 1.97$µm) . It can be stated that fabrication process of hole doesn't initiate the emergence of micro crack then can be affect in generate local stress concentration.

A.3. Machining parameters on the drilling of fiber-reinforced composites

Machining of fiber-reinforced were found different from machining of conventional material such as steel due to the specific behaviour depends on matrix and reinforcement condition. In general, machining parameters on the drilling process will influence surface roughness (R_a) of specimen. The significant differs of R_a at the observation area at hole surface could be indicating a disreputable effect of machining process. From surface roughness measurements on the specimen that used in this study, we found similar R_a (Appendix A.2) from several area at hole surface. It can be noted that the machining parameters have a good influence on surface roughness of fiber-reinforced composites. Previous study [96] informs machining parameters on the drilling of fiber-reinforced composites that producing similar R_a that obtained from our surface roughness test. Since, all the specimens are fully given material, this information could be used as general machining parameters on the fabrication of fiber composite material contains circular notch or hole. Table A.1 gives the information of surface roughness and machining parameters on the drilling of fiber composite where the validity is limited to several factors of the experimentation (material condition and the drill tool).

Table A.1. Surface roughness and machining parameters on the drilling of fiber composite [96]

Levels				Unit	Notation	Parameter	Exp. No
Coded factors		Actual factors					
High	Low	High	Low				
+1	-1	150	75	m/min.	A	Cutting speed	1
+1	-1	20	10	%	B	Volume fraction	2
+1	-1	8	6	mm	C	Drill diameter	3
+1	-1	0.3	0.1	mm/rev.	D	Feed rate	4

Response variable	Actual factors				Coded factors				Exp. No
Ra, µm	D	C	B	A	D	C	B	A	
2.42	0.1	6	10	75	-1	-1	-1	-1	1
1.39	0.1	6	10	150	-1	-1	-1	+1	2
2.24	0.1	6	20	75	-1	-1	+1	-1	3
1.92	0.1	6	20	150	-1	-1	+1	+1	4
1.63	0.1	8	10	75	-1	+1	-1	-1	5
1.92	0.1	8	10	150	-1	+1	-1	+1	6
2.14	0.1	8	20	75	-1	+1	+1	-1	7
2.03	0.1	8	20	150	-1	+1	+1	+1	8
1.76	0.3	6	10	75	+1	-1	-1	-1	9
2.03	0.3	6	10	150	+1	-1	-1	+1	10
2.25	0.3	6	20	75	+1	-1	+1	-1	11
1.82	0.3	6	20	150	+1	-1	+1	+1	12
2.54	0.3	8	10	75	+1	+1	-1	-1	13
2.01	0.3	8	10	150	+1	+1	-1	+1	14
2.33	0.3	8	20	75	+1	+1	+1	-1	15

APPENDIX B

Digital Image Corelation (DIC)

This test is conducted with the aim to ensure that the testing machine and the acquired data are working properly. Testing parameter of load, displacement and strain then compared with the result of DIC. The specimen used is DCFC and GFRP 90° without hole. Fig.B.1 shows the testing set up.
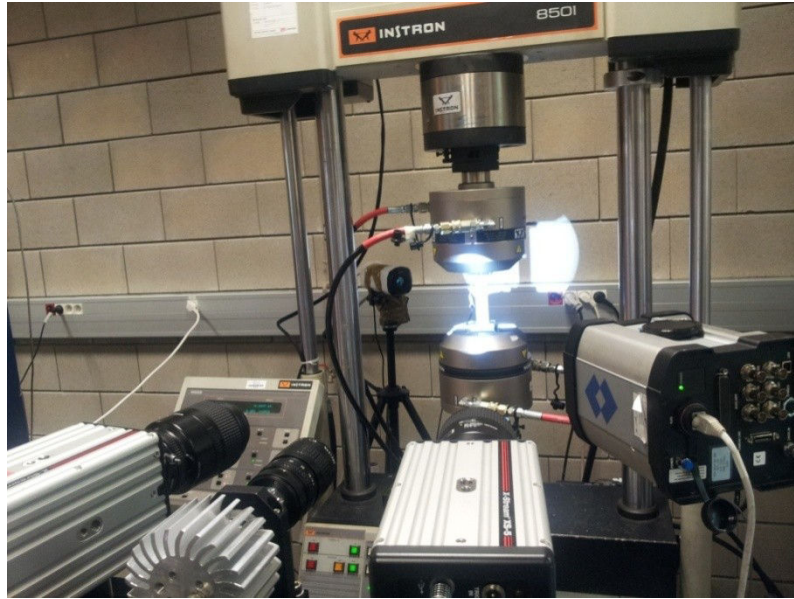
Figure B.1 Test set up

B.1   DIC results of DCFC specimen

This result as seen in Fig.B.2 ilustrates the comparison between DIC and mechanical testing on load, displacement and strain during tensile static test.
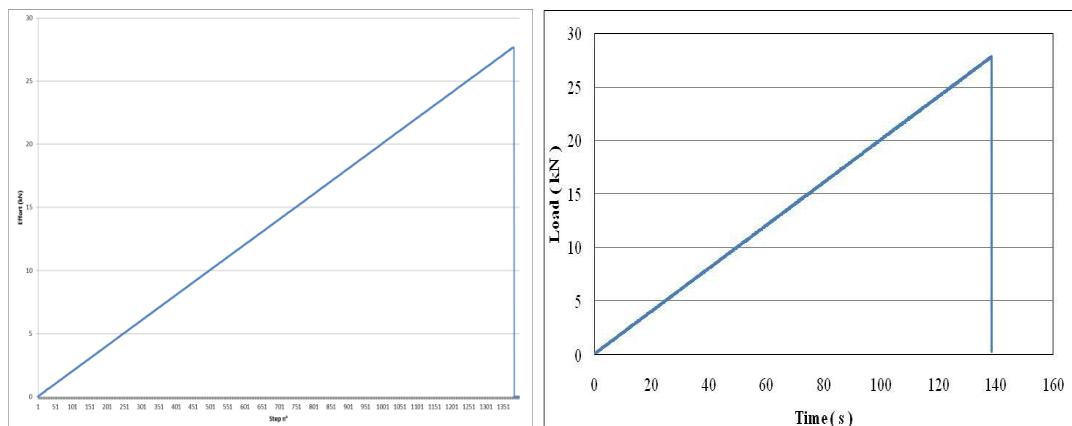
Load acquisition of DIC   Load of mechanical testing
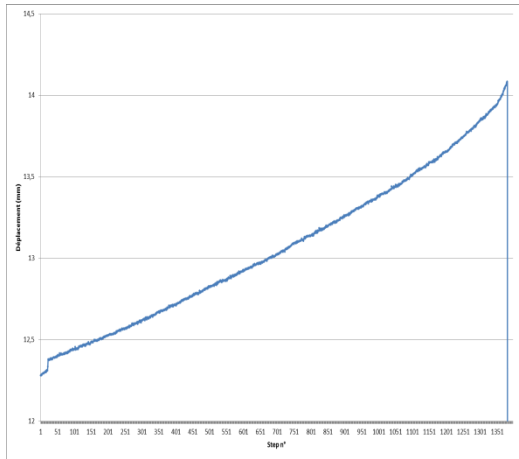
Displacement acquisition of DIC   Displacement of mechanical testing
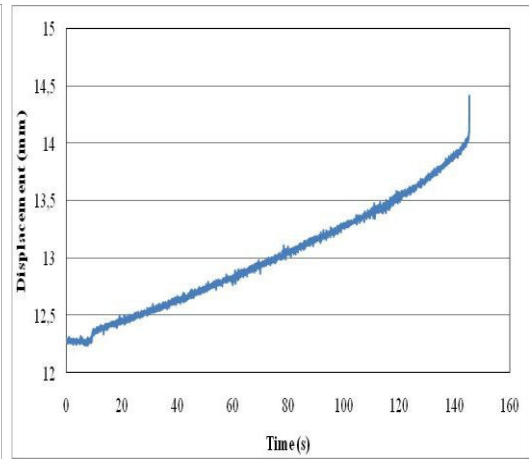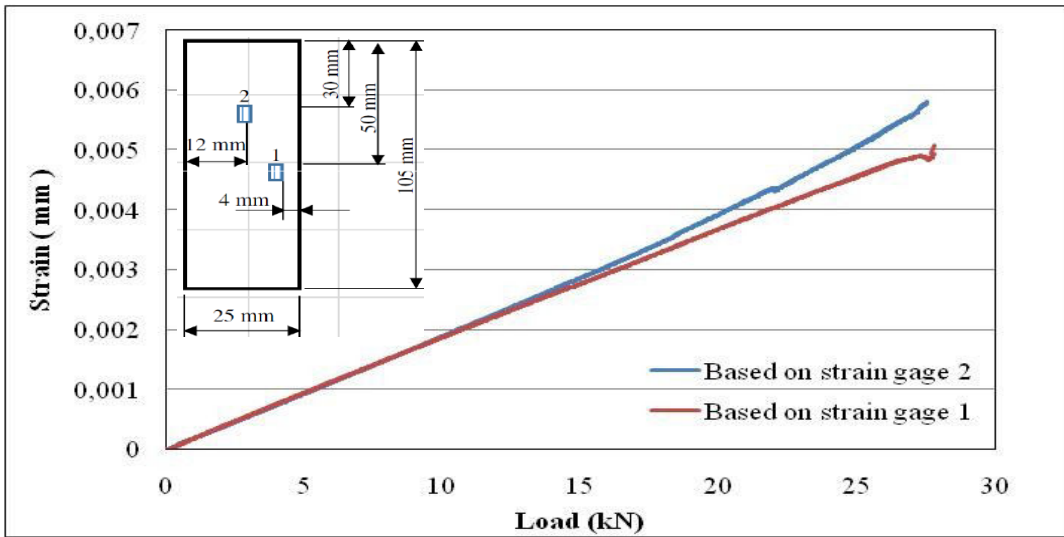
Strain of mechanical testing based on strain gage
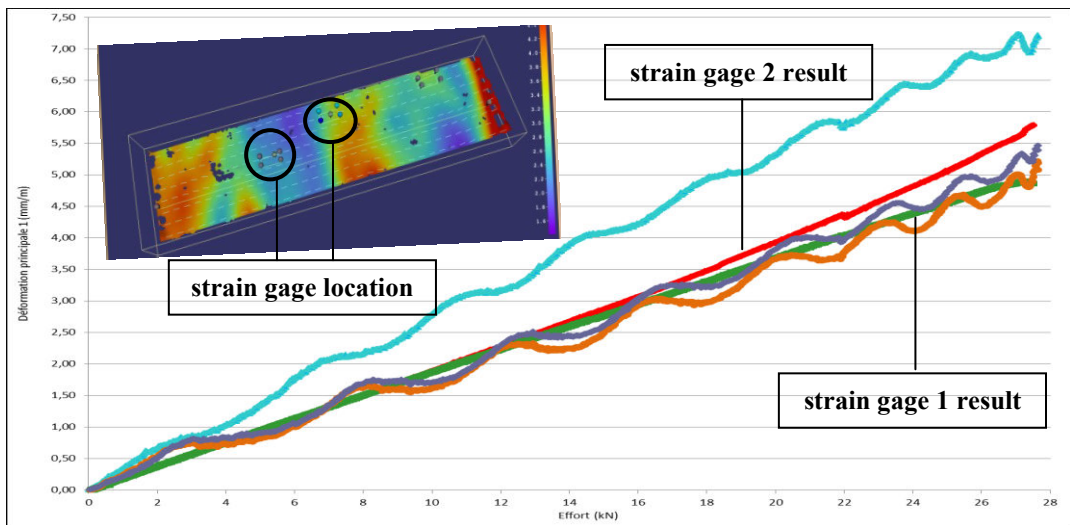
Strain acquisition of DIC

Figure B.2 DIC vs Mecahnical testing of DCFC

B.2   DIC results of GFRP 90° specimen

This result as seen in Fig B.3 ilustrate the comparison between DIC and mechanical testing on load, displacement and strain during tensile static test
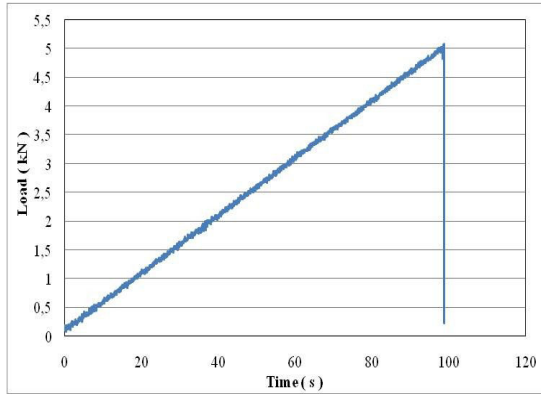
Load acquisition of DIC   Load of mechanical testing
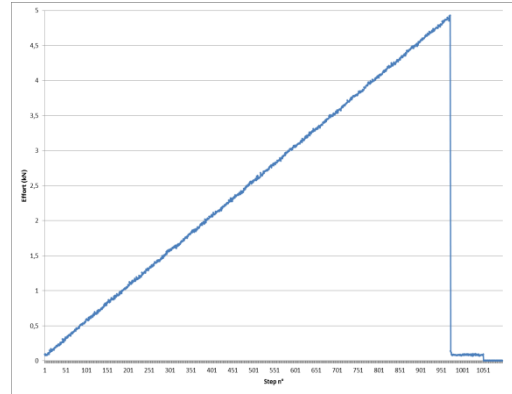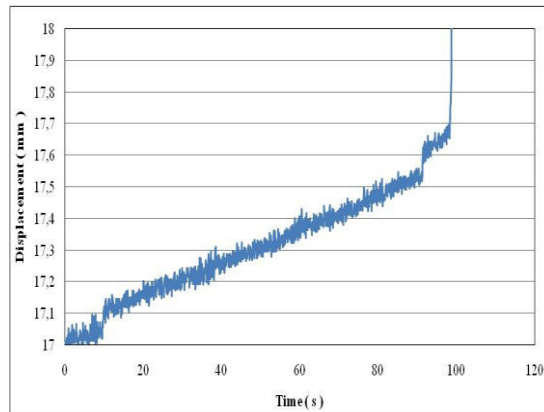
Displacement acquisition of DIC   Displacement of mechanical testing
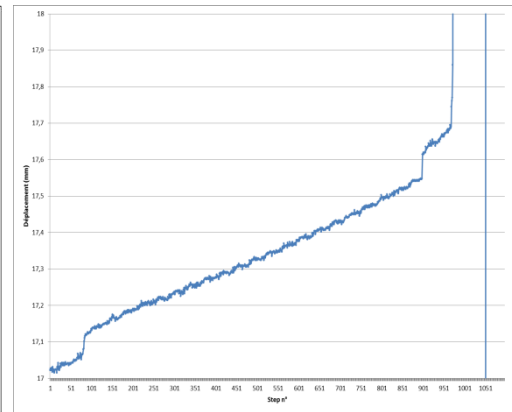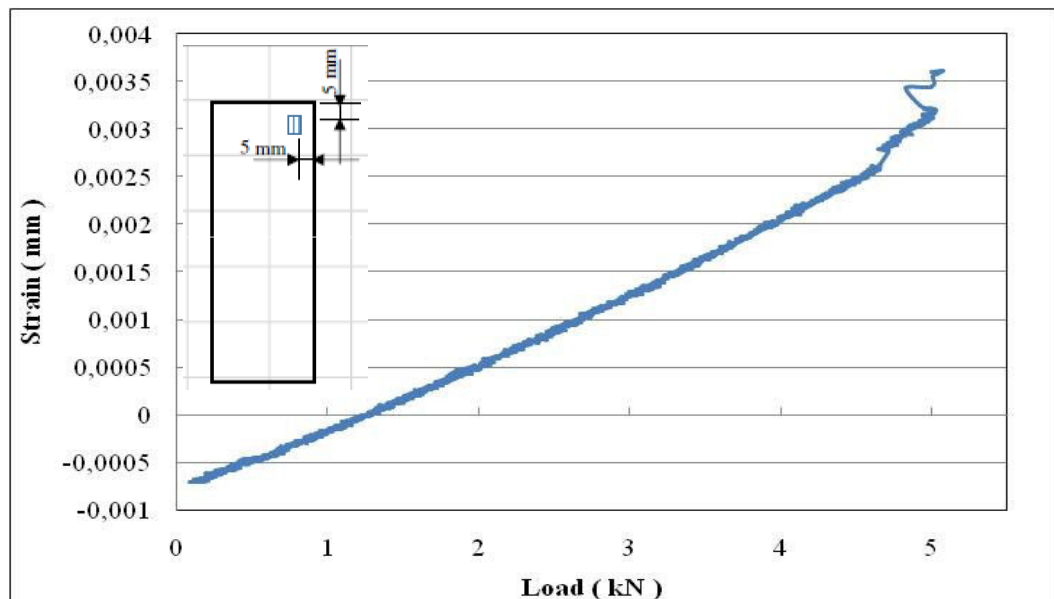
Strain of mechanical testing based on strain gage
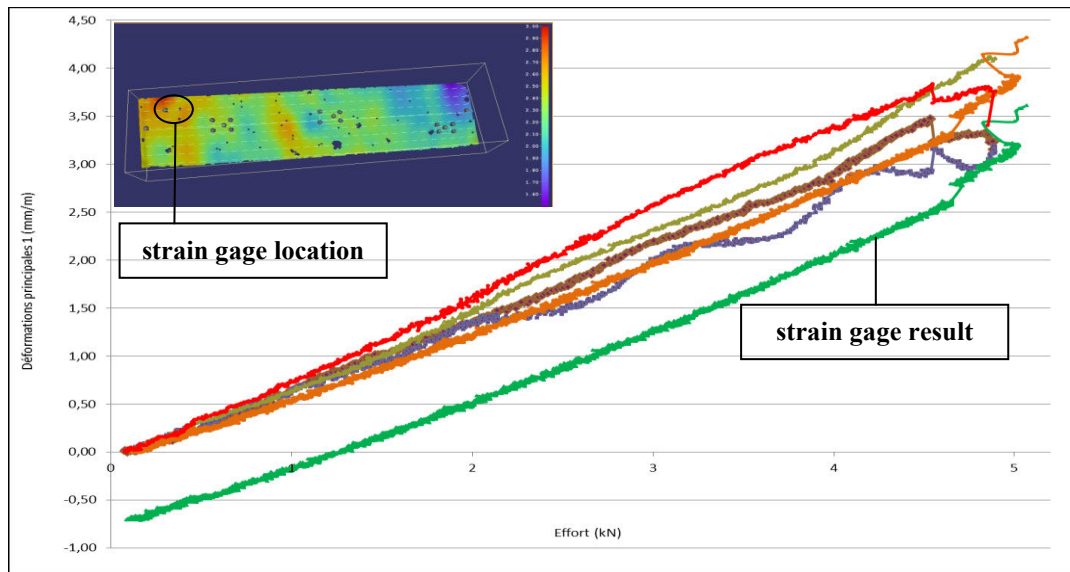
Strain acquisition of DIC

Figure B.3 DIC vs Mecahnical testing of GFRP 90°

From results on Fig.B.2 and Fig.B.3, DIC and mechanical test have a a good confirmation on acquisiition parameter of load, displacement and strain under tensile static testing. It can be noted that, the acquired data can well determined and DIC techniques gives a good identification on mechanical properties for unidirectional fiber composite (GFRP 90°) and randomly discontinuous fiber composite (DCFC).

APPENDIX C

The micromechanical model rule of mixture is the simplest way to calculate stiffness of composite in which all of the fibres are aligned or perpendicular in the direction of the applied load (a unidirectional composite). It is applied to obtain the analytical result. The result then compared with experimental result. This method Composite stiffness can be calculated with the assumptions :

- Fibers are uniformly distributed throughout the matrix

- Perfect bonding between fibers and matrix

- Matrix is free of voids

- Applied loads are either parallel or normal to the fiber direction

- Lamina is initially in a stress-free state (no residual stresses)

- Fiber and matrix behave as linearly elastic materials

1. **Rule of mixture of GFRP specimen**
   Table C.1 shows the properties of GFRP specimen
   Table C.1 The properties of GFRP

	Glass Fiber	Epoxy resin
E (GPa)	$E_f \approx 60$	$E_m \approx 4$
Density (gr/cm^3)	2.5	1.15
Volume (%)	60	40

Following are the steps to calculate stiffness of composite (longitudinal modulus/E_{11} and transverse modulus/E_{22})

- Step 1. Calculate weight fraction (Wf) of fiber and matrix

$$Wf_{fiber} = \frac{2.5 \; gr/cm^3}{cm^3} \times 0.60 = 1.5 \; gr$$

$$Wf_{matrix} = \frac{1.15 \; gr/cm^3}{cm^3} \times 0.40 = 0.46 \; gr$$

- Step 2. Convert weight fraction to volume fraction of fiber (Vf) and matrix (Vm)

$$V_f = \frac{1.5 \; gr}{(1.5 + 0.46)gr} \times 100\% = 76.53\%$$

$$V_m = \frac{0.46 \; gr}{(1.5 + 0.46)gr} \times 100\% = 23.47\%$$

- Calculate longitudinal modulus (E_{11}) and transverse modulus (E_{22})

$$E_{11} = E_f V_f + E_m V_m \; ; E_{11} = 47 \text{ GPa}$$

$$E_{22} = \frac{E_m E_f}{V_m E_f + V_f E_m}; E_{22} = 14 \text{ GPa}$$

The calculation of modulus elastic of composite by rule of mixture, later compared with experimental results, as seen in table C.2

Table C.2 Modulus elastic of GFRP specimen

Relationship	Predicted values (GPa)	Experimental values (GPa)
E_{11} (modulus elastic of GFRP 0° which fibers are aligned with loading direction)	47	45
E_{22} (modulus elastic of GFRP 90° which fibers are perpendicular with loading direction)	14	15 - 17

2. Rule of mixture of DCFC specimen

Table C.3 shows the properties of DCFC specimen

Table C.3 The properties of DCFC

	Carbon Fiber	Epoxy resin
E (GPa)	$E_f \approx 240$	$E_m \approx 4$
Density (gr/cm^3)	1.55	1.15
Volume (%)	57	43
Weight fraction (gr)	0.88	0.5
Volume fraction (%)	63.8	36.2

The calculation stiffness of composite, E_c :

$$E_c = k E_f V_f + E_m V_m \; ; E_c = 32.064 \text{ GPa}$$

where $k = 1/5$ is the reinforcement efficiency for fiber orientation randomly and uniformly distributed within three dimensions in space.

The calculation of modulus elastic of composite by rule of mixture, later compared with experimental results, as seen in table C.4

Table C.4 Modulus elastic of GFRP specimen

Relationship	Predicted values (GPa)	Experimental values (GPa)
E_c (modulus elastic of DCFC with hole based on global strain of crosshead dispalcement)	29.5	27.25

APPENDIX D

D.1. Stress concentration of DCFC specimen

Using the characteristic dimension d_o, that it is possible to calculate the stress concentration factor. Feraboli et.al [86] found d_o as a function of hole diameter for DCFC specimen, as seen in Fig.D.1.
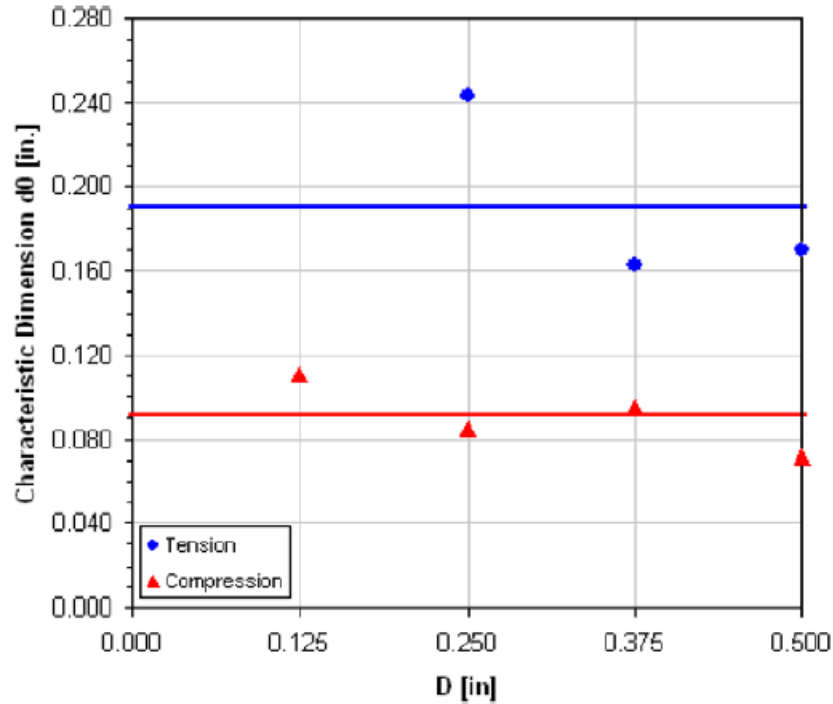
Figure D.1 Characteristic dimension d_o

Calculation the stress concentration factor :

$$K_t = \sqrt{\frac{d + do}{do}} \; ; under \; static \; loading$$

$$K_f = 1 + do \, (K_t - 1); \; under \; fatigue \; loading$$

Using specimen data, d = 10 mm ($\approx$ 0.393 in) and $do \approx 0.192$ in, we found,

$$K_t = \sqrt{\frac{d + do}{do}} = 1.74$$

$$K_f = 1 + do \, (K_t - 1) = 1.14$$

From stress concentration factor, the DCFC specimen shows the sensitivity behaviour due to the presence of the hole (d = 10 mm) under static and fatigue loading.

D.2. Stress concentration for GFRP specimen

Calculate the stress concentration factor around the hole of GFRP under static tensile static test (Assume the plate is uniaxially loaded with a uniform pressure = 1 MPa) . The dimension of the plate is 100 mm x 25 mm with uniform thickness of 4 mm. An open hole is made in the centre of the plate with 5 mm radius. The plate is glass/epoxy composite material with two types of fibers oriented : perpendicular direction with the applied load and pararel direction with the applied load. The material properties are as follows (from experimental results):

Young's modulus in the fiber direction Ex = 45 GPa

Young's modulus in the transverse direction = Ey = 15 GPa

In-plane shear modulus Gxy = 14 GPa

Poisson's ratio V_{12} = 0.05

Experiments :

The effect of an open hole on the stress concentration factor calculated from the theories by performing tensile static test. The specimen was tested in a tensile test machine up to failure under uniaxial tension in the axis-1 direction (Fig.D.2).
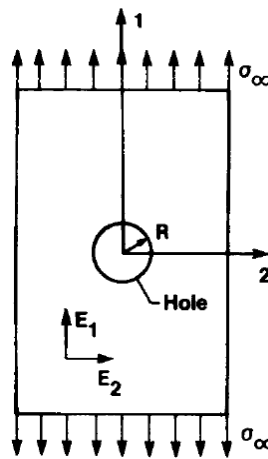
Figure D.2 Loading condition

From the problem specification, the ply engineering elastic constants with respect to the principal elastic axes {L,T} are given by

$E_x = E_L$ = Modulus of elasticity of single ply in fiber direction

$E_y = E_T$ = Modulus of elasticity of single ply transverse to fiber direction

$G_{xy} = G_{LT}$ = shear modulus of single ply associated with {L,T} system

$v_{xy} = v_{LT}$ = poisson's ratio of single ply with respect to {L,T} system

The following is a sample calculation for the stress concentration factor for α =90° and ø = 0 (fiber oriented in parallel direction with loading axis) and α =0° and ø = 90° (fiber oriented in perpendicular direction with loading axis)

1. GFRP 90° (α =0° and ø = 90)

Fig.D.3 shows the ilustration of the loading direction (σ_∞) that perpendicular to the fiber direction.
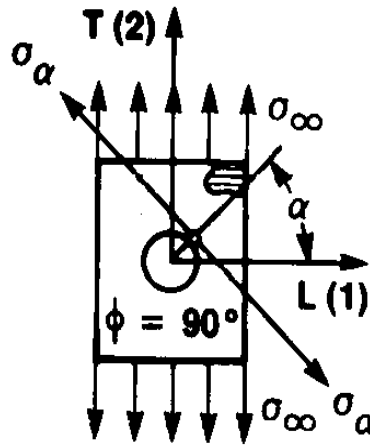
Figure D.3. Ilustration of the loading direction GFRP 90°

Using spesification data, the ply constants with respect to axes {1,2} can be calculated from equation (1) to (4). For θ = 90° fiber orientations,

$E_1 = E_y = 15$ Gpa

$E_2 = E_x = 45$ Gpa

$G_{21} = G_{xy} = G_{yx} = 14$ GPa

The tangential stress,σ_α(or tangential stress concentration factor, $K = \sigma_\alpha / \sigma_\infty$) along the circular hole boundary may be expressed as :

$$K_t = \frac{\sigma_\alpha}{\sigma_\infty} = \frac{E_\alpha}{E_1} \{[-cos^2 \emptyset + (k+n)sin^2 \emptyset]k \, cos^2 \alpha + [(1+n)cos^2 \emptyset -$$

$$k \, sin^2 \emptyset] \, sin^2 \alpha - n \, (1+k+n) \sin \emptyset \cos \emptyset \sin \alpha \cos \alpha \}$$

where E_α is the modulus of elasticity in the α direction (Fig.3) given by :

$$\frac{E_\alpha}{E_1} = 1 / \left[sin^4 \alpha + \frac{E_1}{E_2} cos^4 \alpha + \frac{1}{4} \left(\frac{E_1}{G_{12}} - 2v_{12} \right) sin^2 2\alpha \right]$$

Where k and n are defined by

$$k = \sqrt{\frac{E_1}{E_2}}$$

$$n = \sqrt{2\left(\frac{E_1}{E_2} - v_{12}\right) + \frac{E_1}{G_{12}}}$$

From equation (2) to (4), we obtain the value of E_α/E_1, k and n. The calculation presented below.

$$\frac{E_\alpha}{E_1} = 1/\left[sin^4\alpha + \frac{E_1}{E_2}cos^4\alpha + \frac{1}{4}\left(\frac{E_1}{G_{12}} - 2v_{12}\right)sin^2 2\alpha\right]$$

$$\frac{E_\alpha}{E_1} = 1/\left[sin^4 0 + \frac{15}{45}cos^4 0 + \frac{1}{4}\left(\frac{15}{14} - 2(0.05)\right)sin^2 2(0)\right] = 3$$

$$k = \sqrt{\frac{E_1}{E_2}} = \sqrt{\frac{15}{45}} = 0.577$$

$$n = \sqrt{2\left(\frac{E_1}{E_2} - v_{12}\right) + \frac{E_1}{G_{21}}} = \sqrt{2\left(\frac{15}{45} - 0.05\right) + \frac{15}{14}} \approx 1.3$$

Input the value of E_α/E_1, k and n into equation (1), we found the highest stress concentration factor of GFRP 0° under tensile static test, $K_t = 3$. K value shows that when the loading direction is perpendicular to the fiber direction, the value of K reaches 3 at $\alpha = 0^o$ around the hole area (Fig D.3).

2.   GFRP 0° ($\alpha = 90^o$ and $\phi = 0$)

Fig.D.4 shows the ilustration of the loading direction (σ_∞) that parallel to the fiber direction.
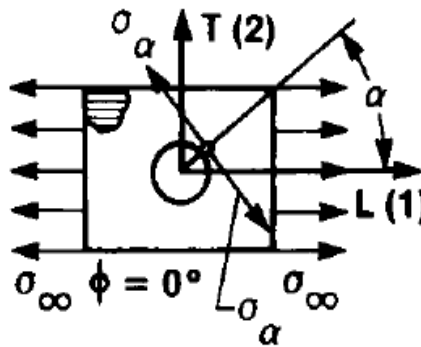
Figure D.4 Ilustration of the loading direction GFRP 0°

Using spesification data, the ply constants with respect to axes {1,2} can be calculated from equation (1) to (4). For $\phi = 0^o$ fiber orientations,

$E_1 = E_x = 45$ Gpa

$E_2 = E_y = 15$ Gpa

$G_{12} = G_{xy} = 14$ GPa

From equation (2) to (4), we obtain the value of E_α/E_1, k and n. The calculation presented below.

$$\frac{E_\alpha}{E_1} = 1\bigg/\left[sin^4\alpha + \frac{E_1}{E_2} cos^4\alpha + \frac{1}{4}\left(\frac{E_1}{G_{12}} - 2v_{12}\right)sin^2 2\alpha\right]$$

$$\frac{E_\alpha}{E_1} = 1\bigg/\left[sin^4 90 + \frac{45}{15} cos^4 90 + \frac{1}{4}\left(\frac{45}{14} - 2(0.05)\right)sin^2 2(90)\right] = 1$$

$$k = \sqrt{\frac{E_1}{E_2}} = \sqrt{\frac{45}{15}} = 1.732$$

$$n = \sqrt{2\left(\frac{E_1}{E_2} - v_{12}\right) + \frac{E_1}{G_{12}}} = \sqrt{2\left(\frac{45}{15} - 0.05\right) + \frac{45}{14}} \approx 3$$

Input the value of E_α/E_1, k and n into equation (1), we found stress concentration factor of GFRP $0°$ under tensile static test, K = 4. K value shows that when the loading direction is parallel to the fiber direction, the value of K reaches 4 at $\alpha = 90°$ around the hole area (Fig.D.4). Stress concentration under fatigue can be defined by :

$$K_f = 1 + q(K_t - 1)$$

$$q = \frac{K_f - 1}{K_t - 1}$$

Since this specimen is very sensitive due to the presence of the hole, where as a value of q = 1, then $K_t \approx K_f$. Table D.1 summarize the results for K for each α.

Table D.1 Stress Concentration Factor

Location of α	Stress Concentration Factor (K)
0	-0.6
30°	0.1
45°	0.36
60°	1.93
75°	3.6
90°	4

The analytical results then compared with the simulation. Following is an example of simulation analysis of GFRP 0°.

A structural solid element (plane 82) was selected in order to construct the graphical image of the geometries of the composite plate, examined using the ANSYS (Advanced Engineering Simulation). Fig.D.5 shows a quarter model of the specimen.
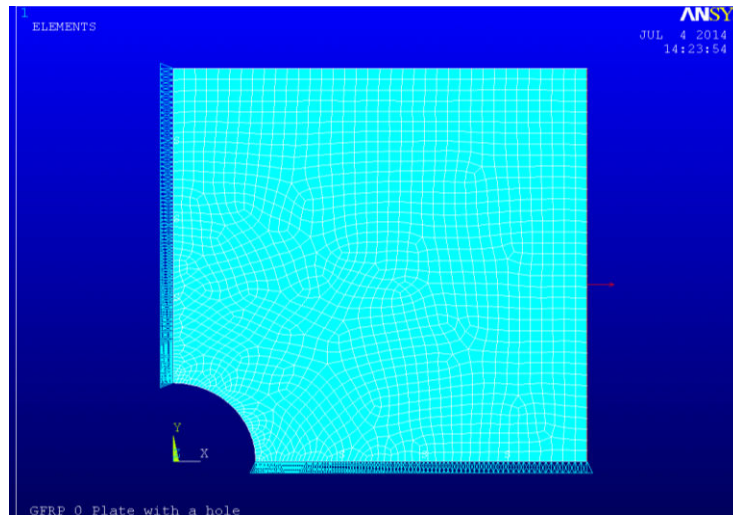
Figure D.5 Boundary conditions of the region to be modeled

The stress distribution contours around the hole for the composite plate having single hole with d = 5 mm (quarter model) is shown in Fig D.6.

Ø (deg)	K
0	-0.74151
2.25	-0.73875
4.5	-0.73171
6.75	-0.71943
9	-0.70462
11.25	-0.6836
13.5	-0.65835
15.75	-0.62786
18	-0.59094
20.25	-0.54774
22.5	-0.50026
24.75	-0.43933
27	-0.37207
29.25	-0.29491
31.5	-0.20976
33.75	-0.11231
36	1.02E-02
38.25	0.11174
40.5	0.2483
42.75	0.40482
45	0.56592
47.25	0.7406
49.5	0.92663
51.75	1.1243
54	1.3324
56.25	1.5491
58.5	1.7745
60.75	2.0073
63	2.2493
65.25	2.4943
67.5	2.7312
69.75	2.9356
72	3.1391
74.25	3.3264
76.5	3.5068
78.75	3.662
81	3.8207
83.25	3.9068
85.5	3.9818
87.75	4.0313
90	4.0526

Figure D.6 Ansys model of stess distribution

From Fig.D.6, we can see that the maximum stress occurs in perpendicular area against the loading direction at the edge of the hole ($\phi = 90^{o}$) . With 1 Mpa tensile stress that using for this ANSYS analysis, maximum stress reaches ≈ 4 times. This simulation analysis has a similar result with analytical based on experimental results. Fig.D.7 shows the simulation and analytical results of stress concentration as a function of ϕ angle degree.
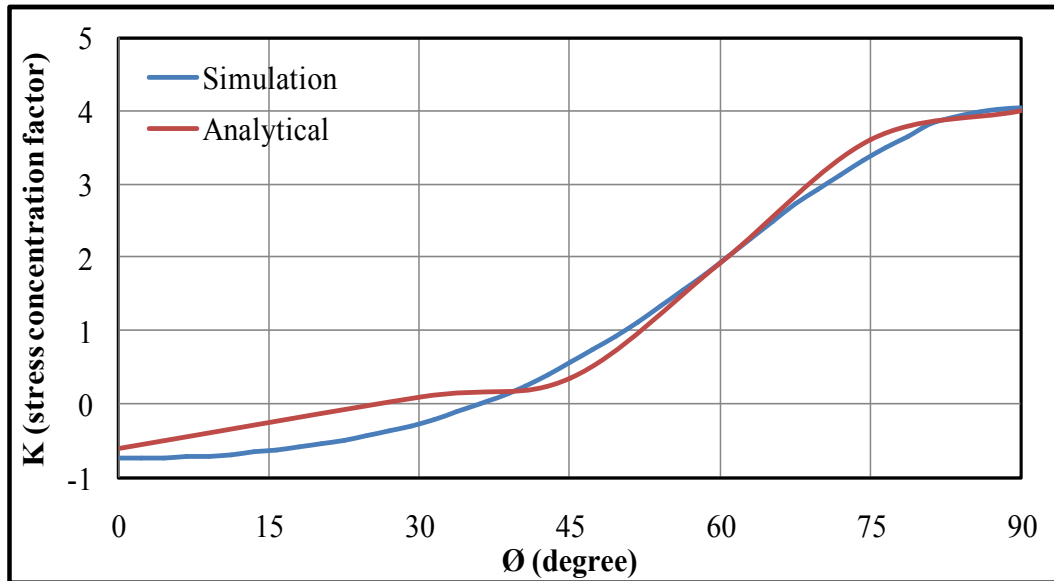
Figure D.7 Simulation vs analytical of K along the hole

From the previous analysis, It was found that the stress concentration factor could be greater or less than 3 (the stress concentration factor for isotropic materials) for GFRP specimen, and the maximum tangential stress points depends on angular coordinate (α) along hole with respect to the loading axis.